ALMA MATER STUDIORUM- UNIVERSITA' DI BOLOGNA

Dottorato di ricerca in

Chimica

Ciclo XXVIII

Settore scientifico-disciplinare di afferenza CHIM/04

Molecular and Supramolecular Engineering of Thiophene Based Materials for Application in Organic Electronics and Bioimaging

Francesca Giulia Di Maria

Coordinatore   Relatore

Prof. Aldo Roda   Prof.ssa Elisabetta Salatelli

Esame Finale Anno 2016

CONTENTS

PUBLISHED ARTICLES

PAPERS DISCUSSED IN THIS THESIS

Facilitated synthesis of functional oligothiophenes application in thin film devices and live cell imaging. F. Di Maria and G. Barbarella.
J. of Sulfur Chemistry, **2013**, *34*, 627-637

Physiological formation of fluorescent and conductive protein microfibers in live fibroblasts upon spontaneous uptake of biocompatible fluorophores. I. Viola, I. E. Palamà, A. M. L. Coluccia, M. Biasiucci, B. Dozza, E. Lucarelli, F. Di Maria, G. Barbarella and G. Gigli.
Integr. Biol., **2013**, *5*, 1057-1066

Live Cell Cytoplasm Staining and Selective Labeling of Intracellular Proteins by Non-toxic Cell-permeant Thiophene Fluorophores. F. Di Maria, I. E. Palamà, M. Baroncini, A. Barbieri, A. Bongini, R. Bizzarri, G. Gigli, G. Barbarella.
Org. Biomol. Chem., **2014**, *12*, 1603-1610

Conformational Polymorphism in Self-Assembled Crystalline Oligothiophene Microfibers and its Effect on the Functional Properties. F. Di Maria, E. Fabiano, D. Gentili, M. Biasiucci, T. Salzillo, G. Bergamini, M. Gazzano, A. Zanelli, A. Brillante, M. Cavallini, F. Della Sala, G. Gigli and G. Barbarella.
Adv. Funct. Mater., **2014**, *31*, 4943-4951

Biocompatible and biodegradable fluorescent microfibers physiologically secreted by live cells upon spontaneous uptake of thiophene fluorophore. I. E. Palamà, F. Di Maria, S. D'Amone, G. Barbarella and G. Gigli.
J. Mater. Chem. B., **2015**, *3*, 151-158

Supramolecular Oligothiophene Microfibers Spontaneously Assembled on Surfaces or Co-assembled with Proteins inside Live Cells. G. Barbarella, F. Di Maria.
Acc. Chem. Res., **2015**, *8*, 2230-2241

Nanoscale characterization and unexpected photovoltaic behaviour of low bandgap sulfur-overrich-thiophene/ benzothiadiazole decamers and polymers. F. Di Maria, M. Biasiucci, F.P. Di Nicola, E. Fabiano, A. Zanelli, M. Gazzano, E.Salatelli, M. Lanzi, F. Della Sala, G. Gigli, G. Barbarella.
J. Phys. Chem. C, **2015**, *119*, 27200-27211

Improving the property-function tuning range of thiophene materials via facile synthesis of oligo/polythiophene-S-oxides and mixed -S-oxides/-S,S-dioxides.
Submitted *Adv. Funct. Mater.*

PAPERS NOT DISCUSSED IN THIS THESIS

Random Laser from engineered nanostructures obtained by surface tension driven lithography.
N. Ghofraniha, I. Viola, F. Di Maria, G. Barbarella, G. Gigli and C. Conti.
Laser Photonics Rev., **2013**, *7*, 432-438

New Biocompatible Polymeric Micelles Designed for Efficient Delivery and Intracellular Release. F. Di Maria, L. Blasi, A. Quarta, G. Bergamini, G. Barbarella, L. Giorgini and M. Benaglia.
J. Mater. Chem. B, **2015**, *3*, 8963-8972

Experimental evidence of replica symmetry breaking in random lasers. N. Ghofraniha, I. Viola, F. Di Maria, G. Barbarella, G. Gigli, L. Leuzzi and C. Conti.
Nature Communications, **2015**, *6*, 6058

Toward efficient OLED lighting: the key role of crystal structure in enhancing FIrpic phosphorescence.
Submitted *Inorganic Chemistry*

CONFERENCES AND INTERNATIONAL MEETINGS

POSTER COMMUNICATIONS

Europolymer Conference EUPOC2015: Synthesis of conjugated Donor-Acceptor Oligomers and Polymers for Application in Bulk Heterojunction (BHJ) and Single Component (SMOC) Solar Cell. F. Di Maria, M. Biasiucci, F. P. De Nicola, A. Zanelli, E. Salatelli, M Lanzi, G. Gigli, G. Barbarella. 24-28 May 2015, Gargnano, Italy.

International Conference on Organic Electronics ICOE2014: Spontaneous self-assembly of sexithiophene into tunable electroactive fluorescent and crystalline microfibers via crystallization synthon T4(SHex)4. F. Di Maria, A. Zanelli, M. Gazzano, M. Zangoli, G. Bergamini, G. Gigli, G. Barbarella. 11-13 June 2014, Modena, Italy.

Challenges in Chemical Renewable Energy ISACS12: Regioregular sulfur overrich thiophene oligomers and polymers for application in organic photovoltaics. F. Di Maria, S. Righi , N. Camaioni and G. Barbarella. 3-6 September 2013, Cambridge, UK.

PERIOD OF RESEARCH ABROAD

Winner of a Marco Polo project -from July 2015 to 20 October 2015- at the School of Chemistry, Faculty of Exact Sciences, Tel Aviv University in the group of Professor Shlomo Rozen to develop new S,S-dioxothiophene oligomers using Rozen's reagent to apply them in photovoltaic devices and nanomedicine.

CHAPTER I: FACILITATED SYNTHESIS OF OLIGO- AND POLYTHIOPHENES

Thiophene based oligomers and polymers are of great current interest from a scientific and technological point of view[1] for their numerous properties: they are electroactive, fluorescent, chemically stable and allow a great diversity in molecular structures and a fine tuning of functional characteristics. They display 'plasticity' in adapting their geometry to the environment in the solid state and in creating supramolecular architectures by self-organization. Moreover, they have the capability to finely interact with biologically relevant molecules such as intracellular proteins. All these properties allow a large number of different applications in fields such as organic electronics and bioimaging which prompted the development of highly efficient and 'user friendly' synthetic approaches for their preparation.

Over the past few years the most investigated procedure for the synthesis of thiophene materials has been the palladium catalyzed cross-couplings between halogenated and metalated thienyls, which allow the regioselective construction of the aromatic backbone starting from functionalized thiophene monomers. Among the numerous different cross coupling procedures reported in the literature the most usually applied ones are the palladium-catalyzed Stille[2] and Suzuki-Miyaura[3] reactions. The Stille reaction consists in the coupling of weakly nucleophilic thienyl stannanes with thienyl halogenides (Br, I) in the presence of a Palladium(0) catalyst. The palladium catalyzed Suzuki-Miyaura reaction uses thienyl boronic acids or esters as nucleophiles in the presence of electrophilic thienyl halides. The boron derivatives are less toxic than the tin derivatives and the reaction is compatible with a greater variety of functional groups and reaction conditions. Both reactions are dependent on the steric and electronic characteristics of the reagents and catalysts and require careful adjustement of experimental conditions. Alternative methods for thienyl-thienyl bond formation have also been proposed[4] but they often do not possess the versatility of the Stille and Suzuki-Miyaura reactions, which allow the preparation of highly regioregular compounds of the most different sizes and functionalization types via stepwise addition of functionalized units. Generally the reactions reported in literature are carried out using homogeneous palladium catalysts and conventional heating. However, in such conditions these reactions present a number of drawbacks, in particular the presence of by-products either originated by the demetalation or dehalogenation of the starting materials or by homo-coupling or metal-halogen exchange side reactions, as well as the presence of catalyst residues. As a consequence, the study of oligo- and polythiopenes as active materials in different applications requires preliminary expensive purification procedures. Achieving high purity is of fundamental importance because the presence of impurities may modify the physico-chemical and optoelectronic properties of the materials. We demonstrated that the implementation of enabling techniques such as microwave and ultrasound irradiation in the synthesis of these materials leads to the expedient, rapid, cost-effective and environment friendly synthesis of ultrapure oligo- and polythiophenes. We also found that the use the use of palladium-supported catalysts and aqueous solvent results in the synthesis of ultrapure thiophene based materials.

I. Enabling technologies: Microwave and Ultrasound Irradiation

Temperature is a major factor that affects the rate of a chemical reactions. In general, most organic reactions are heated by using traditional heat transfer equipment such as oil baths, sand baths and heating jackets. However, these heating techniques are rather slow and an inhomogeneous temperature can develop within the sample. In addition, local overheating can lead to product, substrate and reagent decomposition. In recent years the use of microwave heating has become a widely accepted tool in synthetic chemistry. Indeed, replacing conventional heating with microwave heating, in which heat is generated through the direct microwave-material interaction, leads to more homogeneous and higher temperatures (Fig. 1), faster reaction rates, higher yields, use of aqueous solvents, easy work up and sometimes regio- and stereoselectivity of the reactions.[5]
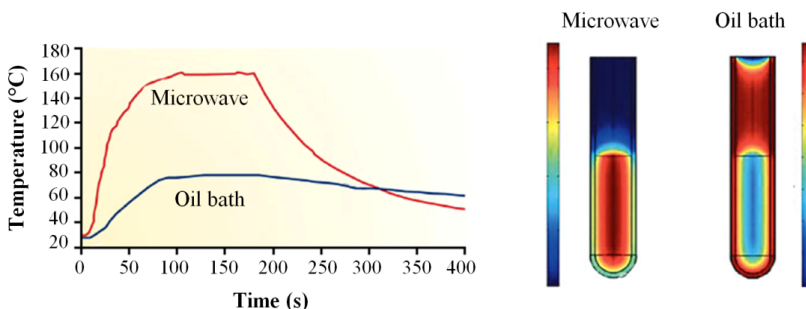

Figure 1. Temperature profiles for ethanol under microwave radiation and open vessel oil bath condition and temperature gradient 1min. after heating. [5]

The last decade has witnessed an increasing interest of organic chemists in microwave-assisted reactions, both in research laboratories and industry, which has led to major improvements in equipment quality and parameters control, in particular temperature and pressure. Microwave assistance has been explored in the synthesis of thiophene oligomers in the solid state as well as in solution.[6,7] Generally, in the presence of microwaves, the formation of the thienyl-thienyl linkage takes place in a very short time, sometimes minutes, and in high yields. The rate of the cross coupling reaction is accelerated with respect to that of halogen-metal exchange and, in consequence, much less undesired products are formed. The yield of the Suzuki-Miyaura reaction depends on many tunable parameters related to the electronic and steric characteristics of reagents and catalyst, solvent, base and temperature which are difficult to optimize. The increase of the reaction rate induced by microwaves irradiation allows the rapid screening of a wide range of experimental conditions allowing the rapid determination of the best combination of parameters. Once this is established, thiophene oligomers are rapidly obtained in high yields and in mixtures that can be easily purified.

Like microwave irradiation, ultrasound irradiation has increasing significance as a non-classical form of energy input in physical and chemical process engineering.[8] Ultrasound is the term used for sound waves in the frequency range 16 kHz to 10 MHz, in other words the frequency range just above the human threshold of audibility. Ultrasound can accelerate reactions in mono- and multi-phase systems that have at least one liquid phase. The reactions occur at low temperatures and in some cases proceed selectively. When ultrasound irradiation is applied during a reaction, pressure and temperature changes displace the system from equilibrium, van der Waals forces are unable to maintain intermolecular cohesion and small cavities, i.e. micro-bubbles, are formed. These bubbles increase in size due to resonance in areas under pressure.[9] Above a certain size the bubbles become unstable and collapse non-symmetrically. Tiny zones of excess heat are formed, where a temperature of 5000 K and a pressure of 50 MPa can occur temporarily (Fig. 2).
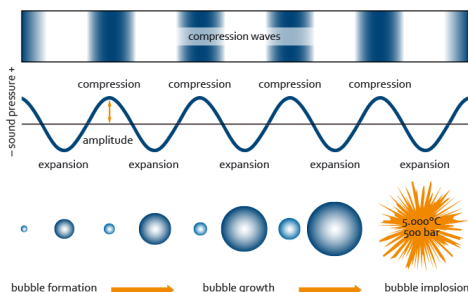

Figure 2. Sound waves interaction with a liquid medium. The bubble growth due to the expansion-compression cycles resulting in the formation of localized "hot spots".

In aqueous systems the tearing of the bubbles can lead to the formation of hydrogen and hydroxyl radicals in the gas zone. These can react further to produce hydrogen peroxide or oxygen directly, or they can dissolve in the water layer surrounding the bubble and then react. The latter process can occur without any difficulty, because a layer of supercritical water is formed temporarily as a result of the pressure and temperature conditions around the bubble. This has hydrophobic properties, in contrast to water under normal conditions.[10] The effects described are not confined to water, in non-aqueous systems acoustic irradiation can also cause the formation of radicals.

II. MICROWAVE AND ULTRASOUND ASSISTED SYNTHESIS OF LARGE-SIZE THIOPHENE OLIGOMERS AND POLYMERS

Well defined large-size monodisperse oligomers should have properties similar to those of polydisperse polythiophenes but be more soluble and much easier to prepare with reproducible properties from batch to batch. We focused on synthetically accessible large-size thiophene oligomers, the 'large-size' being only limited by the possibility to prepare sizeable amounts of

pure oligomer. So far, very few regioregular large-size oligomers have been described in literature.[11]

In Scheme 1 is reported a regiospecific synthesis of sulfur overrich regioregular thiophene octamers, hexadecamers and polymers rapidly prepared making use of ultrasound and microwave irradiation for the bromination and cross-coupling steps, respectively.
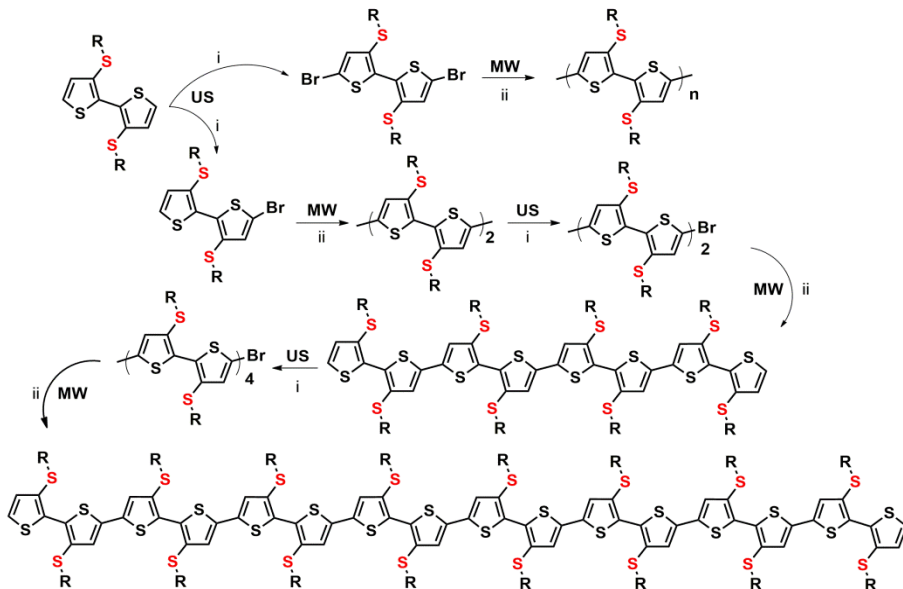
Scheme 1. Microwave (MW) and ultrasound (US) assisted synthesis of octamer, hexadecamer and polymers. *i)* 1 or 2 eq NBS, CH$_2$Cl$_2$, US, room T; *ii)* 4,4,4′,4′,5,5,5′,5′-octamethyl-2,2′-bi-1,3,2-dioxaborolane 0.6 eq, Pd(dppf)Cl$_2$, NaHCO$_3$, THF/H$_2$O 2:1, MW, 80°C.

All the molecules are symmetric and characterized by a repetitive core made of a bithiophene subsystem bearing head-to-head S-hexyl substituents (3,3′-bis(hexylthio)-2,2′-bithiophene),[12,13] with the sulfur atom directly attached to the thiophene ring in the β-position. The regiochemistry of substitution is of the type called 'head-head', a substitution pattern generally avoided since it induces backbone distorsions causing a loss of π−π overlap and the formation of amorphous films. We have choosen this regiochemistry to simplify the synthetic protocol and to obtain regioregular oligomers and polymers in yields higher than 80%.

The rationale behind the use of thioalkyl chains instead of alkyl chains was on one side to strengthen the electron donor properties of bithiophene via the delocalization of the unpaired electrons of the extra sulfur atoms on the aromatic backbone and, on the other, to exploit the non bonding sulfur-sulfur interactions to favour the self-assembling properties of the

compounds in the solid state. The preference for the Suzuki-Miyaura cross-coupling reaction above the other Pd-catalysed cross-coupling reactions is not incidental. The key advantages of the Suzuki-Miyaura coupling are the mild reaction conditions and that the diverse boronic acids formed are environmentally safer than the other organometallic reagents. In addition, the handling and removal of boron-containing byproducts is easy when compared to other organometallic reagents, especially in a large-scale synthesis.

The metalation step was bypassed through the use of commercial 4,4,4′,4′,5,5,5′,5′-octamethyl-2,2′-bi-1,3,2-dioxaborolane (bis(pinacolato)diboron) that in a one pot reaction, in THF/water under microwave irradiation, led to the doubling of the oligomer size in high yield and free of byproducts thus avoiding long, tedious and expensive purifications of the reaction products. In Figure 3 is reported the Palladium catalytic cycle when the bis(pinacolato)diboron compound is used. In our case the boronic esters directly formed in solution (R^1B) react with unreacted halogenated compounds (R^1X) to give oligomers with head to head regiochemistry.
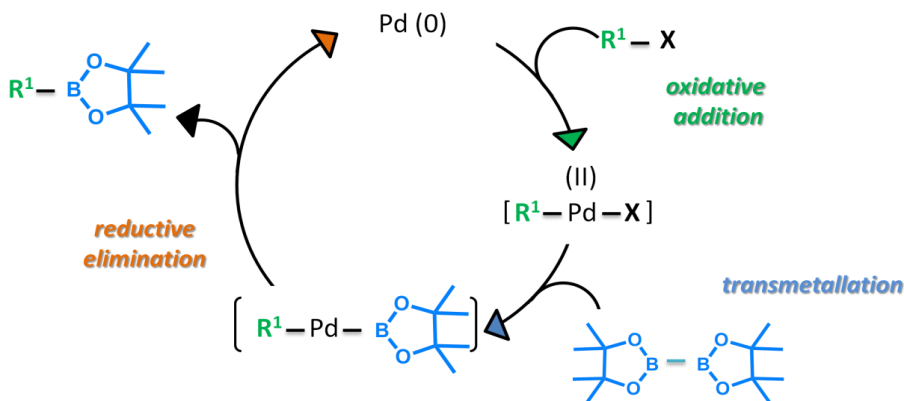

Figure 3. General scheme of palladium-catalyzed borylation with bis(pinacolato) diboron

Efficient monobromination of hexylsulfanyl substituted mono-, di- and quaterthiophenes was achieved in a few minutes with addition of NBS all at once in CH_2Cl_2 under ultrasound irradiation. In the absence of ultrasounds the monobromination of the same substrates required the stepwise addition of NBS in several hours or days leading to higher amount of the dibromo derivative.[14]

As reported in Scheme 2 it is also possible, with the same synthetic pattern, to synthesize with ultrasound and microwave assistance push-pull compounds by connecting bis(3,4'-thioalkyl)-2,2'-bithiophene used as donor building blocks and 2,1,3-benzothiadiazole as acceptor unit. The thioalkyl groups of the electron donor bithiophenes contained either a linear n-hexyl chain (six carbons) or a branched chain of different length, namely 2-methyl-pentyl (six carbons) or 2-ethylhexyl (eight carbons). Thus, the combined use of ultrasound and microwave irradiation

provides a very efficient platform for the rapid, low power, low cost and environmental friendly preparation of regioregular head-to-head thiophene oligomers and polymers.
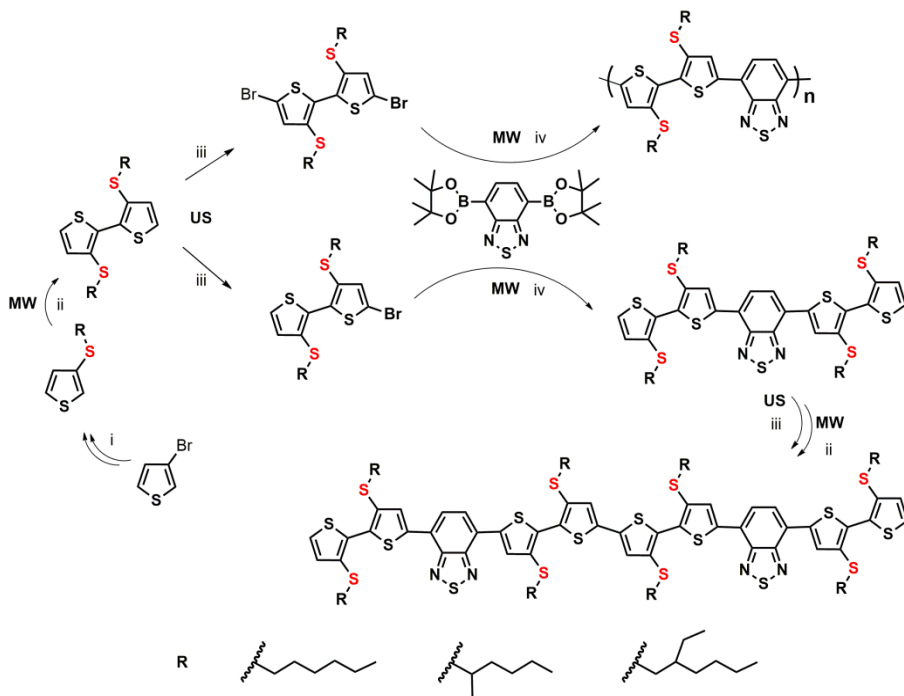
Scheme 2. Synthetic pattern for the preparation of decamers and polymers. i) 1 or 2 eq NBS, CH$_2$Cl$_2$, US, room T; ii) 4,4,4′,4′,5,5,5′,5′-octamethyl-2,2′-bi-1,3,2-dioxaborolane 0.6 eq, Pd(dppf)Cl$_2$, NaHCO$_3$, THF/H$_2$O 2/1, MW, 80°C; iii) 4,7-bis(4,4,5,5-tetramethyl-1,3,2-dioxaborolan-2-yl)-2,1,3-benzothiadiazole, NaHCO$_3$, Pd(dppf)Cl$_2$, THF/H$_2$O.

III. MICROWAVE ASSISTED SYNTHESIS OF THIOPHENE FLUOROPHORES

An advantage of organic fluorophores over other types of luminescent probes is the possibility to employ the methodologies of synthetic chemistry to tailor molecular structure and functionalization. This allows, on one side, to control the optical properties and, on the other, to direct the position of the fluorophore inside live cells by means of appropriate reactive groups forming covalent bonds or supramolecolar interactions with specific biological compounds.[15]

Recently, it has been demonstrated that the functionalization of oligothiophenes with functional groups reactive towards amines such as isothiocyanates or N-succinimidyl esters makes them useful fluorescent dyes for DNA and proteins labelling.[16-18] NHS esters are reactive groups formed by carbodiimide-activation of carboxylate molecules. NHS ester

activated compounds react with primary amines in physiologic to slightly alkaline conditions (pH 7.2 to 9) to yield stable amide bonds by releasing N-hydroxysuccinimide (NHS) (Fig. 4).
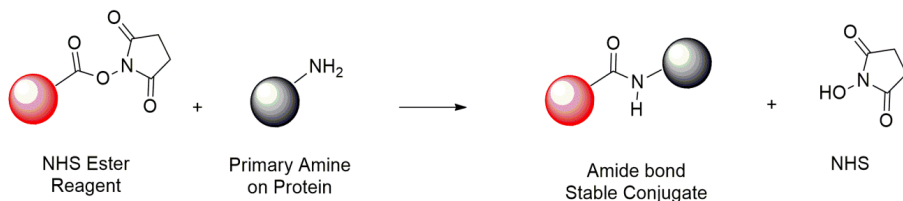

Figure 4. NHS ester reaction scheme for chemical conjugation to a primary amine.

We have developed a rapid and high yield synthetic pattern for the preparation of push pull oligothiophenes functionalized with N-hydroxysuccinimidyl esters and demonstrated that these fluorophores can be covalently linked to biological molecules and can be used to image specific antibody- antigen interactions in tumor cells by fluorescence microscopy or monitor polynucleotides hybridization by fluorescence spectroscopy methods.[19]

Scheme 3 shows the synthetic pattern for the preparation of different push pull compounds - functionalized with N-hydroxysuccinimidyl group as acceptor group and piperidine as donor group.
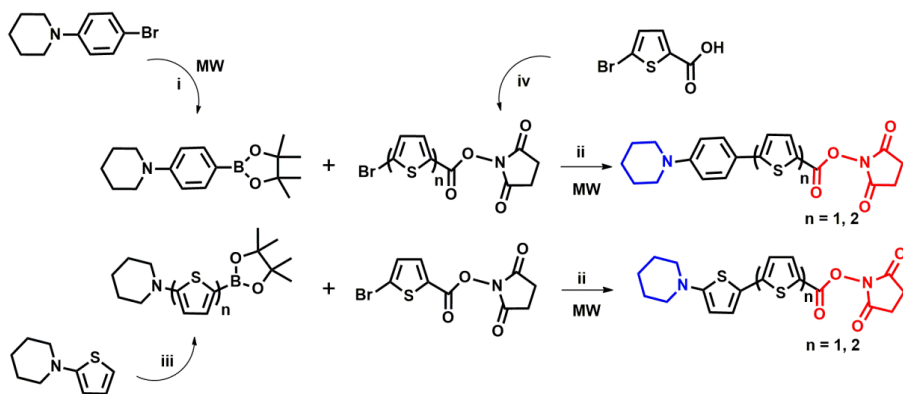
Scheme 3. Synthetic pattern for the preparation of compounds with N-hydroxysuccinimidyl group. i) PdCl$_2$(dppf), bis(pinacolato)diboron, NaHCO$_3$, THF/H$_2$O, MW, 10 min, 80°C; ii) 3 mL DMF/H$_2$O 2:1 v/v, 1 eq of halogenated compound and 3 eq of borylated compound, MW 10 min, 80°C; iii) BuLi 2.5 M, 2-isopropoxy-4,4,5,5-tetramethyl-1,3,2-dioxaborolane, THF, -78°C; iv) NHS, DCC in THF.

The succinimidyl group was introduced starting from commercial 5-bromo-2-thiophenecarboxylic: the carboxylic group was converted to a N-succinimidyl ester by reaction with NHS and dicyclohexylcarbodiimide (DCC) in THF in quantitative yield. N-piperidinyl phenyl and N-piperidinyl thiophene building blocks were synthesized starting from

bromobenzene and 2 iodothiophene through copper-catalyzed amination of the corresponding phenyl and thienyl halogen derivates using N,N-dimethylaminoethanol as a solvent. The last step for the preparation of these fluorophores is a Suzuki cross-copling reaction that with the aid of microwave irradiation was performed in 15 minutes for both compounds with a yield higher than 80%. Although similar products have already been synthesized in our laboratory by the Stille reaction, the Suzuki coupling has a higher efficiency for the preparation ultrapure fluorophores. Thanks to the use of microwave and the precise control of reaction parameters, such as temperature, pressure and power, the yield and purity of the synthesized compounds is highly reproducible and operator independent.

We have also focused our interest in the development of a novel class of thiophene based fluorophores based on dithieno[3,2-b: 2',3'-d]thiophene-4,4-dioxide as a building blocks that it is characterized by intense fluorescence and high quantum yield in solution.[20] This class of fluorophores are capable of spontaneously cross the membrane of live cells and selectively bound through non covalent interactions to specific proteins inside live cells to reveal cellular processes via fluorescence techniques.[21] Scheme 4 reports the synthesis of thiophene 2,6-diphenyl-3,5-dimethyl-dithieno[3,2-b:2',3'-d]thiophene-4,4-dioxide (DTTO).
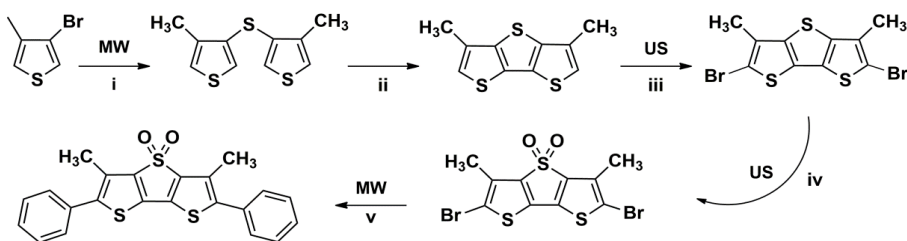
Scheme 4. Synthetic pattern for the preparation of fluorophore named DTTO starting from commercial 3-bromo-4-methylthiophene: (i) bis(tri-n-butyltin)sulphide, Pd(PPh$_3$)$_4$, toluene, 90%; (ii) n-BuLi, CuCl$_2$, ethyl ether, 50%; (iii) NBS, CH$_3$COOH/ CH$_2$Cl$_2$, US, 99%, 80%; (iv) H$_2$O$_2$/CF$_3$COOH in CH$_2$Cl$_2$ or 3-chloroperbenzoic acid, CH$_2$Cl$_2$, under ultrasound assistance, 90%; (v) phenylboronic acid pinacol ester (6 mmol), PdCl$_2$dppf (0.1 mmol) and NaHCO$_3$ (4 mmol) in THF/water 2:1 (3 mL), MW, 15'.

The synthesis starts with the treatment with n-butyllithium of 3-bromo-4-methyl-thiophene leading to regioselective lithiation followed by the reaction with bis-(phenylsulfonyl) sulfide to form the bis-thienyl sulfide. Action of n-butyllithium on this intermediate followed by CuCl$_2$-mediated oxidative ring closure, leads to the formation of the dithienothiophene (DTT) moiety. DTT is then brominated in both α-positions by action of NBS in methylene chloride-acetic acid and subsequently reacted with MCPBA or with H$_2$O$_2$/CF$_3$COOH in dichloromethane with ultrasound assistance to afford the doubly oxigenated dibromurated derivative (DTTO). Finally the dibromurated DTTO is reacted with a phenyl boronic ester in the presence of Pd(dppf)Cl$_2$ under microwave irradiation to yield the final compound. With this procedure DTTO is obtained in a very pure form, with minimal chromatographic purification steps. The green luminescent fluorophore obtained through this procedure displays a remarkable quantum efficiency on the order of 90% and thanks to its peculiar properties, such as the presence of

oxygen atoms in the central position and its molecular symmetry, DTTO display a high affinity towards collagen inside live cells.

IV. ULTRASOUND ASSISTED SYNTHESIS OF OLIGO AND POLYTHIOPHENE-S-OXIDE AND S-S DIOXIDES

The property tuning of oligo- and polythiophenes has as yet mainly been focused on changes in molecular size and shape or on the grafting of various substituents to the aromatic backbone.[1, 22] Much less attention has been devoted to the functionalization of thiophene sulfur (Fig. 5).
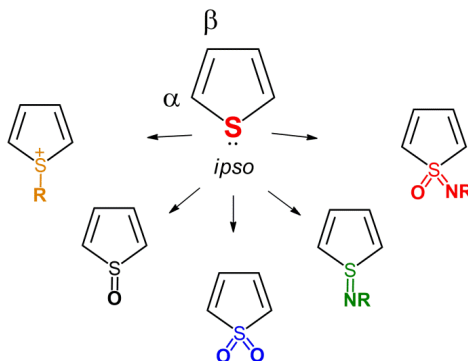

Figure 5. Functionalization of the thiophene sulfur: thiophene-S-oxides, thiophene-S,S-dioxides, thiophene-sulfilimines, thiophene-sulfoximides and thiophene- sulfonium salts.

In thiophene, a 6 π–electrons aromatic system, the sulphur atom has two unshared lone pair electrons, which can be employed in the formation of thiophene-S-oxides,[23] thiophene-S,S-dioxides,[24a] thiophene-sulfilimines,[24b] thiophene-sulfoximides[24bc] and thiophene- sulfonium salts.[25] Removal of thiophene sulfur lone pairs leads to the loss of thiophene aromaticity and consequent changes in frontier orbital energies.[26-27] Until now of all possible thiophene sulfur functionalizations, only sulfur dioxidation has been taken into account in thiophene based materials.[26-28]

The number of reagents shown in Table 1 is necessarily limited and many other examples could have been reported. Our choice was made on the grounds that thiophene S-oxides undergo more facile Diels-Alder type dimerization or other side reactions such as epoxidation of the double bond than thiophene-S,S-dioxides.[23] Rapid dimerization of the transiently formed S-oxides renders difficult the separation of many of these compounds from the reaction medium. However, studies on variously substituted thiophene rings show that stabilization of thiophene-S-oxides can be achieved by introduction of sterically hindering groups, mesomeric effects or fusion of thiophene with phenyl as in dibenzothiophene.[23]

We have found that ultrasound assistance renders possible the stepwise oxidation of thiophene derivatives (Table 1) using H_2O_2 as the oxidizing agent in CF_3COOH:DCM (1:2)[29] at roomT and employing just 1eq H_2O_2 for the S-oxide and 2eq for the -S,S-dioxide. The desired

products were obtained in short reaction times and high yields while only unreacted starting compound was recovered rendering the purification step easier. Other classical oxidizing systems such as MPCBA or dimethyl dioxirane failed to afford the S-oxide in significant amounts.

Table 1. Reagents and conditions for the ultrasound assisted synthesis of brominated thiophene-S-oxides and thiophene-S,S-dioxides.
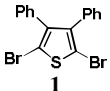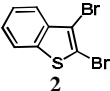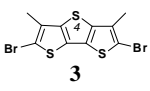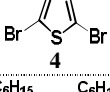
Starting Material	Product		Experimental Conditions	Time (min)	Yield[a] (%)
1 (Ph, Ph; Br, S, Br)	a	SO	DCM:TFA 2:1 H$_2$O$_2$ *1 eq*	30	70
	b	SO$_2$	DCM:TFA 2:1 H$_2$O$_2$ *2 eq* DCM/MPCBA *2 eq*	30 60	80 80
2 (Br, Br)	a	SO	DCM:TFA 2:1 H$_2$O$_2$ *1 eq*	15	99
	b	SO$_2$	DCM:TFA 2:1 H$_2$O$_2$ *2 eq* DCM/MPCBA *2 eq*	15 45	99 >90
3 (Br, S, S, Br)	a	SO	DCM:TFA 2:1 H$_2$O$_2$ *1 eq*	20	75
	b	SO$_2$	DCM:TFA 2:1 H$_2$O$_2$ *2 eq* DCM/MPCBA *2 eq*	15 15	90 80
4 (Br, S, Br)	b	SO$_2$	DCM:TFA 2:1 H$_2$O$_2$ *2 eq* DCM/MPCBA *2 eq*	30 90	80 80
5 (C$_6$H$_{15}$, C$_6$H$_{15}$; Br, S, Br)	b	SO$_2$	DCM:TFA 2:1 H$_2$O$_2$ *2 eq* DCM/MPCBA *2 eq*	20 20	80 80

Table 1 shows that with bromoderivatives and just 1eq H$_2$O$_2$, the thiophene-S-oxide is formed in 15-30 minutes in yields varying in the range 70-99%, depending on the substrate (the full table is reported in chapter II). Times and yields are the same for the formation of the -S,S-dioxide upon addition of a second equivalent of H$_2$O$_2$. We found that also the oxidation of the same substrates with the classical oxidizing agent MPCBA in DCM is facilitated by the assistance of ultrasounds. In this case only the -S,S-dioxide is obtained, although in much shorter times and greater yields than those obtained in the absence of ultrasound irradiation. In our experience, in the absence of ultrasounds, a much greater amount of MPCBA is needed; for example, for the preparation of compound 5, nearly 6 eq were needed for overnight reaction and 52% yield.[30] When no substituents were present in the beta positions of the thiophene ring or when alkyl chains were present the S-oxide could not be isolated, probably due to rapid Diels Alder dimerization.[23,31] The formation of the S,S-dioxide was instead rapid and efficient. The assistance of ultrasounds and the system H$_2$O$_2$/CF$_3$COOH/CH$_2$Cl$_2$ made the yield of 4 (room T, 30 min, 80% isolated yield) competitive with that obtained with Rozen's reagent (room T, 1 hour, 95% yield).[32] The oxidation with MPCBA and US assistance is slower and furnishes the same yield in 90 min. From these results it is seen that the stepwise oxidation of the thiophene sulfur depends on molecular structure, i.e. on the type of

substituents and their position on the thiophene ring. Finally, we found that for some non brominated thiophene derivatives the S-oxide as well as the -S,S-dioxide can be isolated in good yields upon treatment with $H_2O_2/CF_3COOH/CH_2Cl_2$ under ultrasound assistance. Afterwards both oxygenated derivates can be mono or dibrominated in the alpha positions in standard conditions and employed in cross coupling reactions with metalated thiophenes. The brominated S-oxides and -S,S-dioxides of Table 1 were stable compounds and could be purified by silicagel chromatography.

V. MICROWAVE-ASSISTED SYNTHESIS OF OLIGOTHIOPHENES USING CHITOSAN SUPPORTED PALLADIUM CATALYSTS

Heterogeneous catalysts are distinguished from homogeneous catalysts by the different phases present during the reaction. Homogeneous catalysts are present in the same phase as the reactants and products, usually liquid, while heterogeneous catalysts are present in a different phase, usually solid.

The main advantage of using a heterogeneous catalyst is the relative ease of catalyst separation from the product that aids in the purification and creation of a continuous chemical processes.[33] Additionally, heterogeneous catalysts are typically more tolerant of extreme operating conditions than their homogeneous analogues.

In recent years biopolymers have gained attention for their use as support in catalysis.[34] Chitosan, the second most abundant natural polymer after cellulose, is a natural biopolymer produced by the alkaline N-deacetylation of chitin. Due to its countless properties: low-cost, eco-friendly, facile chemical modification, thermal stability, nontoxicity and low solubility in many common solvents, chitosan is an excellent candidate as a support for the development of heterogeneous catalysts.[35]

We developed a family of palladium catalysts supported on chitosan called CHITCATs (Scheme 5) for the synthesis of highly pure thiophene oligomers through microwave-assisted Suzuki cross coupling reactions.
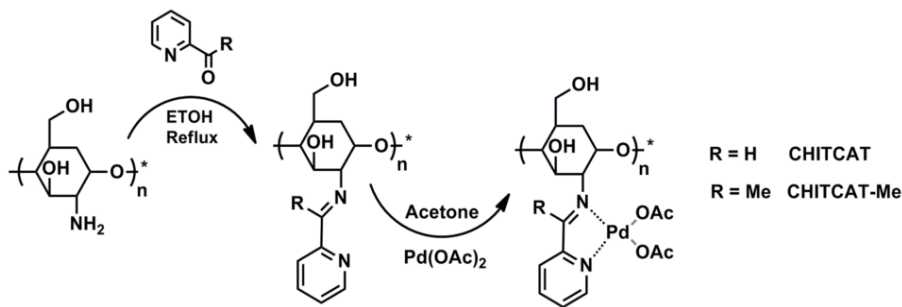

Scheme 5. Molecular structure and synthetic pattern for the preparation of chitosan-supported palladium catalysts CHICAT-Me and CHITCAT.

Our goal was to obtain products not contaminated by traces of metals that can alter charge conduction and other functional properties. Two different palladium chitosan supported

11

catalysts were prepared CHITCAT[36] and CHITCAT-Me, the only difference between the two catalysts is the presence of an additional methyl group in CHITCAT-Me. The methyl group was introduced in the ancillary ligand to increase the reactivity as observed in analogous silica-supported palladium catalysts.[37]

The efficiency of CHITCATs catalysts was tested in the Suzuki-Miyaura reaction under microwave assistance on two commercially available substrates: namely 5-bromo-2-thiophenecarboxaldehyde and a 2-thienylboronic acid derivative (Scheme 6). Since chitosan is a water-tolerant polymer it is possible to carry out the reactions in aqueous media. The use of an aqueous environment is particularly advantageous for an optimal catalytic performance with respect to the use of other organic solvents. This can be ascribed to the higher solubility of the base necessary in the Suzuki cross-coupling as well as to the more efficient absorption of microwaves in aqueous solvents.

With both catalysts (CHITCAT-Me and CHITCAT) the preparation of the 2-bithiophenecarboxaldehyde in presence of KF as the base, in water/ethanol (1:1) as solvent and under microwave irradiation at 130 °C afforded a complete conversion of the starting materials in just 2 min. (Scheme 6).
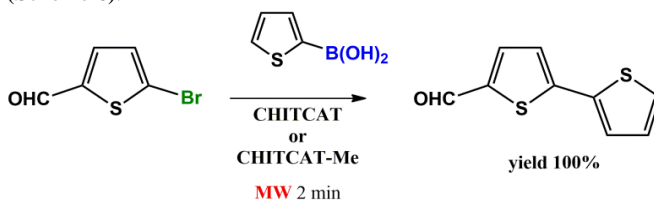
Scheme 6. Model reaction between 5-bromo-2-thiophenecarboxaldehyde and 2-thienylboronic acid.

To establish the heterogeneous nature of the catalytic reaction for both CHITCAT-Me and CHITCAT a hot filtration test on the model reaction was performed (Scheme 6). The reaction was stopped less than half way through completion (~30% conversion) and the catalyst was filtered off; the liquid filtrate and the solid were recovered separately. The reaction mixture without catalyst was then further microwaved for 30 additional minutes and finally quenched. No changes in conversion were observed, excluding the presence of a substantial concentration of palladium leached species in solution (Fig. 6).
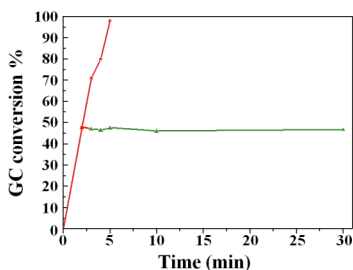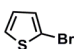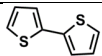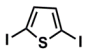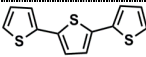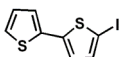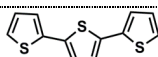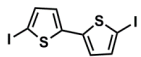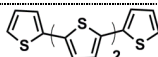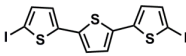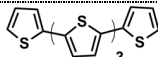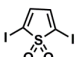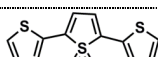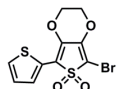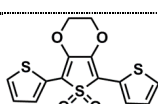

Figure 6. Hot filtration test. Effect of removing the chitosan supported palladium catalyst from the second cycle reaction of 2-thienylboronic acid and the 5-bromo-2-thiophene carboxaldehyde.

The catalysts removed from the reaction mixture by filtration is reusable in consecutive reactions - up to 4 times - without substantial yields variations. For the synthesis of thiophene oligomers, from bi- to quinquethiophene (see Table 2).

Table 2. Products, reagents and experimental conditions of the reaction of thienyl halogenides boronic acid/ester in the presence of CHITCAT-Me.

Starting Material	Product	Solvent 1:1(v/v)	Catalyst	MW[b] Irradiation time (min)	Yield[c] (%)
(structure)	(structure)	ETOH/H$_2$O	CHITCAT-Me	2	100
			CHITCAT	100	20
(structure)	(structure)	ETOH/H$_2$O	CHITCAT-Me	2	100
			CHITCAT	30	87
(structure)	(structure)	DMF/H$_2$O	CHITCAT-Me	3	90
			CHITCAT	30	70
(structure)	(structure)	DMF/H$_2$O	CHITCAT-Me	3	85
			CHITCAT	100	83
(structure)	(structure)	DMF/H$_2$O	CHITCAT-Me	3	86
			CHITCAT	100	37
(structure)	(structure)	ETOH/H$_2$O	CHITCAT-Me	4	71
			CHITCAT	-	-
(structure)	(structure)	ETOH/H$_2$O	CHITCAT-Me	4	60
			CHITCAT	-	-

[b] Fixed T = 140°C (power 300W). [c] GC conversion with respect to n-dodecane as internal standard

The use of CHITCAT-Me considerably reduce the reaction time (from hours to min) leads to higher yields (>80%) than those obtained with the unsubstituded CHITCAT. Moreover only with CHITCAT-Me it is possible the rapid and high yield synthesis of oligomers bearing thiophene-S,S-dioxide unit. Preliminary studies on quater- and quinquethiophene prepared by Suzuki cross-coupling using these new chitosan supported catalysts (CHITCATs) have shown enhanced film forming properties compared to the same material prepared with conventional palladium homogeneous catalysis. In Figure 7 are reported the optical images of melted quinquethiophenes powder prepared with homogeneous (a) and heterogeneous (b) catalysts. The presence of dark aggregates in the melted powder of quinquethiophenes prepared using a homogeneous Pd catalyst, suggest the presence of residues of the catalyst and/or impurities. No evidence of similar impurities are observed in the preparation of quinquethiophenes using CHITCATs. This higher level of purity allow to avoid tedious and energy intensive time consuming purification steps and the need to deal with residual metals contamination.
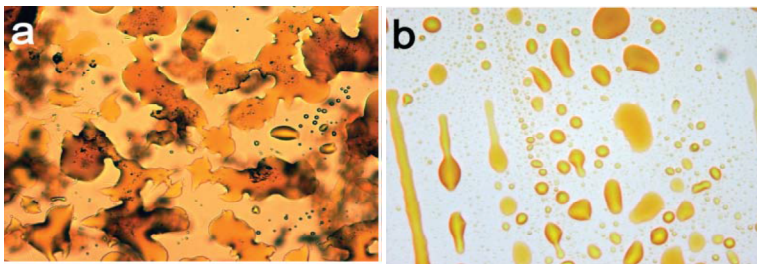
Figure 7. Optical microscopy image of melted T5 powder prepared by (a) conventional homogeneous catalytic method; (b) novel heterogeneously catalyzed protocol.

REFERENCES

[1] Perepichka IF, Perepichka DF, editors. Handbook of Thiophene-Based Materials: Applications in Organic Electronics and Photonics. Wiley: Chichester (UK); **2009**.

[2] Espinet P, Echavarren AM. *Angew. Chem. Int. Ed.,* **2004**, 43, 4704-4734.

[3] Alonso F, Beletskaya IP, Yus M. *Tetrahedron,* **2008**, 64, 3047-3101.

[4] Tanaka S, Tamba S, Tanaka D, Sugie A, Mori A. *J. Am. Chem. Soc.,* **2011**, 133, 16734-16737. (b) Yuan K, Soulé JF, Doucet H. *ACS Catal.*, **2015**, *5*, 978–991 (c)Yamauki T, Shibahara F, Murai T. *Org. Lett.*, **2015**, 17, 5392-5395.

[5] (a) Kappe, CO. *Angew. Chem. Int. Ed.*, **2004**, 43, 6250-6284. (b) Bassyouni FA, Abu-Bakr SM, Rehim MA. *Res. Chem. Intermediat.*, **2012**, 38, 283-322. (c) Kappe CO, Dallinger D. *Nat Rev Drug Discov.,* **2006**, *5*, 51-63.

[6] Melucci M, Barbarella G, Sotgiu G. *J. Org. Chem.,* **2002**, 67, 8877-8884.

[7] Melucci M, Barbarella G, Zambianchi M, Di Pietro P, Bongini A. *J. Org. Chem.,* **2004**, 69, 4821-4828.

[8] Li JT, Wang SX, Chen GF, Li TS. *Curr. Org. Synth.,* **2005**, 2, 415-436.

[9] Suslik KS. *Science,* **1990**, 24, 1439.

[10] Lorimer JP, Mason TJ. *Chem.Soc.Rev*., **1987**, 16, 239.

[11] Thomas JM, Thomas WJ. Principles and Practice of Heterogeneous Catalysis Wiley: Weinheim; **2015**.

[12] Gronnow MJ, Luque R, Macquarrie DJ, Clark JH. *Green Chem.*, **2005**, 7, 552-557.

[13] Macquarrie DJ, Hardy JJE. *Ind. Eng. Chem. Res*., **2005**, 44, 8499-8520.

[14] Alesi S, Di Maria F, Melucci M, Macquarrie DJ, Luqueb R, Barbarella G. *Green Chem.*, **2008**, 10, 517-523.

[15] Macquarrie DJ, Battsengel G, Štefan T. *Platinum Metals Review,* **2001**, 45,102-110.

[16] Cazzato A, Capobianco M, Zambianchi M, Favaretto L, Bettini C, Barbarella G. *Bioconjugate Chem*., **2007**, 18, 318-322.

[17] Barbarella G, Zambianchi M, Ventola A, Fabiano E, Della Sala F, Gigli G, Anni M, Bolognesi A, Polito L, Naldi M, Capobianco M. *Bioconjugate Chem*., **2006**, 17, 58-67.

[18] Zambianchi M, Barbieri A, Ventola A, Favaretto L, Bettini C, Galeotti M and Barbarella G. *Bioconjugate Chem*., **2007**, 18, 1004-1009.

[19] Di Maria F, Palamà IE, Baroncini M, Barbieri A, Bongini A, Bizzarri R, Gigli G, Barbarella G. *Org. Biomol. Chem.*, **2014**, 12, 1603-1610.

[20] Barbarella G, Favaretto L, Sotgiu G, Antolini L, Gigli G, Cingolani R, Bongini A. *Chem. Mater.,* **2001**,13, 4112-4122.

[21] Palamà I, Di Maria F, Viola I, Fabiano E, Gigli G, Bettini C, Barbarella G. *J. Am. Chem. Soc.*, **2011**, 133, 17777-17785.

[22] a). Magurudeniya HD, Huang P, Gunathilake SS, Rainbolt E A, Biewer MC, Stefan MC. Encyclopedia of Polymer Science and Technology, **2014**, John Wiley & Sons, Inc., 1-36. b) Huynha TP, Sharma PS, Sosnowska M, D'Souza F, Kutnera W. *Progress in Polymer Science,* **2015**, 47, 1-25. c) Cinar ME, Ozturk T. *Chem. Rev.*, **2015**, 115, 3036-3140. d) Dou L, Liu Y, Hong Z, Li G, Yang Y. *Chem. Rev.* **2015**, 115, 12633-12665. e) Iyoda M, Shimizu H. *Chem. Soc. Rev.*, **2015**, 44, 6411-6424. f) Rasmussen SC, Evenson SJ, McCausland CB. *Chem. Commun.,* **2015**, 51, 4528-4543. g) Barbarella G, Di Maria F. *Acc. Chem. Res.,* **2015**, 48, 2230-2241. h) Joule JA, Editor, Thiophenes (Topics in Heterocyclic Chemistry) **2015** Edition Springer International Publishing Switzerland.

[23] a) Nakayama J, Sugihara Y. *Sulfur Reports,* **1997**, 19, 349-375. b) Pouzet P, Erdelmeier I, Ginderow D, Mornon JP, Dansette P, Mansuy D. *J. Chem. Soc., Chem. Commun.*, **1995**, 473-474. c) Bongini A, Barbarella G, Zambianchi M, Arbizzani C, Mastragostino M. *Chem. Commun.*, **2000**, 439-440.

[24] a) Nakayama J, Nagasawa H, Sugihara Y, Ishii A. *J. Am. Chem. Soc.*, **1997**, 119, 9077-9078. b) Nakayama J. *Sulfur Reports,* **2000**, 22, 123-149. c) Nakayam J, Sano Y, Sugihara Y, Ishii A. *Tetrahedron Letters,* **1999**, 40, 3785-3788.

[25] Stoffregen A, Heying M, Jenks WS. *J. Am. Chem. Soc.,* **2007**, 129, 15746-15747.

[26] a) Moreno Oliva M, Casado J, LópezNavarrete JT, Patchkovskii S, Goodson T, Harpham MR, Seixas deMelo JS, Amir E, Rozen S. *J. Am. Chem. Soc.,* **2010**, 132, 6231-6242. b) Barbarella G, Favaretto L, Zambianchi M, Pudova O, Arbizzani C, Bongini A, Mastragostino M. *Adv. Mater.,* **1998**, 10, 551-554. c) Barbarella G, Favaretto L, Sotgiu G, Zambianchi M, Antolini L, Pudova O, Bongini A. *J. Org. Chem.*, **1998**, 63, 5497-5506. d) Antolini L, Tedesco E, Barbarella G, Favaretto L, Sotgiu G, Zambianchi M, Casarini D, Gigli G, Cingolani R. *J. Am. Chem. Soc.,* **2000**, 122, 9006-9013. e) Bongini A, Barbarella G, Zambianchi M, Arbizzani C, Mastragostino M. *Chem. Commun.,* **2000**, 439-440.

[27] a) Biwang J, Tilley TD. *J. Am. Chem. Soc.,* **1999**, 121, 9744-9745. b) Su MC, Biwang J, Tilley TD. An Efficient, Modular. *Angew. Chem. Int. Ed.,* **2000**, 39, 2870-2873.

[28] Rozen S, Bareket Y. *J. Org. Chem.,* **1997**, 62, 1457-1462. b) Amir E, Rozen S. *Angew. Chem. Int. Ed.,* **2005**, 44, 7374-7378. c) Shefer N, Harel T, Rozen S. *J. Org. Chem.,* **2009**, *74*, 6993-6998. d) Rozen S. *Acc. Chem. Res.,* **2014**, 47, 2378-2389.

[29] Pouzet P, Erdelmeier PI, Ginderow D, Mornon JP, Dansette P, Mansuy D. *J. Chem. Soc., Chem. Commun.,* **1995**, 473-474.

[30] Barbarella G, Favaretto L, Sotgiu G, Zambianchi M, Arbizzani C, Bongini A, Mastragostino M. *Chem.Mater.*, **1999**, 11, 2533-2541.

[31] Baldo MA, Lamansky S, Burrows PE, Thompson ME, Forrest SR. *Appl. Phys. Lett.,* **1999**, 75, 4-6.

[32] Kalinowski J, Stampor W, Cocchi M, Virgili D, Fattori V, Di Marco P. *Chem. Phys.,* **2004**, 297, 39-48.

[33] (a) Kreyes A, Amirkhani M, Lieberwirth I, Mauer R, Laquai F, Landfester K, Ziener U. *Chem. Mater.*, **2010**, 22, 6453-6458 (b) Azumi R, Mena-Osteritz E, Boese R, Benet-Buchholz J, Baüerle P. *J. Mater. Chem*., **2006**, 16, 728. (c) Jestin I, Frère P, Mercier N, Levillainn E, Stievenard D, Roncali J. *J. Am. Chem. Soc*., **1998**, 120, 8150.

[34] Di Maria F, Olivelli P, Gazzano M, Zanelli A, Biasiucci M, Gigli G, Gentili D, D'Angelo P, Cavallini M, Barbarella G. *J. Am. Chem. Soc*., **2011**, 133, 8654-8661.

[35] Di Maria F, Gazzano M, Zanelli A, Gigli G, Loiudice A, Rizzo A, Biasiucci M, Salatelli E, D'Angelo P, Barbarella G. *Macromolecules,* **2012**, 45,8284-8291.

[36] Arsenyan P, Paegle E, Belyakov S. *Tetrahedron Lett.,* **2010**, 51, 205-208.

[37] (a) Jing, C, Cornish VW. *Acc. Chem. Res*., **2011**, 44, 784-792. (b) Wombacher R, Cornish VW. *J. Biophotonics,* **2011**, 4, 391-402.(c) Chen Z, Jing C, Gallagher SS, Sheetz MP, Cornish VW. *J. Am. Chem. Soc,* **2012**, 134, 13692-13699.

CHAPTER II: PROPERTY-FUNCTION CONTROL IN THIOPHENE MATERIALS BY STEPWISE OXIDATION OF THIOPHENE SULFUR

The tuning of the properties of oligo and polythiophenes is generally achieved by grafting different functional groups to the aromatic backbone or through size and shape changes, while much less attention has been devoted to thiophene sulfur functionalization. In this chapter, we report the facile, ultrasound-assisted, chemoselective synthesis of brominated thiophene-S-oxides and thiophene-S,S-dioxides in short times, mild conditions and high yields. The many possible combinations of these unexpensive 'Lego-like' building blocks with metalated thiophenes via microwave assisted cross coupling reactions afforded unprecedented oligo- and polythiophene-S-oxides and mixed -S-oxides/-S,S-dioxides. We oberved that depending on the number, type and sequence alternation of non-oxygenated, mono-oxygenated and di-oxygenated thiophene units a very wide property-function tuning can be achieved spanning from frontier orbital energies and energy gaps, to charge transport characteristics. In particulars polymers containing thiophene-S-oxide units in the backbone showed ambipolar charge transport properties whereas they displayed n-type charge conduction when only thiophene-S,S-dioxide moieties were present. We also found that small fluorescent oligomers with one inner thiophene S-oxide or thiophene S,S-dioxide were spontaneously internalized by living fibroblast. However, while the -S,S-dioxides were not cytotoxic and co-assembled inside the cells with type-I collagen affording fluorescent microfibers, the corresponding S-oxides were unable to form fluorescent microfibers and some of them were even toxic the cells.The simple chemical strategy outlined in this study opens a wide range of opportunities for the development of innovative thiophene materials with tailored properties and function.

I. INTRODUCTION

Oligo- and polythiophenes are of outstanding importance in organic materials science and technology.[1] The synthetic versatility of thiophene and the easy property tuning of its oligomers and polymers by means of appropriate functionalization, the possibility to modulate and optimize electrical, photoluminescence, recognition and self-assembly properties through minor structural changes, the easy deformability of the thiophene ring and its geometric adaptability to the most diverse environments, have resulted in countless papers describing thiophene materials in the last two decades. Numerous studies on their basic chemical and physical features, their applications as active device components in organic electronics and bioelectronics, as selective chemosensors and biosensors for a variety of target analytes and as fluorescent reporters in bioimaging have been published. Applications in photovoltaic cells[2] and field-effect transistors[3] have achieved performances among the best ever obtained for organic materials. Brigthly fluorescent oligothiophenes are capable of selective identification of protein aggregates associated with Alzheimer's disease[4a-c] and of selective detection of distinct cells, including cancer cells.[4b] Small fluorescent thiophene oligomers are effective membrane probes with high mechanosensitivity.[5] The continuous flow of publications on thiophene materials of the last two decades is not likely to come to a stop since there are still many unexplored sides of these multifaceted materials, as we will try to demonstrate with the present study. To time the property tuning of oligo- and polythiophenes has mainly been focused on changes in molecular size and shape or on the grafting of various substituents to the aromatic backbone.[1] Much less attention has been devoted to the functionalization of thiophene sulfur, although it is expected to deeply affect the aromatic character of the ring hence the frontier orbital energies and energy gaps of oligo- and polythiophenes, crucial parameters for the performance in organic devices. In thiophene, a 6 π−electrons aromatic system, sulphur has two unshared lone pair electrons, which can be employed in the formation of thiophene-S-oxides,[6] thiophene-S,S-dioxides,[7a] thiophene-sulfilimines,[7b] thiophene-sulfoximides[7b,c] and thiophene-sulfonium salts.[8] Removal of thiophene sulfur lone pairs leads to the loss of thiophene aromaticity and consequent changes in frontier orbital energies.[9a] Until now of all possible thiophene sulfur functionalizations, only sulfur dioxidation has been taken into account. Several classes of oligo- and polythiophene-S,S-dioxides have been prepared and investigated, from the first oligomers.[9,10] to all-SO2 oligothiophenes and polymers oxidized with Rozen's reagent.[11] Oligo- and polythiophene-S,S-dioxides display smaller energy gaps, greater electron affinities and greater ionization energies than their non oxygenated all-aromatic counterparts. Very recently, the peculiar electrical and optical properties of some of these materials have been deeply investigated.[12,13] In single-molecule junctions, oligomers containing thiophene-S,S-dioxide groups display dominant charge carriers changing from holes to electrons depending on the length of the molecular backbone and the number of these groups present in the molecular structure.[12a] Oligomers and polymers containing thiophene-S,S-dioxide groups can undergo efficient intramolecular singlet fission and are consequently candidates for the development of the next generation of photovoltaic devices based on multiple exciton-generation processes.[12b] A quinque-thiophene containing one central thiophene-S,S-dioxide group has been employed

for the first experimental demonstration of replica symmetry breaking in random lasers.[14] Also several biological applications of small thiophene oligomers containing thiophene-S,S-dioxide units have been reported.[5,15] A disadvantage due to the presence of thiophene-S,S-dioxide units in the molecular structure is that the materials become rapidly insoluble and intractable as the number of these units increases, probably due to increased aggregation capabilities via H-bonding promoted by the presence of the two oxygens in the thiophene ring.[9e] Furthermore, the presence of thiophene-S,S-oxide units in the molecular structure leads to a large increase in the oxidation potential with respect to the all-thiophene counterpart.[9a] In this context a challenging frontier is represented by investigations on synthetic approaches to the as yet unexplored classes of oligo/polythiophene-S-oxides and mixed S-oxized/S,S-dioxized. These compounds should indeed be more soluble than the dioxidized counterparts due to the non planarity of the SO group,[6] have similar electron affinities but smaller oxidation potentials and energy gaps,[9c] hence extending the range of structure-property tunability of thiophene materials. Owing to its low reactivity, the oxidation of thiophene sulfur is not easy to achieve and requires strong oxidants such as MPBA[6] or the Rozen's reagent.[11] While the oxidation with Rozen's reagent cannot be stopped at the S-oxide stage, oxidation with MPCBA in the presence of a Lewis acid may lead to the desired S-oxide although in very low yield.[6] Thiophene S-oxides are more reactive than the corresponding thiophene -S,S-dioxides and undergo more facile Diels-Alder type dimerization or other side reactions such as epoxidation of the double bond.[6] Rapid dimerization of the transiently formed S-oxides renders difficult the separation of many of these compounds from the reaction medium. However, studies on variously substituted thiophene rings have shown that stabilization of thiophene-S-oxides can be achieved by introduction of sterically hindering groups, mesomeric effects or fusion of thiophene with phenyl as in dibenzothiophene.[6] To date, very few oligothiophene-S-oxides[16] and no polythiophene-S-oxides have been prepared, owing to the difficulty to synthesize thiophene-S-oxide building blocks. In this work, we report the ultrasound assisted synthesis of mono and dibromo thiophene-S-oxides and -S,S-dioxides. We show that the cross coupling reaction of these building blocks with metalated thiophenes affords innovative oligo- and polythiophenes containing thiophene-S-oxides or mixed thiophene-S-oxide and thiophene -S,S-dioxide moieties in the desired number and position of the molecular backbone. The presence of mono oxigenated thiophene units and their alternation with thiophene or thiophene-S,S-dioxide moieties allow for the fine modulation of properties of oligo and polythiophenes such as the frontier orbital energies, p- or n-type charge transport, photo and electroluminescence and even the biological activity inside live cells.

II.   RESULTS AND DISCUSSION

2.1. Synthesis. Ultrasound assistance has already been employed in the selective bromination of thiophene oligomers.[17,18] We have found that ultrasound assistance renders also easier the stepwise oxidation of thiophene derivatives. The oxidizing agent chosen for the ultrasound assisted chemoselective oxidation of thiophene bromides was H_2O_2 in CF_3COOH:DCM (1:2), described in 1995 by Pouzet P. et al. for the preparation of 2,5-diphenyl-thiophene-1-oxide.[19]

At T = 0°C, after addition of 4eq. H_2O_2 to 2,5-diphenyl-thiophene, 4 hours reaction time and flash chromatography on deactivated neutral alumina, the authors were able to obtain the S-oxide in 25% isolated yield. Further addition of the oxidizing agent led to the -S,S-dioxide. Other classical oxidizing systems such as MPCBA or dimethyl dioxirane failed to afford the S-oxide in significant amounts.

Table 1. Reagents and conditions for the ultrasound assisted synthesis of brominated thiophene-S-oxides and thiophene-S,S-dioxides

	Starting materials	Product		Experimental conditions	Time (min)	Yield[a] (%)
1		a	SO	DCM:TFA 2:1 H_2O_2 *1 eq*	30	70
		b	SO₂	DCM:TFA 2:1 H_2O_2 *2 eq* DCM/MPCBA *2 eq*	30 60	80 80
2		a	SO	DCM:TFA 2:1 H_2O_2 *1 eq*	15	99
		b	SO₂	DCM:TFA 2:1 H_2O_2 *2 eq* DCM/MPCBA *2 eq*	15 45	99 >90
3		a	SO	DCM:TFA 2:1 H_2O_2 *1 eq*	15	99
		b	SO₂	DCM:TFA 2:1 H_2O_2 2 eq DCM/MPCBA *2 eq*	15 45	99 >90
4		a	SO	DCM:TFA 2:1 H_2O_2 *1 eq*	15	>90
		b	SO₂	DCM:TFA 2:1 H_2O_2 *2 eq* DCM/MPCBA *2 eq*	15 45	99 >90
5		a	SO	DCM:TFA 2:1 H_2O_2 *1 eq*	20	75
		b	SO₂	DCM:TFA 2:1 H_2O_2 2 eq DCM/MPCBA 2 eq	15 15	90 80
6		a	SO	DCM:TFA 2:1 H_2O_2 *1 eq*	20	30
		b	SO₂	DCM:TFA 2:1 H_2O_2 *2 eq* DCM/MPCBA *2 eq*	20 45	90 80
7		b	SO₂	DCM:TFA 2:1 H_2O_2 *2 eq* DCM/MPCBA *2 eq*	30 90	80 80
8		b	SO₂	DCM:TFA 2:1 H_2O_2 *2 eq* DCM/MPCBA *2 eq*	20 20	80 80
9		b	SO₂	DCM:TFA 2:1 H_2O_2 *2 eq* DCM/MPCBA *2 eq*	20 20	80 80
10		b	SO₂	DCM:TFA 2:1 H_2O_2 *2 eq* DCM/MPCBA *2 eq*	25 60	60 70

[a] Isolated yield

We found that use of ultrasound irradiation allowed the stepwise oxidation of brominated thiophenes to take place in much milder conditions: room T and just 1eq H_2O_2 for the S-oxide and 2eq for the -S,S-dioxide (Table 1). The desired products were obtained in much shorter reaction times (from hours to minutes) and in high yields, while only the unreacted reagent was recovered rendering the purification step easier. Table 1 shows that with bromoderivatives 1-6 and just 1eq H_2O_2, the thiophene-S-oxide is formed in 15-30 minutes in yields varying in the range 70-99%, depending on the substrate. Times and yields are the same for the formation of the -S,S-dioxide upon addition of a second equivalent of H_2O_2. We found that also the oxidation of the same substrates with the classical oxidizing agent MPCBA in DCM is facilitated by the assistance of ultrasounds. In this case only the -S,S-dioxide is obtained, although in much shorter times and greater yields than those obtained in the absence of ultrasound irradiation. In our experience, in the absence of ultrasounds, a much greater amount of MPCBA is needed; for example, for the preparation of compound 9b, nearly 6 eq were needed for overnight reaction and 52% yield.[20] Synthetic details are reported in experimental section. When no substituents were present in the beta positions of the thiophene ring or when alkyl chains were present (items 7-9 in Table 1) the S-oxide could not be isolated, probably due to rapid Diels Alder dimerization.[6,21] The formation of the -S,S-dioxide was instead rapid and efficient. The assistance of ultrasounds and the system $H_2O_2/CF_3COOH/CH_2Cl_2$ made the yield of 7b (room T, 30 min, 80% isolated yield) competitive with that obtained with Rozen's reagent (room T, 1 hour, 95% yield).[22] The oxidation with MPCBA and US assistance is slower and furnishes the same yield in 90 min. Note that until recently 7b obtained in reasonable yield only via the preparation of 2,5-disilylated thiophene and its conversion to the 2,5-dibromo derivative.[23] From these results it is seen that the stepwise oxidation of the thiophene sulfur depends on molecular structure, i.e. on the type of substituents and their position on the thiophene ring. Finally, we found that for some non brominated thiophene derivatives (Table S2) the S-oxide as well as the -S,S-dioxide can be isolated in good yields upon treatment with $H_2O_2/CF_3COOH/CH_2Cl_2$ under ultrasound assistance. Afterwards both oxygenated derivates can be mono or dibrominated in the alpha positions in standard conditions and employed in cross coupling reactions with metalated thiophenes. The brominated S-oxides and -S,S-dioxides of Table 1 and Table S2 were stable compounds and could be purified by silicagel chromatography. Their characterization is reported in experimental section. IR, UV, and NMR of the S-oxides were in agreement with those reported for the thiophene-S-oxides described in the literature.[7a] Oligo- and poly-thiophenes having thiophene-S-oxide and/or thiophene-S,S-dioxide groups in precise position and number inside the molecular backbone could easily be prepared by reacting compounds 1a-6a and/or 1b-6b with metalated thiophenes via palladium catalyzed cross-coupling Stille or Suzuki reactions[24] to obtain the formation of the desired products in high yields. A few examples of the innumerable structures that can be prepared on the basis of the simple chemical strategy described above are given in Schemes 1-4.

Scheme 1. Preparation of oligomers and polymers from 2,5-dibromo-3,4-diphenyl-thiophene-1-oxide 1a and 1,1-dioxide 1b
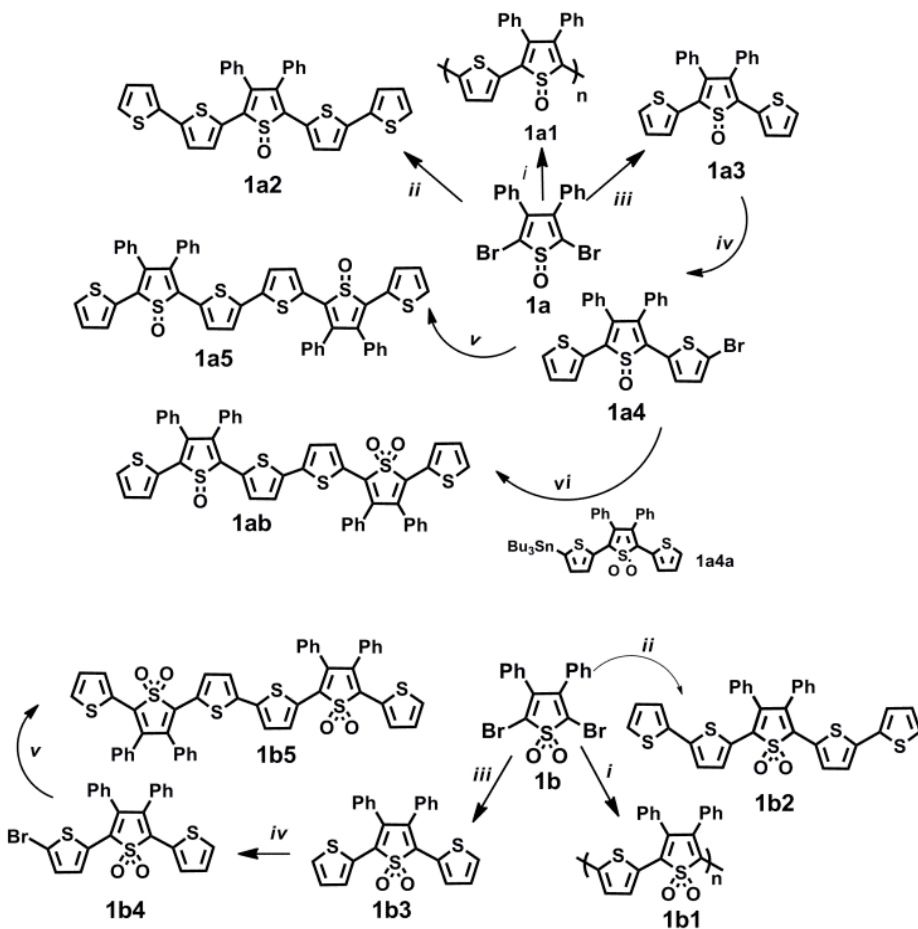
i) 2,5-bis(tributylstannyl)thiophene, ii) 2-tributylstannyl-2:2'.bithiophene, iii) 2-(tributylstannyl) thiophene, Pd (PPh₃)₄, toluene, reflux overnight; iv) N-bromosuccinimide, CH₂Cl₂:CH₃COOH, US; v) Bis (pinacolato)diboron, PdCl₂dppf, NaHCO₃, THF:H₂O 2:1, MW, 80°C; vi) 1a4a, Pd(PPh₃)₄, toluene, reflux overnight. US= ultrasound assistance, MW = microwave assistance.

Scheme 2. Preparation of V-shaped oligomers from 2,3-dibromo-benzo[b]thiophene-S-oxide 3a an -S,S-dioxide 3b.
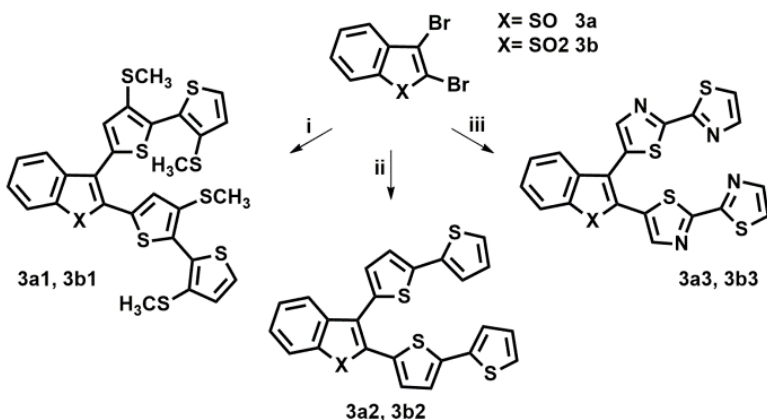
i) 5-tributylstannyl-3,3'-bis(methylthio)-2,2'-bithiophene, ii) 2-tributylstannyl-2,2'-bithiophene, iii) 5-tributylstannyl-2,2'-bithiazole, Pd(PPh₃)₄, toluene, reflux overnight..

Scheme 3. Preparation of oligomers from 2,6-dibromo-3,5-dimethyl-dithieno[3,2-b:2′,3′-d]thiophene -4-oxide 5a and 4,4-dioxide 5b.
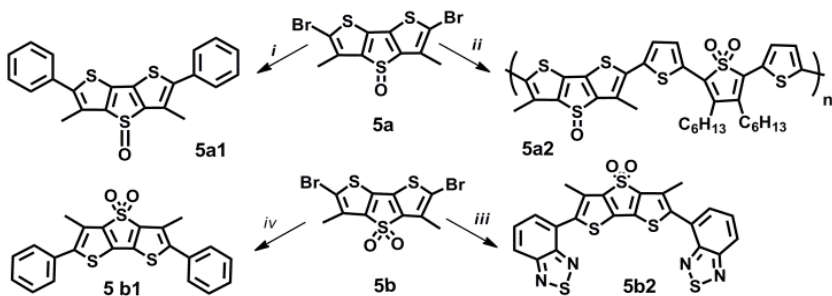
i) 5a (1 mmol), phenylboronic acid pinacol ester (3 mmol), PdCl₂dppf (0.05 mmol) and NaHCO₃ (2 mmol) in THF/ H₂O 2:1 (3 mL), MW, 15'; ii) 5a, 3',4'-dihexyl-5,5''-bis(tributyl stannyl)-[2,2':5',2''-terthiophene]1',1'-dioxide iii) 5b (1 mmol, 4-(4,4,5,5-tetramethyl-1,3,2-dioxaboralan-2-yl)-2,1,3-benzothiadiazole (3 mmol), PdCl₂dppf, NaHCO₃, THF/H₂O 2:1, MW; iv) 5b, phenylboronic acid pinacol ester, PdCl₂dppf, NaHCO₃, THF/H2O 2:1, MW. For 5b1 see reference 15c.

Scheme 4. Preparation of pentamers from 2,5-dibromo-3,4-dihexyl-thiophene-1,1-dioxide 9b and 2-bromo-3,4-dihexyl-thiophene-1,1-dioxide 10b.
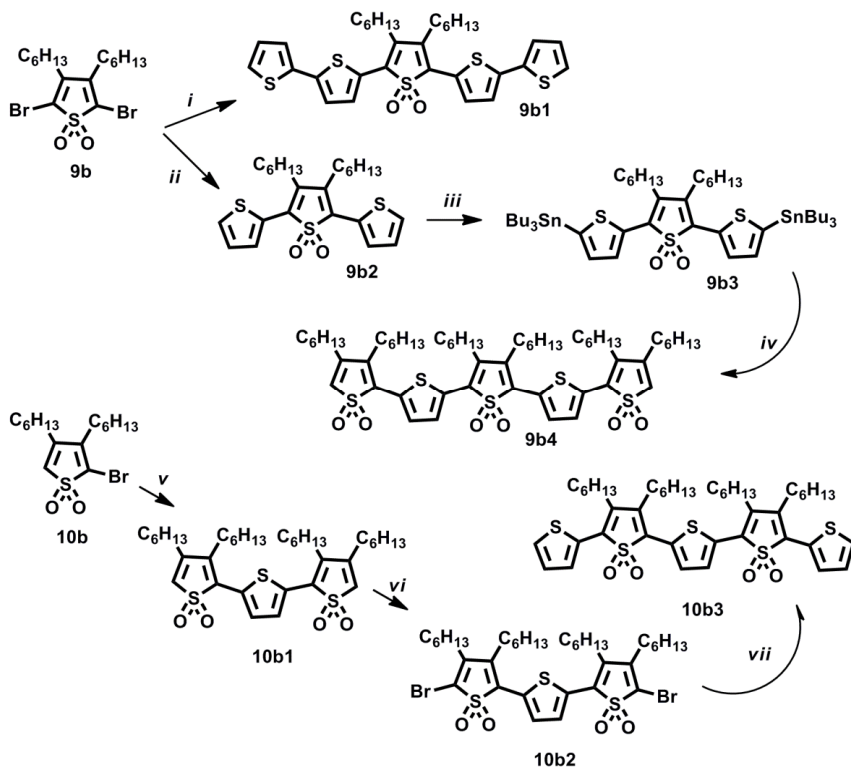
i) (tributylstannyl)-2,2'-bithiophene, ii) 2-(tributylstannyl)- thiophene, Pd(PPh₃)₄, toluene, reflux overnight; iii) THF, BuLi, Bu₃SnCl; iv) 9b, v) 2,5-bis(tributyl)- thiophene, Pd(PPh₃)₄, toluene, reflux overnight; vi) N-bromosuccinimide, CH₂Cl₂ : CH₃COOH, US; vii) 2-tributyl stannyl)-thiophene, Pd(PPh₃)₄, toluene, reflux overnight.

Scheme 1 shows the synthetic pattern to prepare oligomers and polymers starting from dibromo derivatives 1a and 1b. The polymers (1a1,1b1) are made of alternating 3,4-diphenyl-thiophene and 3,4-diphenyl-thiophene-S-oxide or -S,S-dioxide units. The oligomers are trimers (1a3,1b3) or pentamers (1a2,1b2) with one central thiophene-S-oxide or -S,S-dioxide and hexamers bearing two thiophene-S-oxide or -S,S-dioxide groups (1a5 and 1b5, respectively) or one thiophene-S-oxide and one thiophene-S,S-dioxide group (1ab). Scheme 2 illustrates the preparation of V-shaped[25] oligomers obtained from 3a and 3b, while Scheme 3 describes the

24

pattern to obtain the polymer, 5a2, with alternating mono- and dioxygenated thiophene units. Scheme 4 describes the preparation of a quinquethiophene having one (9b1), two (10b3) and three (9b4) thiophene-S,S-dioxide groups in the backbone. It was found that oligomers and polymers containing only thiophene-S-oxide units are much more soluble in common organic solvents than those containing alternating thiophene-S-oxides and thiophene-S,S-dioxides and even more soluble than those containing only thiophene-S,S-dioxides units.

2.2. Electrochemical characterization. Cyclic Voltammetry was used to measure the redox potentials of the newly synthesized oligomers and polymers and to estimate the HOMO-LUMO electrochemical energy gaps. Table 2 reports the oxidation and reduction potentials and the corresponding energy gaps as well as HOMO and LUMO energies calculated according to the modalities indicated in reference 26. Representative CV scans are shown in Figure 1-2. All plots are reported in experimental section (Figures S19-S24).

Table 2. Redox potentials of oligo/polythiophene-S-oxides, -S,S-dioxides and mixed S-oxides/-S,S-dioxides

	E_{ox}^{onset}	E_{rid}^{onset}	E_g eV	HOMO	LUMO
1a1	0.69[a]	-0.56[a]	1.25	5.37	4.12
1b1	0.98[c]	-0.49[a]	1.37	5.66	4.19
5a2	0.95[a]	-0.97[c]	1.92	5.63	3.71
1a3	1.29[c]	-1.25[b]	2.54	5.97	3.43
1b3	1.47[c]	-1.11[a]	2.58	6.15	3.57
1a5	1.08[b]	-1.19[b]	2.27	5.76	3.49
1b5	1.42[c]	-0.92[b]	2.34	6.10	3.76
1ab	1.14[c]	-1.04[c]	2.18	5.82	3.64
1a2	1.04[b]	-1.18[c]	2.22	5.72	3.50
1b2	1.16[c]	-1.03[c]	2.19	5.84	3.65
3a1	1.04[c]	-1.31[c]	2.35	5.72	3.37
3b1	1.09[b]	-1.25[c]	2.35	5.72	3.37
3a2	1.20[c]	-1.28[c]	2.48	5.88	3.40
3b2	1.35[a,d]	-1.19[a,d]	2.54	6.03	3.49
3a3	>1.6	-1.08[c]	>2.68	>6.28	3.60
3b3	>1.6	-0.9[c]	>2.51	>6.28	377
5a1	1.23[c]	-1.53[b]	2.76	5.91	3.15
5b1	1.47[c]	-1.48[c]	2.95	6.15	3.20
5b2	1.46[b]	-1.25[c]	2.71	6.14	3.43
9b1	1.22[a]	-1.20[a]	2.42	5.90	3.48
10b3	1.38[b]	-1.00[a], -1.00[c]	2.38	6.06	3.68
9b4	1.46[b]	-0.94[c]	2.40	6.14	3.74

a Reversible. b Irreversible. c Quasi-reversible. d Reference 35.

It is seen that the presence of thiophene S-oxides results in lower oxidation potentials and lower (more negative) reduction potentials than the presence of thiophene-S,S-dioxides in the corresponding molecular structure. Compare, for example, polymer 1a (0.69, -0.56 V) with

polymer 1b (0.98, -0.49 V) or pentamer 1a5 (1.08, -1.19 V) with pentamer 1b5 (1.42, -0.92V). Generally, the shift of the oxidation potential is more significant than that of the reduction one. As a result of the trend of variation in redox potentials, the electrochemical energy gaps of oligo/polythiophene-S-oxides are smaller than those of the corresponding oligo/polythiophene-S,S-dioxides. Polymers 1a1, 1b1 and 5a2 whose CV plots are shown in Figure 1, having the HOMO-LUMO energy gap < 2 V, are all Low Band Gap polymers.[27] The optical energy gaps, estimated by the onset point of the absorption bands in solution (Figure 1) are in agreement with the electrochemical energy gaps. Polymer 1a1 has one of the lowest electrochemical gaps of polythiophenes described to date, 1.25 V. Remarkably, both polymers 1a1 and 1b1 display reduction potentials similar to those of PCBM,[28] indicating significant electron affinities. The reduction potential of the mixed polymer 5a2, with a different molecular structure, is sizeably more negative than that of the other two polymers while the energy gap is much higher (1.92 V). Of the series of hexamers bearing two oxidized thiophenes, namerly compounds 1a5 (two S-oxides), 1b5 (two -S,S-dioxides) and 1ab (one S-oxide and one -S,S-dioxide) - see the CV plots in Figure S19- the former displays the lowest oxidation potential (1.08V), the second the highest (1.42V) while the third is intermediate between the two (1.14V). The comparison of the redox potentials of pentamers 9b1, 10b3 and 9b4 (see CV plots in Figure S20) shows that passing from one thiophene-S,S-dioxide unit to two and three in the same molecular skeleton leads to a progressive increase in ionization potential paralleled by a progressive increase in reduction potential. Thus, the advantage of increasing the electron affinity of the system is paid by the increase in the ionization energy. The three dithienothiophene derivatives, 5a1, 5b1 and 5b2 – see CV plots in Figure S21 – display quasi-reversible oxidation waves. On the contrary, only 5b1 with two terminal benzothiadiazole units, displays a reversible reduction wave, the other two being irreversible. Note that the oxidation potential of 5b2 is very close to that of 5b1 having two phenyl groups, suggesting that the HOMO of the former is mainly concentrated on the dithienothiophene-S,S-dioxide unit.

2.3. Optical properties. Absorption and emission wavelenghs and molar absorption coefficients of all oligomers and the absorption wavelength of all poymers are reported in Table S3. The corresponding spectra are shown in Figures S25-S30.To time the photophysical properties of oxygenated thiophene derivatives have been poorly investigated. Very recently, Busby, E. et al. have reported that the photodynamics of compounds containing thiophene-S,S-oxide moieties is profoundly different from that of the non-oxygenated counterparts.[29] The difference is due to the formation of fast singlet deactivation pathways which reduce the excited state lifetime by several orders of magnitude depending on the number and sequence of oxygenated thiophene units present in the molecular structure. Probably due to analogous reasons, none of polymers 1a1, 1b1 and 5a2 displays light emission in the visible and NIR range upon irradiation at the maximum absorption wavelength. The oligomers having only one single inner thiophene-S,S-dioxide or thiophene-S-oxide moiety - whether in linear trimers (1a3, 1b3, Figure S30) and pentamers (1a2, 1b2, Figure S26) or in V-shaped systems (3a1-3, 3b1-3, Figure S27) or in dithienothiophene derivatives (5a1, 5b1, 5b2, Figure S29) - display photoluminescence in the visible region upon irradiation at the maximum wavelength

absorption. However, on increasing the number of oxygenated units present in the molecular backbone, the intensity of the photoluminescence signal progressively decreases. This effect is nicely illustrated by the sequence of pentamers 9b1, 10b3 and 9b4 having one, two and three thiophene-S,S-dioxide moieties, respectively, in the backbone. Figure S25 shows that the photoluminescence progressively vanishes as the number of S,S-dioxide moieties increases. A similar effect is observed for the hexamers having two thiophene-S-oxide groups (1a5), two thiophene-S,S-dioxide groups (1b5) and and one thiophene-S,S-dioxide group (1ab), which display the same absorption spectra and extremely weak photoluminescence spectra in solution (Figure S28). Of the three hexamers only the former one displays a sizeable photoluminescence signal in cast film (Figure S28). From the comparison of the data concerning the S-oxides and the corresponding S,S-dioxides reported in this study we infer that the photophysical behavior of the former compounds is very similar to that of the latter ones. As an exemple of such a similarity, Figure S31 shows the photophysical characterization of 3a1 and 3b1 in 1.0×10^{-5} M solution in DCM, in thin film 0.1wt% in PMMA and in neat film (100%). It is seen that passing from isolated monomers dispersed into the PMMA inert matrix to the neat film there is a considerable red shift indicating the formation of aggregate absorbing states (dimers). The isolated monomer absorption profile for both oligomers finely match with that obtained in solution. The corresponding photoluminescence spectra, also reported in Figure S31, show that the spectral profiles change considerably passing from 3a1 or 3b1 0.1% in PMMA to the pure dye for which a marked red shift is again observed. The red shift of about 60 nm in both oligomers can be ascribed to the interaction of adjacent molecules leading to the formation of dimer emitting states. It is interesting to note how for both compound there is a strong blue shift passing from the diluted solution to the isolated molecule in inert matrix, probably related to greater rotational and vibrational degrees of freedom in solution. For both 3a1 and 3b1 multiple photoluminescence decay times were also observed, as illustrated in Figure S32 and Table 3.

Table 3. Maximum emission wavelengths, decay times $\tau 1$, $\tau 2$, $\tau 3$ and photoluminescence quantum yields of 3a1 and 3b1.

	λ (nm)	$\tau 1$ (ns)	$\tau 2$ (ns)	$\tau 3$ (ns)	PLQY %
3b1 1.0^{-5} M in DCM	650	0.8		5.3	a
3b1 0.1% in PMMA	600	1.1		5.6	19%
3b1 100 %	650	0.6	2.0	4.4	0.7%
3a1 1.0^{-5} M in DCM	650	0.8		5.6	a
3a1 0.1% in PMMA	650	1.0		5.6	11%
3a1 100 %	650	0.7	2.6	7.8	0.4%

The analysis of lifetime decays shown in Figure S32 in PMMA and in diluted solution shows that both compounds follow a biexponential behaviour, most probably due to a double emitting state already described for some thiophene derivatives.[30] Table 3 shows that in the neat films a third decay time ($\tau 3$) was found that can be ascribed to the de-excitation of the aggregates. Table 3 shows that the highest photoluminescence quantum yields (PLQY) are those of the samples 0.1 % in PMMA ($\Phi PL \sim 0.1$, 0.2) and the lowest those of the pure samples ($\Phi PL = 0.04$, 0.07), possibly due to quenching activities of the excited states by molecular oxygen

and/or self-quenching phenomena. Despite the fact that our data point to the similarity in photophysical properties of S-oxides and S,S-dioxides, we are aware of the fact that only precise photophysical studies - far beyond the objective of the present study - will allow to unambiguously shed light on that matter.

2.4. Single crystal x-ray structure of hexamer 1a5. We were able to obtain single crystals for hexamer 1a5 having a backbone containing two thiophene-S-oxide units. The X-ray diffraction molecular structure and packing of 1a5 are reported in Figure 1.
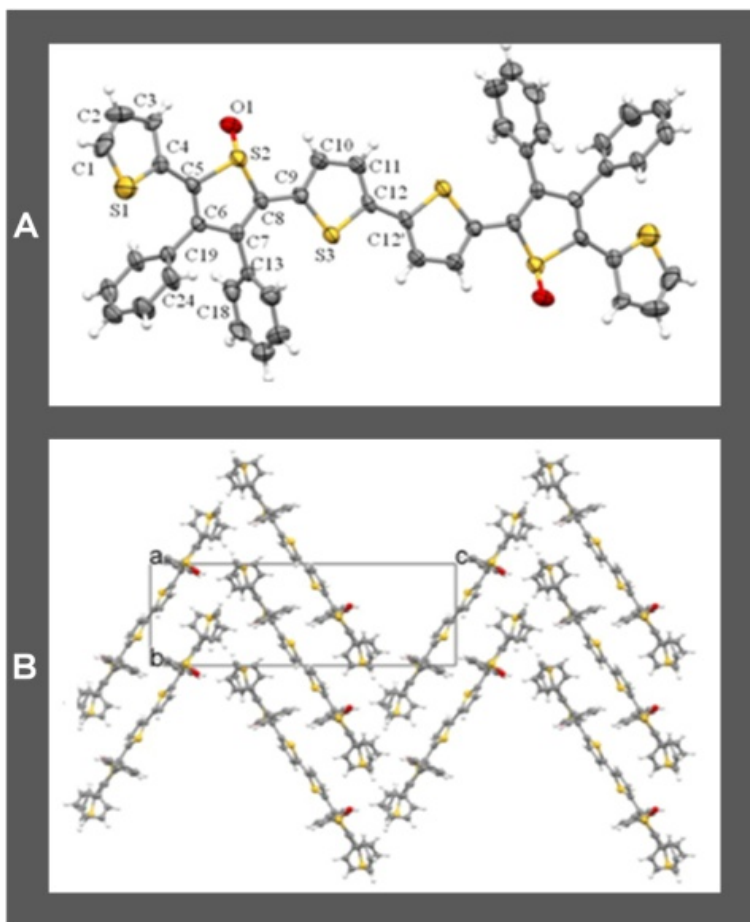

Figure 1. Crystal structure of hexamer 1a5 containing two thiophene-S-oxide moieties. A) Molecular conformation. The labeled atoms are related to the unlabelled ones by the symmetry operation –x+1, -y, -z+1. B) View down the a axis of the crystal packing.

28

The compound has a crystallographic inversion centre in the middle of the C-C bond connecting the inner thienyl rings. The orientation of the sulfur atoms in the adjacent rings is transoid. The central bithiophene unit is planar and is connected in the 2-positions to the thiophene-1-oxide rings bearing two phenyl groups in 3 and 4 and a thienyl ring in 5. The ring containing the oxidized sulfur atom loses its aromatic character and shows a diene structure with C5-C6, C6-C7 and C7-C8 bond distances of 1.354(7), 1.474(7) and 1.380(7) Å, respectively. In agreement with X-ray data already reported for thiophene-S-oxides,[31,9a] the oxidized sulfur atom exhibits a pyramidal geometry and lies 0.186(8) Å out of the C5-C6-C7-C8 least-square plane. In addition the S2-C bonds (S2-C5 1.816(5) and S2- C8 1.794(6) Å) are longer than the S-C distances in the other thiophene rings that fall in the range 1.683 -1.749(5) Å. The C5-C6-C7-C8 mean plane makes dihedral angles of 20.1(3) and 8.7(3)° with the outer and inner thienyl rings, respectively. The deviation from planarity of the thiophene-S-oxide sulfur is small, indicating the possibility that some π-delocalization may still occur. In the crystal the molecules adopt a pseudo-herringbone mode (Figure 1B). The molecules pack in a parallel slipped arrangement but without π−π stacking (distance between the molecular plane 4.45 Å). The intermolecular interactions between the different stacks are mainly C-H…π interactions (H20-centroid C19-C24) 3.43 Å. It is worth noticing that the crystal conformation of 1a5 closely resembles the recently reported substituted hexamer having butyl groups in place of the phenyl rings, one methyl group in the outer thiophene ring and two thiophene -S,S-dioxides instead of two thiophene-S-oxide moieties.[32]

2.5. Thin film devices

2.5.1 Field-effect transistors with polymers 1a1, 1b1 and 5a2. All polymers were tested as active materials in staggered top-gate FETs operating both in p- and n-accumulation regimes. A staggered architecture was adopted since it typically suffers less from charge injection limitations at the contacts,[33] and a top-gate configuration with a low-k polymer dielectric, in this case PMMA, offers a dielectric/polymer interface which is more ideal for charge transport.[33] The measured transfer curves (Figure 2B) for the fabricated devices highlight a capability of all three materials for electron transport, while only 1a1 and 5a2 - having thiophene-S-oxide units - can appreciably conduct holes. It is to stress how the ambipolarity feature of the latter two materials is fairly balanced with respect to the opposite charged species. The extracted mobility values for the materials are summarized in Figure 2Bd. To date FET charge mobilities of polymers bearing thiophene-S,S-dioxides moieties into the aromatic backbone have been assessed only in two cases. The first case concerns a polythiophene with varying ratios of alkylated thiophene to thiophene-S,S-dioxide units in the backbone. According to that study I-V measurements showed that the polymers never exhibited clear field-effect behavior in either hole or electron accumulation regimes. Moreover, the authors report that the SO2 functionality was labile on heating and increasing above 50% the number of oxygenated thiophene units present in the backbone resulted in significant degradation negatively impacting on charge-transport properties. In particular they report that an

incorporation of oxygenated thiophene higher than 20% led to complete failure of the FETs after a 110 °C thermal annealing.
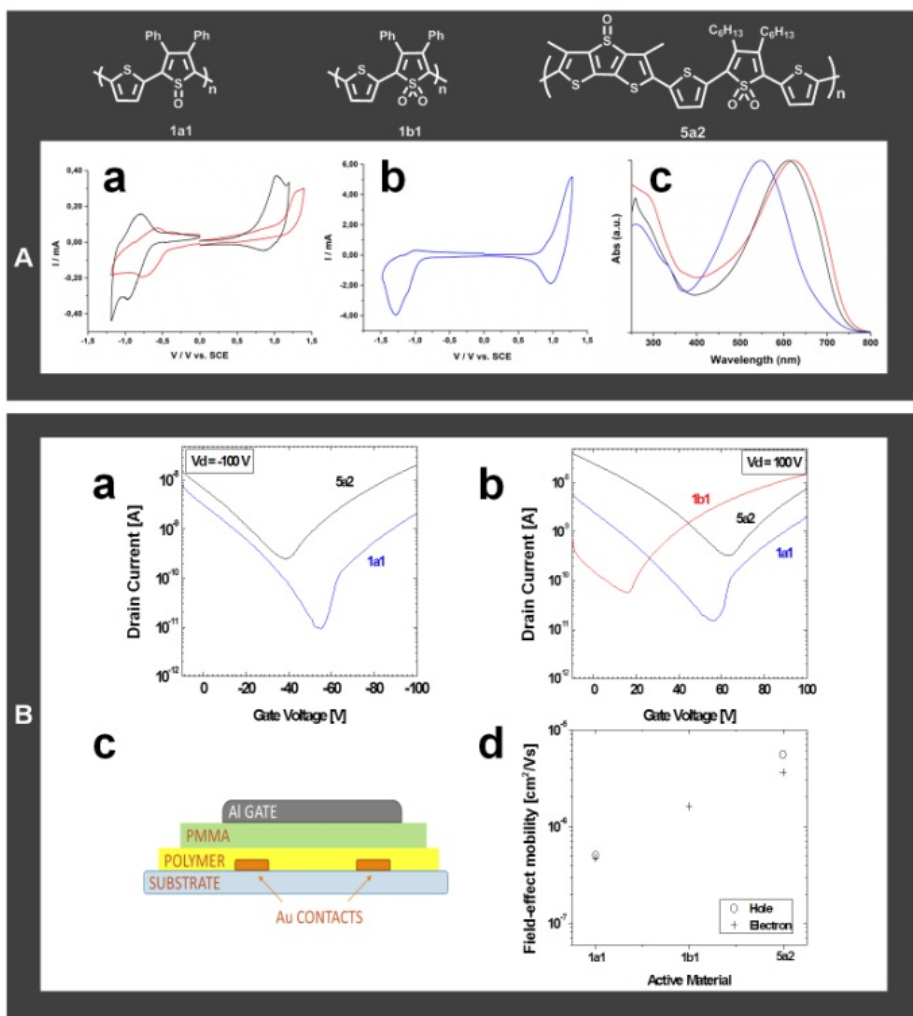
Figure 2. A) Cyclic voltammetries of polymers 1a1, 1b1, 5a2 and their absorption spectra in DCM. B) The FETs stack. Geometrical dimensions for the FETs channel are L = 20 µm and W = 10 mm C) Transfer curves for the fabricated FETs in a) hole accumulation regime (Vdrain = -100 V) and b) electron accumulation regime (Vdrain = 100 V), c) the FETs stack and d) the extracted Field-Effect charge mobilities for the polymers. Geometrical dimensions for the FETs channel are L = 20 µm for polymers 5a2 and 1b1, L = 10 µm for polymer 1a1 and W = 10 mm in all cases.

30

By contrast, the FET devices reported here, realized using active materials featuring 30 to 50% incorporation, showed proper field-effect behavior even after a thermal annealing at 150 °C. The second case concerns two polymers alternating acenaphtho [1,2-c]thiophene-S,S-dioxide units and thieno-thiophene or benzo [1,2-b:4,5-b']dithiophene units.[34b] The polymers displayed p-type charge mobility on the order of 10-3 – 10-4 Vcm-1s-1. It is well known that FET charge mobilities can be enhanced by optimizing device fabrication and film morphology[33,35,36] or appropriate surface treatment.[37] The optimization of film morphology requires a good knowledge of the self-assembly properties of oligomers and polymers bearing thiophene oxidized moieties in the backbone. Although some data are available on single crystal X-ray structure of oligothiophene-S,S-dioxides[38] and powder X-ray studies of polythiophene-S,S-dioxides outlining the importance of H-bonding on molecular packing,[34,39] no detailed investigations have been carried out so far on the self-assembly pathways in thin films of oligomers and polymers containing thiophene oxigenated units. It is reasonable to expect that these studies will result in the preparation of thin films with optimized morphology and consequently higher charge mobility values than those reported in Figure 2B. However, independently of the FET charge mobility values, our data unambiguously indicate that charge carrier types in thiophene materials can be modulated via mono- or di-oxygenation of thiophene sulfur. Our data also indicate that the compounds containing thiophene-S-oxide units in the backbone display ambipolar charge conduction. We suggest that this property is related to lower oxidation potentials than those of the correponding compounds with thiophene-S,S-dioxide units.

2.5.2. Light emitting devices with oligomers 3a1 and 3b1. V-shaped thiophene-S,S-dioxides are active materials in electroluminescent devices.[25] They form non centro-symmetric thin films and one member of the series displays second order susceptibility χ(2) values as high as the reference LiNbO3 single crystal, without poling processing.[40] To time no data are available for the corresponding S-oxides. Light emitting diodes were fabricated using either the neat films of both 3a1 and 3b1 or films where the compounds were dispersed in 15% concentration (chosen following optimized photoluminescence quantum yield yield measurements) within two different host matrices: BCPO, namely ambipolar 9,9′-(4,4′-(Phenylphosphoryl) bis-(4,1-phenylene))bis(9H-carbazole) and TPBI, namely electron transporting 1,3,5-tris-(N-phenylbenzimidazole-2-yl)-benzene. Both compounds were electroluminescent systems as shown in Figure 3, Figure S33 and Figure S34. Note that these are the first electroluminescence data ever reported for thiophene-S-oxides. Figure 3 shows that the electroluminescent spectra are in accordance with the photophysical characterization displaying emission peaks around 620 nm (3a1) and 635 nm (3b1) for the host-guest system light emitting diodes (LEDs) and around 645 nm and 660 nm, respectively, for LEDs with neat films. Due to self-quenching phenomena in the neat films, high current density values are measured, demonstrating an inefficient exciton radiative recombination within the emitting layers, which leads to low luminance and low current efficiencies. In the case of host-guest systems better results were obtained in terms of luminance and current efficiencies. Figure 3 shows that the S-oxide 3a1 exhibits close values of electroluminescence efficiency in both

matrices with the highest one being obtained for the film dispersed within the ambipolar BCPO matrix. By contrast, there is a much greater difference in the electroluminescence efficiency of 3b1 dispersed into the two different matrices, the highest value being attained when the compound is dispersed within the electron transporting TPBI matrix. Since the electro-optical characteristics of the devices depend on the intrinsic transport properties of the active materials[41] one can argue that the S-oxide 3a1 has ambipolar charge transport properties whereas 3a2 has a predominant electron transporting behaviour. This result is consistent with the charge transport properties measured in FET devices for polymers 1a1 and 5a2 containing thiophene-S-oxide moieties (ambipolar semiconductors) and 1b1 containing only thiophene-S,S-dioxide moieties (n-type semiconductor).
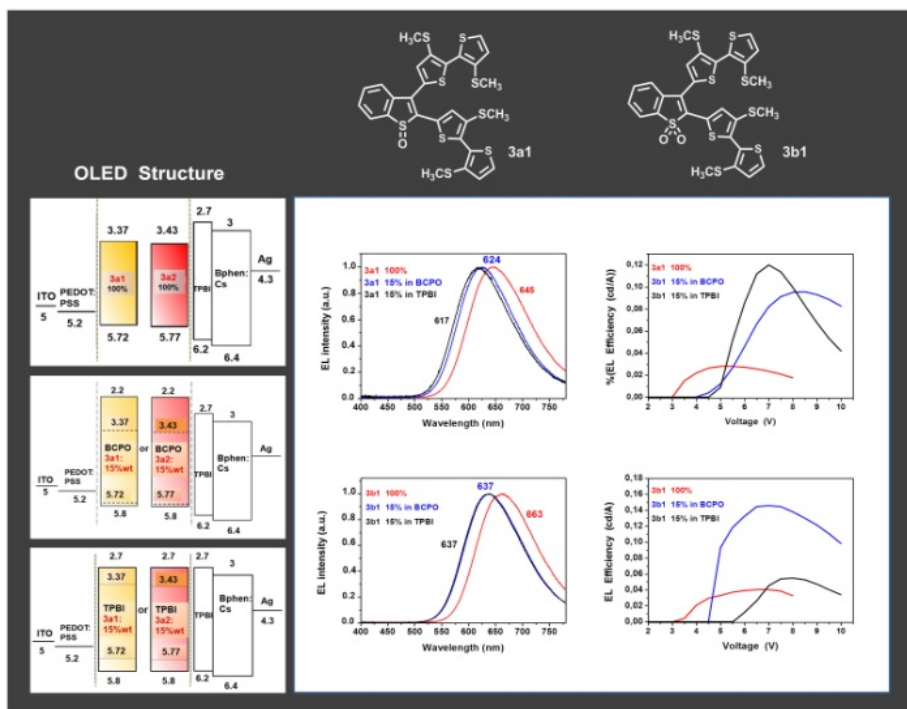
Figure 3. Structure of electroluminescent devices, electroluminescence intensity and efficiency of V-shaped oligomers 3a1 and 3b1 in thin films, 15% in BCPO, namely bipolar 9,9′-(4,4′-(Phenylphosphoryl)bis-(4,1-phenylene))bis(9H-carbazole) and 15% in TPBI, namely electron transporting 1,3,5-tris-(N-phenylbenzimidazole-2-yl)-benzene.

2.6. Oligomers 5a1, 5b1 and 5b2 inside live cells. The presence of thiophene-S,S-dioxide moieties into the molecular backbone not only changes the frontier orbital energies but also affects the aggregation properties through the formation of H-bondings involving the oxygen

atoms. We have already reported that the green fluorescent dithienothiophene -S,S-dioxide 5b1 is able to spontaneously cross the membrane of live mouse and bone-marrow human tumour fibroblasts.[11a,c] In the perinuclear region 5b1 is recognized by the hydroxy proline component of protocollagen polypeptide chains through the formation of hydrogen bondings between the O-H group of hydroxyproline and the oxygen atom of the O=S=O group. As a consequence, the formation of co-assembled fluorescent and conductive type-I collagen-5b1 microfibers is observed inside the cells (Figure 4A).[11a,c]
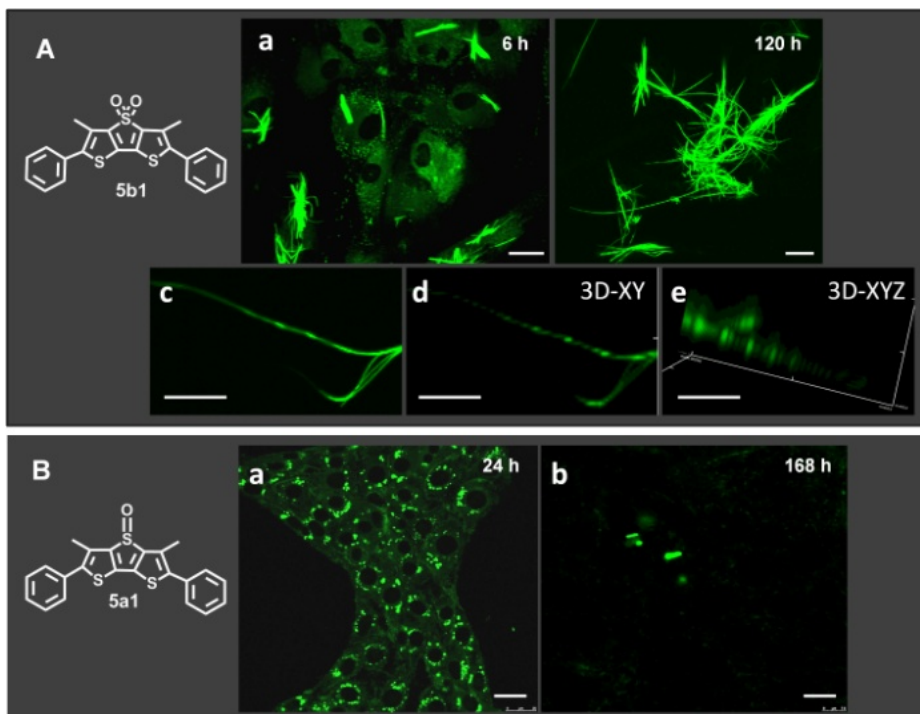
Figure 4. LSCM images of live fibroblasts upon spontaneous uptake of DTTSO2Ph (5b1) and DTTSOPh (5a1). A) View (a,b) of the cell culture after 6 and 120 hours from uptake of 5b1 by human fibroblasts showing the formation of green fluorescent microfibers on the surface of the cells (scale bars: 25 µm), a detail of the microfibers structure (c) and the corresponding 3D spatial reconstruction (d,e) displaying the helical morphology of the microfibers (scale bars: 50 µm (c); 25 µm (d,e)). B) LSCM images of live N3 HT3 fibroblasts 24h (a) and 168h (b) from spontaneous uptake of 5a1 showing that in this case there is no formation of fluorescent microfibers (scale bars: 75 µm).

Having now the possibility to prepare in fair amount and free of contaminants the corresponding S-oxide, 5a1, we could repeatedly and reproducibly test its behaviour inside live cells in the same conditions. The results are reported in Figure 4A and Figure 4B comparing the

behavior of the -S,S-dioxide 5b1 with that of the - S-oxide 5a1. Figure 4A shows the formation of fluorescent microfibers after 6 hours (a) and 120 h (b) upon spontaneous uptake of 5b1 by live human fibroblasts. The diffusion of 5b1 inside the cells is rather uniform as the cytoplasm appears entirely stained, while the compound does not enter the nucleus of the cells which remains dark. Figure 4A(c-e) shows that most microfibers display helical supramolecular organization, as shown by the 3D Laser Scanning Confocal Microscopy (LSCM) reconstruction. The fluorescent microfibers are mainly made of type-I collagen co-assembled with 5a1, as demonstrated by SDS-PAGE and immunoblotting analysis.[11a,c] Similar to sulfone 5b1, sulfoxide 5a1 - also green fluorescent - is able to be spontaneously internalized by live NIH 3T3 mouse fibroblast cells without altering their viability and proliferation ability. Figure 5 reports the MTT cytotoxicity tests24 on NIH 3T3 cells treated with some S-oxides, including 5a1, and -S,S-dioxides. The corresponding cytotoxicity test for 5b1 is reported in reference 11a. Contrary to the -S,S-dioxide 5b1, the S-oxide 5a1 once internalized by the the cells is not recognized by any intracellular component and is physiologically and progressively eliminated by the cells. Figure 4B shows that after 24h from spontaneous uptake by the fibroblasts, 5a1 accumulates in the perinuclear region forming bright green fluorescent spots. However, there is no sign of formation of fluorescent fibers and after 168h (7 days) only a few fluorescent aggregates of 5a1 are still present inside the cells.
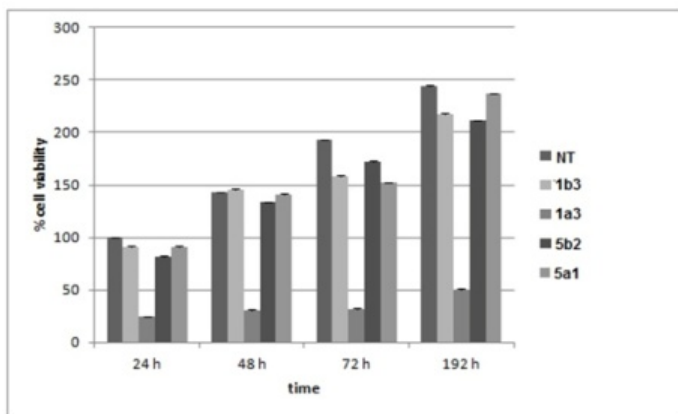
Figure 5. MTT cytotoxicity tests on NIH 3T3 cells treated with T3PhSO2 (1b3), T3PhSO (1a3), DTTSO2Ph (5b1) and DTTSOPh (5a1) compared to untreated cells (NT). Representative measurements of three distinct sets of data and no significant difference between values at different time points is observed at $P < 0.05$ with t-Student test. See reference 11a for 5b1.

To account for the different behaviour of -S,S-dioxide 5b1 and S-oxide 5a1 inside the cells we performed a theoretical study using the density functional theory at the BLOC-D3/def2-TZVPP level.[42] Since the fluorescent microfibers generated by the cells upon uptake of 5b1 are mainly made of type-1 collagen, the theoretical investigation considered a model system consisting of

one molecule (either 5b1 or 5a1) sandwiched between two collagen strands simulated by a sequence of three tripeptide Gly-Pro-HyPro (Figure 6).
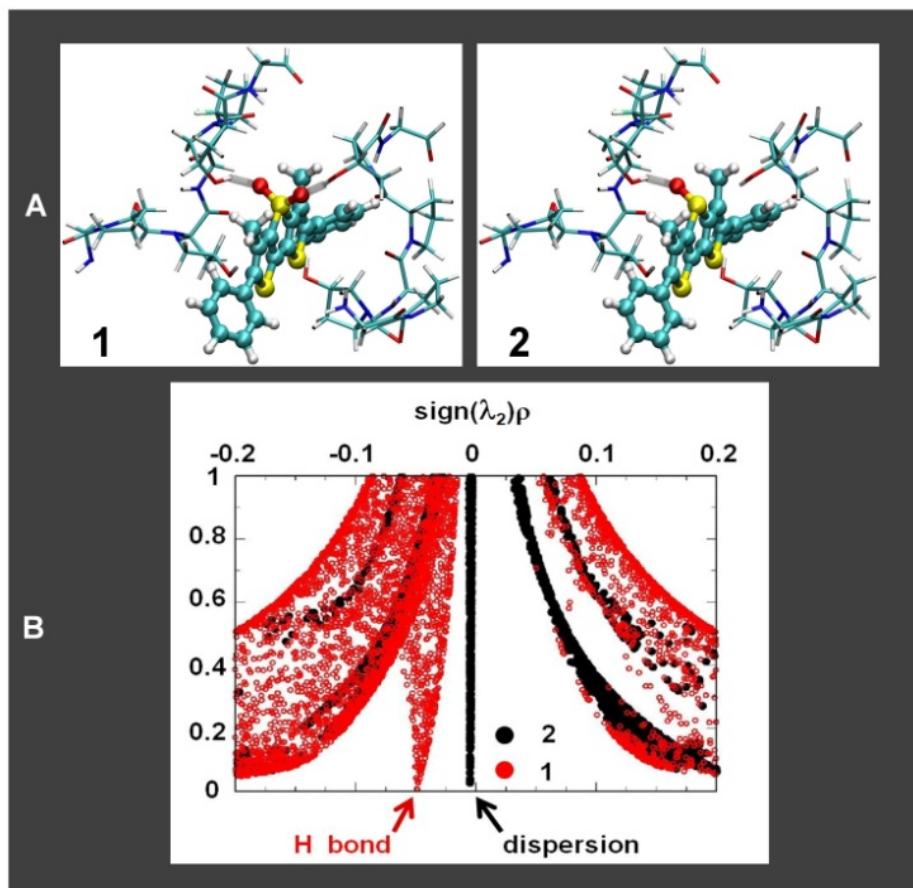
Figure 6. A) Model systems considered for DFT calculations with 5b1 (1) and 5a1 (2) interacting with two collagen strands build up of three Gly-Pro-HyPro tripeptide chains. B) NCI indicator analysis of the bonding region between the Collagen-Fluorophore and the additional collagene strand in cases 1 and 2. In the x-axis label ρ denotes the electron density and $\lambda 2$ the second eigenvalue of the electron-density Hessian.

A similar model for collagen but with only a single tripeptide chain was also used in reference 11a. To elucidate the nature of the non-covalent interaction between the S-oxide and collagen, and especially the role of the hydrogen bonding, an analysis of the reduced gradient as a function of the electron density (ρ) times the second eigenvalue of the electron-density Hessian

35

(λ2) was performed in the collagen-5a1 (5b1) Collagen [C-5a1 (5b1)...C] bonding region. This is the so called NCI indicator, which is able to characterize different kinds of non-covalent bonds.[43] The results of this analysis, reported in Fig. 6B, unambiguously show the importance of oxygen to promote a H-bonding between the oxidized compounds and the collagen strand. In fact, in the case of -S,S-dioxide 5b1 a clear hydrogen bond nature is observed due to the interaction of the oxygen atoms with the hydrogen atoms of the HyPro rings in front of it. By contrast, when the corresponding S-oxide 5a1 is considered, where no oxygen atom is present to mediate the interaction between C-F and the second collagen strand, no signature of hydrogen bonding was found in the relevant bonding region and the interaction between 5a1 and the collagen strand is only due to dispersion contributions. These results further confirm our interpretation according to which the collagen-5b1 co-assembly inside live fibroblasts is mainly due to the hydrogen bonding capabilities of the sulfone groups and provide a key to understand why 5a1 does not lead to the physiological formation of fluorescent microfibers. We can anticipate that we have tested several other thiophene-S,S-dioxides and the corresponding S-oxides for their behaviour inside live fibroblasts. We have found that the former were not toxic to the cells (for example, see the MMT tests of Figure 5 for 1b3 and 5b2) and always formed fluorescent microfibers inside the cells, the composition of which varies with the molecular structure and is currently under study. On the contrary, the corresponding S-oxides never led to the formation of fluorescent microfibers inside live cells and some of them were even toxic to the cells (see, for example, the MMT test for 1a3 in Figure 5).

III. CONCLUSION

What we intend to demonstrate with this study is that there is still much to explore in the vast land of thiophene materials. In the present work, we have shown that the availability of reliable ultrasonic equipments and microwave laboratory reactors provides the means to develop simple synthetic procedures for the easy and low cost preparation of regioregular thiophene-based oligomers and polymers having the thiophene sulfur functionalized with oxygen. We have reported the facile synthesis of two new classes of air stable, low band gap oligomers and polymers, - namely oligo and poly-thiophene-S-oxides and mixed S-oxides/-S,S-dioxides - and shown that selective functionalization of thiophene sulfur with one or two oxygens provides a new means to finely tune frontier orbitals energy and band gaps, p- and n-type charge transport, photo- and electroluminescence properties of these materials and even their fate inside living cells. It is evident that the number of oligo and poly-thiophene-S-oxides and mixed S-oxides/-S,S-dioxides which could be synthesized through the simple chemical strategy described here exceeds the few examples reported in the present study and that a much larger variety of multifunctional thiophene materials could be prepared and investigated. We believe that there are many potentialities for oligo/polythiophene-S-oxides and S-oxides/-S,S-dioxides in fields such as organic electronics or fluorescent imaging of biological processes inside live cells. One of these is, for example, the possibility to exploit the pyramidality of the sulfur atom of the thiophene-S-oxide group for the preparation of chiral oligomers and polymers. Recent studies have demonstrated that chiral organic molecules on surfaces can act as electron spin filters at

room temperature opening up the possibility of innovative electronic devices such as spin-OLEDs that do not require magnetic elements to define the spin orientation.[44] Furthermore, it should be taken into account that there are still more types of functionalization of thiophene sulfur that have not at all been explored so far in the preparation of thiophene based materials. New organic materials could be obtained through the preparation of thiophene sulfinimides, sulfoximides and sulfonium salts. All functionalization types should be capable to deeply affect the properties of thiophene materials, including their self-organization capabilities into functional supramolecular structures. We hope that the present study stimulates further developments in this directions

IV EXPERIMENTAL SECTION

4.1. General

4.1.1. Synthesis and characterization. The synthesis of thiophene-S-oxides (Table 1) was performed in a FALC LBS1 50KHz Ultrasonic bath. Cross coupling reactions involving boron derivatives were carried out under microwave assistance in a Milestone Microsynth Labstation operating at 2450 MHz monitored by a proprietary control unit. All operations were carried out under a dry, oxygen-free nitrogen atmosphere. Organic solvents were dried by standard procedures. TLC was carried out with 0.2-mm thick of silica gel 60 F254 (Merck). Visualization was accomplished by UV light or phosphomolybdic acid solution. Preparative column chromatographies was performed on glass columns of different sizes hand packed with silica gel 60 (particle sizes 0.040-0.063 mm, Merck). H-1 and C-13 NMR spectra were recorded with a Varian Mercury-400 spectrometer equipped with a 5-mm probe. Chemical shifts were calibrated using the internal $CDCl_3$ resonance which was referenced to TMS. Mass spectra were collected on a Thermo Scientific TRACE 1300 gas chromatograph. UV-Vis spectra were recorded using a Agilent Technologies CARY 100 UV-Vis spectrophotometer. Photoluminescence spectra were collected on a Perkin Elmer LS50 spectrofluorometer.

4.1.2. Cyclic Voltammetry. Solid state CVs were obtained employing an AMEL 5000 electrochemical cell under argon. Working electrodes were solid films of the oligomers or polymers deposited on ITO. An electrolytic solution of anhydrous propylene carbonate (Sigma-Aldrich) containing 0.1 mol L-1 tetraethylammonium tetrafloroborate (Fluka for electrochemical analysis) was used. The oxidation potential of ferrocene/ferricinium (Fc/Fc+ = -4.84 eV) vs. aqueous saturated calomel electrode (SCE) was 0.50 V. The CVs of 1 mmol L-1 oligomers were performed on Pt disc-electrode in DCM (Sigma-Aldrich, distilled on P2O5 and stored under Ar) 0.1 mmol L-1 tetrabutyl-ammonimum perchlorate (Fluka, recrystalized form methanol) where Fc/Fc+ = 0.47 V vs. SCE.

4.1.3. X-Ray Diffraction. Crystallographic Data Collection and Structure Determination. Single crystals of hexamer 1a5 were grown from toluene. The X-ray intensity data of the compound were measured on a Bruker Apex II CCD diffractometer. Cell dimensions and the orientation matrix were initially determined from a least-squares refinement on reflections measured in three sets of 20 exposures, collected in three different ω regions, and eventually

refined against all data. A full sphere of reciprocal space was scanned by 0.3° ω steps. The software SMART[45] was used for collecting frames of data, indexing reflections and determination of lattice parameters. The collected frames were then processed for integration by the SAINT program,[45] and an empirical absorption correction was applied using SADABS.[46] The structure was solved by direct methods (SIR 2004[47]) and subsequent Fourier syntheses and refined by full-matrix least-squares on F2 (SHELXTL[48]) using anisotropic thermal parameters for all non-hydrogen atoms. All the hydrogen atoms were added in calculated positions, included in the final stage of refinement and refined with U(H)=1.2Ueq(C) and allowed to ride on their carrier atoms. The oxygen atom of the sulphoxide group was found to be disordered over two sites with occupancy factor of 0.90 and 0.10, respectively. The SQUEEZE routine of the PLATON software[49] revealed that the structure contains solvent accessible voids (352Å3/unit cell), filled with disordered solvent molecules (99 electrons/unit cell) that is most likely disordered toluene. Molecular graphics were generated by using Mercury 3.3.[50] Color codes for all molecular graphics: orange (Cu), blue (N), red (O), grey (C), white (H). Crystal data and details of data collections for compound A are reported in Table S4.

4.1.4. Field-effect transistors. Top-gate, staggered Field-Effect Transistors (FETs) operating both in p- and n- accumulation regimes were fabricated using polymers 1a1, 1b1, 5a2 as the active materials. Low alkali 1737F Corning glass was used as substrate, cleaned sequentially in an ultrasonic bath of deionized water, acetone and 2-propanol for 10 minutes each, then exposed to oxygen plasma at 100 W for 10 minutes. Bottom source and drain electrodes were defined by photolithography and evaporation of 1.5 nm of Cr and 25 nm of Au. The defined patterns feature a channel width W=10mm and channel length L=20μm or L=10 μm. Solutions of the three polymers with a concentration of 5 g/L in chloroform were prepared and deposited via spin-coating at 1000 rpm in nitrogen atmosphere, then the samples were annealed at 150 °C for 8 hours. Poly(methylmethacrylate), PMMA, was purchased from Sigma-Aldrich and dissolved in n-butyl acetate with a concentration of 80 g/L, then spin-coated over the active material layer at 1500 rpm yielding a 500-nm-thick dielectric layer. The devices were then annealed at 80 °C for 30 mn. The gate electrodes were defined via evaporation of Al through a shadow mask. Electrical characterization was performed in a nitrogen atmosphere using an Agilent B1500A Semiconductor Parameter Analyzer.

4.1.5. Photoluminescence measurements in thin films. Emission spectra were obtained with an Edinburgh FLS980 spectrometer equipped with a peltier-cooled Hamamatsu R928 photomultiplier tube (185-850 nm). An Edinburgh Xe900 450 W Xenon arc lamp was used as exciting light source. Emission lifetimes in the ns-μs range were determined with the single photon counting technique by means of the same Edinburgh FLS980 spectrometer using a laser diode as excitation source (1 MHz, λexc = 407 nm, 200 ps time resolution after deconvolution) and the above-mentioned PMT as detector. Analysis of the luminescence decay profiles vs time was accomplished with the Decay Analysis Software provided by the manufacturer. Photoluminescence yields were calculated by corrected emission spectra obtained from an apparatus consisting of a barium sulphate coated integrating sphere (4 inches), a 450W Xe lamp (λexc = tunable by a monochromator supplied with the instrument) as light sources, and a R928

photomultiplayer tube as signal detectors, following the procedure described by De Mello et al.[51] Experimental uncertainties are estimated to be ± 8% for lifetime determinations, ± 20% for emission quantum yields, ± 2 nm and ± 5 nm for absorption and emission peaks, respectively. Absorption spectra were recorded with a Cary 5000 UV-Vis-Nir Varian spectrophotometer.

4.1.6. OLEDs fabrication and characterization. The OLEDs were fully fabricated by high vacuum thermal evaporation in a Kurt J. Lesker multiple high vacuum chamber system. The electrical-optical characteristics of the devices were measured under vacuum with an Optronics OL770 spectrometer, coupled, through an optical fiber, to the OL610 telescope unit for the luminance measurements, with an experimental uncertainty of around ± 10%. The whole system was National Institute of Standards and Technology (NIST) calibrated using a standard lamp and was directly connected by RS232 cable to a Keithley 2420 current-voltage source meter.

4.1.7. Cell viability. Mouse embryonic fibroblasts (NIH-3T3) were seeded at a density of 100,000 cells in tissue culture plate in 1 mL of complete culture medium. Compounds 5a1, 5b1, 5b2 were dissolved in the minimum amount of DMSO in order to obtain a stock solution and then were administered to the cells by adding the appropriate dilution in DMEM serum free to obtain the final concentration of 0.05 mg/mL and incubated at 37°C in 5% CO_2, 95% relative humidity for 1h. At the end of the incubation period, the cell cultures were repeatedly washed with DMEM medium serum free. The cells were examined after 1, 24, 48, 72 hours and 7 days upon treatment by laser scanning confocal microscopy (LSCM). Confocal micrographs were taken with Leica confocal scanning system mounted into a Leica TCS SP5 (Leica Microsystem GmbH, Mannheim, Germany), equipped with a 63X oil immersion objective and spatial resolution of approximately 200 nm in x-y and 100 nm in z. After an appropriate incubation period, the cultures were removed from the incubator and the MTT (3-(4,5-dimethylthiazol-2-yl) -2,5-diphenyl tetra- zolium bromide) solution added in an amount equal to 10% of the culture volume. Then the cultures were returned to incubator and incubated for 3 hours. After the incubation period, the cultures were removed from the incubator and the resulting MTT formazan crystals were dissolved with acidified isopropanol solution to an equal culture volume. The plates were read within 1 hour after adding acidified isopropanol solution. The absorbance was spectrophotometrically measured at wavelength 570 nm and the background absorbance measured at 690 nm substracted. The percentage viability is expressed as the relative growth rate (RGR) by equation:

$$RGR = (Dsample/ Dcontrol) *100\%$$

where Dsample and Dcontrol are the absorbances of the sample and the negative control. Representative measurements of three distinct sets of data are reported (Student t- test, P < 0.05).[52]

4.2. Synthesis. General. Unless otherwise noted, all operations were carried out under a dry, oxygen-free nitrogen atmosphere. Organic solvents were dried by standard procedures. TLC was carried out with 0.2-mm thick of silica gel 60 F254 (Merck). Visualization was

accomplished by UV light or phosphomolybdic acid solution. Preparative column chromatographies was performed on glass columns of different sizes hand packed with silica gel 60 (particle sizes 0.040-0.063 mm, Merck). Phenylboronic acid pinacol ester, 4-bromo-2,1,3-benzothiadiazole, 2-(tributylstannyl)thiophene, 2-(tributylstannyl)-2:2'.bithiophene, 2,3-dibromobenzo[b]thiophene, thianaphthene, thieno[3,2-b]thiophene, tributyltin chloride, 2,5-bis(tributylstannyl)thiophene, 2-hexylthiophene, 3,4-dihexylthiophene, hydrogen peroxide solution (30 wt. % in H$_2$O), 1,1′-bis(diphenylphosphino)ferrocene palladium(II)chloride dichloromethane complex (PdCl2dppf),n-butyllithium 2.5 M solution in hexane, N-bromosuccinimide, sodium bicarbonate, tributylstannyl chloride, potassium tert-butoxide and trifluoroacetic acid were purchased from Sigma-Aldrich Co; 2-isopropoxy-4,4,5,5-tetramethyl-1,3,2-dioxaborolane, Bis(pinacolato)diboron from Alfa Aesar GmbH & Co KG. All reagents and solvents were used as received. Microwave experiments were carried out in a Milestone Microsynth Labstation operating at 2450 MHz monitored by a proprietary control unit. The oven was equipped with magnetic stirring, pressure and temperature sensors. Reactions were performed in a glass vessel (capacity 10 mL) sealed with a septum. The microwave method was power controlled (100 W maximum power input) and the samples were irradiated with the required power output (setting at the maximum power) to achieve the desired temperature (80°C). Reactions with ultrasound were performed in a FALC LBS1 50KHz Ultrasonic bath. Melting points were determined on Kofler bank apparatus and are uncorrected. All 1H NMR and 13C NMR spectra were recorded on a Varian Mercury-400 spectrometer equipped with a 5-mm probe. Chemical shifts were calibrated using the internal CDCl$_3$ resonance which was referenced to TMS. Mass spectra were collected on a Thermo Scientific TRACE 1300 gas chromatograph. UV-Vis spectra were recorded using a Agilent Technologies CARY 100 UV-Vis spectrophotometer. Photoluminescence spectra were collected on a Perkin Elmer LS50 spectrofluorometer. Fluorescence measurements were performed using an excitation wavelength corresponding to the maximum absorption lambda. Ultrasound assisted reactions were performed on a ELMASONIC S 40 (H).

General procedure for the synthesis of bromothienyl-derivatives: To a solution of the starting materials (1 mmol) in CH$_2$Cl$_2$: CH$_3$COOH (6:4 v/v), 1 mmol or 2 mmol of NBS were added. The reaction mixture was sonicated for 30 min at room temperature. The solvent was removed and the products were purified by flash chromatography on silica gel.

2,5-dibromo-3,4-diphenylthiophene → Cyclohexane: CH$_2$Cl$_2$ (80:20). Yield 100%. Pale yellow solid; EI-MS m/z 394 (M+); 1H NMR (400 MHz, CDCl$_3$, TMS/ppm): δ 7.25-7.22 (m, 6H), 7.07-7.05 (m, 4H).

2-bromobenzo[b]thiophene → EI-MS m/z 213(M+); 1H NMR (400 MHz, CDCl$_3$, TMS/ppm): δ 7.87-7.83 (m, 2H), 7.50-7.40 (m, 3H).

2-bromo-3,4-dihexylthiophene 1,1-dioxide → EI-MS m/z 362(M+); 1H NMR (400 MHz, CDCl$_3$, TMS/ppm): δ 6.41 (s, 2H), 2.39-2.34 (m, 4H), 1.57-1.29 (m, 16H), 0.92-0.88 (m, 6H).

2,6-dibromo-3,5-dimethyldithieno[3,2-b:2',3'-d]thiophene → White solid;EI-MS m/z 382(M+); 1H NMR (400 MHz, CDCl$_3$, TMS/ppm): δ 2.37 (s, 6H).

2,5-dibromothieno[3,2-b]thiophene → EI-MS m/z 298 (M+); 1H NMR (400 MHz, CDCl$_3$, TMS/ppm): δ 7.17 (s, 2H).

5-bromo-3',4'-diphenyl-[2,2':5',2''-terthiophene] 1'-oxide (1a4) → Cyclohexane : CH$_2$Cl$_2$: AcOEt (70:25:5). Yield 60%. Dark orange solid; EI-MS m/z 494(M+); 1H NMR (400 MHz, CDCl$_3$, TMS/ppm): δ 7.63 (d, J=3.6, 1H), 7.63 (d, J=3.6, 1H), 7.35-7.27 (m, 6H), 7.13-7.12 (m, 4H), 7.06 (dd, 3J=3.6Hz, 3J=1.2 Hz, 1H), 7.02 (d, J=3.6, 1H).

5-bromo-3',4'-diphenyl-[2,2':5',2''-terthiophene] 1',1'-dioxide (1b4) → Cyclohexane : CH$_2$Cl$_2$ (70:30). Yield 74%. Dark orange solid; EI-MS m/z 511(M+); 1H NMR (400 MHz, CDCl$_3$, TMS/ppm): δ 7.74 (d, 3J=4 Hz, 4J=1.2 Hz, 1H), 7.51 (d, J=4, 1H), 7.34-7.25 (m, 6H), 7.11-7.06 (m, 6H), 7.02 (d, J=4, 1H).

5,5''-dibromo-3,3'',4,4''-tetrahexyl-[2,2':5',2''-terthiophene]-1,1,1'',1''-tetraoxide (10b2) → Cyclohexane : CH$_2$Cl$_2$: AcOEt (65:30:5). Yield 60%. Pale orange solid; EI-MS m/z 804 (M+); 1H NMR (400 MHz, CDCl$_3$, TMS/ppm): δ 7.67 (s, 2H), 2.67-2.63 (m, 4H), 2.49-2.45 (m, 4H), 1.62-1.24 (m, 32H), 0.92-0.84 (m, 12H).

General procedure for the synthesis of thienyl-S-oxides and -S,S-dioxides.

METHOD A: To a solution of the starting material (1 mmol) in CH$_2$Cl$_2$/ CF$_3$COOH (2:1 v:v), were added 1 mmol of H$_2$O$_2$ (as a solution in H$_2$O 30 wt. %) for the synthesis of sulfoxide derivatives or 2 mmol of H$_2$O$_2$ (as a solution in H$_2$O 30 wt. %) for the synthesis of the sulfone derivatives. The reaction mixture was sonicated in a closed vessel by immersion in an ultrasonic bath (see table 1 for the reaction times of the different substrates). The crude product was extracted with NaHCO$_3$ sat. and the organic layers were collected. The solvent was removed under reduced pressure and the products were purified by flash chromatography.

METHOD B: To a solution of the starting material (1 mmol) in CH$_2$Cl$_2$, 2 mmol of meta-chloroperoxybenzoic acid (mCPBA) were added for the synthesis of the sulfone derivatives. The reaction mixture was sonicated in a closed vessel by immersion in an ultrasonic bath (see table 1 for the reaction times of different substrates). The solvent was removed and the products were purified by flash chromatography.

2,5-dibromo-3,4-diphenylthiophene-1-oxide (1a) → METHOD A: Cyclohexane: CH$_2$Cl$_2$: AcOEt (80:15:5). Yield 70%. Pale orange solid; EI-MS m/z 410 (M+); 1H NMR (400 MHz, CDCl$_3$, TMS/ppm): δ 7.32-7.24 (m, 6H), 7.06-7.04 (m, 4H).

2,5-dibromo-3,4-diphenylthiophene-1,1-dioxide (1b) → Cyclohexane: CH$_2$Cl$_2$: AcOEt (80:15:5). Yield 80% with METHOD A, 80% with METHOD B. Pale yellow solid; EI-MS m/z 426 (M+); 1H NMR (400 MHz, CDCl$_3$, TMS/ppm): δ 7.35-7.28 (m, 6H), 7.04-7.02 (m, 4H).

2-bromobenzo[b]thiophene-1-oxide (2a) → METHOD A: Cyclohexane: CH$_2$Cl$_2$:AcOEt (80:15:5). Yield 99%. White solid; EI-MS m/z 229 (M+); 1H NMR (400 MHz, CDCl$_3$, TMS/ppm): δ 7.92 (d, J=8 Hz, 1H), 7.66-7.54 (m, 3H), 7.27 (s, 1H).

2-bromobenzo[b]thiophene-1,1-dioxide (2b) → Cyclohexane : CH$_2$Cl$_2$: AcOEt (80:15:5). Yield 80% with METHOD A, 80% with METHOD B. White solid; EI-MS m/z 245 (M+); 1H NMR (400 MHz, CDCl$_3$, TMS/ppm): δ 7.73-7.55 (m, 4H), 6.96 (s, 1H).

2,3-dibromobenzo[b]thiophene-1-oxide (3a) → METHOD A: Cyclohexane: CH$_2$Cl$_2$: AcOEt (80:15:5). Yield 99%. White solid; EI-MS m/z 308 (M+); 1H NMR (400 MHz, CDCl$_3$, TMS/ppm): δ 7.87 (d, J=8 Hz, 1H), 7.63-7.51 (m, 3H).

2,3-dibromobenzo[b]thiophene-1,1-dioxide (3b) → Cyclohexane : CH$_2$Cl$_2$: AcOEt (80:15:5). Yield 80% with METHOD A, 80% with METHOD B. White solid; EI-MS m/z 324 (M+); 1H

NMR (400 MHz, CDCl$_3$, TMS/ppm): δ 7.76 (d, J=8 Hz, 1H), 7.69-7.65 (m, 1H), 7.61-7.57 (m, 2H).

5-bromobenzo[b]thiophene-1-oxide (4a) → METHOD A: Cyclohexane : CH$_2$Cl$_2$: AcOEt (80:15:5). Yield > 90%. White solid; EI-MS m/z 229 (M+); 1H NMR (400 MHz, CDCl$_3$, TMS/ppm): δ 7.96 (d, J=8 Hz, 1H), 7.70-7.57 (m, 3H), 7.29 (s, 1H).

5-bromobenzo[b]thiophene-1,1-dioxide (4b) → Cyclohexane : CH$_2$Cl$_2$: AcOEt (80:15:5). Yield 80% with METHOD A, 80% with METHOD B. White solid; EI-MS m/z 245 (M+); 1H NMR (400 MHz, CDCl$_3$, TMS/ppm): δ 7.74-7.56 (m, 4H), 6.97 (s, 1H).

2,6-dibromo-3,5-dimethyldithieno[3,2-b:2',3'-d]thiophene-4-oxide (5a) → METHOD A: Cyclohexane : AcOEt : CH$_2$Cl$_2$ 80:15:5. Yield 75%. Yellow solid; EI-MS m/z 398 (M+); 1H NMR (400 MHz, CDCl$_3$, TMS/ppm) 2.39 (s, 6H).

2,6-dibromo-3,5-dimethyldithieno[3,2-b:2',3'-d]thiophene-4,4-dioxide (5b) → Cyclohexane : AcOEt : CH$_2$Cl$_2$ 80:15:5. Yield 80% with METHOD A, 80% with METHOD B. Yellow microcrystals; EI-MS m/z 414 (M+); 1H NMR (400 MHz, CDCl$_3$, TMS/ppm) 2.34 (s, 6H).

2,5-dibromothieno[3,2-b]thiophene-1-oxide (6a) → METHOD A: Cyclohexane : CH$_2$Cl$_2$: AcOEt (80:15:5). Yield 30%. Pale yellow oil; EI-MS m/z 314 (M+); 1H NMR (400 MHz, CDCl$_3$, TMS/ppm): δ 7.37 (s, 1H), 7.12 (s,1H).

2,5-dibromothieno[3,2-b]thiophene 1,1-dioxide (6b) → Cyclohexane : CH$_2$Cl$_2$: AcOEt (80:15:5). Yield 80% with METHOD A, 80% with METHOD B. Pale yellow solid; EI-MS m/z 330 (M+); 1H NMR (400 MHz, CDCl$_3$, TMS/ppm): δ 7.28 (s, 1H), 7.08 (s,1H).

2,5-dibromothiophene-1,1-dioxide (7b) → Cyclohexane : CH$_2$Cl$_2$: AcOEt (80:15:5). Yield 80% with METHOD A, 80% with METHOD B. Pale yellow solid; EI-MS m/z 274 (M+); 1H NMR (400 MHz, CDCl$_3$, TMS/ppm): δ 6.91 (s, 2H).

2-bromo-5-hexylthiophene-1,1-dioxide (8b) → Cyclohexane: CH$_2$Cl$_2$: AcOEt (80:15:5). Yield 80% with METHOD A, 80% with METHOD B. Pale yellow solid; EI-MS m/z 246 (M+); 1H NMR (400 MHz, CDCl$_3$, TMS/ppm): δ 6.76 (d, J=4.8 Hz, 1H), 6.36 (d, J=4.8 Hz, 1H), 2.50 (m, 2H), 1.65 (m, 2H), 1.30 (m, 6H), 0.90 (m, 3H).

2,5-dibromo-3,4-dihexylthiophene 1,1-dioxide (9b) → Cyclohexane : CH$_2$Cl$_2$: AcOEt (80:15:5). Yield 80% with METHOD A, 80% with METHOD B. Pale yellow solid; EI-MS m/z 442 (M+); 1H NMR (400 MHz, CDCl$_3$, TMS/ppm): δ 2.41 (t, 4H), 1.53-1.28 (m, 16H), 0.89 (t, 6H).

General procedure for the synthesis of tributyl stannanes: To a solution of the starting material (1 mmol) in anhydrous THF (10 mL) at -78°C, LDA (1 mmol). The mixture was left rising to room temperature and after 1.5 h was lowered to -78°C and Bu$_3$SnCl (1.1 mmol) was added. The reaction mixture was stirred for 12 h at room temperature. The mixture was extracted with water and then the organic phase was evaporated under reduced pressure.

3',4'-dihexyl-5,5''-bis(tributylstannyl)-[2,2':5',2''-terthiophene]-1',1'-dioxide (9b3) → The compound was prepared starting from 9b2. Orange oil; EI-MS m/z 1026 (M+); 1H NMR (400 MHz, CDCl$_3$, TMS/ppm) δ 7.85 (d, 3J=3.2 Hz, 2H), 7.22 (d, 3J=3.2 Hz, 2H), 1.64-1.49 (m, 20H), 1.41-1.27 (m, 20H), 1.18-1.09 (m, 10H), 0.93-0.88 (m, 24H).

3',4'-diphenyl-5-(tributylstannyl)-[2,2':5',2''-terthiophene]-1',1'-dioxide (1b6) → The compound was prepared starting from 1b4. Yield 60%. Orange solid; EI-MS m/z 722(M+); 1H

NMR (400 MHz, CDCl$_3$, TMS/ppm): δ 7.82 (d, J=3.2, 1H), 7.74 (d, 3J=3.2 Hz, 4J=0.8 Hz, 1H), 7.3-7.24 (m, 6H), 7.12-7.09 (m, 6H), 7.06 (dd, 3J=5.6 Hz, 3J=4 Hz, 1H), 1.47-1.41 (m, 6H), 1.31-1.21 (m, 6H), 1.02-0.98 (m, 6H), 0.85 (t, 9H).

3,3'-bis(methylthio)-[2,2'-bithiophen]-5-yl)tributylstannane → Brown-yellow oil; EI-MS m/z 547 (M+); Yield 90%. 1H NMR (400 MHz, CDCl$_3$, TMS/ppm) δ 7.36 (d, 3J=5.6 Hz, 1H), 7.08 (s, 1H), 7.07 (d, 3J=5.6 Hz, 1H), 2.42-2.40 (m, 6H), 1.60-1.56 (m, 6H), 1.36-1.32 (m, 8H), 1.15-1.11 (m, 4H), 0.94-0.89 (m, 9H).

5-(tributylstannyl)-2,2'-bithiazole → Yellow oil; EI-MS m/z 457 (M+); Yield 60%. 1H NMR (400 MHz, CDCl$_3$, TMS/ppm) δ 7.88 (d, 3J=3.6 Hz, 1H), 7.79 (s, 1H), 7.40 (d, 3J=3.6 Hz, 1H), 1.63-1.53 (m, 6H), 1.38-1.09 (m, 12H), 0.92-0.88 (m, 9H).

Synthesis of 4-(4,4,5,5-tetramethyl-1,3,2-dioxaboralan-2-yl)-2,1,3-benzothiadiazole: A mixture of 4-bromo-2,1,3-benzothiadiazole (1 mmol), bis(pinacolato)diboron (1.2 mmol) and potassium acetate (2.86 mmol) was dissolved in dry 1,4-diossane (5 mL). The solution was purged with nitrogen for 20 min and then PdCl2(dppf) (0.05 mmol) was added. The reaction mixture was heated, with stirring, at 105°C. After 24h the cooled mixture was extracted with diethyl ether and the solvent was evaporated under reduced pressure. Yield 90%. Dark white solid; EI-MS m/z 287; 1H NMR (400 MHz, CDCl$_3$, ppm) δ 8.17 (d, J=6 Hz, 1H), 8.11 (d, J=9 Hz, 1H), 7.60 (t, J=6 Hz, 1H) 1.45 (s, 12H). 13C NMR: (400 MHz, CDCl$_3$, ppm) δ 157.0, 154.4, 138.5, 128.5, 124.3, 84.1, 24.7.

General procedure for the synthesis of 5a1, 5b2. A mixture of the appropriate bromo compound (1 mmol), boronic ester derivatives (3 mmol), PdCl$_2$dppf (0.05 mmol) and NaHCO$_3$ (2 mmol) in THF/water 2:1 (3 mL) was irradiated with microwaves at 80°C for 15 min. The reaction mixture was brought to room temperature and the solvent was evaporated under reduced pressure.

2,6-Diphenyl-3,5-dimethyl-dithieno[3,2-b:2',3'-d]thiophene-4-oxide (5a1) (DTTSO2Ph2) The compound was prepared starting from 5a and phenylboronic ester. → Cyclohexane : CH$_2$Cl$_2$: AcOEt (80:15:5). Yield 95% (0.390 g). Yellow solid; EI-MS m/z 392 (M+); 1H NMR (400 MHz, CDCl$_3$, TMS/ppm) δ 7.47-7.46 (m, 8H), 7.42-7.37 (m, 2H), 2.53 (s, 6H); 13C NMR (CDCl$_3$, TMS/ppm) d 149.8, 135.9, 133.3, 131.0, 128.9, 128.7, 128.2, 12.96; UV/Vis: λmax 410 nm (ε 18220 cm-1M-1), λem. 534 nm in CH$_2$Cl$_2$. IR: νmax (NaCl) 3462, 2919, 1732, 1598, 1442, 1028 cm-1.

2,6-bis(benzo[c][1,2,5]thiadiazol-4-yl)-3,5-dimethyldithieno[3,2-b:2',3'-d]thiophene   4,4-dioxide (5b2) (DTTSO2Bthia2) The compound was prepared starting from 5b and 4-(4,4,5,5-tetramethyl-1,3,2-dioxaboralan-2-yl)-2,1,3-benzothiadiazole.→ Petroleum ether : CH$_2$Cl$_2$: AcOEt (80:15:5). Yield 60%. Dark orange solid; EI-MS m/z 549 (M+); 1H NMR (400 MHz, CDCl$_3$, TMS/ppm) δ 8.07 (d, 3J=8.4 Hz, 2H), 7.74-7.67 (m, 4H), 2.55 (s, 6H); 13C NMR (400 MHz, CDCl$_3$, TMS/ppm) d 155.2, 153.1, 143.0, 137.6, 135.2, 131.2, 129.8, 129.2, 125.9, 122.0, 13.2; UV/Vis: λmax 426 nm (ε 21420 cm-1M-1), λem. 549 nm in CH$_2$Cl$_2$. IR: νmax (NaCl) 3462, 2919, 2850, 1716, 1620, 1541, 1299, 1142 cm-1.

General procedure for the synthesis of 1a5, 1b5: A mixture of the bromothienyl-derivative (1 mmol), bis(pinacolato)diboron (0.6 mmol), PdCl$_2$dppf (0.05 mmol), NaHCO$_3$ (2 mmol) in THF/water 2:1 (3 mL) was irradiated with microwaves at 80°C for 30 min. The reaction

mixture was brought to room temperature and the solvent was evaporated under reduced pressure. All compounds were purified by flash chromatography with increasing amounts of CH$_2$Cl$_2$ in cyclohexane as eluent.

3',3'''',4',4''''-tetraphenyl-[2,2':5',2'':5'',2''':5''',2''':5'''',2'''''-sexithiophene]-1',1''''-dioxide (1a5) (T6Ph2bisSO) The compound was prepared starting from 1a4. → Cyclohexane : CH$_2$Cl$_2$: AcOEt (60:35:5). Yield 70%. Deep purple solid; mp 240-242°C; EI-MS m/z 830(M+); 1H NMR (400 MHz, CDCl$_3$, TMS/ppm): δ 7.57 (d, 3J =3.6 Hz, 4J=1.2 Hz, 2H), 7.40 (d, 3J=4.4 Hz, 4J=1.6 Hz, 2H), 7.28-7.23 (m, 12H), 7.21 (d, 3J =5.2 Hz, 4J=1.2 Hz, 2H), 7.09-7.05 (m, 8H), 6.99 (dd, 3J=5.2 Hz, 3J=3.6 Hz, 2H), 6.88 (d, 3J=4.4 Hz, 4J=1.2 Hz, 2H).13C NMR: (400 MHz, CDCl$_3$) δ 140.3, 140.2, 140.15, 140.12, 139.3, 139.2, 138.94, 138.91, 138.7, 133.3, 133.1, 133.0, 132.8, 129.8, 129.4, 129.3, 129.0, 128.94, 128.9, 128.85, 128.8, 128.1, 127.3, 124.5. IR: vmax 3394, 2918, 2361, 1718, 1589, 1482, 1436, 1232, 1044, 789, 696. UV/Vis: λmax 528 nm (ε 38100 cm-1M-1) in CH$_2$Cl$_2$.

3',3'''',4',4''''-tetraphenyl-[2,2':5',2'':5'',2''':5''',2''':5'''',2'''''-sexithiophene] 1',1',1'''',1''''-tetraoxide (1b5) (T6Ph2SO2SO2) The compound was prepared starting from 1b4. → Cyclohexane : CH$_2$Cl$_2$: AcOEt (60:30:10). Yield 70%. Deep red solid; mp > 300°C; EI-MS m/z 862(M+); 1H NMR (400 MHz, CDCl$_3$, TMS/ppm): δ 7.74 (d, J =4 Hz, 2H), 7.56 (d, J=4 Hz, 2H), 7.33-7.21 (m, 10H), 7.10-7.05 (m, 14H), 6.93 (d, J=4 Hz, 2H). IR: vmax 3442, 2921, 2358, 1728, 1599, 1463, 1300, 1135, 1073, 806, 701. UV/Vis: λmax 526 nm (ε 27000 cm-1M-1 poor solubility), in CH$_2$Cl$_2$.

General procedure for the Stille cross coupling reaction: A mixture of the appropriate bromo compound (1 mmol), stannane derivatives (1 mmol or 2 mmol), Pd(PPh$_3$)$_4$ (0.05 mmol) in Toluene (10 mL) was refluxed for 24 h. The reaction mixture was brought to room temperature and the solvent was evaporated under reduced pressure. The title compound was isolated by flash chromatography on silica gel.

3,3'',4,4''-tetrahexyl-[2,2':5',2''-terthiophene] 1,1,1'',1''-tetraoxide (10b1) The compound was prepared starting from 2-bromo-3,4-dihexylthiophene 1,1-dioxide and 2,5-Bis(tributylstannyl)thiophene. → Cyclohexane : CH$_2$Cl$_2$: AcOEt (65:30:5). Yield 50%. Pale yellow solid; EI-MS m/z 644 (M+); 1H NMR (400 MHz, CDCl$_3$, TMS/ppm): δ 7.67 (s, 2H), 7.41 (s, 2H), 2.62-2.58 (m, 4H), 2.43-2.38 (m, 4H), 1.63-1.25 (m, 32H), 0.93-0.87 (m, 12H).

3',3''',4',4'''-tetrahexyl-[2,2':5',2'':5'',2''''-quinquethiophene] 1',1',1''',1'''-tetraoxide (10b3) (T5O4) The compound was prepared starting from 5,5''-dibromo-3,3'',4,4''-tetrahexyl-[2,2':5',2''-terthiophene] 1,1,1'',1''-tetraoxide and 2-(tributylstannyl)thiophene. → Cyclohexane: CH$_2$Cl$_2$: AcOEt (60:35:5). Yield 70%. Red solid; mp 95-97°C; EI-MS m/z 812(M+); 1H NMR (400 MHz, CDCl$_3$, TMS/ppm): δ 7.77-7.57 (m, 4H), 7.53 (d, 3J=5.2 Hz, 4J=1.2 Hz, 2H), 7.20 (d, 3J =5.2 Hz, 4J=4 Hz, 2H), 2.72-2.66 (m, 8H), 1.65-1.62 (m, 16H), 1.36-1.32 (m, 16H), 0.94-0.90 (m, 12H); 13C NMR (400 MHz, CDCl$_3$) δ 138.8, 137.0, 130.9, 130.8, 129.7, 129.5, 129.0, 128.4, 128.2, 31.4, 31.3, 31.0, 29.8, 29.7, 29.6, 28.7, 28.5, 27.4, 27.0, 22.6, 22.56, 14.1,14.0. IR: vmax (NaCl) 3436, 2955, 2924, 2850, 2083, 1643, 1464, 1420, 1303, 1142, 1086, 800.UV/Vis: λmax 480 nm (ε 27000 cm-1M-1) in CH$_2$Cl$_2$.

3,3'',3'''',4,4'',4''''-hexahexyl-[2,2':5',2'':5'',2''':5''',2''''-quinquethiophene]1,1,1'',1'',1'''', 1''''-hexaoxide (9b4) (T5O6)The compound was prepared starting from 2-bromo-3,4-

44

dihexylthiophene 1,1-dioxide and 3',4'-dihexyl-5,5"-bis(tributylstannyl)-[2,2':5',2"-terthiophene]1',1'-dioxide.→ Cyclohexane : CH$_2$Cl$_2$: AcOEt (65:25:10). Yield 70%. Deep red solid; mp 135-137°C; EI-MS m/z 1012(M+); 1H NMR (400 MHz, CDCl$_3$, TMS/ppm): δ 7.75 (d, 3J =4.4 Hz, 2H), 7.72 (d, 3J=4.4 Hz, 2H), 6.43 (s, 2H), 2.62-2.60 (m, 8H), 2.44-2.39 (m, 4H), 1.63-1.33 (m, 22H), 0.93-0.89 (m, 18H); 13C NMR (400 MHz, CDCl$_3$) δ 149.1, 138.7, 137.0, 131.7, 130.9, 130.8, 130.3, 129.9, 129.7, 122.6, 31.5, 31.4, 31.36, 29.7, 29.69, 28.9, 28.6, 28.5, 28.4, 27.3, 27.1, 26.9, 22.6, 22.5, 14.0. IR: νmax (NaCl) 3467, 2955, 2927, 2857, 2066, 1637, 1465, 1300, 1168, 1090, 800. UV/Vis: λmax 475 nm (ε 32700 cm-1M-1), λem. 580 nm in CH$_2$Cl$_2$.

3',4'-diphenyl-[2,2':5',2''-terthiophene] 1'-oxide (1a3) (T3PhSO)The compound was prepared starting from 1a and 2-(tributylstannyl)thiophene. → Cyclohexane: CH$_2$Cl$_2$:AcOEt (65:30:5). Yield 77%. Orange solid, mp 188-190°C; EI-MS m/z 416(M+); 1H NMR (400 MHz, CDCl$_3$, TMS/ppm): δ 7.75 (d, 3J=4 Hz, 4J=1.2 Hz, 2H), 7.31-7.25 (m, 8H), 7.11-7.09 (m, 4H), 7.06 (dd, 3J=4 Hz, 3J=5.2 Hz, 2H).13C NMR: (400 MHz, CDCl$_3$) δ 140.1, 139.2, 133.2, 133.1, 129.4, 128.9, 128.8, 128.7, 127.9, 127.2. IR: νmax (NaCl) 3460, 3102, 2929, 2362, 1605, 1420, 1051 cm-1. UV/Vis: λmax 443 nm, λem. 555 nm in CH$_2$Cl$_2$.

3',4'-diphenyl-[2,2':5',2''-terthiophene] 1',1'-dioxide (1b3) (T3PhSO2) The compound was prepared starting from 1b and 2-(tributylstannyl)thiophene. → Cyclohexane: CH$_2$Cl$_2$:AcOEt (65:30:5). Yield 77%. Orange solid, mp 228-230°C; EI-MS m/z 432(M+); 1H NMR (400 MHz, CDCl$_3$, TMS/ppm): δ 7.75 (d, 3J=3.6Hz, 4J=1.2 Hz, 2H), 7.31-7.25 (m, 8H), 7.11-7.09 (m, 4H), 7.06 (dd, 3J=5.2 Hz, 3J=3.6 Hz, 2H).13C NMR: (400 MHz, CDCl$_3$) δ 135.5, 131.5, 131.1, 129.5, 129.3, 129.2, 129.18, 129.0, 128.9, 127.4. IR: νmax (NaCl) 3450, 1613, 1420, 1301, 1143 cm-1. UV/Vis: λmax 429 nm, λem. 535 nm in CH$_2$Cl$_2$.

3',3'''',4',4''''-tetraphenyl-[2,2':5',2'':5'',2''':5''',2'''':5'''',2'''''-sexithiophene] 1',1',1''''-trioxide (1ab) (T6Ph2SOSO2) The compound was prepared starting from 1a4 and 1b6.→ Cyclohexane: CH$_2$Cl$_2$:AcOEt (60:30:10). Yield 65%. Deep purple solid; mp 270-272°C; EI-MS m/z 830(M+); 1H NMR (400 MHz, CDCl$_3$, TMS/ppm): δ 7.73 (d, 3J =3.6 Hz, 1H), 7.57-7.56 (m, 2H), 7.41-7.38 (m, 2H), 7.32-7.24 (m, 8H), 7.21-7.20 (m, 2H), 7.10-7.05 (m, 12H), 7.00 (dd, 3J=4 Hz, 3J=5.2 Hz, 1H), 6.93 (d, J=4, 1H), 6.89-6.87 (m, 1H). IR: νmax 3491, 2962, 2263, 1743, 1618, 1422, 1304, 1141,1094, 913, 797, 700. UV/Vis: λmax 527nm (ε 35000 cm-1M-1) in CH$_2$Cl$_2$.

3'',4''-diphenyl-[2,2':5',2'':5'',2''':5''',2''''-quinquethiophene] 1''-oxide (1a2) (T5Ph2SO) The compound was prepared starting from 1a and 2-(tributylstannyl)bithiophene. → Cyclohexane : CH$_2$Cl$_2$: AcOEt (60:30:10). Yield 60%. Red solid; mp 240-242°C EI-MS m/z 580 (M+); 1H NMR (400 MHz, CDCl$_3$, TMS/ppm): δ 7.47 (d, 3J =4.4 Hz, 2H), 7.72-7.27 (m, 6H), 7.19 (d, 3J=4.4 Hz, 4J=0.8 Hz, 2H), 7.12-7.08 (m, 4H), 7.06 (d, 3J =3.6 Hz, 2H), 7.02 (d, 3J =3.6 Hz, 4J=0.8 Hz, 2H), 6.95 (dd, 3J=4.4 Hz, 3J=3.6 Hz, 2H).13C NMR: (400 MHz, CDCl$_3$) δ 138.8, 132.9, 132.25, 132.12, 131.1, 129.8, 129.7, 129.3, 129.2, 129.0, 128.9, 128.8, 127.8, 125.2, 124.4, 123.8. IR: νmax 3435, 2921, 2850, 2087, 1645, 1442, 1261, 1045, 790, 698. UV/Vis: λmax 506 nm (ε 42200 cm-1M-1), λem. 620 nm in CH$_2$Cl$_2$.

3'',4''-diphenyl-[2,2':5',2'':5'',2''':5''',2''''-quinquethiophene] 1'',1''-dioxide (1b2) (T5Ph2SO2) The compound was prepared starting from 1b and 2-(tributylstannyl)

bithiophene.→ Cyclohexane : CH$_2$Cl$_2$: AcOEt (60:30:10). Yield 60%. Red solid; mp 275-277°C; EI-MS m/z 596 (M+); 1H NMR (400 MHz, CDCl$_3$, TMS/ppm): δ 7.64 (d, 3J =3.6 Hz, 2H), 7.73-7.27 (m, 6H), 7.21 (d, 3J=5.2 Hz, 4J=1.2 Hz, 2H), 7.14-7.11 (m, 6H), 7.02 (d, 3J =3.6 Hz, 4J=1.2 Hz, 2H), 6.95 (dd, 3J=5.2 Hz, 3J=3.6 Hz, 2H). 13C NMR: (400 MHz, CDCl$_3$) δ 140.8, 136.3, 135.0, 131.4, 130.9, 130.5, 129.3, 129.28, 129.2, 129.0, 128.97, 128.2, 127.9, 125.6, 124.8, 124.0. IR: vmax 3447, 2954, 2854, 2095, 1654, 1440, 1289, 1130, 1068, 793.UV/Vis: λmax 504 nm (ε 38450 cm-1M-1), λem. 615 nm in CH$_2$Cl$_2$.

2,3-di([2,2'-bithiophen]-5-yl)benzo[b]thiophene 1-oxide (3a2) (V-SOT2) The compound was prepared starting from 4a and 2-(tributylstannyl)bithiophene.→ Cyclohexane : CH$_2$Cl$_2$: AcOEt (80:15:5). Yield 85%. Orange solid, mp 150-153°C; EI-MS m/z 478 (M+); 1H NMR (400 MHz, CDCl$_3$, TMS/ppm) δ 7.96 (d, J=6.8 Hz, 1H), 7.59 (d, 3J=3.6 Hz, 1H), 7.55-7.45 (m, 2H), 7.42 (d, J=6.8 Hz, 1H), 7.30-7.28 (m, 2H), 7.26 (d, 3J=3.6 Hz, 1H), 7.22 (d, 3J=5.2 Hz, 4J=1.6 Hz, 1H), 7.16 (d, 3J=3.6 Hz, 1H), 7.14-7.12 (m, 2H), 7.06 (dd, 3J=5.2 Hz, 3J=3.6 Hz, 1H), 6.97 (dd, 3J=5.2 Hz, 3J=3.6 Hz, 1H); 13C NMR: (400 MHz, CDCl3) δ 143.6, 142.0, 141.0, 140.8, 140.0, 136.4, 136.5, 132.6, 131.5, 131.0, 130.6, 130.3, 130.0, 128.6, 128.0, 127.9, 126.3, 125.5, 125.2, 124.7, 124.5, 124.3, 124.0, 123.9. IR: vmax 3468, 3067, 2336, 1577, 1458, 1067, 1033, 838, 801, 695. UV/Vis: λmax 430 nm (ε 11900 cm-1M-1), λem. 578 nm in CH$_2$Cl$_2$. IR: vmax (NaCl) 3442, 2923, 2361, 1621, 1446, 1034 cm-1.

2,3-bis(3,3'-bis(methylthio)-[2,2'-bithiophen]-5-yl)benzo[b]thiophene 1-oxide (3a1) (V-SOT2SCH3) The compound was prepared starting from 3a and 3,3'-bis(methylthio)-[2,2'-bithiophen]-5-yl)tributylstannane.→ Cyclohexane : CH$_2$Cl$_2$: AcOEt (80:18:2). Yield 65%. Red solid, mp 105-107°C; EI-MS m/z 662 (M+); 1H NMR (400 MHz, CDCl$_3$, TMS/ppm) δ 7.97 (d, J=6.8 Hz, 1H), 7.67 (s, 1H), 7.57-7.43 (m, 3H), 7.42 (d, 3J=5.2 Hz, 1H), 7.37 (d, 3J=5.2 Hz, 1H), 7.22 (s, 1H), 7.09 (d, 3J=5.2 Hz, 1H), 7.04 (d, 3J=5.2 Hz, 1H), 2.46-2.36 (m, 12H); 13C NMR: (400 MHz, CDCl$_3$) δ 143.3, 142.2, 139.6, 134.4, 134.1, 134.0, 133.9, 133.6, 133.4, 132.6, 132.5, 131.5, 131.4, 131.3, 130.9, 129.8, 129.5, 129.4, 129.2, 128.9, 126.6, 126.5, 126.3, 124.1, 18.9, 18.8, 18.7, 18.6. IR: vmax (NaCl) 3430, 3078, 2917, 2361, 1654, 1560, 1432, 1314, 1158, 1064, 1036, 970, 844, 717. UV/Vis: λmax 430 nm (ε 12800 cm-1M-1), λem. 602 nm in CH$_2$Cl$_2$.

2,3-bis(3,3'-bis(methylthio)-[2,2'-bithiophen]-5-yl)benzo[b]thiophene 1,1-dioxide (3b1) (V-SO2T2SCH3) The compound was prepared starting from 4b and 3,3'-bis(methylthio)-[2,2'-bithiophen]-5-yl)tributylstannane.→ Cyclohexane: CH$_2$Cl$_2$:AcOEt (80:18:2). Yield 60%. Red solid, mp 178-180°C; EI-MS m/z 678 (M+); 1H NMR (400 MHz, CDCl$_3$, TMS/ppm) δ 7.85 (d, J=6.8 Hz, 1H), 7.77 (s, 1H), 7.63-7.52 (m, 2H), 7.47 (d, J=6.8 Hz, 1H), 7.44 (d, 3J=5.6 Hz, 1H), 7.38 (d, 3J=5.2 Hz, 1H), 7.25 (s, 1H), 7.10 (d, 3J=5.6 Hz, 1H), 7.05 (d, 3J=5.2 Hz, 1H), 2.48-2.36 (m, 12H); 13C NMR: (400 MHz, CDCl$_3$) δ 135.3, 135.2, 134.7, 134.2, 134.18, 134.1, 134.0, 133.8, 133.5, 131.7, 131.6, 131.5, 129.9, 129.86, 129.8, 129.7, 129.5, 129.2, 128.0, 127.1, 126.8, 126.7, 124.0, 121.5 19.0, 18.8, 18.77, 18.7. IR: vmax (NaCl) 3435, 3078, 2918, 2361, 1654, 1580, 1420, 1303, 1154, 1121, 1054, 970, 845, 718. UV/Vis: λmax 435 nm (ε 12500 cm-1M-1), λem. 642 nm in CH$_2$Cl$_2$

2,3-di([2,2'-bithiazol]-5-yl)benzo[b]thiophene 1-oxide (3a3) (V-SOT2DTZ). The compound was prepared starting from 3a and 5-(tributylstannyl)-2,2'-bithiazole.→Cyclohexane:

CH$_2$Cl$_2$:AcOEt (80:15:5). Yield 40%. Yellow solid, mp 210-212°C; EI-MS m/z 482 (M+); 1H NMR (400 MHz, CDCl$_3$, TMS/ppm) δ 8.43 (s, 1H), 8.04-8.02 (m, 1H), 7.99 (s, 1H), 7.95 (d, J=3.2 Hz, 1H), 7.86 (d, J=3.2 Hz, 1H), 7.59-7.57 (m, 2H), 7.56 (d, J=3.2 Hz, 1H), 7.48 (d, J=3.6 Hz, 1H), 7.41-7.39 (m, 1H); 13C NMR: (400 MHz, CDCl$_3$) δ 164.6, 163.4, 160.8, 160.7, 145.8, 145.1, 144.3, 144.0, 142.7, 138.9, 132.9, 130.7, 129.7, 129.4, 127.9, 126.7, 124.0, 121.9. IR: νmax 3418, 3073, 2918, 2360, 1715 1540, 1471, 1374, 1251, 1062, 1036, 918, 870. UV/Vis: λmax 404 nm (ε 19500 cm-1M-1), λem. 530 nm in CH$_2$Cl$_2$.

2,3-di([2,2'-bithiazol]-5-yl)benzo[b]thiophene 1,1-dioxide (3b3) (V-SO2T2DTZ). The compound was prepared starting from 4b and 5-(tributylstannyl)-2,2'-bithiazole.→ Cyclohexane : CH$_2$Cl$_2$: AcOEt (80:15:5). Yield 40%. Yellow solid, mp 150-153°C; EI-MS m/z 498 (M+); 1H NMR (400 MHz, CDCl$_3$, TMS/ppm) δ 8.52 (s, 1H), 8.01 (s, 1H), 7.96 (d, 3J=3.2 Hz, 1H), 7.92-7.89 (m, 1H), 7.86 (d, 3J=3.2 Hz, 1H), 7.65-7.62 (m, 2H), 7.57 (d, 3J=3.2 Hz, 1H), 7.49 (d, 3J=3.2 Hz, 1H), 7.42-7.40 (m, 1H); 13C NMR: (400 MHz, CDCl$_3$) δ 165.2, 163.8, 160.6, 160.4, 146.2, 145.5, 144.4, 144.3, 135.3, 134.4, 133.7, 132.6, 130.9, 127.3, 126.2, 124.9, 123.9, 122.4, 122.3, 121.9; IR: νmax 3467, 2074, 1637, 1307, 1250, 1157, 1052, 920, 868. UV/Vis: λmax 401 nm (ε 12800 cm-1M-1), λem. 470 nm in CH$_2$Cl$_2$.

3,3'',4,4''-tetrahexyl-2,2':5',2''-terthiophene (T3hex4) The compound was prepared starting from 2-bromo-3,4-dihexylthiophene and 2,5-Bis(tributylstannyl)thiophene.→ Cyclohexane : CH$_2$Cl$_2$ (90:10). Yield 65%. Yellow oil; EI-MS m/z 584 (M+); 1H NMR (400 MHz, CDCl$_3$, TMS/ppm) δ 7.04 (s, 2H), 6.86 (s, 2H), 2.71 (t, 4H), 2.53 (t, 4H), 1.68-1.62 (m, 4H), 1.57-1.51 (m, 4H), 1.43-1.29 (m, 24H), 0.93-0.87 (m, 12H)

3',3'',4',4'''-tetrahexyl-2,2':5',2'':5'',2''':5''',2''''-quinquethiophene (T5Hex4) The compound was prepared starting from 5,5''-dibromo-3,3'',4,4''-tetrahexyl-2,2':5',2''-terthiophene and 2-(tributylstannyl)thiophene → Cyclohexane : CH$_2$Cl$_2$ (90:10). Yield 70%. Yellow solid; EI-MS m/z 748 (M+); mp <50. 1H NMR (400 MHz, CDCl$_3$, TMS/ppm) δ 7.31 (d, 3J=5.2 Hz, 4J=1.2 Hz, 2H), 7.14 (d, 3J=3.6 Hz, 4J=1.2 Hz, 2H), 7.08 (s, 2H), 7.07 (dd, 3J=3.6 Hz, 3J=5.2 Hz, 2H), 2.76-2.68 (m, 8H), 1.62-1.54 (m, 8H), 1.46-1.30 (m, 24H), 0.92-0.89 (m, 12H)
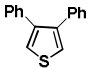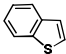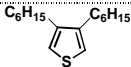
Synthesis of polymers 1a1, 1b1 and 5a2

PSOSO2 (5a2). The compound was prepared starting from 5a and 3',4'-dihexyl-5,5''-bis(tributylstannyl)-[2,2':5',2''-terthiophene]1',1'-dioxide → Yield 70%. Dark violet solid, mp > 300°C; 1H NMR (400 MHz, CDCl$_3$, TMS/ppm) δ 7.80-7.70 (m), 7.60-7.50 (m), 7.40-7.24 (m), 2.75-2.70 (m), 1.70-1.14 (m), 0.98-0.92 (m). GPC: Mn= 30700, Mw = 40800, PDI = 2.06, DP = 55. UV/Vis: λmax 550 nm in CH$_2$Cl$_2$. Td 160.1 °C (34.2% residual weight). Tg= -46.51. IR νmax 3418, 2923, 1731, 1644, 1455, 1380, 1299, 1260, 1139, 1057, 799, 699. Mn = 30700, Mw/Mn = 2.1, DPn = 44 (Determined by GPC in THF and polystyrene standard);Td = 208°C (Determined by TGA under nitrogen); Tg = 34.2°C (Determined by DSC)

PSO (1a1)The compound was prepared starting from 1a and 2,5-bis(tributylstannyl)thiophene. → Yield 60%. Dark blue solid, mp > 300°C; 1H NMR (400 MHz, CDCl$_3$, TMS/ppm) δ 7.73-7.68 (m), 7.31-7.21 (m), 7.15-7.09 (m), 7.06-6.92 (m), 6.84-6.81 (m), 6.77-6.70 (m). GPC: Mw 5881 Mn 3213, PDI = 1.83, DP = 17. UV/Vis: λmax 625 nm in CH$_2$Cl$_2$. Td 171.9 °C (69.4% residual weight). IR: νmax 3467, 2922, 2362, 1721, 1619, 1441, 1054. Mn(g/mol) = 5100,

Mw/Mn = 1.7, DPn = 15 (Determined by GPC in THF and polystyrene standard); Td = 153°C (Determined by TGA under nitrogen).

*PSO2 (1b1)*The compound was prepared starting from 1b and 2,5-Bis(tributylstannyl) thiophene. → Yield 60%. Dark blue solid, mp > 300°C; 1H NMR (400 MHz, CDCl₃, TMS/ppm) δ 7.73-7.68 (m), 7.31-7.21 (m), 7.15-7.09 (m), 7.06-6.92 (m), 6.84-6.81 (m), 6.77-6.70 (m). GPC: Mw 5320 Mn 2907, PDI = 1.83, DP = 15. UV/Vis: λmax 610 nm in CH₂Cl₂. Td 158.0 °C (38.5% residual weight). IR: vmax 3461, 2921, 1612, 1619, 1439, 1309, 113 Characteristics of polymers **1a1**, **1b1** and **5a2**. Mn = 4200, Mw/Mn = 1.8, DPn = 12 (Determined by GPC in THF and polystyrene standard);Td = 153°C (Determined by TGA under nitrogen).

Table S2. Reagents and conditions for the ultrasound assisted synthesis of thiophene-S-oxides and –S,S-dioxides

|	Starting Material	Product	Experimental Conditions	Time (min)	Yield (%)
11	Ph ⟍ Ph (thiophene, S)	**SO**	CH₂Cl₂:CF₃COOH 2:1/ H₂O₂ **1eq**	20	60
		SO2	CH₂Cl₂:CF₃COO 2:1 / H₂O₂ **2eq**	20	75
			CH₂Cl₂ / MPCBA **2 eq**	20	75
12	(benzothiophene, S)	**SO**	CH₂Cl₂:CF₃COOH 2:1/ H₂O₂ **1eq**	15	>90
		SO2	CH₂Cl₂:CF₃COO 2:1 / H₂O₂ **2eq**	15	>90
			CH₂Cl₂ / MPCBA **2 eq**	45	>90
13	C₆H₁₅ ⟍ C₆H₁₅ (thiophene, S)	**SO2**	CH₂Cl₂:CF₃COO 2:1 / H₂O₂ **2eq**	15	80
			CH₂Cl₂ / MPCBA **2 eq**	60	45

4.3. Cyclic Voltammetry
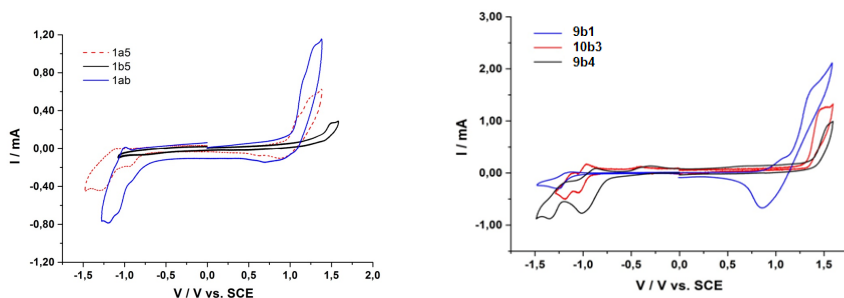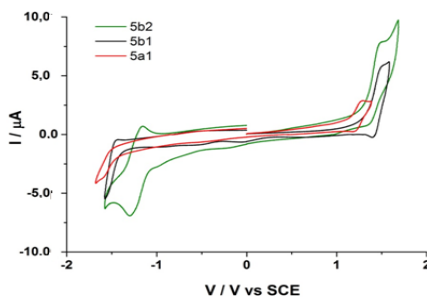
Figure S19-S20-S21. Cyclic voltammetry of hexamers 1a5, 1b5 and 1ab, pentamers 9b1, 10b3 and 9b4 and dithienothiophene derivative 5a1, 5b1 and 5b2 respectively.
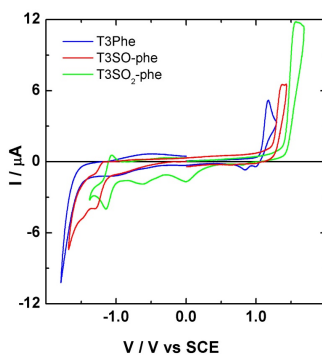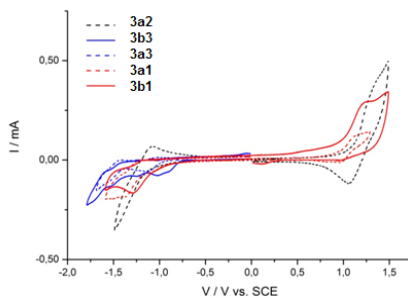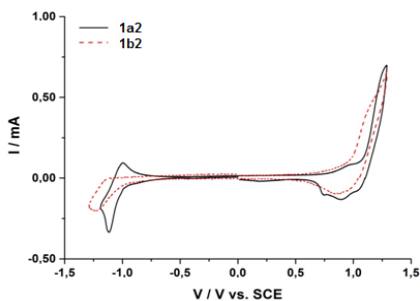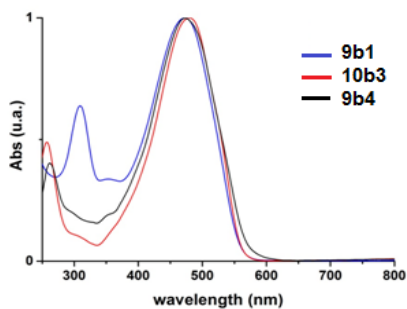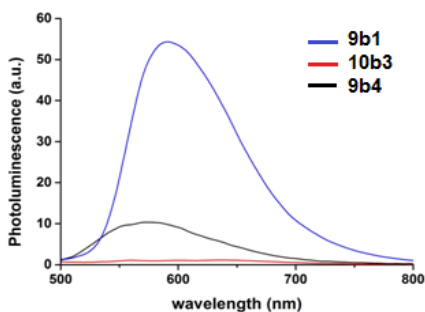

Figure S22- S23- S24. Cyclic voltammetry of pentamers 1a2 and 1b2, V-shaped oligomers 3a2, 3b3, 3a3, 3a1 and 3b1 and trimers 1a3 (T3SO-Phe), 1b3 (T3SO$_2$-Phe) and the corresponding non oxygenated terthiophene (T3Phe) respectively.

4.4. Optical properties

Table S3. Absorption (λ_{max}, nm) and emission (λ_{PL}, nm) wavelengths and molar coefficients (ε, cm^{-1}mol^{-}1) in CHCl$_3$ of compounds.

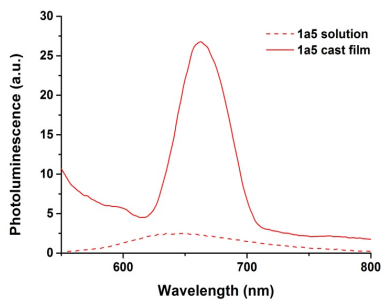| Item	λ_{max}	λ_{PL}	ε	Tag	Item	λ_{max}	λ_{PL}	ε
1a1	622			DTTSOPh	5a1	409	534	18200
1b1	612			DTTSO2Ph	5b1	408	514	
5a2	548			DTTSO2BT	5b2	426	549	21400
1a3	443	555	7553	T5O2	8b1	470	590	
1b3	429	535	9164	T5O4	9b2	480		27000
1b5	528	650,662(solid)	38100	T5O6	8b3	475	580	32700
1b5	526	~650	27000					
1ab	527	~650	35000					
1a2	506	620	42200					
1b2	504	615	38450					
3a1	428	602	12800					
3b1	435	642	12500					
3a2	430	578	11900					
3b2	429	520	10700					
3a3	404	530	19500					
3b3	401	470	12800					

Figure S25. Absorption and emission spectra of pentamers 9b1, 10b3 and 9b4 ~10^{-5} M in CH_2Cl_2
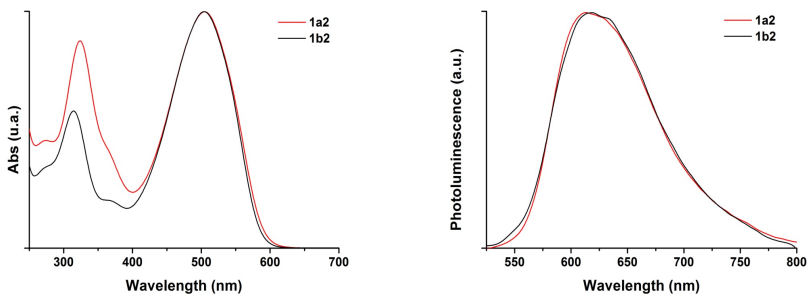

Figure S26. Absorption and emission spectra of pentamers 1a2 and 1b2 ~10^{-5} M in CH_2Cl_2.
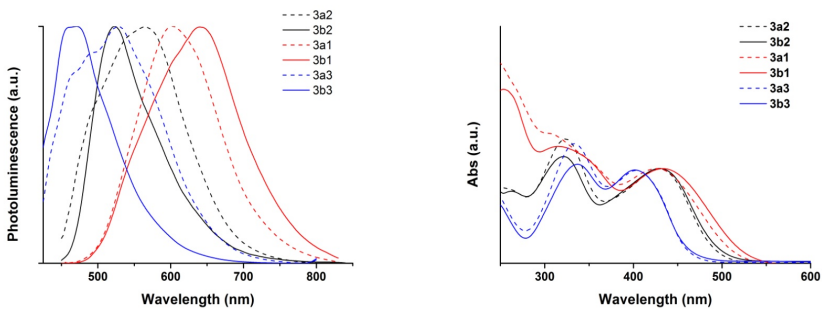
Figure S27. Absorption and emission spectra of V-shaped compounds ~10^{-5} M in CH_2Cl_2
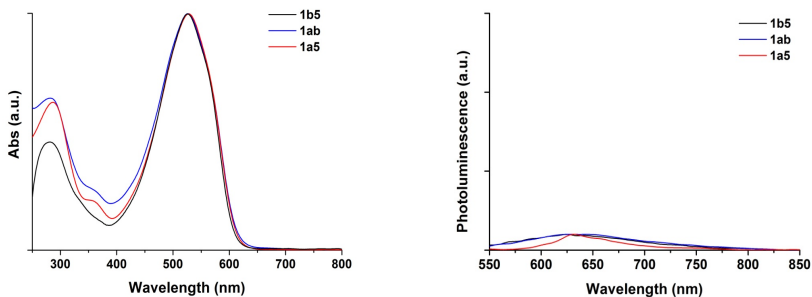
Figure S28. Absorption and emission spectra of hexamers 1a5, 1b5 and 1ab ~10^{-5} M in CH$_2$Cl$_2$.
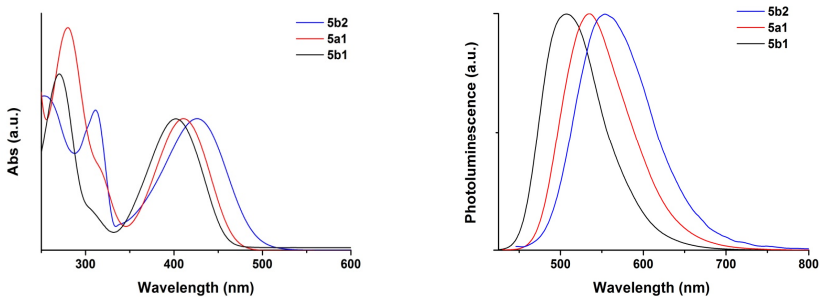
Figure S29. Absorption and emission spectra of dithienothiophene derivatives 5a1, 5b1 and 5b2 ~10^{-5} M in CH$_2$Cl$_2$.
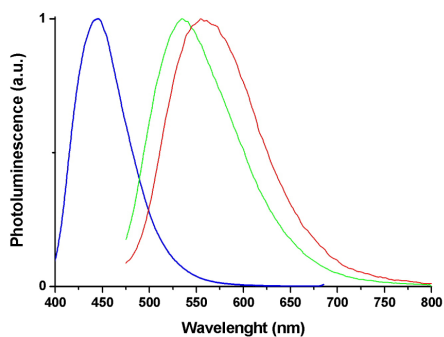
Figure S30. Photoluminescence spectra of 1a3 (red), 1b3 (green) and the corresponding non oxygenated terthiophene (blue) ~10^{-5} M in CH$_2$Cl$_2$.

4.5. Photophysical characterization and and electroluminescence properties of V-shaped oligomers 3a1 and 3b1
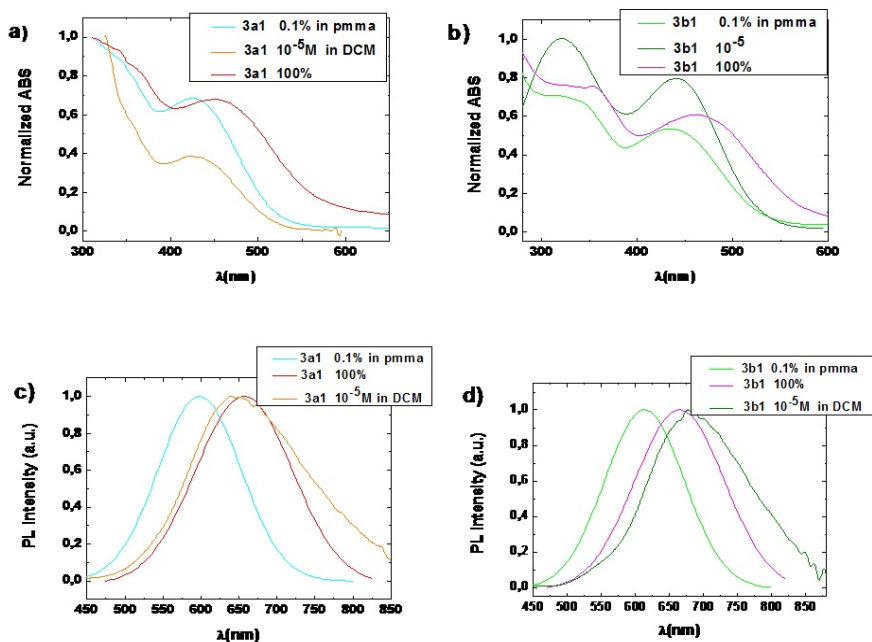
Figure S31. Photophysical characterization of 3a1 and 3b1 1.0×10^{-5} M in DCM, thin film 0.1wt% in PMMA and neat film: a), b) normalized absorption spectra, c), d) normalized photoluminescence spectra.
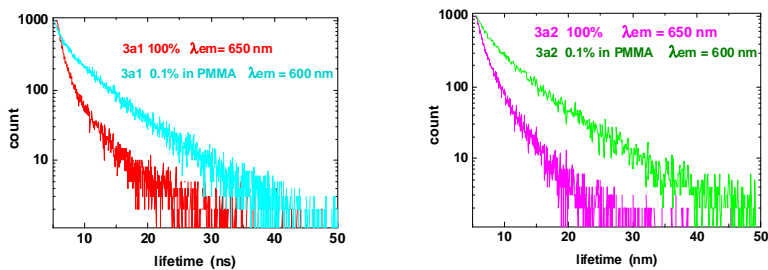
Figure S32. Decay times of 3a1 and 3b1 0.1% in PMMA and in neat films.

The complete OLED structures:

SO_OLED_1:   ITO / PEDOT:PSS / **3a1 neat film** / TPBI / Bphen:Cs / Ag

SO_OLED_2:   ITO / PEDOT:PSS / **BCPO:3a1 15wt%** / TPBI / Bphen:Cs / Ag

SO_OLED_3:   ITO / PEDOT:PSS / **TPBI:3a1 15wt%** / TPBI / Bphen:Cs / Ag

SO$_2$_OLED_1:   ITO / PEDOT:PSS / **3b1 neat film** / TPBI / Bphen:Cs / Ag

SO$_2$_OLED_2:   ITO / PEDOT:PSS / **BCPO:3b1 15wt%** / TPBI / Bphen:Cs / Ag

SO$_2$_OLED_3:   ITO / PEDOT:PSS / **TPBI:3b1 15wt%** / TPBI / Bphen:Cs / Ag
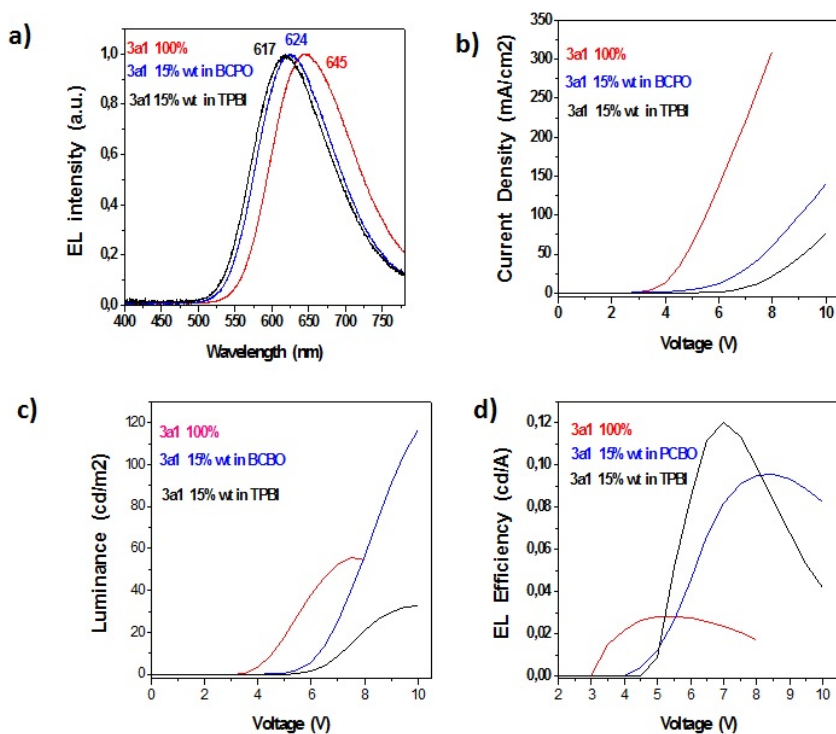
Figure S33. Electrical characterization of 3a1 based OLEDs.

Figure S34. Electrical characterization of 3b1 based OLEDs.

4.6. Structural data of 1a5

Table S4. Crystal Data and Structure Refinement for Compound A.

compound	A
formula	$C_{48}H_{30}O_2S_6$
FW	831.08
Crystal symmetry	Monoclinic
Space group	$P2_1/c$
a, Å	10.748(5)
b, Å	8.699(4)
c, Å	25.388(11)
α, °	90

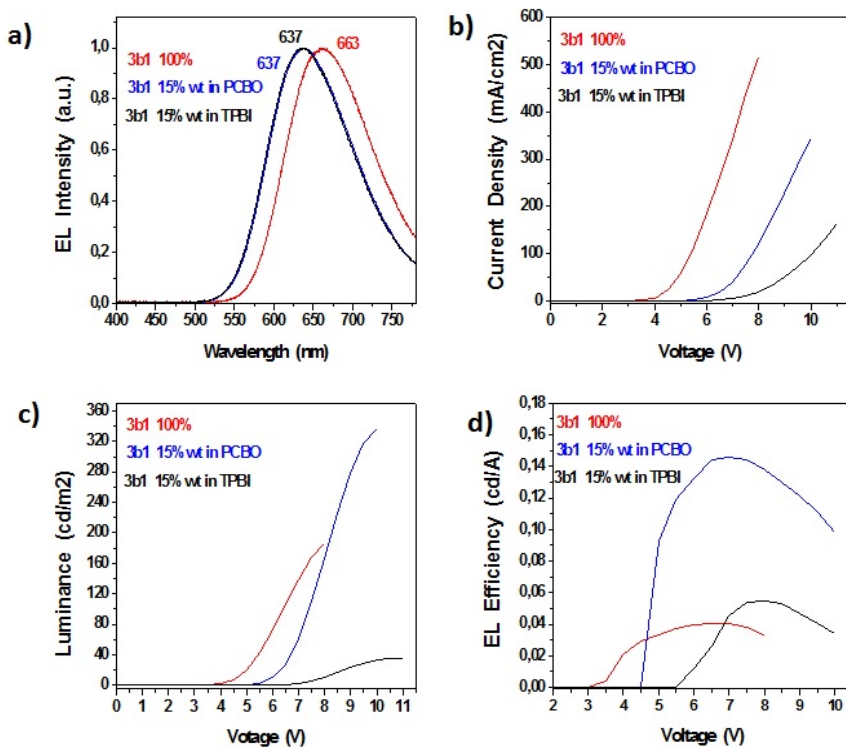|	
β, °	94.919(4)
γ, °	90
cell volume, Å^3	2365.0(17)
Z	2
D_c, Mg m^{-3}	1.167
μ(Mo Kα), mm^{-1}	0.324
F(000)	860
crystal size, mm	0.20×0.10×0.05
T, K	296
θ limits, °	1.61-24.87
Refl. collected	12171
unique refl. (R_{int})	3922 [R(int) = 0.0844]
GooF on F^2	0.892
$R_1(F)^a$, $wR_2(F^2)^b$	0.0753, 0.1697
largest diff. peak and hole, e Å^{-3}	0.251 and -0.297

[a] $R_1 = \sum||F_o| - |F_c|/\sum|F_o|$. [b] $wR_2 = [\sum w(F_o^2 - F_c^2)^2/\sum w(F_o^2)^2]^{1/2}$, where w = $1/[\sigma^2(F_o^2) + (aP)^2 + bP]$ where P = $(F_o^2 + 2F_c^2)/3$. CCDC number 1445836 contains the supplementary crystallographic data for this paper. These data can be obtained free of charge from The Cambridge Crystallographic Data Center via www.ccdc.cam.ac.uk/data_request/cif.

REFERENCES

[1] (a) Magurudeniya HD, Huang P, Gunathilake SS, Rainbolt EA, Biewer MC, Stefan MC. Encyclopedia of Polymer Science and Technology. **2014**, John Wiley & Sons, Inc., 1-36. (b) Huynha TP, Sharma PS, Sosnowska M, D'Souza F, Kutnera W. *Progress in Polymer Science,* **2015**, 47, 1-25. (c) Cinar ME, Ozturk T. *Chem. Rev.* **2015**, 115, 3036-3140. (d) Dou L, Liu Y, Hong Z, Li G, Yang Y. *Chem. Rev.* **2015**, 115, 12633-12665. (e) Iyoda M, Shimizu H. *Chem. Soc. Rev.*, **2015**, 44, 6411-6424. (f) Rasmussen SC, Evenson SJ, McCausland CB. *Chem. Commun.* **2015**, 51, 4528-4543. (g) Handbook of Thiophene-Based Materials: Applications in Organic Electronics and Photonics. Perepichka I, Perepichka DF. Eds. **2009**, John Wiley & Sons, Ltd. (h) Thiophenes (Topics in Heterocyclic Chemistry) **2015** Edition. Joule. J. A. Editor, Springer International Publishing Switzerland 2015.
[2] (a) Malytskyi V, Simon JJ, Patrone L, Raimundo JM. *RSC Adv.,* **2015**, 5, 354-397. (b) Qin P, Kast H, Nazeeruddin MK, Zakeeruddin SM, Mishra A, Bäuerle P, Grätzel M. *Energy Environ. Sci.,* **2014**, 7, 2981-2985.
[3] (a) Takimiya K, Osaka I, Mori T, Nakano M. *Acc. Chem. Res.,* **2014**, 47, 1493-1502. (b) Ashraf RS, Kronemeijer AJ. *Chem. Commun.*, **2012**, 48, 3939-3941. (c) Facchetti A. *Chem. Mater.,* **2011**, 23, 733-758.

[4] (a) Johansson LBG, Simon R, Bergström G, Eriksson M, Prokop S, Mandenius CF, Heppner FL, Åslund AKO, Nilsson KPR. *Biosensors and Bioelectronics,* **2015**, 63, 204-211. (b) Ciéslar-Pobuda A, Bäck M, Magnusson K, Jain MV, Rafat M, Ghavami S, Nilsson KPR, Łos MJ. *Cytometry Part A,* **2014**, 85A, 628-635. (c) Ries J, Udayar V, Soragni A, Hornemann S, Nilsson KPR, Riek R, Hock C, Ewers H, Aguzzi AA, Rajendran L. *ACS Chem. Neurosci.,* **2013**, 4, 1057-1061.

[5] Dal Molin M, Verolet Q, Colom A, Letrun R, Derivery E, Gonzalez-Gaitan M, Vauthey, E, Roux A, Sakai N, Matile S. *J. Am. Chem. Soc.,* **2015**, 137, 568-571.

[6] (a) Nakayama J, Sugihara Y. *Sulfur Reports,* **1997**, 19, 349-375. (b) Pouzet P, Erdelmeier I, Ginderow DJP, Mornon P, Dansette PM, Mansuy D. *J. Chem. Soc., Chem. Commun.,* **1995**, 473-474. (c) Bongini A, Barbarella G, Zambianchi M, Arbizzani C, Mastragostino M. *Chem. Commun.,* **2000**, 439-440. (d) Thiemann T, Dongol KG. *J. Chem. Research (M),* **2002**, 0701–0719.

[7] (a) Nakayama J, Nagasawa H, Sugihara Y, Ishii A. *J. Am. Chem. Soc.*, **1997**, 119, 9077-9078. (8b) Nakayama J. *Sulfur Reports*, **2000**, 22, 123-149. (c) Nakayama J, Sano Y, Sugihara, Y, Ishii A. *Tetrahedron Letters*, **1999**, 40, 3785-3788.

[8] Stoffregen A, Heying M, Jenks WS. *J. Am. Chem. Soc.*, **2007**, 129, 15746-15747.

[9] (a) Barbarella G, Favaretto L, Zambianchi M, Pudova O, Arbizzani C, Bongini A, Mastragostino M. *Adv. Mater.*, **1998**, 10, 551-554. (b) Barbarella G, Favaretto L, Sotgiu G, Zambianchi M, Antolini L, Pudova O, Bongini A. *J.Org.Chem.*, **1998**, 63, 5497-5506. (c) Bongini A, Barbarella G, Zambianchi M, Arbizzani C, Mastragostino M. *Chem. Commun.,* **2000**, 439-440. (d) Antolini L, Tedesco E, Barbarella G, Favaretto L, Sotgiu G, Zambianchi M, Casarini D, Gigli G, Cingolani R. *J. Am. Chem. Soc.,* **2000**, 122, 9006-9013. (e) Antolini L, Tedesco E, Barbarella G, Favaretto L, Sotgiu G, Zambianchi M, Casarini D, Gigli, G, Cingolani R. *J. Am. Chem. Soc.,* **2000**, 122, 9006-9013.

[10] (a) Biwang J, Tilley TD. *J. Am. Chem. Soc.,* **1999**, 121, 9744-9745. (b) Su MC, Biwang J, Tilley TD. *Angew. Chem. Int. Ed.,* **2000**, 39, 2870-2873.

[11] (a) Rozen S, Bareket Y. *J. Org. Chem.,* **1997**, 62, 1457-1462. (b) Amir E, Rozen S. *Angew. Chem. Int. Ed.*, **2005**, 44, 7374-7378. (c) Shefer N, Harel T, Rozen S. *J. Org. Chem.,* **2009**, 74, 6993-6998. (d) Rozen S. *Acc. Chem. Res.,* **2014**, 47, 2378-2389.

[12] (a) Dell EJ, Capozzi B, Xia J, Venkataraman L, Campos LM. *Nat. Chem.,* **2015**, 7, 209-214. (b) Busby E, Xia J, Wu Q, Low JZ, Song R, Miller JR, Zhu XY, Campos LM, Sfeir MY. *Nat. Mater.,* **2015**, 14, 426-433. (c) Capozzi B, Xia J, Adak O, Dell EJ, Liu ZF, Taylor JC, Neaton JB, Campos LM, Venkataraman L., *Nat. Nanotechnol.* **2015**, 10, 522-527. (d) Busby E, Xia J, Low JZ, Wu Q, Hoy J, Campos LM, Sfeir MY. *J. Phys. Chem. B*, **2015**, 119, 7644-7650. (e) Dell EJ, Campos LM. *J. Mater. Chem.,* **2012**, 22, 12945-12952.

[13] Moreno Oliva M, Casado J, LópezNavrrete JT, Patchkovskii S, Goodson T, Harpham MR, SeixasdeMelo JS, Amir E, Rozen S. *J. Am. Chem. Soc.,* **2010**, 132,6231-6242.

[14] Ghofraniha N, Viola I, Di Maria F, Barbarella G, Gigli G, Leuzzi L, Conti C. *Nat. Commun.,* **2015**, 6, article 6058.

[15] (a) Palamà IE, Di Maria F, D'Amone S, Barbarella G, Gigli G. *J. Mater. Chem. B*, **2015**, 3, 151-158. (b) Ji P, Xu X, Ma S, Fan J, Zhou Q, Mao X, Qiao C. *ACS Med. Chem. Lett.,* **2015**, 6,

1010-1014. biology 2015. (c) Palamà IE, Di Maria F, Viola I, Fabiano E, Gigli G, Bettini C, Barbarella G. *J. Am. Chem. Soc.,* **2011**, 133, 17777–17785.

[16] Santato C, Favaretto L, Melucci M, Zanelli A, Gazzano M, Monari M, Isik D, Banville D, Bertolazzi S, Loranger S, Cicoira F. *J.Mater.Che*m., **2010**, 20,669-676.

[17] (a) Lindley J, Mason T. *J. Chem. Soc. Rev.,***1987**,16, 275-311. (b) Arsenyan P, Paegle E, Belyakov S. *Tetrahedron Lett.,* **2010**, 51, 205-208.

[18] (a) Kappe CO. *Angew Chem Int Ed.*, **2004**, 43, 6250-6284. (b) Melucci M, Barbarella G, Zambianchi M, Di Pietro P, Bongini, A. *J. Org. Chem.*, **2004**, 69, 4821-4828.

[19] Pouzet P, Erdelmeier I, Ginderow D, Mornon JP, Dansette P, Mansuy D. *J., Chem. Soc., Chem. Commun.,* **1995**, 473-474.

[20] Barbarella G, Favaretto L, Sotgiu G, Zambianchi M, Arbizzani C, Bongini A, Mastragostino M. *Chem.Mater.,* **1999**, 11, 2533-2541.

[21] Raasch S. Chemistry of Heterocyclic Compounds, Thiophene and its Derivatives, ed. S. Gronowitz, Wiley, New York, **1985**, 44, 871.

[22] Rozen S, Bareket Y. *J. Org. Chem.,* **1997**, 62, 1457-1462.

[23] Furukawa N, Hoshiai H, Shibutani T, Higaki M, Iwasaki F, Fujihara H. *Heterocycles*, **1992**, 34, 1085-1088.

[24] Johansson Seechurn CCC, Kitching MO, Colacot TJ, Snieckus, V. *Angew. Chem. Int. Ed.*, **2012**, 51, 5062-5085.

[25] Barbarella G, Favaretto L, Zanelli A, Gigli G, Mazzeo M, Anni M, Bongini A. *Adv. Funct. Mater.,* **2005**, 15, 664-670.

[26] (a) Cardona CM, Li W, Kaifer AE, Stockdale D, Bazan GC. *Adv. Mater.*, **2011**, 23, 2367-2371. (b) Trasatti S. *Pure Appl. Chem.*, **1986**, 58, 955-966, (c) Gratzner G, Kuta J. *Pure Appl. Chem.*, **1984**, 56, 461-466.

[27] Bundgaard E., Krebs FC. *Sol. Energ. Mat. Sol. C,* **2007**, 91, 954-985.

[28] (a) Echegoyen L, Echegoyen LE. *Acc. Chem. Res.*, **1998**, 31, 593-601. (b) Damlin P, Hätönen M, Domínguez SE, Ääritalo T, Kivelä H, Kvarnström C., *RSC Adv.*, **2014**, 4, 8391-8401.

[29] Busby E, Xia J, Low JZ, Wu Q, Hoy J, Campos LM, Sfeir MY. *J. Phys. Chem. B,* **2015**, 119, 7644-7650.

[30] Dias FB, Bourdakos KN, Jankus V, Moss KC, Kamtekar KT, Bhalla V, Santos J, Bryce MR, Monkman AP. *Adv. Mater.,* **2013**, 25, 3707-3714.

[31] Lukevics E, Arsenyan P, Belyakov S, Pudova O. *Chem. Heterocycl. Comp.,* **2002**, 38, 632-645.

[32] Pappenfus TM, Melby JH, Hansen BB, Sumption DM, Hubers SA, Janzen DE, Eubank PC, McGee KA, Burand MW, Mann KR, *Org. Lett.*, **2007**, 9, 3721-3724.

[33] Sirringhaus H. *Adv.Mater.,* **2005**, 17, 2411-2425.

[34] (a) Cochran JE, Amir E, Sivanandan K, Ku SY, Seo JH, Collins BA, Tumbleston JR, Toney MF, Ade H, Hawker CJ, Chabiny ML. *J. Polym. Sci., Part B: Polym. Phys.,* **2013**, 51, 48-56. (b) Shin YR, Lee WH, Park JB, Kim H, Lee SK, Shin WS, Hwang DH, Kang, IN. *J. Pol. Sci Part A: Pol. Chem.*, **2015**, 54, 449-581.

[35] Natali D, Caironi M. *Adv. Mater.*, **2012**, 24, 1357-1387.

[36] (a) Murphy AR, Fréchet JM. *J. Chem.Rev.*, **2007**, 107, 1066-1096. (b) Facchetti A. *Chem. Mater.,* **2011**, 23, 733-758.

[37] Chua LL, Zaumseil J, Chang JF, Ou ECW, Ho PKH, Sirringhaus H, Friend RH. *Nature,* **2005**, 434, 194-199.

[38] Antolini L, Tedesco E, Barbarella G, Favaretto L, Sotgiu G, Zambianchi M, Casarini D, Gigli G, Cingolani R. *J.Am.Chem.Soc.*, **2000**, 122, 9006 9013.

[39] (a) Amir E, Sivanandan K, Cochran A. *Polym Chem.,* **2011**, 49, 1933-1941. (b)Pasini M, Destri S, Porzio W, Botta C, Giovanella U. *J. Mater. Chem.*, **2003**, 13, 807-813.

[40] Favaretto L, Barbarella G, Rau I, Kajzar F, Caria S, Murgia M, Zamboni R. *Optics Exspress,* **2009**, 17, 2557-2564.

[41] Meerheim R, Lussem B, Leo K. *Proceedings of the IEEE,* **2009**, 97, 1606-26.

[42] (a) Constantin LA, Fabiano E, Della Sala F. *Phys. Rev. B,* **2012**, 86, 035130. (b) Constantin LA, Fabiano E, Della Sala, F. *J. Chem. Theory Comput.*, **2013**, 9, 2256-2263, (c) Constantin LA, Fabiano E, Della Sala F. *Phys. Rev. B,* **2013**, 88, 125112.

[43] (a) Contreras-Garcia J, Johnson ER, Keinan S, Chaudret R, Piquemal JP, Beratan DN, Yang W. *J. Chem. Theory Comput.,* **2011**, 7, 625-632 (b) Contreras-Garcia J, Yang W, Johnson ER. *J. Phys. Chem. A,* **2011**, 115, 12983-12990.

[44] Mondal PC, Kantor-Uriel N, Mathew SP, Tassinari F, Fontanesi C, Naaman R. *Adv. Mater.,* **2015**, 27, 1924-1927.

[45] SMART & SAINT Software Reference Manuals, version 5.051 (Windows NT Version), Bruker Analytical X-ray Instruments Inc.: Madison, WI, **1998**.

[46] Sheldrick, G. M. SADABS, program for empirical absorption correction, University of Göttingen, Germany, **1996**.

[47] Burla MC, Caliandro R, Camalli M, Carrozzini B, Cascarano GL, De Caro L, Giacovazzo, C, Polidori G, Spagna R. *J. Appl. Crystallogr.,* **2005**, 38, 381-388.

[48] Sheldrick GM. SHELXTLplus (Windows NT Version) Structure Determination Package, Version 5.1. Bruker Analytical X-ray Instruments Inc.: Madison, WI, USA, **1998**.

[49] Spek AL. *Acta Crystallogr.*, **2009** 148-155.

[50] Macrae CF, Bruno IJ, Chisholm JA, Edgington PR, McCabe P, Pidcock E, Rodriguez-Monge L, Taylor R, Van de Streek J, Wood P. A. *J. Appl. Crystallogr.,* **2008**, 41, 466-470.

[51] De Mello JC, Wittmann F, Friend RH. *Adv. Mater.*, **1997**, 9, 230-232.

[52] Denizot F, Lang R. *J. Immunol. Methods,* **1986**, 89, 271-277.

CHAPTER III: SUPRAMOLECULAR ORGANIZATION, FUNCTIONAL PROPERTIES AND APPLICATION IN DEVICES OF SULFUR OVERRICH OLIGOMERS AND POLYMERS

We have developed a new class of oligo and polythiophenes characterized by the presence of an extra sulfur atom per ring ("sulfur overrich") directly attached to one β-carbon to induce ordered self-aggregation via S...S interactions. On the basis of literature data, we envisioned that the directionality of S...S interactions and the large polarizability of the sulfur would induce the formation of highly anisotropic supramolecular systems. Here two studies are reported:

1) Spontaneous self assembly of sulfur overrich octamers into functional polymorphic crystalline microfibers. We observed that the arrangement of the same molecule in two diverse supramolecular architectures leads to markedly different electronic, optical and charge mobility properties. The microfibers - straight and yellow emitting or helical and red emitting - exhibited p-type charge transport characteristics, with the yellow ones showing charge mobility and I_{on}/I_{off} ratio one and three orders of magnitude, respectively, greater than the red ones. We also observed that the organization of the octamers into microfibers resulted in additional intresting properties. Indeed, both forms showed circular dichroism signals, with significant differences from one form to the other, even though the molecules hadn't chiral centers.

2) Sulfur overrich decamers and polymers induce a supramolecular organization in thin films that allows charge transport of both hole and electrons in single material solar cells (SMOCs). In agreement with Kelvin Probe Force Microscopy results, photovoltaic behaviour was observed for all compounds with power conversion efficiencies in line with the best results obtained so far for the few donor-acceptor molecules already shown to perform in single-component solar cells.

Part I: Polymorphism in Crystalline Microfibers of Achiral Octithiophene: The Effect on Charge Transport, Supramolecular Chirality and Optical Properties

I. INTRODUCTION

Polymorphism in organic crystals, namely the existence of different crystalline forms for the same substance, is a phenomenon of considerable fundamental and technological relevance.[1] The intermolecular interactions and the mechanisms leading to different crystal arrangements are matter of intense studies aimed to achieve the control and prediction of solid-state structures.[2] Polymorphism has acquired great importance for organic solids of pharmaceutical interest, since the solid-state packing may affect biological activity or other features such as rate of dissolution or shelf life.[3] In conjugated materials, which are of major importance in nanotechnologies, solid-state molecular packing plays a crucial role in controlling the functional properties. Cases of polymer-induced[4] or solvent-[5] and substrate-induced[6] polymorphism observed in pentacene and its derivatives have been described and related to charge transport properties. The relationship between polymorphism and functional properties in other families of π-conjugated oligomers[7-8] and polymers, including poly(3-hexyl-thiophene)[9-11] has also been explored. A few cases of polymorphism in thiophene oligomers have been reported, most of them concerning *conformational* polymorphism in single crystals,[12-13] where different conformations of the same molecule pack in different ways. Conformational polymorphism generally occurs with molecules with flexible torsions.[1] A thiophene derivative, ROY, namely 5-methyl-2-[(2-nitrophenyl) amino]-3-thiophene carbonitrile, an intermediate in the production of the pharmaceutical olanzapine, has seven stable and a few unstable, structurally characterized, conformational polymorphs.[14-15] The name ROY derives from the color of its red, orange, and yellow polymorphs and the polymorphism is due to variations in the C-N-C-S torsion angle. Early studies on unsubstituted quater- and sexithiophene have shown that these compounds form different polymorphs having either a completely flat or a slightly tilted conformation with trans-trans configuration of adjacent rings and different packing arrangements.[16-19] Orange and yellow single crystals of a head-to-head S-CH$_3$ substituted quaterthiophene[20-21] and a tetramethyl substituted sexithiophene with the same regiochemistry of substitution,[22] were separated at room temperature and displayed different conformations and crystal packings. In other cases the conformational polymorphism was induced by alkyl side chains which were either nearly perpendicular or parallel to the molecular backbone [23] or by a trans-trans or cis-trans configuration of the thiophene rings.[24]

We report here the first case of polymorphism in octithiophene crystalline microfibers spontaneously self-assembled on solid substrates. The octithiophene in question is a "sulfur overrich" oligomer with one S-hexyl substituent per ring and head-to-head regiochemistry of substitution.[25] The octamer was designed as part of a chemical strategy aimed to obtain oligothiophenes with an intrinsic tendency to self-assemble anisotropically in nano and microfibers by virtue of intra- and inter-molecular sulfur-sulfur non-bonding interactions controllable via organic synthesis with different building blocks.[25] It formed thermodynamically very stable, red emitting, crystalline microfibers displaying the same helical

morphology independently of the type of surface on which they were grown. We have now been able to obtain polymorphic crystalline microfibers of the octithiophene, stable, straight and yellow emitting, which can be separately grown on solid substrates and characterized. We demonstrate that the yellow microfibers display significantly different electronic, optical and charge transport properties from the red emitting ones. Theoretical calculations on conformational energies and aggregation tendencies of the octithiophene, together with X-ray diffraction data, indicate that the polymorphism observed for the microfibers is the result of the interplay of slightly different conformations and different packing organizations.

II. RESULTS AND DISCUSSION

The molecular structure of the microfibers forming octithiophene, namely 3,3',3''',3'''',3''''',4'',4'''',4'''''-octakis(hexylsulphanyl)-octi-thiophene (1), is reported in Figure 1.
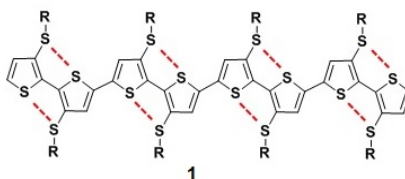
Figure 1. Molecular structure of octithiophene **1** (R = C_6H_{13}). Dotted red lines highlight intramolecular S···S interactions according to DFT calculations (S···S distance = 3.07-3.09 Å).

Octithiophene 1, with one S-hexyl chain per ring and head-to-head substitution pattern was synthesized through a sequence of selective monobrominations and Suzuki coupling steps, as already described.[25] When 1 was synthesized for the first time it was separated as a dark-red, red-emitting, microcrystalline powder. We have now been able to obtain the same compound in the form of a yellow, yellow-emitting, microcrystalline powder (Figure 2).

Figure 2. Plots of X-ray analysis of the microcrystalline powders of octamer **1**. The insets are microscopy fluorescence images of the red and yellow forms.

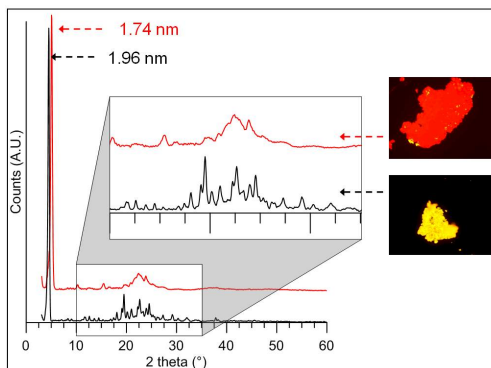In CDCl$_3$ the yellow and red powders display the same mass spectrum and the same proton and carbon-13 spectra, corresponding to those already described. However, they show different differential scanning calorimetry (DSC) plots: a peak at 73.0°C (onset 63.3°C) and a ΔH value of 24.5 J/g for the red powder and a peak at 70.7°C (onset 64.2°C) and a ΔH value of 31.4 J/g for the yellow one, indicating that the latter is slightly more stable than the former (Figure 4S, Figure 5S). No signs of interconversion of one form to the other were observed. The yellow and red powders showed different X-ray diffraction profiles (Figure 2). A very intense small angle reflection was present in both profiles (yellow d=1.96 nm; red d=1.74 nm). The profile of the yellow form showed sharper and more resolved reflections indicating that the crystalline domains are of better quality than those of the red form, which shows broadened and overlapped reflections. The identification of the yellow powder was the result of an empirical search (for more details see experimental section.) Currently, we are pursuing efforts to acquire full control on the formation of the yellow or red powders from solutions of 1. However, having in hand both forms, we can control the formation of one or the other simply by seeding with a previous crystal of the desired form. Microfibers from the yellow or red powder (Figure 3A,C) were separately prepared starting from 1mg/1mL solution (6.3 x 10^{-4} M) of the powder in toluene, a solvent in which 1 is very soluble. Drops of the solution were put on a solid support (glass or ITO or SiO$_2$ of a field-effect transistor device with gold contacts) located inside a glass cylinder containing at the bottom CH$_3$CN, a solvent in which 1 is insoluble (Figure 3B).
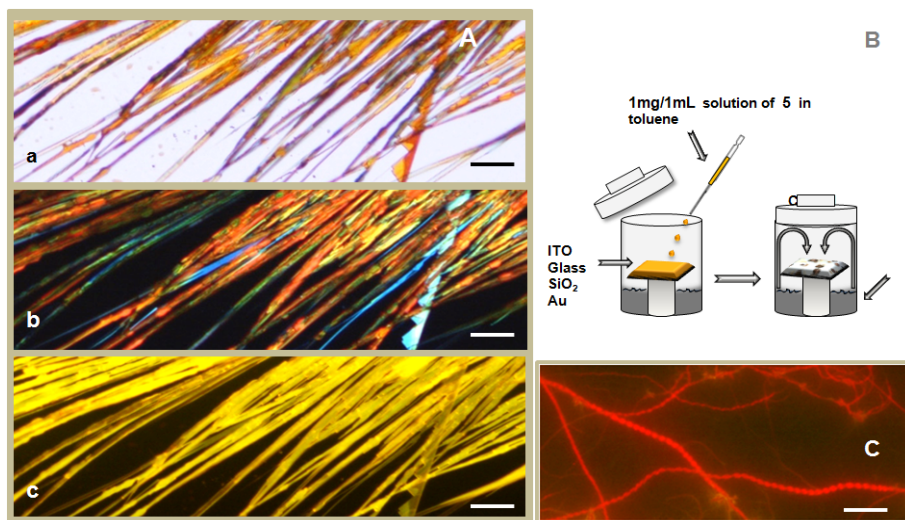
Figure 3. A) Light transmission microscopy image (a), microscopy image with cross polarizers oriented parallel and perpendicular to the images axes (b) and fluorescence microscopy image (c) of the yellow microfibers grown on glass from the yellow powder. Bars: 50 μm. B) Sketch illustrating the preparation of the microfibers. C) Fluorescence microscopy image of helical red microfibers obtained from the red powder (see also reference 25). Bar: 50 μm.

The drops of octamer in toluene diffuse on the substrate and when the CH$_3$CN vapours come in

touch with the toluene solution crystallization in the form of microfibers takes place. Afterwards the substrate is removed and allowed to dry on a Petri dish. The process takes place at ambient T. The formation of the microfibers (Figure 3 and Figure 6S, Figure 7S, Figure 8S) is highly reproducible provided the concentration of the starting solution in toluene is kept between 10^{-3} and 10^{-4} M. It is known that nucleation to form specific polymorphs is often driven by self-association in solution.[1,26] On this basis our hypothesis is that at the concentration employed octithiophene **1** is still partially aggregated as it was in the powder and the aggregates act as crystallization nuclei for the formation of the microfibers. This hypothesis is in agreement with the fact that: 1) X-ray diffraction data (see below) indicate that the crystal phase of the microfibers is the same as that of the respective powders, 2) when a mixture of yellow and red powders is employed (at the same concentration in toluene), mixed yellow and red microfibers are obtained (Figure 11S). The yellow and red microfibers shown in Figure 3 are very stable and always display the same morphology independently of the type of solid support employed. Figure 3A shows the light transmitted microscopy image with parallel (a) and crossed (b) polarizers and the fluoresce microscopy image (c) of the microfibers obtained on glass from the yellow powder. When using crossed polarizers they exhibit birefringence and by rotating progressively the polarized light by 360° extinguish in four positions, indicating that they are crystalline. No matter what the substrate employed is, the yellow microfibers invariably display a high aspect ratio being tens of micrometers long and a few micrometers wide, while their thickness is submicrometric (Figure 10S). For a satisfying identification and characterization of polymorphs a combination of various techniques is required.[1] Hence, a comprehensive description of the yellow microfibers is reported below in parallel with that of the red microfibers, for comparison.

2.1. Structural characterizations. Figure 4 compares the X-ray diffraction plots and the Raman spectrum in the 600-2000 cm^{-1} region of the yellow and red microfibers separately grown on glass from the corresponding powders. Concerning the X-ray plots, the yellow microfibers show several sharp intense reflections attributable to further orders (up to the seventh) of the 1.96 nm periodicity, while the red microfibers only show two main peaks (d=1.74, 1.54 nm). The full width at half-maximum (FWHM) of the most intense peaks of the yellow and red microfibers are FWHM = 0.079° and 0.173°, respectively. The length of the crystal domains, estimated with Scherrer method, are L = 102 nm and L = 46 nm, respectively. Furthermore, both types of microfibers show a high crystal orientation, in particular in the yellow phase as demonstrated by the high order of repetition of the main reflection. Peak widths indicate that the length of the coherent domains of the yellow polymorph is twice that of the red one. Concerning the Raman spectra reported in Figure 4B, it is seen that both the yellow (yellow plot) and red (red plot) microfibers display exactly the same pattern. The 600-2000 cm^{-1} spectral region shows the vibrations typical of oligothiophenes.[27] In particular, near 1450 cm^{-1} the C=C and C-C stretching are present, while near 1200 cm^{-1} there is the signal of the inter-ring C-C vibrations and near 730 cm^{-1} the signal corresponding to the vibration of ring C-S-C deformation. Thus, the Raman spectra show that the yellow and red microfibers are made of the same molecular material. Unfortunately, the signals in the 0-200 cm^{-1} region, related to the crystalline network, are too weak to allow any sound description of the differences between the two polymorphs (Figure 9S).
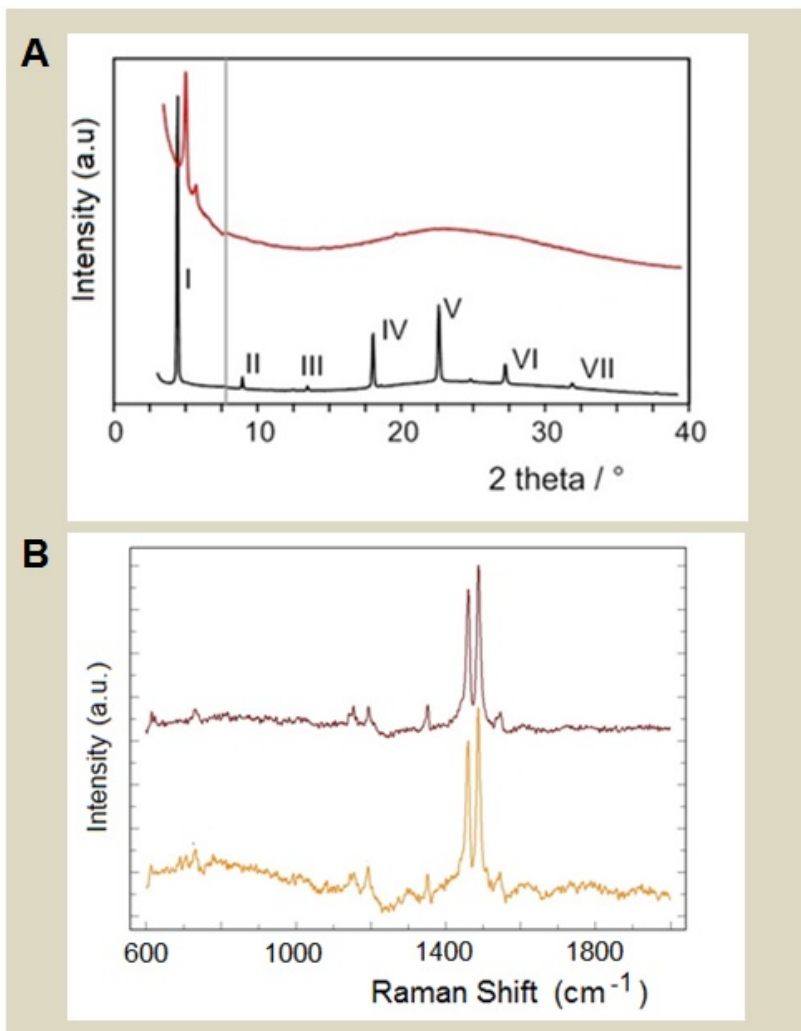
Figure 4. A) (a) X-ray diffraction pattern of yellow (black trace) and red (red trace) microfibers grown on glass. The romans highlight the consecutive orders of the 1.96 nm periodicity. **B)** Raman spectrum in the 600-2000 cm^{-1} region of the yellow (yellow trace) and red (red trace) microfibers on glass.

2.2. Optical characterizations. Figure 5A displays the laser scanning confocal microscopy (LSCM) image and the spatially resolved spectra of the yellow microfibers grown on ITO. The LSCM image and spatially resolved spectra of a sample with yellow and red microfibers grown on ITO from mixed yellow and red powders are reported in Figure 11S showing that the emission wavelength of the red microfibers is red-shifted by about 70 nm, indicating that the different assembly and the different intermolecular interactions result in a lower energy excited state formation.
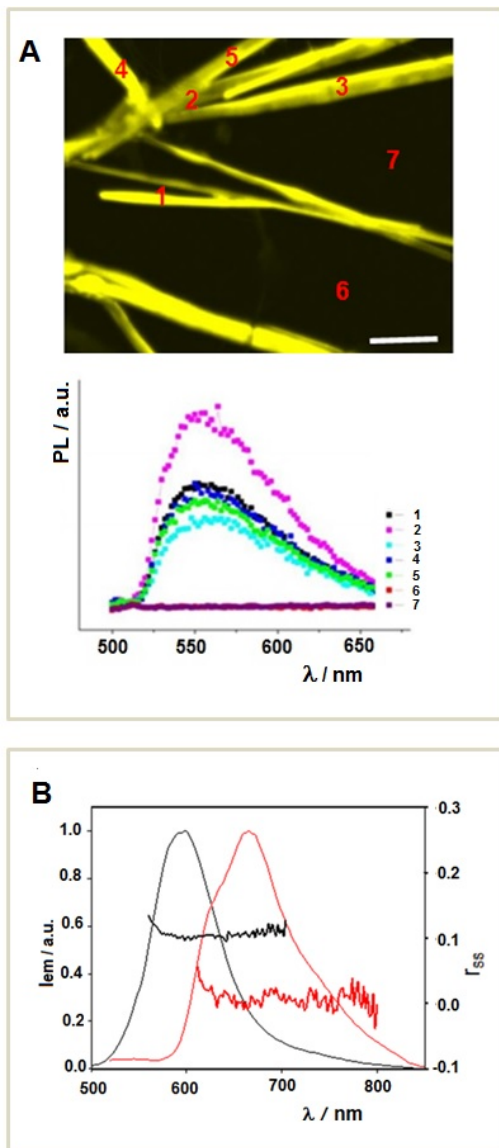
Figure 5. A) Laser Scanning Confocal Microscopy image and spatially resolved photoluminescence spectra of the yellow microfibers grown on ITO. Bar: 20 μm. B) Normalised fluorescence spectra and steady state anisotropy of yellow (black line) and red microfibers (red line) grown on glass (λ_{ex} =480 nm). Note that in Figure 5A each one of the spectra is relative to a single fiber while the spectrum of Figure 5B is relative to the envelope of fibers included into the surface of the irradiation spot (4- 9 mm^2).

To complete the optical characterizations, circular dichroism (CD) spectra were run for the

yellow and red microfibers separately grown on glass. For each type of microfibers the spectra of two different samples (reversed in sign) are reported are reported in Figure 6.

Figure 6. Circular dichroism spectra of two different samples of the yellow (A) and red (B) microfibers grown on glass.

The CD spectra of the red microfibers are the same as those already reported by us and interpreted as being due to the interplay of molecular and supramolecular helicity.[25] Since octamer 1 lacks asymmetrically substituted carbon atoms, no CD signal is observed in solution. The optical activity observed in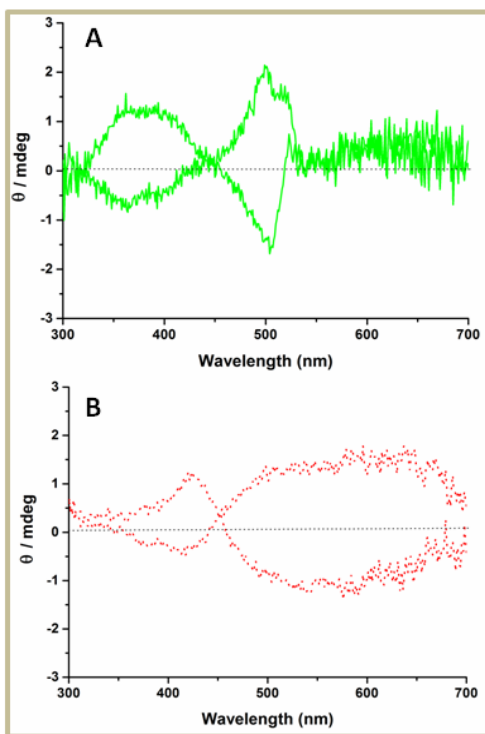 the solid state is the effect of hindered rotations about the thienyl-thienyl interring bonds caused by the freezing of the molecule on the solid support.[33] Hindered rotations about a thienyl-thienyl linkage have the potentiality to generate enantiomers, as in the case of tetra-*ortho* substituted biphenyls in which the freezing of the interring C-C rotation generates stereoisomers displaying axial chirality.[34] The phenomenon is named *atropisomerism* and has profound implications in drugs synthesis.[35-36] When 1, which has seven inter-ring bonds, is deposited on a solid support, scalemic (enantiomerically enriched) mixtures are formed, which are made of different conformers in the yellow and red polymorphs. As soon as the first molecule of 1 is locked on the surface of the substrate, it looses all symmetry elements and becomes chiral.[33] The handedness of the first molecule then induces preferential handedness of the same sign on the following ones, causing chirality

amplification. Since the one or the other handedness sign of the first molecule have equal probabilities, different samples may display opposite chiralities, as is indeed shown in Figure 6. In the red microfibers the weak intermolecular interactions due to the helical morphology induce an additional supramolecular component to the overall chirality of the system. Figure 6B shows that the CD spectra of the red microfibers present extensively enlarged bands with respect to those of the yellow polymorph, which are precisely the signature of supramolecular helicity.[37-39] It is worth noting that, as far as we know, the yellow microfibers are the first example reported so far of microfibers with straight morphology displaying a CD spectrum. Apparently, a helical morphological habit only adds a supramolecular component to the chirality but it is not a necessary condition to observe a CD spectrum. This finding is important since the non linear optical properties related to the chirality of supramolecular assemblies may open the door to a new generation of functional materials.[40]

2.3. Electrical characterization. The semiconducting properties of the yellow and red microfibers were measured using them as active layers in organic field-effect transistors (OFETs) built in bottom-gate, bottom-contact architecture.[41] The microfibers were directly grown on interdigitated gold source and drain microelectrodes prefabricated on the octa-decyltrichlorosilane (OTS) self-assembled monolayer (SAM)-treated Si/SiO_2 substrate (experimental section for details). Saturated charge mobilities were measured in vacuum (10^{-5} mbar) with a drain voltage $V_D = -60$ V and calculated by estimating the coverage of the device on the basis of optical microscopy images. In addition, to ensure full consistency between the devices based on different microfibers, bias range and voltage steps were kept constant. Figure 7A and Figure 7B show the optical images of the OFET devices with separately grown yellow and red microfibers (a), the output features (b), the AFM images (c) with details (d) and the corresponding AFM profiles (e). The electrical transfers in saturation regime are displayed in Figure 12S. It is seen that the AFM images show the peculiar features of yellow and red microfibers, namely straight morphology for the former and helical morphology for the latter, with comparable submicrometric thickness. Both types of microfibers exhibit p-channel field-effect characteristics. However, the OFET based on yellow microfibers clearly shows a better field-effect performance than that based on red microfibers. Saturated hole mobility, μ_{sat}, and I_{ON}/I_{OFF} ratio are indeed one and three orders of magnitude higher, respectively, than those obtained with the red microfibers. In particular, μ_{sat}, threshold voltage (V_T), and I_{ON}/I_{OFF} are determined to be 2.20×10^{-4} cm^2 V^{-1} s^{-1} (maximum value = 6.83×10^{-4} cm^2 V^{-1} s^{-1}), -25 V, and 10^4 for the yellow microfibers and 2.05×10^{-5} cm^2 V^{-1} s^{-1} (maximum value = 2.64×10^{-5}), -22 V, and 10^1 for the red ones. The modest charge mobilities reported could certainly be increased by optimization of the OFET devices or manipulation of the organization of the microfibers on the surface. For example, we have already demonstrated that controlling the self-assembly of microfibers forming thiophene oligomers by confinement effects provides an increase in charge mobility up to three orders of magnitude.[42] However, to this stage our objective was only to demonstrate that the microfibers were electroactive and displayed very different characteristics. Considering that the yellow and red microfibers are polymorphic structures, the results indicate that the different electrical properties are strongly related to the molecular packing, which in the case of the yellow polymorph favors significantly the charge transport. This result is in agreement with the X-ray diffraction data reported above, showing that the interlayer distance

in the red phase is greater than in the yellow one. The yellow phase, both in powder or microfibers, has a higher tendency to form more ordered crystalline domains, allowing better orbitals overlap and more efficient electron transfer.

Figure 7. (A) Optical micrographs (a) (scale bar: 50 µm), output plots at various gate voltages (b), AFM topography (c and d) and AFM profile (e) of yellow microfibers grown directly on the interdigitated el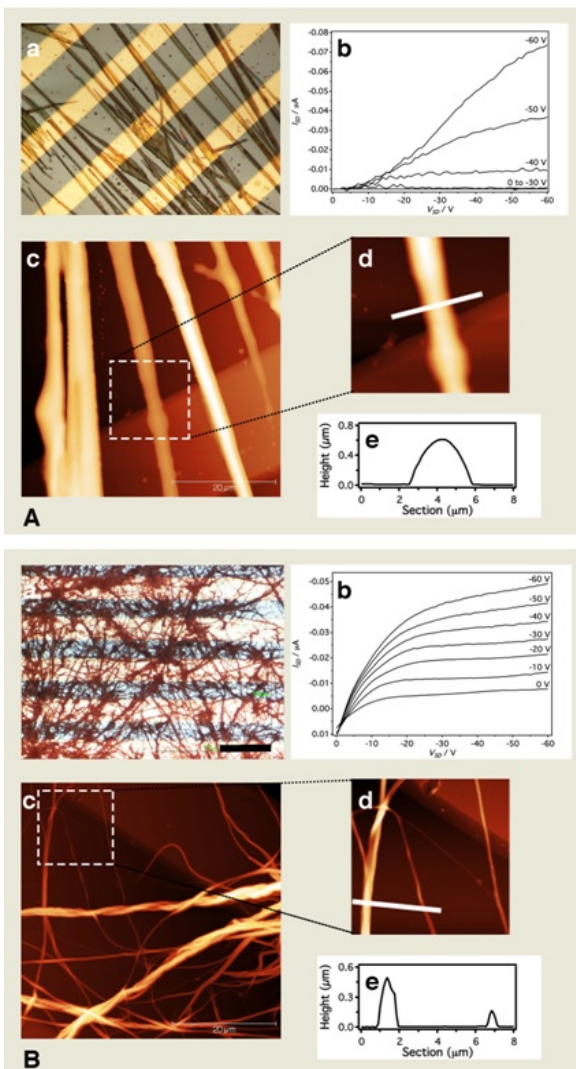ectrodes/SiO_2 surface of a bottom-contact field-effect transistor. (B) Optical micrographs (a) (scale bar: 50 µm), output plots at various gate voltages (b), AFM topography (c and d) and AFM profile (e) of red microfibers grown directly on the interdigitated electrodes/SiO_2 surface of a bottom-contact field-effect transistor.

2.4. Electrochemical characterization. A comparison of the cyclic voltammograms of yellow and red microfibers separately grown on ITO electrodes is reported in Figure 8. The current was normalized to compensate the differences in coating masses. The oxidation onset potential of the yellow microfibers was E_{ox}(onset) = 0.70 V vs. SCE (0.20 V vs. Fc/Fc$^+$) and the reduction onset potential was E_{red}(onset) = -1.50 V vs. SCE (-1.70 V vs. Fc/Fc$^+$). In agreement with the UV-vis blue-shift, the electrochemical band gap of the yellow microfibers was 2.20 eV, that is 0.08 eV (99 nm) smaller than that of the red microfibers, mainly because of the decrease in the HOMO energy (-5.30 eV).
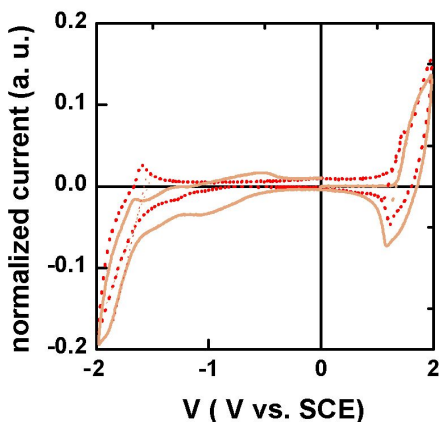

Figure 8. Voltammograms of yellow and red microfibers in PC-0.1 M TEABF$_4$ (yellow and dotted red line, respectively). The microfibers were separately grown on the ITO substrate.

2.5. Theoretical Calculations. Owing to the heavy computational requirements due to the large number of sulfur atoms, no high level theoretical calculations have been carried out so far on sulfur overrich octamers. To elucidate the capability of octamer **1** to self-aggregate in different forms, we have now calculated the conformational preferences and aggregation modalities for the octamer substituted with S-CH$_3$ instead of S-C$_6$H$_{13}$ groups. The calculations have been performed at the density functional theory level using the BLOC-D3 eta-GGA functional[43] (which includes semiempirical D3 dispersion corrections). A preliminary screening of possible equilibrium geometries was carried out using the def2-SV(P) basis set.[44] Final calculations were performed using a def2-TZVPP basis set.[45] The consistency of the obtained results was evaluated by comparing them with PBE-D3/def2-TZVPP[46-47] calculations: similar results were obtained in all cases. All calculations were performed with the TURBOMOLE program package.[48] The calculations show that the S¨S intramolecular interactions (indicated with dotted lines in Figure 1), favor the planar arrangement of adjacent rings (dihedral angle < 1 degree; S¨S distance about 3.07-3.09 Å). Some torsional flexibility is observed instead in the bonds between bithiophene subsystems. As a result, a quaterthiophene made of two adjacent bithiophene subsystems is planar with a small distortion in the central bond (torsional angle of about 10 degrees) and a similar torsional angle is found for the central

C-C bond of the octamer made of four bithiophene subsystems. This type of bonding pattern leads to the existence of two quasi-degenerate minimum-energy conformations for octamer **1**, separated by less than 1 kcal/mol in energy and differing for the relative orientation of the three main C-C torsional angles between bithiophene subsystems. The first slightly more stable conformation is characterized by torsions of opposite sign in the carbon-carbon single bonds and is therefore, on average, almost planar (Figure 9A). The second conformation, on the opposite, displays the three torsions in the same directions (Figure 9B) and is in consequence significantly twisted with respect to the main molecular axis. The orientation of the side chains was found to play a negligible role in gas phase, with the orientation perpendicular to the average molecular plane being slightly favored with respect to the orientation on the average molecular plane. When the aggregate formed by two stacked molecules is considered, the situation is different. In general, packing interactions shall favor the planarization of the octamer units, independently of whether the starting monomers were in the 'planar' or 'twisted' configuration. However, in this case, a significant role was found to be played by the orientation of the side chains. When the SCH_3 side groups lay in a planar configuration with respect to the octamer's main body, they do not contribute substantially to the intermolecular interaction. Therefore, the whole complex tends to be planar, due to the prevalence of stacking forces (Figure 9C). This geometrical configuration is ascribable to the yellow fibers. On the contrary, when a perpendicular configuration is considered for the side chains, steric interactions are present between the CH_3 units and the thiophene rings of the other molecule. As a result, small and diffuse distortions of the molecular backbone are promoted. In consequence, the complex assumes a twisted geometry (Figure 9D), which can be ascribed to the red fibers. We remark that, despite the conformational differences and the existence in the latter aggregate of steric interactions which promote a distortion of the molecular backbone, the binding interaction in both cases is determined by stacking forces. Therefore, since at room temperature the orientation of the side chains in non-aggregated octamer can be assumed to be random, we expect the two conformations to have very similar probabilities to form. Moreover, the presence of perpendicular side chains is only causing a small destabilization of the binding and the planar aggregate is only 27 kcal/mol lower in energy than the twisted one. Finally, to support our assignment of the two structures to the yellow and red microfibers, we performed additional time-dependent density functional theory calculations at the PBE/def2 -TZVPP level to compute the lowest optically active excited states of both systems. The calculations yielded a difference in excitation energy of 0.11 eV, compatible with the yellow-red color difference. Figure 9E,F shows a sketch comparing the proposed supramolecular organization of the yellow and red microfibers. In both cases the molecules which, given the intense fluorescence signal, are likely to be in a J-type arrangement,[25] are organized in platelets forming crystalline domains. In the yellow microfibers the platelets are parallel with interchain stacking and strongly $\pi-\pi$ interacting building blocks (Figure 9E). Instead, in the red microfibers, owing to the twisted conformation, the platelets tend to bend forming curves and curls (Figure 9F), as already described in reference 25. The proposed model is in agreement with the difference in OFET charge mobility measured for the yellow and red microfibers. Indeed, in π-conjugated materials, charge transport takes place by interchain hopping,[41] a mechanism which is is more efficient between parallel lamellae.
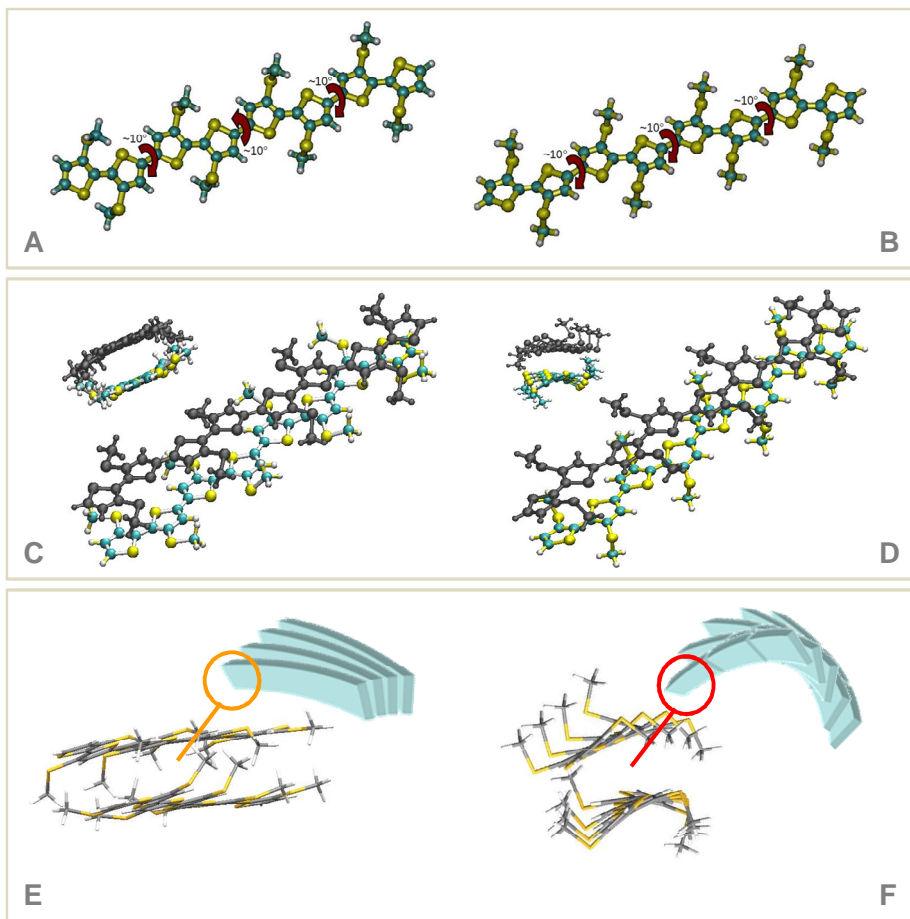
Figure 9. A,B) Calculated preferred conformations of octamer 5 (R=SCH₃). C,D) Calculatd geometries of the aggregate made of two molecules of 5 in A or B conformation. E,F) Sketch of the proposed supramolecular organization of the yellow and red microfibers.

III. CONCLUSION

In summary, we reported the first case of fully characterized polymorphic, stable and crystalline, microfibers formed by an achiral octithiophene spontaneously self-assembling at room temperature on several surfaces (glass, ITO, SiO₂/Au) with the same reproducible morphology. Theoretical evidence points to the microfibers as being the manifestation of *conformational* polymorphism. The control of the self-assembly process leads to polymorphic linear arrays of the octithiophene being micrometric in length and width and submicrometric in thickness, held together by non covalent interactions and displaying markedly different

morphological and functional properties. The polymorphs, one made by straight and the other by helical microfibers, are not only fluorescent and electroactive but also chiral, with the latter being characterized by an additional supramolecular component of the CD spectrum. Incidentally, we note that the importance of addressing stereochemistry in the development and application of functional thiophene materials in the solid state has been largely overlooked so far. Our results indicate that in the field of thiophene oligomers and their supramolecular assemblies - very promising materials for application in photonics, biosensors, (opto)electronics - it is time to broadly use polymorph screening as a tool to control and optimise the quality and efficiency of the final materials, in analogy with what is currently done in pharmaceutical industry for drug substances.

IV. EXPERIMENTAL SECTION

4.1 General

4.1.1. Synthesis of 3,3', 3''',3'''', 3''''''',4'',4'''',4''''''-octakis(hexylsulphanyl)-octi-thiophene 1. Compound **1** was synthesized in ultrapure form *via* a sequence of ultrasound-assisted selective monobrominations and microwave-assisted Suzuki cross coupling reactions according to the modalities described in reference 25 (see also F. Di Maria et al., *Journal of Sulfur Chemistry*, 2013, 34, 627-637). The synthesis was repeated several times and, after chromatograhy on silica gel using cyclohexane:CH_2Cl_2 as the eluant, the product was obtained either as a dark red or yellow microcrystalline powder. Both powders, redissolved in $CDCl_3$, displayed the same proton and carbon-13 spectra, identical to those shown in reference 25 for compound **1**. The melting point of both microcristalline forms was strongly dependent on the amount of solvent absorbed into the powder. After drying under high vacuum the melting point of both forms stabilized around 70°C. The Differential Scanning Calorimetry plots below indicate that the yellow form melts at 70,69 °C and the red form at 72,98 °C.

To time it is not clear which are the factors determining the formation of one or the other type of powder and our results are mainly due to a trial and error procedure. Our feeling of synthetic chemists is that the degree of purity and the exact proportions of the eluants used in silicagel chromatography play a major role. Attempts to put our feelings on a more objective basis are under way.

4.1.2. X-ray diffraction. The investigations were carried out on films of the yellow and red microfibers separately grown on glass slides using a PANalytical X'Pert diffractometer equipped with a copper anode (λmean = 0.15418 nm) and a fast X'Celerator detector.

4.1.3. Raman spectra. A Renishaw System 1000 was employed for the region 600-2000 cm^{-1} using a 782.5 nm laser as exciting source. The spectrum in the region 10-150 cm^{-1} was obtained with a Raman Jobin Yvon T64000 spectrometer using a 752.1 nm laser as exciting source.

4.1.4. Optical Microscopy and Fluorescence Microscopy. Optical micrographs were recorded with a Nikon i-80 microscope equipped with epi-illuminator and cross polars. Fluorescence images were recorded with a Nikon i-80 microscope equipped with epi-fluorescence and a commercial Nikon CCD DS-2Mv camera. The illumination was performed using a 100 W halogen lamp at fixed power (12 V) and fixed acquisition time (500 ms).

4.1.5. Atomic Force Microscopy. The AFM images of Figure 7 were obtained using a Solver Pro, NT-MDT instrument working in semicontact mode. The AFM images of Figure 10S were carried out using a Multimode 8 instrument controlled by Nanoscope V (Bruker-AXS). Line profiles of height versus lenght were measured by Nanoscope 8.

4.1.6. LSCM. The Laser Scanning Confocal Microscopy images and the spatially resolved photoluminescence spectra of thin films of the microfibers on ITO, separately grown from the corresponding powders or grown together from mixed yellow and red powders, were collected using a Fluo-View1000 (Olympus) confocal microscope with spatial resolution of 200 nm in xy and 100 nm in z. The excitation source was a FV5-LD505-2 Laser Diode (Olympus) at 405 nm coupled with a 405/488 nm dichroic mirror and a 60X objective was used for the acquisitions. The optical images were obtained with a CCD color camera coupled to the microscope. Spatially-resolved PL spectra were collected with 2 nm wavelength resolution and 200 nm spatial resolution.

4.1.7. Circular Dichroism. All measurements were carried out with a JASCO J-715 spectropolari-meter under ambient conditions using films of the yellow and red microfibers separately grown on glass slides.

4.1.8. Cyclic Voltammetry. Cyclic voltammetries have been performed at room temperature, after Ar purging, with AMEL 5000 electrochemical system in an home made three compartment cell with Pt wire counter electrode and aqueous KCl Saturated Calomel Electrode (SCE = -0.50 V vs. ferrocene/ferricinium). Supporting electrolyte was propylene carbonate (Aldrich, distilled under reduced pressure) and 0.1 M tetraethylammonium tetrafluoborate (TEBF$_4$, Fluka, puriss. vacuum dried). Yellow and red fibers were separately prepared on indium tin oxide/glass slides (ITO, Balzers, 23 ohm/square).

4.1.9. Field-Effect Transistors. Spectroscopic grade quality solvents and octadecyltrichloro-silane (OTS) were purchased from Sigma Aldrich. For bottom-gate, bottom contact OFETs, heavily n-type doped silicon wafers with a thermally grown silicon dioxide layer 200 nm thick (C_i = 17.25 nF/cm^2) are used as substrates. Gold source-drain interdigitated electrodes with different channel length (L = 20, 40 µm) and width (W = 11200, 22400 µm) were prepatterned on the substrates. Before fibers formation, gate dielectric was functionalized with a self-assembled monolayer of OTS by vapor phase deposition. The substrates were cleaned by sonication in acetone for 10 min, then in 2-propanol for 10 min, dried in a stream of nitrogen and heated at 100°C for 15 min. After treatment in UV-ozone for 20 min, the substrates were kept in a desiccator with a few drops of OTS. The desiccator was evacuated for 10 min and placed in an oven at 110 °C for 3 h. The substrates were removed from the desiccator, thoroughly rinsed with isopropanol, and dried under a nitrogen flow.

Fibers of red or yellow octamer 5 were deposited on the OTS-treated substrates by solvent/non-solvent vapor-induced crystallization. 20 µL of 1 mg/mL toluene solution of 5 was drop cast on the substrate and exposed to saturated acetonitrile (non-solvent) vapor atmosphere at room temperature for 24 in an airtight container. Before characterization, the samples were aged in atmospheric conditions for 2 hours.

4.2. ^{1}H and ^{13}C NMR spectra and Mass spectrum of the yellow and red powders in solution. The polymorfic yellow and red powders, separately redissolved in CDCl$_3$, displayed identical proton and carbon-13 NMR spectra, the same already shown for compound **1** in the

experimental section of reference 25. Mixing the yellow and red powders in various proportions and dissolving the mixture in CDCl$_3$ always afforded the same spectra. Figure 1S and Figure 2S show the ^{1}H and ^{13}C spectra of a 1:1 (w:w) mixture of yellow and red powders dissolved in CDCl$_3$. Comparison of these spectra with the spectra displayed in reference 25 for 1 shows that both types of powders are made by the same molecular material.
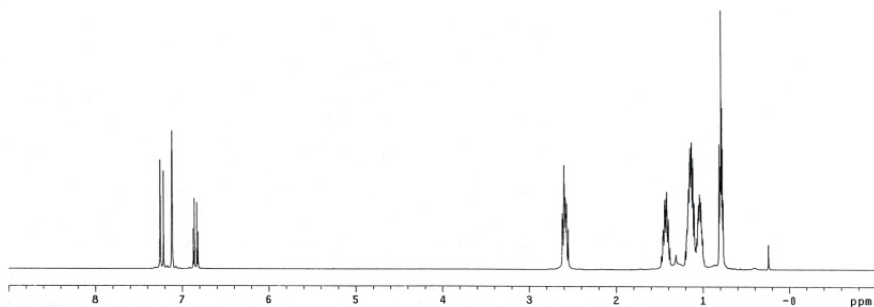
Figure 1S. ^{1}H NMR spectrum of a 1:1 (w:w) mixture of yellow and red powders redissolved in CDCl$_3$.
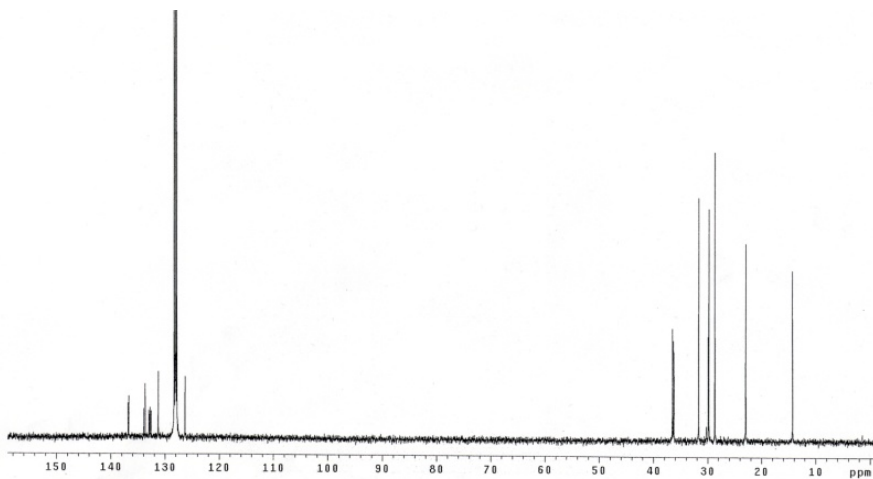
Figure 2S. ^{13}C NMR spectrum of a 1:1 (w:w) mixture of yellow and red powders redissolved in CDCl$_3$.
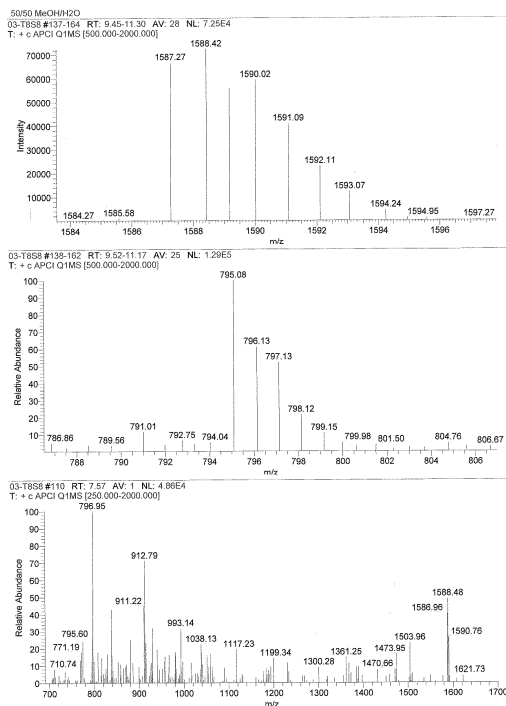
Figure 3S. Mass spectrum of a 1:1 (w:w) mixture of yellow and red powders redissolved in MeOH/H$_2$O.

The same spectrum was obtained starting from the isolated red or yellow powders or from any mixture of yellow and red powders.

4.3. Differential Scanning Calorimetry of the yellow and red powders
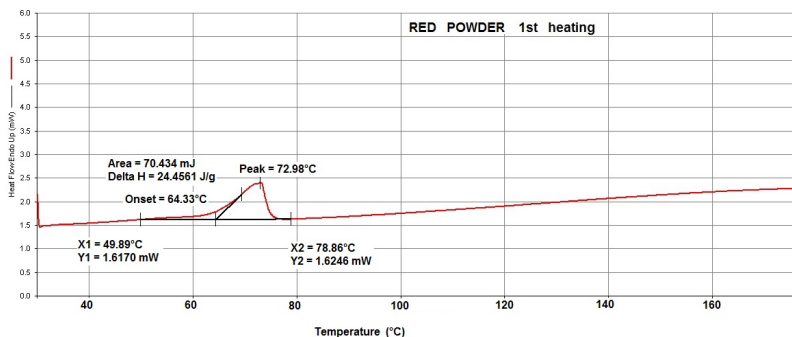
Figure 4S. DSC of the yellow powder. No peaks were present in the cooling and second heating cycles.
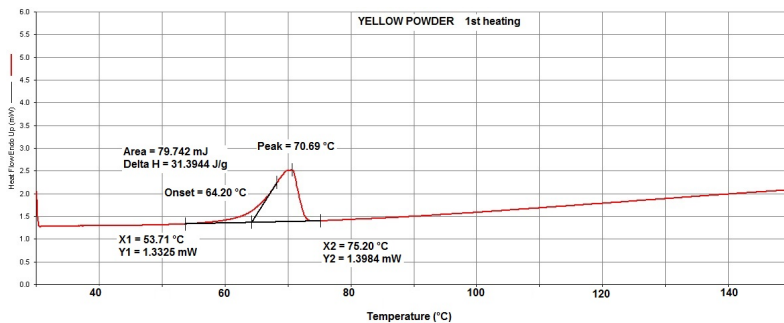
Figure 5S. DSC of the red powder. No peaks were present in the cooling and second heating cycles.

The melting enthalpy of the yellow powder (31.4 J/g) is greater than that of the red powder (24.4 J/g) indicating greater stability.

4.4. Light transmission and fluorescence images of yellow and red microfibers
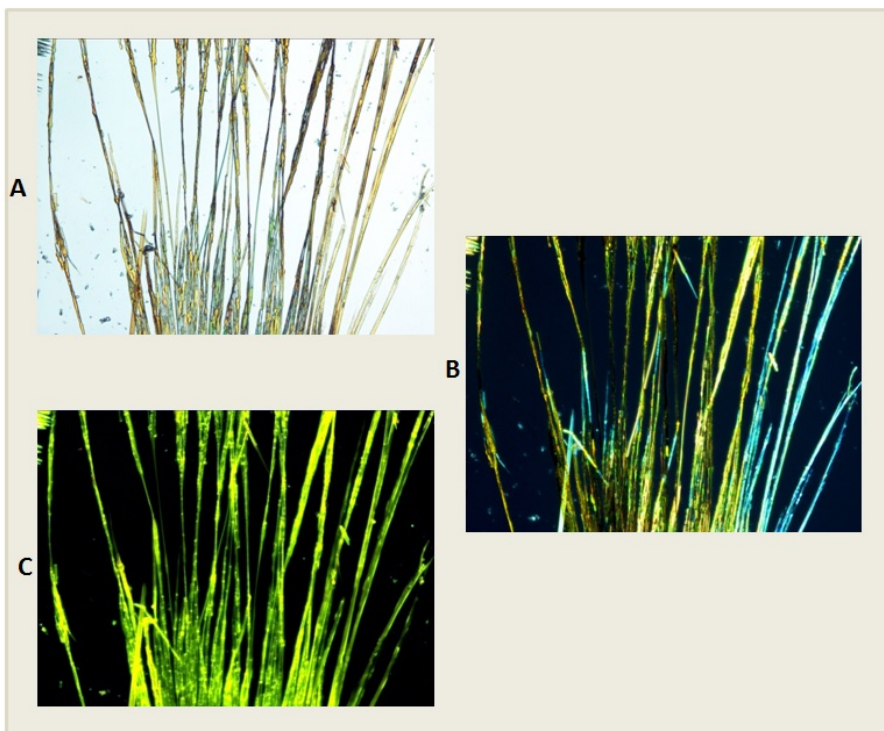
Figure 6S. A) Light transmission microscopy, B) optical microscopy image with cross polarizers oriented parallel and perpendicular to the images axes and **C)** fluorescence microscopy image of the yellow microfibers grown on glass from the yellow powder.

77
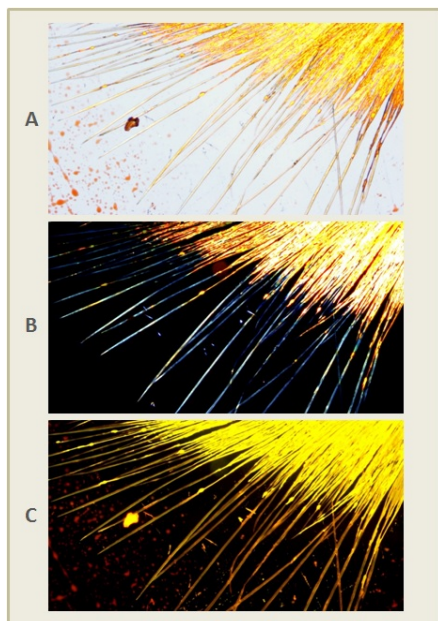
Figure 7S. As in Figure 1S: **A)** Light transmission microscopy, **B)** optical microscopy image with cross polarizers oriented parallel and perpendicular to the images axes and **C)** fluorescence microscopy image of the yellow microfibers grown on glass from the yellow powder.
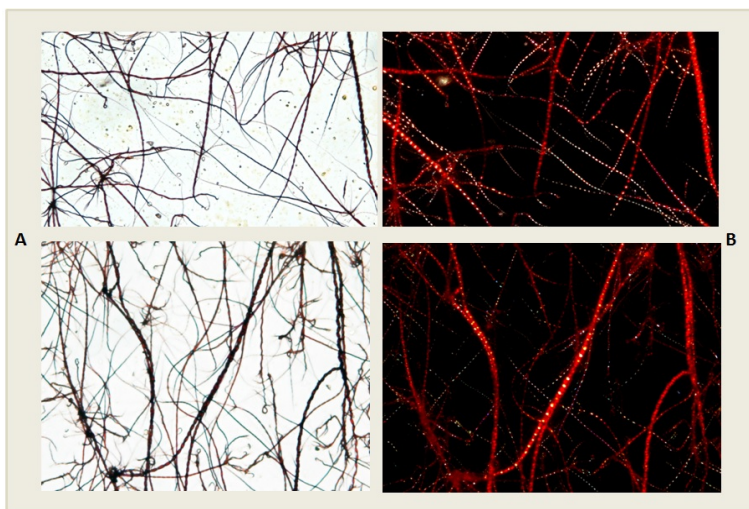
Figure 8S. A) Light transmission microscopy and B) optical microscopy images with cross polarizers oriented parallel and perpendicular to the images axes of the red microfibers grown on glass from the red powder.

4.5. Raman spectra of yellow and yellow and red microfibers
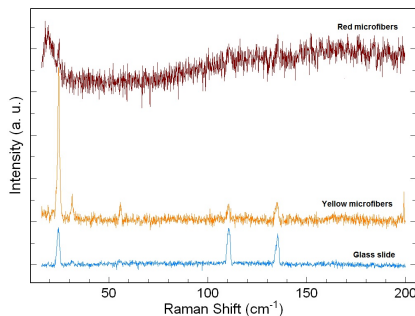
Figure 9S. Raman spectra of the 0-200 cm^{-1} region of red and yellow microfibers separately grown on glass.

4.6. Atomic Force Microscopy of yellow microfibers
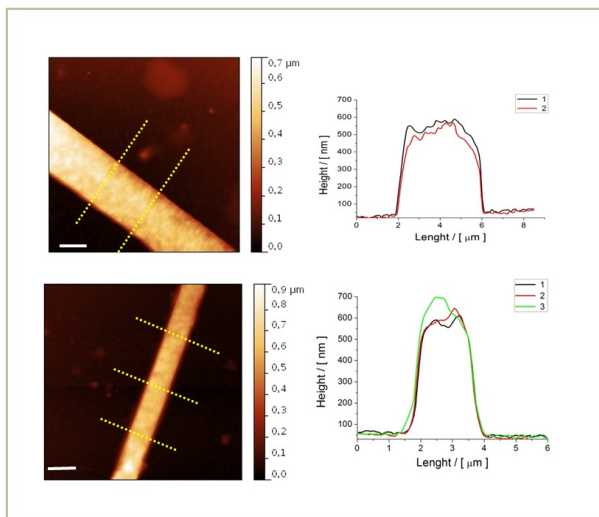
Figure 10S. AFM images (15 micron x 15 micron) of the yellow microfibers grown on ITO (bars: 2 micron) and corresponding scanning linear profiles in the region of the dot yellow lines.

4.7. Optical characterizations of yellow and red microfibers.

Laser Scanning Confocal Microscopy measurements were carried out on samples with mixed yellow and red fibers grown on glass from mixed yellow and red powders. Initial measurements of microfibers quantum yields using an integrating sphere indicated that both types of fibers are characterized by quantum yields < 5%, with the yellow ones having a quantum yield nearly twice that of the red fibers. The fluorescence lifetimes are 1.8 ns for the yellow microfibers and 2.1 ns for the red ones.
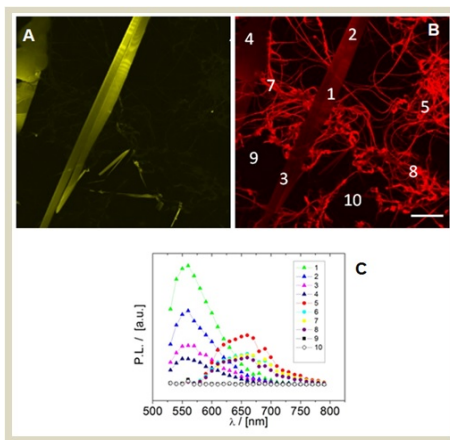
Figure 11S. Laser Scanning Confocal Microscopy images of yellow and red microfibers grown on glass from mixed red and yellow powders. Bars: 50 µm. A) Spectral region 567-591 nm. B) Spectral region 592-800 nm. C) Spatially resolved emission spectra.

4.8. Electrical characterization of yellow and red microfibers. All the electrical measurements were performed in vacuum (10^{-5} mbar), using a Keithley 2612 source measure units. The mobility in the saturation regime (μ_{sat}) was calculated using the equation $I_{DS} = (W/2L)C_i\mu_{sat}(V_G-V_T)^2$, where W and L are channel widths and lengths, respectively, C_i is the capacitance of the insulating SiO_2 layer, and V_{th} is the threshold voltage extracted from the square root of the drain current ($I_{DS}^{1/2}$) versus gate voltage (V_G) characteristics for a fixed drain voltage (V_{DS}). All measured values were averaged on at least three devices. Finally, it should be mentioned that thin films of **1** fabricated by spin coating do not exhibit measurable charge transport properties.
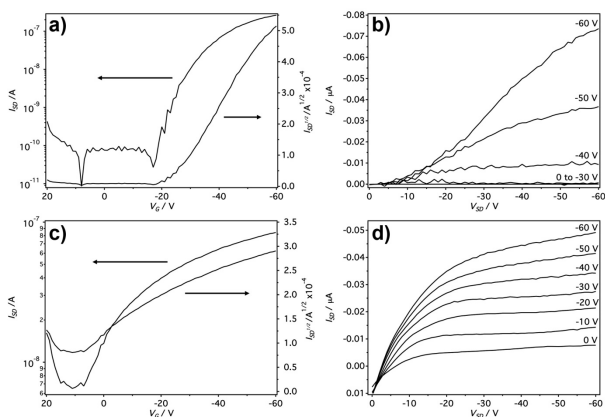
Figure 12S. Transfer plots at $V_D = -60$ V and output curves at various gate voltages V_G corresponding to OFETs functionalized with OTS and based on yellow (a and b) and red (c and d) microfibers.

REFERENCES

[1] Brog JP, Chanez CL, Crochet A, Fromm KM. *RSC Adv.,* **2013**, 3, 16905-16931.

[2] Davey RJ, Schroeder SLM, ter Horst JH. *Angew. Chem. Int. Ed,.* **2013**, 52, 2166-2179.

[3] Nangia A. *Acc. Chem. Res.*, **2008**, 41, 595-604.

[4] Chen J, Shao M, Xiao K, He Z, Li D, Lokitz BS, Hensley DK, Kilbey SM, Anthony JE, Keum JK, Rondinone AJ, Lee WY, Hong S, Bao Z. *Chem. Mater.,* **2013**, 25, 4378-4386.

[5] Chen J, Shao M, Xiao K, Rondinone AJ, Loo YL, Kent PRC, Sumpter BG, Li D, Keum JK, Diemer PJ, Anthony JE, Jurchescu OD, Huang J. *Nanoscale* **2014**, 6, 449-456.

[6] Schiefer S, Huth M, Dobrinevski A, Nickel B. *J. Am. Chem. Soc.,* **2007**, 129, 10316-10317.

[7] Gu X, Yao J, Zhang G, Yan Y, Zhang C, Peng Q, Liao Q, Wu Y, Xu Z, Zhao Y, Fu H, Zhang D. *Adv. Funct. Mater.,* **2012**, 22, 4862-4872.

[8] Dikundwar AG, Dutta GK, Guru Row TN, Patil S. *Cryst. Growth Des.,* **2011**, 11, 1615-1622.

[9] Poelking C, Andrienko D. *Macromol.,* **2013**, 46, 8941-8956.

[10] Koch FPV, Heeney M, Smith P. *J. Am. Chem. Soc.,* **2013**, 135, 13699-13709.

[11] Yuan Y, Zhang J, Sun J, Hu J, Zhang T, Duan Y. *Macromol.* **2011**, 44, 9341-9350.

[12] Bernstein J, Hagler AT. *J. Am. Chem. Soc.,* **1978**, 100, 673-681.

[13] Bernstein J. *Acc. Chem. Res.,* **1995**, 28, 193-200.

[14] Yu L. *Acc. Chem. Res.,* **2010**, 43, 1257- 1266.

[15] Chen S, Guzei IA, Yu L. *J. Am. Chem. Soc.,* **2005**, 127, 9881-9885

[16] Antolini L, Horowitz G, Kouki F, Garnier F. *Adv. Mater.,* **1998**, 10, 382-385.

[17] Siegrist T, Kloc C, Laudise RA, Katz HE, Haddon RC. *Adv. Mater.,* **1998**, 10, 379-382.

[18] Siegrist T, Fleming RM, Haddon RC, Laudise RA, Lovinger AJ, Katz HE, Bridenbaugh P, Davis DD. *J. Mater. Res.,* **1995**, 10, 2170-2173.

[19] Garnier F. *Acc. Chem. Res.,* **1999**, 32, 209-215.

[20] Barbarella G, Zambianchi M, Di Toro R, Colonna M, Antolini L, Bongini A. *Adv. Mater.,* **1996**, 8, 327-330.

[21] Barbarella G, Zambianchi M, Del Fresno M, Marimon I, Antolini L, Bongini A. *Adv. Mater.,* **1997**, 9, 484-487.

[22] Barbarella G, Zambianchi M, Antolini L, Ostoja P, Maccagnani P, Bongini A, Marseglia EA, Tedesco E, Gigli G, Cingolani R. *J. Am. Chem. Soc.,* **1999**, 121, 8920-8926.

[23] Pan H, Liu P, Li Y, Wu Y, Ong BS, Zhu S, Xu G. *Adv. Mater.,* **2007**, 19, 3240-3243.

[24] Sokolov AN, Sumrak JC, MacGillivray LR. *Chem. Commun.*, **2010**, 46, 82-84.

[25] Di Maria F, Olivelli P, Gazzano M, Zanelli A, Biasiucci M, Gigli G, Gentili D, D'Angelo P, Cavallini M, Barbarella G. *J. Am. Chem. Soc.,* **2011**, 133, 8654-8661.

[26] Leclère P, Surin M, Viville P, Lazzaroni R, Kilbinger AFM, Henze O, Feast WJ, Cavallini M, Biscarini F, Schenning APHJ, Meijer EW. *Chem. Mater.,* **2004**, 16, 4452-4466.

[27] Brillante A, Bilotti I, Biscarini F, Della Valle RG, Venuti E. *Chem. Phys.*, **2006**, 328, 125-131.

[28] Lakowicz JR. *Principles of Fluorescence Spectroscopy*. Springer, Singapore, 3rd edn, **2006**.

[29] Sauer M, Hofkens J, Enderlein J. *Handbook of Fluorescence Spectroscopy and Imaging.*, Wiley-VCH rlag GmbH & Co. KGaA Weinheim **2011**.

[30] Vicinelli V, Bergamini G, Ceroni P, Balzani V, Vögtle F, Lukin O. *J. Phys. Chem. B*, **2007**, 111, 6620-6627.

[31] Bergamini G, Marchi E, Ceroni P, Balzani V. "Enlightening Structure and Properties of Dendrimers by Fluorescence Depolarization", in Designing Dendrimers, eds. S. Campagna, P. Ceroni, F. Puntoriero, John Wiley & Sons, Hoboken, **2012**, ch. 11, 341-366.

[32] Gierschner J, Ehni M, Egelhaaf HJ, Medina BM, Beljonne D, Benmansour H, Bazan GC. *J. Chem. Phys.*, **2005**, 123, 144914.

[33] Simbrunner C. *Semicond. Sci. Technol.,* **2013**, 28, 053001.

[34] Eliel EL, Wilen SH, Mander LN. Stereochemistry of Organic Compounds. John Wiley and Sons, **1994**, 1142-1145.

[35] Clayden J, Moran WJ, Edwards PJ, LaPlante SR. *Angew. Chem. Int. Ed.,* **2009**, 48, 6398-6401.

[36] Leroux F. *ChemBioChem,* **2004**, 5, 644-649.

[37] Suárez M, Branda N, Lehn JM, Decian A, Fischer J. *Helv. Chim. Acta*, **1998**, 81, 1-13.

[38] Crego-Calama M, Reinhoudt DN. *Top. Curr. Chem.*, **2006**, 265.

[39] Micali N, Engelkamp H, van Rhee PG, Christianen PCM, Monsu` Scolaro L, Maan JC. *Nat. Chem.*, **2012**, 4, 201-207.

[40] Xu J, Semin S, Niedzialek D, Kouwer PHJ, Fron E, Coutino E, Savoini M, Li Y, Hofkens J, Uji-I H, Beljonne D, Rasing T, Rowan AE. *Adv. Mater.,* **2013**, 25, 2084-2089.

[41] Wang C, Dong H, Hu W, Liu Y, Zhu D. *Chem. Rev.,* **2012**, 112, 2208-2267.

[42] Gentili D, Di Maria F, Liscio F, Ferlauto L, Leonardi F, Maini L, Gazzano M, Milita S, Barbarella G, Cavallini M. *J. Mater. Chem.,* **2012**, 22, 20852-20856.

[43] Constantin LA, Fabiano E, Della Sala F. *J. Chem. Theory Comput.*, **2013**, 9, 2256-2263.

Part II: Nanoscale Characterization and Unexpected Photovoltaic Behaviour of Low Bandgap Sulfur-Overrich-Thiophene/Benzothiadiazole Decamers and Polymers

I. INTRODUCTION

The synthesis of conjugated polymers alternating donor and acceptor building blocks is a well known strategy to obtain low band gap materials finding application in organic devices such as field-effect transistors and photovoltaic cells.[1-3] Low band gap conjugated materials are roughly defined as having a band gap below 2eV and a variety of polymers with this characteristic have been described. The search for the best donor and acceptor moieties to ensure the most efficient polymers, in particular in photovoltaic applications, is a topic of large current interest.[4-8] The engineering of molecular structures for application in organic devices requires appropriate building blocks to be covalently linked *via* organic synthesis to obtain the desired electronic properties and the appropriate aggregation modalities in thin films.[9] Furthermore, the synthetic patterns employed should be reproducible, ecocompatible, amenable to large-scale production and the resulting compounds should be soluble and processable in non-chlorinated solvents. This holds particularly true for organic solar cells, which are expected in the near future to provide renewable energy sources compatible with low-cost/large-area production technologies.[10-12] The most widely employed acceptor building blocks are benzothiadiazole and its variants, substituted with long alkyl or alkoxy chains to make the polymers soluble, while among the most investigated donor building blocks are linear and fused thiophene derivatives or substituted pyrroles and benzothiophenes. Various types of alternation of donor and acceptor building blocks have been described leading to tunable molecular packings and film morphologies.[1-13] Here we report the synthesis of a novel class of decamers and polymers having a conjugated backbone alternating sulfur-overrich bis(3,4'-S-alkyl)-2,2'-bithiophenes electron donor units and benzothiadiazole electron acceptor units (Scheme 1). Sulfur-overrich oligothiophenes are so named since they have an extra sulfur atom per ring directly attached to one of the carbons β to thiophene sulfur.[14] The main aim of our work was to investigate the effect of the additional sulfur atom, attached to alkyl chains of different length and branching, on the solid state electronic properties, redox potentials and band gaps of thiophene-benzothiadiazole oligomers and polymers as well as on their packing and nanoscale morphologies. To this purpose we developed a synthetic protocol exploiting the use of enabling technologies such as ultrasound and microwave assistance[15] to make the reactions more rapid and clean. To check the applicability of the newly synthesized decamers and polymers in photovoltaic devices we carried out Kelvin Probe Force Microscopy[16-17] measurements to obtain surface photovoltage maps under illumination of spin-coated films of the pure materials and, for comparison, of their blends with [6,6]-phenyl-C61-butyric acid methyl ester (PCBM), the fullerene derivative most often employed as electron acceptor in bulk heterojunction photovoltaic cells (BHJ).[18] To our surprise, KPBM data showed that under illumination charge generation and separation were obtained in both cases and with a similar trend. This result suggested that spin-coated films of pure **1-6** had the appropriate electrical characteristics and morphology to be employed as donor-acceptor materials in single-material organic solar cells (SMOCs[19]). SMOCs are organic solar cells employing only one single photoactive material,

containing donor and acceptor moieties in the same molecule and capable of ensuring all the required tasks normally achieved by separate donor and acceptor materials in BHJ cells, namely the efficient absorption of light, the dissociation of the formed excitons and the transport of holes and electrons. Different types of materials with these characteristics have already been described, spanning from block copolymers to "double cable" polymers to donor-acceptor conjugated oligomers and polymers.[19-23] The highest power conversion efficiencies for SMOC devices - in the range 1.7-1.9% - have been achieved with block copolymers based on dyads of poly(3-hexylthiophene) and fullerene C60[22] or oligo(p-phenylenevinylene) and C70.[24] Lower power conversion efficiencies have been obtained with donor-acceptor molecular or polymeric materials.[19] Very recently, SMOC devices based on an air stable donor-acceptor DPP-thieno-TTF copolymer have been described displaying a power conversion efficiency of 0.3%,[25] a value comparable to those obtained for most of the SMOCs based on donor-acceptor conjugated materials. Although these power conversion efficiencies are one order of magnitude lower than those achieved to date with bulk heterojunction cells,[26] the research in the direction of single material solar cells is prompted by the huge technological simplification of the fabrication process of this type of device. In agreement with KPBM results, compounds **1-6** displayed photovoltaic behaviour in SMOC devices with power conversion efficiencies in the range 0.24-0.54%, in line with the best results obtained so far for the few donor-acceptor molecules already reported in the literature as photoactive materials in single-component solar cells.[19-25] To our knowledge, this is the first time that thiophene-benzothiadiazole conjugated oligomers and polymers are shown to be useful materials for application in single-component solar cells.

II. RESULTS AND DISCUSSION

The molecular structure of decamers 1-3 and polymers 4-6 and the corresponding synthetic routes are outlined in Scheme 1. Compounds 1-6 were obtained by connecting electron donor bis(3,4'-thioalkyl)-2,2'-bithiophene with the electron acceptor 2,1,3-benzothiadiazole. The S-alkyl groups contained either a linear *n*-hexyl chain (R=Hex) or branched chains of different length, namely 2-methyl-pentyl (R=Branched1, six carbons) or 2-ethylhexyl (R=Branched2, eight carbons).

2.1. Synthesis and characterization. Ultrasound and microwave irradiations (US, MW) were employed for bromination reactions and Suzuki cross couplings, respectively.[15] Bromination reactions were carried out in CH_2Cl_2 at room temperature, while Suzuki reactions were carried out in THF/H_2O at 80 °C. This synthetic protocol allowed us to obtain the decamers in yields higher than 80% and the polymers with highly reproducible molecular weights and polydispersities (scheme 1). In addition, products purification was facilitated by the small amount of by-products formed. ^1H and ^{13}C NMR spectra of final products and intermediates are shown in Figures S1-S27. GPC, DSC and TGA of polymers 4-6, are reported in Table 1. All polymers showed good thermal stability in air which increased under nitrogen atmosphere. It can be noticed that the decomposition temperatures (T_d) of the samples with branched side chains are lower with respect to the derivative bearing hexyl side chains, both in air and under nitrogen, probably due to a less compact packing. The DSC thermograms of 4-6 reveal only

second order thermal transitions attributable to glass transition (T_g) with the absence of any crystallization peak, indicative of an essentially amorphous structure of these materials in the solid state. The T_g values appear in the order polymer 5 (R=Branched1) > polymer 6 (R=Branched2) ≈ polymer 4 (R=Hex) owing to the greater stiffness of the side chains in polymer 5 (R=Branched1) that somewhat reduces the macromolecules mobility in the solid state.
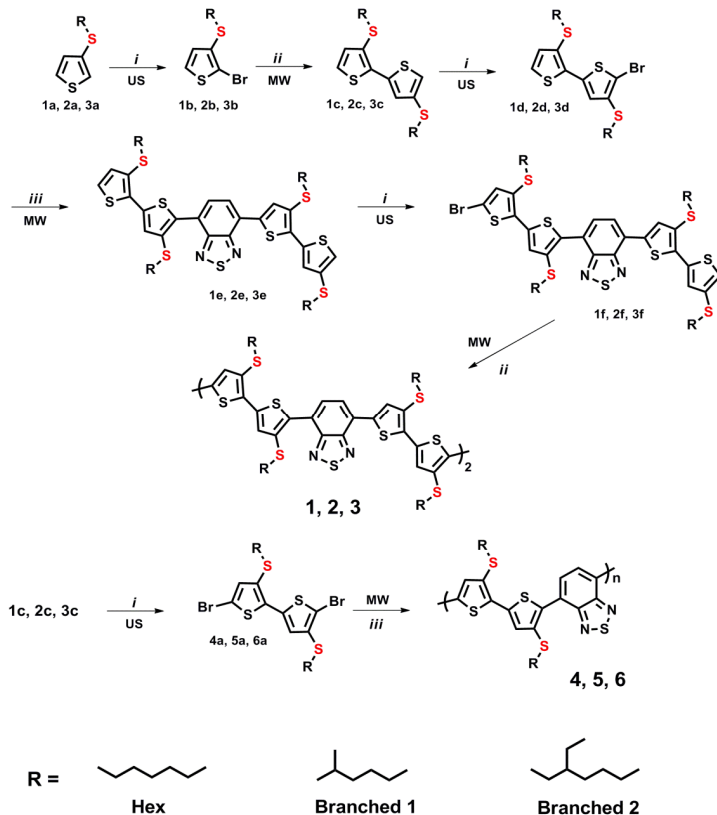
Scheme 1. Ultrasound (US) and microwave (MW) assisted synthesis of compounds **1-6**. *i)* 1 or 2 eq NBS, CH$_2$Cl$_2$, US, room T; *ii)* 4,4,5,5-tetramethyl-1,3,2-dioxaborolane 0.6 eq, Pd(dppf) Cl$_2$, NaHCO$_3$, THF/H$_2$O 2/1, MW, 80°C; *iii)* 4,7-bis(4,4,5,5-tetramethyl-1,3,2-dioxaborolan-2-yl)-2,1,3-benzothiadiazole, NaHCO$_3$, Pd(dppf)Cl$_2$, THF/H$_2$O.

Table 1. Molecular weights and Thermal Properties of Polymers 4-6.

Sample	M$_n$[a] (g/mol)	M$_w$[a]/M$_n$	DP$_n$[b]	T$_d$[c] (°C)	T$_g$[d] (°C)
polymer 4 (**4**)	9300	1.62	17.5	330, 360	59.6
polymer 5 (**5**)	8000	1.60	15.9	276, 296	63.5
polymer 6 (**6**)	12400	1.48	21.1	265, 346	59.1

[a] Determined by GPC in THF and polystyrene standard. [b] Average degree of polymerization relative to repeating units. [c] Determined by TGA in air or under nitrogen, respectively. [d] Determined by DSC.

2.2. Optical properties. Table 2 shows the maximum absorption and emission wavelengths (λ_{max}, λ_{em}) and molar absorption coefficients (ε) of compounds 1-6 (1.1×10^{-4} M) in CH_2Cl_2 as the solvent and in thin solid films obtained by spin-coating from CH_2Cl_2 and 70:30 toluene:acetonitrile. The corresponding UV-vis spectra are shown in Figure 1.

Table 2. UV–vis maximum absorption and emission wavelengths of decamers 1-3 and polymers 4-6 in solution and in thin films.

Item	Material	λ_{max} (nm)[a]	λ_{em} (nm)[a]	ε ($M^{-1}cm^{-1}$)[a]	λ_{max} (nm)[b]	λ_{max} (nm)[c]
1	decamer 1	514	715	52100	560	610
2	decamer 2	518	700	53400	556	554
3	decamer 3	522	715	58000	562	556
4	polymer 4	538	727		614	603
5	polymer 5	546	707		602	590
6	polymer 6	612	748		672	670

a) In CH_2Cl_2. b) Films deposited from CH_2Cl_2. c) Films deposited from 70:30 toluene:acetonitrile (v:v).

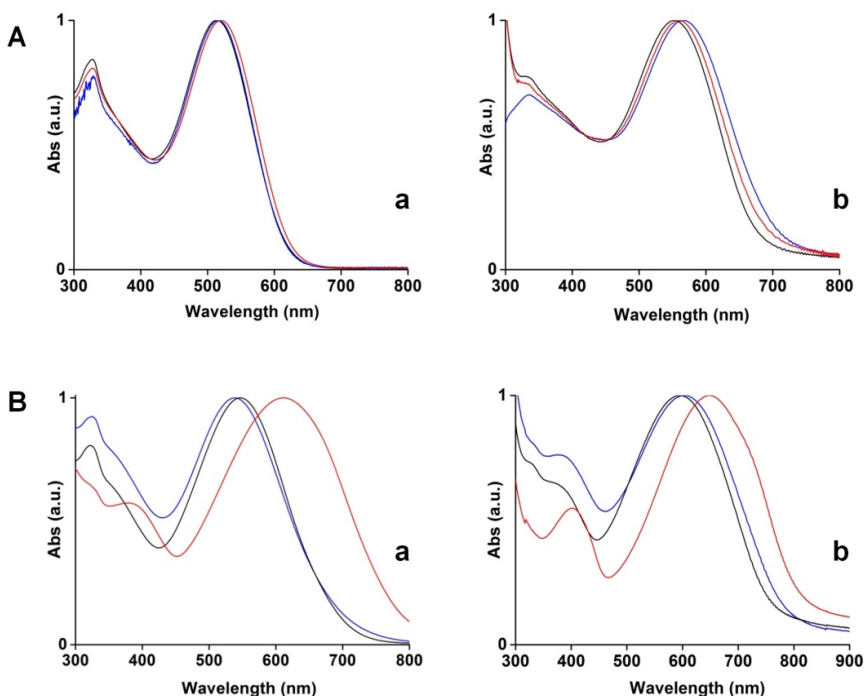**Figure 1.** Normalized absorption spectra of decamers (A) and polymers (B) in CH_2Cl_2 (a) and as spin-coated films from CH_2Cl_2 (b). Blue: decamer 1 and polymer 4; black: decamer 2 and polymer 5; red: decamer 3 and polymer 6.

Several non chlorinated organic solvents were checked but only minor changes were observed for the absorption spectra in solution passing from one to another. The same result was

obtained with spin-coated films from the different solutions. In this case a significant change (50 nm) was only observed for decamer 1 (R=Hex) on passing from CH_2Cl_2 to 70:30 toluene:acetonitrile as deposition solvent. Most probably this result was due to the greater capability of linear alkyl side-chains to promote structural ordering in the solid state compared to branched ones also trough side-chains interdigitation. Table 2 and Figure 1A (a) show that the maximum absorption wavelength of decamers 1-3 increases progressively in CH_2Cl_2 when R changes from R=Hex to R= Branched1 to R=Branched2. The same but more accentuated trend is observed for polymers 4-6 Figure 1B (a). In particular, polymer 6 (R=Branched2) shows a bathochromic shift of 74 nm with respect to polymer 4 (R=Hex) and of 66 nm with respect to polymer 5 (R=Branched1). In solution a large Stokes shift from absorption to emission is observed for both decamers and polymers, in the range 135-201 nm, probably in most part due to the planarization of the aromatic backbone in the excited state. Going from solution to spin-coated film a bathochromic shift of a few tens of nm is observed for both decamers Figure 1A (b) and polymers Figure 1B (b), the largest, 76 nm, being those of polymer 4 (R=Hex) for the film spin-coated from CH_2Cl_2 and of decamer 1 (R=Hex), 96 nm, for the film spin-coated from toluene:acetonitrile. As mentioned above, decamer 1 (R=Hex) is the only compound showing a remarkably different absorption spectrum in film spin-coated from toluene:acetonitrile with respect to that spin-coated from CH_2Cl_2. Side-chains effects on the optical properties of conjugated oligomers and polymers are largely dependent on the molecular system under investigation. In our case S-alkylated chains are involved and S···S non bonding intra and intermolecular interactions are likely to play a significant role. However, further studies on the self-assembly properties of compounds **1-6** are required before sound hypotheses can be made.

2.3. Structural Characterization and Theoretical Analysis of the Crystalline Film of Decamer 1 (R=Hex). Figure 2 (A-B) shows the absorption spectrum of the spin-coated films of decamer **1** (R=Hex) deposited from CH_2Cl_2 (black trace) and from toluene:acetonitrile (red trace) and the corresponding X-ray diffraction plots. The figure shows that the former film is amorphous while the latter is crystalline and displays the presence of one narrow reflection at 4.8° (1.8 nm) in the diffraction pattern.
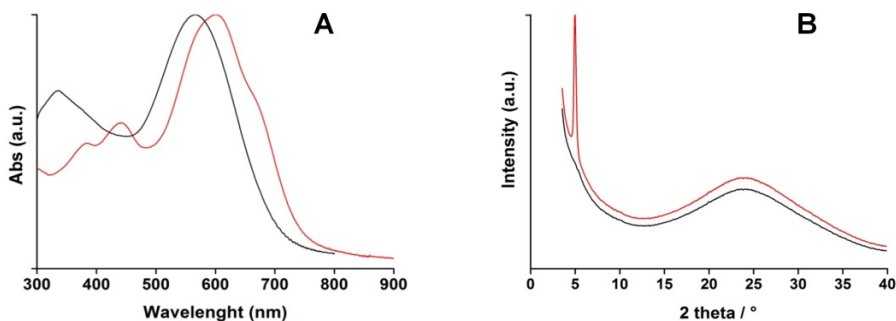

Figure 2. A) Absorption spectra and B) X-ray diffraction patterns of decamer (**1**) spin-coated film from CH_2Cl_2 (black trace) and toluene:acetonitrile 70:30 (red trace).

To get some clues on the way molecules containing our donor and acceptor components tend to pack in the solid state we performed a computational study using Density Functional Theory (DFT) with full periodic boundary conditions to simulate the molecular aggregation in solids. Because for such an investigation considering the decamer leads to a too high computational cost, which prevents a full study of all possible configurations, we used as a model the pentamer (Figure 3A), which is expected to provide all valuable information without exceeding our computational capability. The calculations have been carried out with the VASP progBranched1 using PBE-PAW pseudopotentials and the APBE exchange-correlation potential with a D3 dispersion correction. All Brillouin zone integrations were performed on Γ-centered symmetry-reduced Monkhorst-Pack k-point meshes, using the tetrahedron method with Blöch corrections. For all the calculations a 4x4x4 k-mesh grid was applied and a plane-wave cutoff of 600 eV was chosen.[27-30] Figure 3B-D shows the conformation of the molecule and its calculated arrangement within the primitive cell. According to the calculations, the molecules are planar with the S-CH$_3$ substituents almost perpendicular to the aromatic backbone. They are stacked in columns with a stacking distance of 3.5 Angstrom. As shown in Figure 3B, two stacked molecules have the benzothiazole unit arranged in opposite directions in order to optimize the interaction and minimize the steric repulsion. Moreover, the molecules are slightly shifted so that the benzothiazole rings are only partially superimposed. On the basis of the calculations on the model pentamer, it is reasonable to assume that the decamer is also planar in the solid state, an assumption also supported by the fact that the inner quaterthiophene tends to assume a planar conformation in the solid state.[14,31,32]
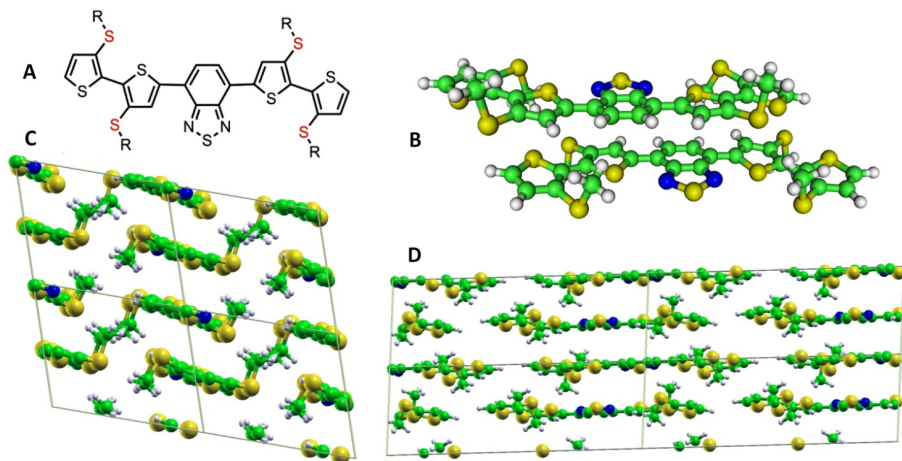
Figure 3. Molecular structure of the model pentamer (A) employed for DFT calculations. (B) Dimer, (C,D) two different views of the 3D periodic crystal structure.

Figure 4 shows a possible model of the supramolecular organization of the crystalline film of decamer **1** built on the basis of the indications obtained from the calculations and taking into account the XRD pattern of the sample obtained from toluene acetonitrile (Figure 2B).
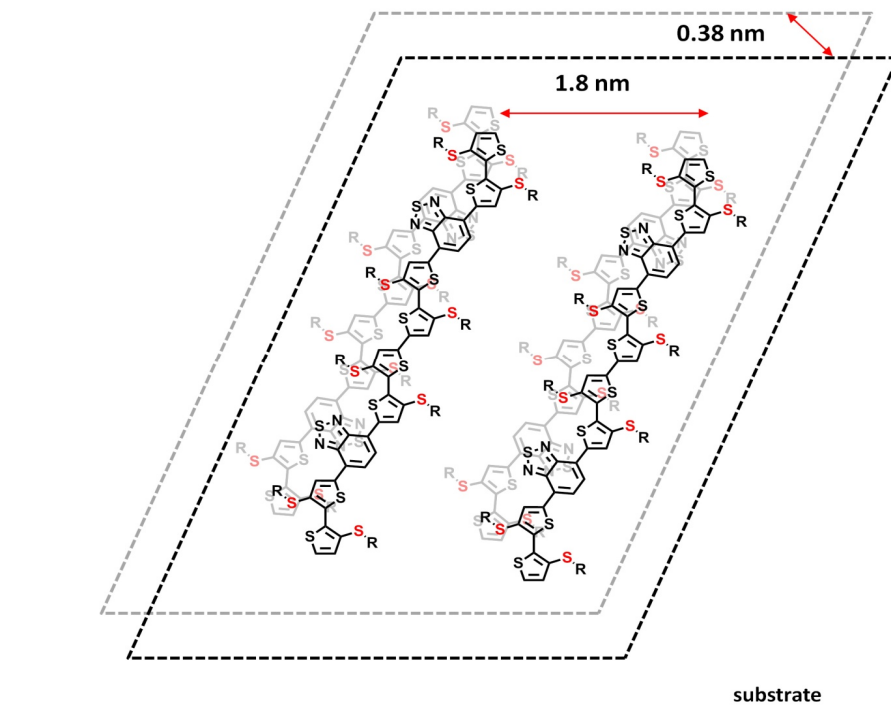
Figure 4. Proposed model for the supramolecular organization of decamer **1** (R=Hex) in crystalline thin film spin-coated from toluene:acetonitrile 70:30 v:v.

Decamer **1** is planar and exhibits a layered structure with the π-conjugated backbones of all molecules parallel to one another. Consecutive planes are stacked by 0.38 nm, a distance equivalent to an angle (2θ=23.4°) whereas a broad halo is detected. The distance between the thiophene molecules belonging to the same plane is 1.8 nm. The presence of S-alchil substituents almost perpendicular to the main molecular plain was not a novelty.[14,31,32] This packing is sometimes preferred to the 'herringbone' arrangement typical of thiophene materials where the conjugated planes have face to edge contacts. It occurs, for example, in a regioregular β-alkylated dodecylthiophene.[33] The increased flexibility of side chains due to the sulfur atom presence will adapt them to the most suitable conformations that best pack in the crystal.

2.4. Cyclic voltammetry. Table 3 shows the onset potentials of the oxidation and reduction waves of decamers 1-3 and polymers 4-6 thin films, estimated from cyclic voltammetries, and the corresponding HOMO and LUMO energy values.[34] Figure 5 (A, B) shows the cyclic voltammetries of decamer 1 (R=Hex) deposited from toluene:acetonitrile and CH$_2$Cl$_2$ and those of the films of decamer 3 (R=Branched2) and polymer 6 deposited from 70:30 toluene:acetonitrile. The corresponding cyclic voltammetries of decamer 2 (R=Branched1) and polymers 4,5 are shown in Figure 28S.

Table 3. Solid-state cyclovoltammetry data of compounds 1-6 deposited from 70:30 toluene:acetonitrile estimated from the onset of the oxidation and reduction waves (1st cyclic voltammetry) and the corresponding HOMO and LUMO energy values.

Item	Materials	E^{onset}_{red} V *vs.* SCE	E^{onset}_{ox} V *vs.* SCE	LUMO eV	HOMO eV	EG eV
1	decamer 1	-1.00 (-1.17)*	0.67 (0.77)*	-3.68 (-3.51)*	-5.35 (-5.45)*	1.67 (1.84)*
2	decamer 2	-1.08	0.88	-3.60	-5.56	1.96
3	decamer 3	-1.09	0.80	-3.59	-5.48	1.89
4	polymer 4	-1.10	0.81	-3.58	-5.49	1.91
5	polymer 5	-1.11	0.86	-3.57	-5.54	1.97
6	polymer 6	-1.16	0.76	-3.52	-5.44	1.92

*Values in parenthesis are relative to the film deposited from CH_2Cl_2.
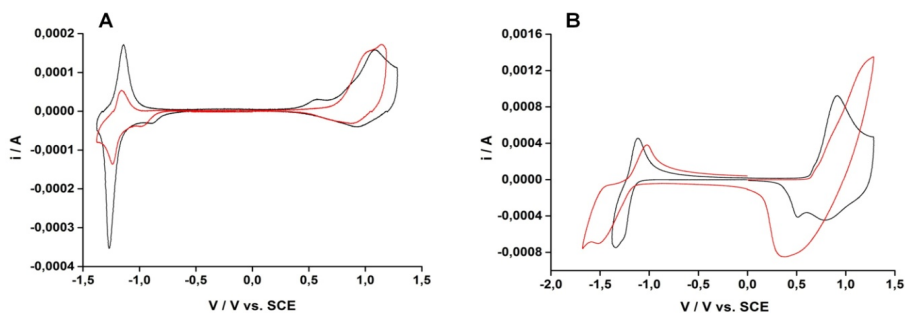
Figure 5. Cyclic voltammetries of the films of A) decamer **3** (R=Branched2, red trace) and polymer **6** (R=Branched2, black trace) deposited from toluene:acetonitrile; B) decamer **1** (R=Hex) deposited from toluene:acetonitrile (black trace) and CH_2Cl_2 (red trace).

The oxidation potentials vary within 210 mV, the lowest value (0.67 V) being that of the crystalline film of compound 1 deposited from toluene:acetonitrile (0.77 V for the amorphous film deposited from CH_2Cl_2). Among the polymers, polymer 6, displays the lowest oxidation potential (0.76 V). The reduction potentials vary within a range of only 170 mV, the less negative value (-1.0 V) being that of the crystalline film of decamer 1 (R=Hex) (-1.17 V for the amorphous film). The corresponding HOMO energy levels of compounds 1-6 are the in the range 5.35 to 5.56 eV and the LUMO energy levels in the range 3.51-3.68 eV with energy gaps varying from 1.67 to 1.89 eV, the lowest energy gap being that of the crystalline film of decamer 1 (R=Hex). It should be noticed that compared to most donor-acceptor alternating oligomers and polymers reported in the literature[35] compounds 1-6 are characterized by less negative reduction potentials, i.e. higher electron affinities. This result is in agreement with previously reported data according to which a thiophene hexadecamer with one S-alkyl chain per ring displays in thin film a greater electron affinity than the corresponding hexadecamer having alkyl- instead of S-alkyl chains.[32] A sketch illustrating the relative energy levels of

HOMO and LUMO orbitals of compounds 1-6 compared to the corresponding levels of PEDOT:SS, P3HT and PCBM, the most popular components of BHJ, is reported in Figure S29. The cyclovoltammetry data are consistent with the results of DFT calculations on an isolated decamer (R=SCH₃) performed with the TURBOMOLE program Package,[36] using a PBE0 exchange-correlation functional[37] and a def2-TZVP basis set,[38] which can also be used to inspect the electron distribution within the orbitals. An isodensity plot of the HOMO and LUMO is reported in Figure 6. The figure shows that the HOMO displays a larger effective conjugation length, being concentrated on the inner quaterthiophene while the LUMO is concentrated on the two separate benzothiazole groups.
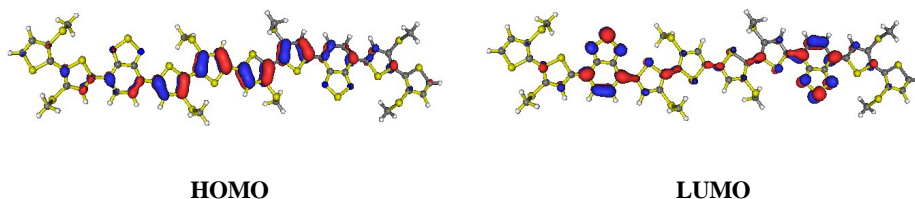

HOMO　　　　　　　　　　　　　　　　　　　**LUMO**

Figure 6. Frontier molecular orbital distribution of decamer (R= SCH₃) calculated with the TURBOMOLE program.[35]

2.5. Kelvin Probe Force Microscopy (KPFM). The electronic properties of thin films can be investigated with nanoscale resolution by KPFM, which allows the determination of the surface potential of nano-objects[16-17] and the explorations of the photovoltaic effect in real time.[39] We performed KPFM measurements on spin-coated films of pure 1-6 and, for comparison, on spin-coated films of their blends with PCBM, to obtain surface photovoltage maps correlating morphological and surface electronic properties. KPFM is a powerful tool to measure the surface potential and the photoinduced surface photovoltage with a lateral resolution better than 100 nm and correlate this with the topography of the film examined.[40] It allows, in particular, to investigate charge carrier generation under illumination after dissociation of excitons.[16] This technique, performed by means of a noncontact AFM tip with a conductive coating, makes it possible to obtain a quantitative measurement of the surface potential (SP) through the difference between the tip potential and the local surface potential.[40] Being contactless, it does not perturb significantly the system under study. For this reason it is also used for the in situ exploration of operating electronic devices. Our objective was to obtain information on the ability of charge generation under illumination of the spin-coated films of pure 1-6 and, for comparison, also of the spin-coated films of their blends with PCBM. The formation of charges can be revealed by a shift of the surface potential under illumination with respect to the dark (ΔSP$_{light-dark}$). The films were all prepared by spin coating from a 70:30 toluene:acetonitrile solution. KPFM images were obtained over the same area of the sample under three different conditions: i) without light (labeled "dark 1"), ii) under illumination (labeled "light"), and iii) after illumination (labeled "dark 2") using an experimental setup described in other works.[41] The surface potential curves were calculated from the expression ΔSP = ϕsample −ϕtip. The

work function of the tip was measured by calibrating the cantilever on a highly oriented pyrolytic graphite (HOPG) reference sample as previously reported.[41] Figure 7 and Figure 8 illustrate the results for decamer 3 (R=Branched2) and polymer 6 (R=Branched2). Other data are reported in Figure 30S and Figure 31S.
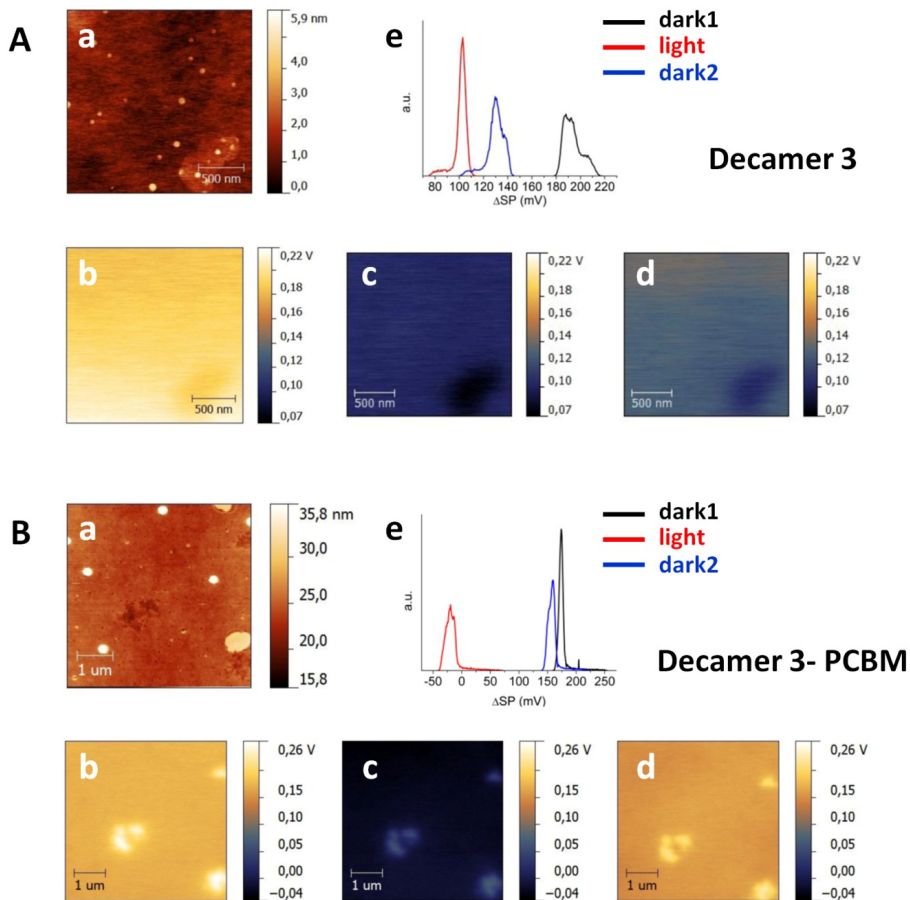
Figure 7. A) (a) Surface topography images of a spin-coated film from toluene:acetonitrile of decamer 3 (R=Branched2); (b,c,d) the corresponding KPFM images (dark1, light, dark2) and (e) surface potential distributions. B) The same for decamer 3 in blend with PCBM.
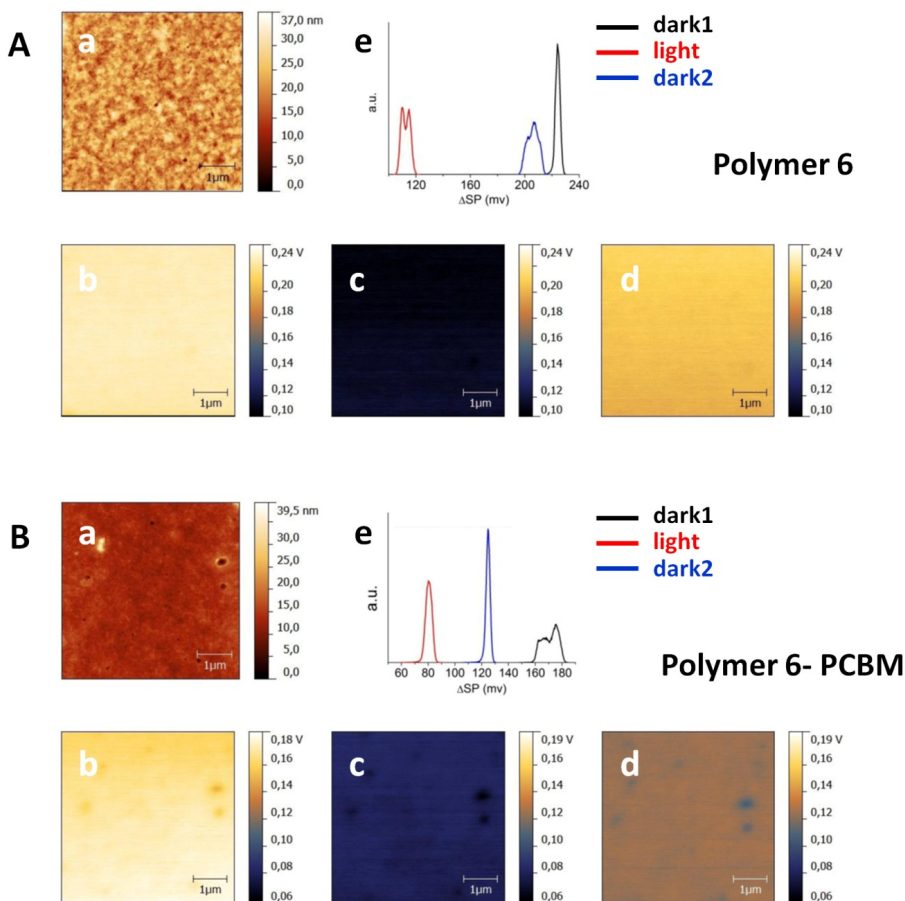
Figure 8. A) (a) Surface topography images of a spin-coated film from toluene:acetonitrile of polymer 6 (R=Branched2); (b,c,d) the corresponding KPFM images (dark1, light, dark2) and (e) surface potential distributions. B) The same for polymer 6 in blend with PCBM.

Considering the films of Figures 7 B (a-e) and 8 B (a-e), formed by the blends of compounds 3 or 6 with PCBM, free charges are photogenerated under illumination at the interfaces of the heterojunction after dissociation of excitons. The formation of charges is revealed by a shift of the surface potential under illumination and in the dark ($\Delta SP_{light-dark1}$). Switching off the illumination ('dark 2'), the surface potential shifts to values close to those measured before illumination ('dark 1'), indicating that the surface potential shift is not due to artifacts but it is the consequence of a reversible process. Interestingly, the trend of variation of the surface potential under illumination shown in Figure 7 A (a-e) and Figure 8 A (a-e) for the films made of pure 3 or 6 is the same as that of their blends with PCBM. This means that there is photovoltaic activity under illumination also in the films of the pure materials that consequently can be checked in single-material organic solar cells. A table of $\Delta SP_{light-dark1}$ values for all

compounds alone or blended with PCBM is reported in experimental section (Table S1). It is worth noting that the surface potential depends on the presence of surface or bulk charges, on dipoles, and on the interfacial electronic states in the heterostructures.[42] When the illumination is switched off the carriers recombination rate should, in principle, give to the surface potential the time necessary to recover the initial value showed in Dark1. However, the surface potential values decay exhibits both a slow surface (~minutes to hours) component associated with the filling and emptying of deep traps and a fast (~milliseconds or faster) component associated with the recombination of excess free carriers.[43] In our experiments we noticed a slow decay (not reported), with most of the photovoltage dissipating on time scales of ~ hours. This slow recombination of the excess carrier population in OPV is the reason why a difference is observed between the surface potential distribution values in Dark1 and Dark2.

2.6. Photovoltaic behaviour of films of 1-6. Based on the results of KPFM measurements, the photovoltaic behaviour of compounds 1-6 was tested in SMOC devices[19] using the pure compounds as single photoactive components. An ITO electrode coated with a film of PEDOT-PSS and an aluminum cathode were employed (see experimental section). In agreement with KPFM data, all compounds displayed photovoltaic behaviour in single component photovoltaic devices. The photovoltaic characteristics of the SMOC devices are reported in Table 4 and the corresponding I-V plots in Figure S32.

Table 4. Photovoltaic characteristics of spin-coated films of 1-6 in SMOC devices.[a]

Item	Materials	J_{SC} (mAcm^{-2})	V_{OC} (V)	FF %	η %
1	decamer 1[b]	1.37	0.50	0.35	0.24
		(6.06)	(0.51)	(0.35)	(1.07)
	decamer 1[c]	1.55	055	0.45	0.38
2	decamer 2	1.22	0.38	0.38	0.35
		(7.18)	(0.55)	(0.33)	(1.30)
3	**decamer 3**	**2.36**	**0.51**	**0.45**	**0.54**
		(8.34)	(0.62)	(0.35)	(1.80)
4	polymer 4	1.05	0.37	0.37	0.12
		(4.33)	(0.44)	(0.35)	(0.67)
5	polymer 5	0.98	0.40	0.40	0.15
		(5.42)	(0.47)	(0.34)	(0.86)
6	polymer 6	1.52	0.49	0.40	0.30
		(9.67)	(0.58)	(0.28)	(1.56)

[a] Values in parenthesis are relative to blends of **1-6** with PCBM (1:1 weight ratio) in BHJ devices. [b]Spin-coated film from CH$_2$Cl$_2$. [c]Spin-coated film from toluene-acetonitrile (70:30 v:v). The values reported are averaged values obtained from three different devices prepared under the same operative conditions.

The results of Table 4 - which were obtained without any attempt to optimize the cell structure or the morphology of the film through, for example, annealing or addition of additives - unambiguously indicate that compounds **1-6** act as donor-acceptor materials in SMOC devices. The best efficiency is that of the decamer functionalized with the S-(2-ethylhexyl) group (decamer 3) showing a 0.54% value. So far, for most SMOCs based on donor-acceptor compounds conversion efficiency values in the range 0.002-0.51% have been reported[19], and

only one single paper reports a value of 1.50% obtained with an optimized device.[44] Since thiophene-benzothiadiazole derivatives generally act as electron donors in BHJ devices,[1-13] the behaviour of blends of 1-6 with PCBM was also tested in BHJ devices. The photovoltaic characteristics of the BHJ devices are reported in parentheses in Table 4 while the corresponding I-V plots are shown in Figure S32. Also in BHJ devices the highest efficiency (1.8%) is that of decamer 3 (R=Branched2). It is worth noting that conversion efficiency values similar to those obtained for 3 have been reported by Roncali et al. for a star-shaped donor-acceptor system having a triphenylamine core and a peripheral thienyl cyano group (namely 0.40% for the SMOC device and 1.85% for the same material in BHJ device).[45] The very recently reported donor-acceptor conjugated DPP-thieno-TTF copolymer displays a conversion efficiency of 0.3% in SMOC device and of 1.8 in BHJ device for the blend of the same copolymer with PC$_{71}$BM.[25] Although phase segregation is not a prerequisite to obtain the generation of a measurable photovoltage in single material polymeric films,[46,47] owing to the fact that compounds 1-6 are photoactive materials in SMOC devices, donor and acceptor nanodomains must be present in their spin-coated films in order to ensure not only light absorption and charge-separation but also the basic function of charge-transport. In other words, the self-assembled films must contain substructures on nanometer scale (that is, a scale comparable to the mean exciton diffusion length) having the appropriate organization for separate hole and electron transport. We suggest that the formation of appropriate nanoscale substructures are driven by sulfur···sulfur intra and intermolecular interactions, which have already been demonstrated to be a powerful tool to promote self-organization in sulfur-overrich oligothiophenes.[14] It is worth noting that for single component solar cells (as well as for the corresponding BHJ devices) the decamers, monodisperse and with well defined molecular structure, display better performance than the corresponding polymers. Table 4 shows that in the decamers as well as in the polymers changing the side chain leads to sizeable variations of all parameters of the photovoltaic devices, in agreement with already published work on the influence of side chains on photovoltaic properties of BHJ cells.[48-49] In this respect, it is again worth noting that the trend of variation with the side chains of all parameters displayed in Table 4 for SMOC devices is the same as that of the corresponding BHJ devices. Finally, Table 4 shows that the performance of decamer 1 (R=Hex) increases for the crystalline film spin-coated from toluene:acetonitrile compared to the amorphous film spin-coated from dichloromethane. This result suggests that there is much room to improve the efficiency of solar cells having the title compounds as active materials, in particular as single photoactive components, through the appropriate choice of the S-alkyl groups (chain length and/or branching) and deposition solvent.

III. CONCLUSION

In summary, we have demonstrated that newly synthesized linear conjugated compounds alternating electron donor 'sulfur-overrich' thiophene units and electron acceptor benzothiadiazole units may act as donors and acceptors in single material organic solar cells (SMOCs[19]) and can be viewed as paintable organic solar materials. To our knowledge no other thiophene-benzothiadiazole co-oligomers or co-polymers of the many described in the literature have been reported to display similar characteristics. We ascribe this result to the presence of

the extra sulfur atoms directly attached to the β-carbons of the thiophene ring of the S-alkyl side chains ensuring the structural control of inter-chain interactions and self-aggregation modalities via S···S non bonding interactions. These interactions have already been demonstrated to be dominant in the formation of 'sulfur-overrich' oligothiophene microfibers.[14] In compounds 1-6 they promote the nanoscale self-organization in spin-coated films in such a way that nanodomains for separate hole and electron transport are formed. SMOCs based on conjugated donor-acceptor moieties represent the ultimate stage of simplification of solar cells[19] and although their conversion efficiences are currently more than one order of magnitude lower than those of bulk heterojunction solar cells, it is reasonable to predict that more extensive investigations on molecular structures and functioning mechanisms, in particular charge generation and recombination dynamics, will rapidly lead to much better results. In our study, to identify synthesized donor-acceptor compounds capable to act as donor and acceptors in SMOCs, we employed Kelvin Probe Force Microscopy measurements, showing that under illumination charge generation and separation were obtained in thin films of the pure materials with a similar trend to that observed in thin films of blends of the materials with PCBM. One point to stress is that compounds 1-6 are very easy to prepare in high yields and very pure form thanks to the possibility to employ ultrasound and microwave assistance, which greatly facilitate the synthesis of thiophene derivatives. Moreover, compounds **1-6** are air stable, very soluble and easy to deposit from solution in single-layer. We believe that further investigations on conjugated compounds alternating ''sulfur overrich'' thiophene moieties and benzothiadiazole will lead to the identification of the most appropriate alternation sequence of donors and acceptors and to the definition of correct structure-property correlations hence to more adequate design of materials and much better performance in SMOC devices.

IV. EXPERIMENTAL SECTION

4.1. General

4.1.1. Materials and Methods. Reactions with ultrasound irradiation were performed in a FALC LBS1 50KHz Ultrasonic bath at room temperature. Microwave irradiation was performed in a Milestone Microsynth Labstation operating at 2450 MHz equipped with pressure and temperature sensors. All ^{1}H NMR and ^{13}C NMR spectra were recorded on a Varian Mercury-400 spectrometer equipped with a 5-mm probe. Mass spectra were collected on a Finningan Mat GCQ spectrometer. UV-Vis spectra were recorded on a Perkin Elmer Lambda 20 spectrometer. Photoluminescence spectra were recorded on a Perkin Elmer LS50 spectrofluorometer exciting at a wavelength corresponding to the maximum absorption wavelength. Number-average (M_n) and weight-average (M_w) molecular weights of the polymers and their polydispersity indexes (M_w/M_n) were determined by gel permeation chromathography (GPC) in THF solution using a HPLC Lab Flow 2000 apparatus, equipped with an injector Rheodyne 7725i, a Phenomenex Phenogel Mixed 5μ MXL column and a UV-Vis detector Linear Instruments model UVIS-200, working at 254 nm. Calibration curve was recorded using several monodisperse polystyrene standards. The initial thermal decomposition temperature (T_d) of the polymers was determined by using a TA Instruments SDT-Q600 thermogravimetric analyser operating at a heating rate of 20°C/min under nitrogen or in air.

The glass transition temperatures of the polymers (T_g) were determined by differential scanning calorimetry (DSC) on a TA Instruments Q2000 DSC Modulated apparatus equipped with RCS cooling system, at a heating rate of 10°C/min under nitrogen after one preliminary heating-cooling cycle. Spin-coated films were grown using a home-made spin-coater operating at 1000 rpm for 1 minute.

4.1.2. X-ray diffraction. XRD investigations were carried out on spin-coated films deposited on glass slides using a PANalytical X'Pert diffractometer (reflection mode, Bragg-Brentano geometry) equipped with a copper anode ($\lambda_{mean} = 0.15418$ nm) and a fast X'Celerator detector.

4.1.3. Cyclic voltammetry. CVs have been performed at 100 mV s^{-1} with an electrochemical systems AMEL 5000 in a three compartment electrochemical cell under Ar pressure. Working electrodes were solid films of the decamers or the polymers on deposited on ITO coated glass (Balzers) disc (diameter 1 mm). The electrolytic solution, carefully purged, was anhydrous propylene carbonate (Sigma-Aldrich) with 0.1 mol L^{-1} tetraethylammonium tetrafloroborate (Fluka for electrochemical analysis stored under vacuum) where the oxidation potential of ferrocene/ferricinium (Fc/Fc$^+$ = -4.84 eV) resulted 0.50 V *vs.* aqueous saturated calomel electrode (SCE).

4.1.4. Kelvin Probe Force Microscopy. KPFM images were obtained with a commercial AFM system (Bruker-AXS) MultiMode AFM equipped with a Nanoscope V controller operating in lift mode (typical lift height 20 nm) and using silicon tips with PtIr coating (SCM- PIT) with k ≈ 3 N m^{-1}, tip radius ≈ 20 nm, and resonant frequency ≈ 80 kHz.

4.1.5. Photovoltaic Device Fabrication and Testing. ITO/(PEDOT:PSS) (40 nm)/ oligo-polymer (or oligo-polymer:PCBM) (~100nm)/ Al (150 nm). BHJ PV cells were fabricated on patterned ITO-coated glass substrates as the anode. ITO glass (2.5 x 2.5 cm) was first cleaned in an ultrasonic bath using a non-foaming glass detergent in deionized water. It was then rinsed sequentially in double distilled water, isopropanol and acetone. PEDOT:PSS was diluted 1:1 with isopropanol and deposited by doctor blading on the top of the cleaned ITO glass. After baking the films in vacuum at 130°C for 30 min, the active layer film was deposited and the thickness was measured by AFM to be about 100 nm. A solution of 70:30 toluene:acetonitrile was used for the oligomers and a solution of 60:20:20 toluene:acetonitrile:chlorobenzene was for the polymers and PCBM (1:1 weight ratio) which were deposited by doctor blading on the PEDOT:PSS layer. Finally, 150 nm of Al was thermally deposited under the vacuum of 6 x 10^{-7} Torr by means of an Edwards E306A vacuum coating apparatus equipped with a diffusive and a turbo-molecular pump. The current-voltage characteristics were measured using a Keithley 2401 source meter under the illumination of a Abet Technologies LS 150 Xenon Arc Lamp Source AM1.5 Solar Simulator, calibrated with an ILT 1400-BL photometer. The reported PCE results were the averaged values obtained from three different devices prepared under the same operative conditions. The results obtained clearly showed a good reproducibility, with a maximum standard deviation of about 5%.

4.2.   Synthesis *General*. Lithiation and cross coupling reactions were carried out under nitrogen atmosphere using organic solvents dried following standard procedures. Bis(pinacolato)diboron (2-isopropoxy-4,4,5,5-tetramethyl-1,3,2-dioxaborolane) was from Alfa Aesar GmbH & Co KG; sodium bicarbonate from Sigma-Aldrich Co; 1,1′-bis(diphenylphosphino)ferrocene palladium(II)chloride dichloromethane complex (PdCl$_2$dppf),

n-butyllithium 2.5 M solution in hexane from Acros Organics. Solvents and reagents were used as received without further purification. Reactions with ultrasound were performed in a FALC LBS1 50KHz Ultrasonic bath at room temperature. Microwave irradiation was performed in a Milestone Microsynth Labstation operating at 2450 MHz equipped with pressure and temperature sensors. Melting points (uncorrected) were measured using a Kofler bank apparatus. All ^{1}H NMR and ^{13}C NMR spectrum were recorded on a Varian Mercury-400 spectrometer equipped with a 5-mm probe. Chemical shifts are referenced to TMS. Mass spectrum were collected on a Finningan Mat GCQ spectrometer. UV-Vis spectrum were recorded using a Perkin Elmer Lambda 20 spectrometer. Photoluminescence spectrum were obtained from a Perkin Elmer LS50 spectrofluorometer exciting at a wavelength corresponding to the maximum absorption wavelength. Number-average molecular weights (M_n) and weight-average molecular weight (M_w) of the polymers and their polydispersity indexes (M_w/M_n) were determined by gel permeation chromathography (GPC) in THF solution using a HPLC Lab Flow 2000 apparatus, equipped with an injector Rheodyne 7725i, a Phenomenex Phenogel Mixed 5□ MXL column and a UV-Vis detector Linear Instruments model UVIS-200, working at 254 nm. Calibration curve was recorded using several monodisperse polystyrene standards.

The initial thermal decomposition temperature (T_d) of the polymers was determined by using a TA Instruments SDT-Q600 thermogravimetric analyser operating at a heating rate of 20 °C/min under nitrogen or in air. The glass transition temperatures of the polymers (T_g) were determined by differential scanning calorimetry (DSC) on a TA Instruments Q2000 DSC Modulated apparatus equipped with RCS cooling system, at a heating rate of 10°C/min under nitrogen after one preliminary heating–cooling cycle.

***General procedure for the synthesis of compounds* 1a-3a.** To a solution of 3-bromothiophene (25 mmol, 2.34 mL) in anhydrous diethyl ether (25 mL) at -78° C under a nitrogen atmosphere a solution of *n*-butyllithium in hexane (2.5 M, 25 mmol, 10 mL) was added dropwise. After 2.5 h at -78°C sublimed sulfur (25 mmol, 0.804 g) was added and the reaction mixture was stirred for 2 h and then quenched with 100 mL of water. The resulting mixture was extracted with 3x25 mL of a acqueous solution of NaOH 1M. The combined aqueous phases were cooled at 0° C and acidified with 10% hydrochloric acid to liberate the thiol from its sodium salt. The product was then extracted with diethyl ether (3x50 mL). The combined organic phases were dried over anhydrous sodium sulphate and the solvent was removed under reduced pressure. A clear yellow oil (3-mercapto-thiophene, yield 86%) was obtained: EI-MS *m/z* 116(M$^+$); ^{1}H NMR (400 MHz, CDCl$_3$, TMS/ppm): δ 7.31 (dd, ^3J=5.2 Hz, ^4J=3.2 Hz, 1H), 7.19–7.17 (m, 1H), 6.99 (dd, ^3J=5.2 Hz, ^4J=1.6 Hz, 1H), 3.39 (s, 1H). To the previously obtained 3-mercapto-thiophene (21 mmol, 2.4 g) a solution of potassium tert-butoxide (30 mmol, 6.7 g) in anhydrous ethanol (20 mL) was added at 0°C under a nitrogen atmosphere. The mixture was stirred for 30 min at 0°C and after that 1-bromohexane (21 mmol, 2.9 mL) or 2-bromopentane or 2-ethylhexyl bromide was slowly added and the mixture refluxed for 2 h before quenching with 100 mL of water. The product was extracted with diethyl ether (3x30 mL). The combined organic layers were dried over anhydrous sodium sulphate and the solvent was removed under reduced pressure. The residue was isolated by flash chromatography (100% cyclohexane).

3-(hexylsulphanyl)thiophene (**1a**) → Yield 90%. Colorless oil; EI-MS *m/z* 200 (M$^+$); ^{1}H NMR (400 MHz, CDCl3, TMS/ppm): δ 7.30 (dd, ^3J = 5.2 Hz, ^4J = 3.2 Hz, 1H), 7.11 (dd, ^3J = 2.8 Hz, ^4J = 1.2 Hz, 1H), 7.02 (dd, ^3J = 4.8 Hz, ^4J = 1.2 Hz, 1H), 2.85 (t, 2H), 1.66-1.59 (m, 2H), 1.45–

1.38 (m, 2H), 1.34-1.27 (m, 4H), 0.90 (t, 3H).

3-(hexan-2-ylsulfanyl)thiophene (**2a**) → Yield 88%. Colorless oil; EI-MS *m/z* 200 (M$^+$); ^{1}H NMR (400 MHz, CDCl3, TMS/ppm): δ 7.30 (dd, ^3J = 4.8 Hz, ^4J = 3.2 Hz, 1H), 7.24 (dd, ^3J = 3.2 Hz, ^4J = 1.2 Hz, 1H), 7.04 (dd, ^3J = 4.8 Hz, ^4J = 1.2 Hz, 1H), 3.10-3.01 (m, 1H), 1.60-1.40 (m, 4H), 1.24 (d, 3H), 0.93-0.89 (m, 3H).

3-(2-ethylhexylsulfanyl)thiophene (**3a**) → Yield 85%. Colorless oil; EI-MS *m/z* 228 (M$^+$); ^{1}H NMR (400 MHz, CDCl3, TMS/ppm): δ 7.31 (dd, ^3J = 4.8 Hz, ^4J = 2.8 Hz, 1H), 7.08 (dd, ^3J = 3.2 Hz, ^4J = 1.6 Hz, 1H), 7.02 (dd, ^3J = 4.8 Hz, ^4J = 1.2 Hz, 1H), 2.85 (d, 2H), 1.58-1.35 (m, 5H), 1.32-1.24 (m, 4H), 0.91-0.86 (m, 6H).

***General procedure for the synthesis of bromothienyl derivatives* 1b-3b, 1d-3d, 4a-6a *and* 1f-3f.** To a solution of **1a-3a, 1c-3c, 1e-3e** (1 mmol) in CH$_2$Cl$_2$, 1 mmol or 2 mmol of NBS were added. The reaction mixture was sonicated for 20min at room temperature. The solvent was removed and the products were purified by flash chromatography.

2-bromo-3-(hexylsulphanyl)thiophene (**1b**) → Cyclohexane 100%. Yield >90%. Pale yellow oil; EI-MS *m/z* 278 (M$^+$); ^{1}H NMR (400 MHz, CDCl3, TMS/ppm): δ 7.25 (d, ^3J = 5.6 Hz, 1H), 6.92 (d, ^3J = 5.6 Hz, 1H), 2.84 (t, 2H), 1.62-1.55 (m, 2H), 1.43–1.36 (m, 2H), 1.32-1.25 (m, 4H), 0.88 (t, 3H).

2-bromo-3-(hexan-2-ylsulphanyl)thiophene (**2b**) → Cyclohexane 100%. Yield >90%. Pale yellow oil; EI-MS *m/z* 278 (M$^+$); ^{1}H NMR (400 MHz, CDCl3, TMS/ppm): δ 7.25 (d, ^3J = 5.6 Hz, 1H), 6.94 (d, ^3J = 5.6 Hz, 1H), 3.21-3.13 (m, 1H), 1.61-1.40 (m, 4H), 1.24 (d, 3H), 0.93-0.89 (m, 3H).

2-bromo-3-(2-ethylhexylsulphanyl) thiophene (**3b**) → Cyclohexane 100%. Yield >90%. Pale yellow oil; EI-MS *m/z* 308 (M$^+$);^{1}H NMR (400 MHz, CDCl3, TMS/ppm): δ 7.25 (d, ^3J = 5.6 Hz, 1H), 6.93 (d, ^3J = 5.2 Hz, 1H), 2.83 (d, 2H), 1.54-1.31 (m, 5H), 1.28-1.20 (m, 4H), 0.89-0.86 (m, 6H).

5-bromo-3,3'-bis(hexylsulphanyl)-2,2'-bithiophene (**1d**) → Cyclohexane : CH$_2$Cl$_2$ (98:2). Yield 78%. Yellow oil; EI-MS *m/z* 478 (M$^+$);^{1}H NMR (400 MHz, CDCl3, TMS/ppm): δ 7.36 (d, ^3J = 5.2 Hz, 1H), 7.06 (d, ^3J = 5.2 Hz, 1H), 7.03 (s, 1H), 2.78 (q, ^3J = 7.2 Hz, 4H), 1.58-1.50 (m, 4H), 1.34–1.22 (m, 12H), 0.88-0.84 (m, 6H).

5-bromo-3,3'-bis(hexan-2-ylsulphanyl)-2,2'-bithiophene (**2d**) → Cyclohexane : CH$_2$Cl$_2$ (98:2). Yield 70%. Yellow oil; EI-MS *m/z* 478 (M$^+$);^{1}H NMR (400 MHz, CDCl3, TMS/ppm): δ 7.34 (d, ^3J = 5.2 Hz, 1H), 7.06 (d, ^3J = 5.2 Hz, 1H), 7.03 (s, 1H), 3.11-3.01 (m, 2H), 1.56-1.33 (m, 8H), 1.19-1.17 (m, 6H), 0.88-0.84 (m, 6H).

5-bromo-3,3'-bis(2-ethylhexylsulphanyl)-2,2'-bithiophene (**3d**) → Cyclohexane : CH$_2$Cl$_2$ (98:2). Yield 72%. Yellow oil; EI-MS *m/z* 534 (M$^+$);^{1}H NMR (400 MHz, CDCl3, TMS/ppm): δ 7.34 (d, ^3J = 5.2 Hz, 1H), 7.06 (d, ^3J = 5.2 Hz, 1H), 7.03 (s, 1H), 2.77 (t, 4H), 1.50-1.15 (m, 18H), 0.89-0.80 (m, 12H).

4-[3,3'-bis(hexylsulphanyl)-2,2'-bithien-5-yl]-7-[5'-bromo-3,3'-bis(hexylsulphanyl)-2,2'-bithien-5-yl]-2,1,3-benzothiadiazole (**1f**) → Cyclohexane : CH$_2$Cl$_2$ (90:10). Yield 72%. Red oil; ^{1}H NMR (400 MHz, CDCl3, TMS/ppm): δ 8.19 (s, 1H), 8.16 (s, 1H), 7.87 (s, 2H), 7.41 (d, ^3J = 5.2 Hz, 1H), 7.12 (d, ^3J = 5.2 Hz, 1H), 7.07 (s, 1H), 2.93-2.82 (m, 8H), 1.64-1.54 (m, 8H), 1.27-1.25 (m, 24H), 0.87-0.83 (m, 12H).

4-[3,3'-bis(hexan-2-ylsulphanyl)-2,2'-bithien-5-yl]-7-[5'-bromo-3,3'-bis(hexan-2-ylsulphanyl)-2,2'-bithien-5-yl]-2,1,3-benzothiadiazole (**2f**) → Cyclohexane : CH$_2$Cl$_2$ (90:10).

Yield 70%. Red oil;^{1}H NMR (400 MHz, CDCl3, TMS/ppm): δ 8.18 (s, 1H), 8.15 (s, 1H), 7.88 (s, 2H), 7.40 (d, ^3J = 5.2 Hz, 1H), 7.12 (d, ^3J = 5.6 Hz, 1H), 7.07 (s, 1H), 3.25-3.13 (m, 4H), 1.62-1.40 (m, 16H), 1.29-1.21 (m, 12H), 0.92-0.84 (m, 12H).

4-[3,3'-bis(2-ethylhexylsulphanyl)-2,2'-bithien-5-yl]-7-[5'-bromo-3,3'-bis(2-ethylhexylsulphanyl)-2,2'-bithien-5-yl]-2,1,3-benzothiadiazole (**3f**) → Cyclohexane : CH$_2$Cl$_2$ (92:8). Yield 68%. Red oil; ^{1}H NMR (400 MHz, CDCl3, TMS/ppm): δ 8.20 (s, 1H), 8.17 (s, 1H), 7.86 (s, 2H), 7.40 (d, ^3J = 5.6 Hz, 1H), 7.16 (d, ^3J = 5.2 Hz, 1H), 7.07 (s, 1H), 2.92-2.89 (m, 4H), 2.84 (d, 4H), 1.72-1.02 (m, 36H), 0.94-0.74 (m, 24H).

5,5'-dibromo-3,3'-bis(hexylsulphanyl)-2,2'-bithiophene (**4a**) → Cyclohexane : CH$_2$Cl$_2$ (90:10). Yield > 99%. Pale yellow solid; EI-MS *m/z* 529 (M$^+$);^{1}H NMR (400 MHz, CDCl3, TMS/ppm): δ 7.01 (s, 2H), 2.79-2.76 (t, 4H), 1.57-1.52 (m, 4H), 1.38-1.21 (m, 12H), 0.89-0.85 (t, 6H).

5,5'-dibromo-3,3'-bis(hexan-2-ylsulphanyl)-2,2'-bithiophene (**5a**) → Cyclohexane : CH$_2$Cl$_2$ (90:10). Yield > 99%. Pale yellow oil; EI-MS *m/z* 529 (M$^+$);^{1}H NMR (400 MHz, CDCl3, TMS/ppm): δ 7.01 (s, 2H), 3.12-3.04 (m, 2H), 1.57-1.34 (m, 8H), 1.20 (d, 6H), 0.90-0.86 (m, 6H).

5,5'-dibromo-3,3'-bis(2-ethylhexylsulphanyl)-2,2'-bithiophene (**6a**) → Cyclohexane : CH$_2$Cl$_2$ (90:10). Yield > 90%. Pale yellow oil; EI-MS *m/z* 585 (M$^+$);^{1}H NMR (400 MHz, CDCl3, TMS/ppm): δ 7.01 (s, 2H), 2.77 (d, 4H), 1.49-1.18 (m, 18H), 0.90-0.82 (m, 12H).

General procedure for the synthesis of compounds **1e-3e**

A mixture of the 2,1,3-Benzothiadiazole-4,7-bis(boronic acid pinacol ester) (1 mmol), a bromo derivatives **1d-3d** (2.2 mmol), PdCl$_2$dppf (0.1 mmol) and NaHCO$_3$ (5 mmol) in THF/water 2:1 (3 mL) was irradiated with microwaves at 80°C for 20 min. The reaction mixture was brought to room temperature and the solvent was evaporated under reduced pressure.

4,7-bis[3,3'-bis(hexylsulphanyl)-2,2'-bithien-5-yl]-2,1,3-benzothiadiazole (**1e**) → Cyclohexane : CH$_2$Cl$_2$ (90:10).Yield 85%. Red oil;^{1}H NMR (400 MHz, CDCl3, TMS/ppm): δ 8.18 (s, 2H), 7.87 (s, 2H), 7.41 (d, ^3J = 5.2 Hz, 2H), 7.12 (d, ^3J = 5.6 Hz, 2H), 2.91 (t, 4H), 2.85 (t, 4H), 1.72-1.54 (m, 8H), 1.42-1.32 (m, 8H), 1.29-1.20 (m, 16H), 0.88-0.81 (m, 12H).

4,7-bis[3,3'-bis(hexan-2-ylsulphanyl)-2,2'-bithien-5-yl]-2,1,3-benzothiadiazole (**2e**) → Cyclohexane : CH$_2$Cl$_2$ (90:10). Yield 78%. Dark Red oil; ^{1}H NMR (400 MHz, CDCl3, TMS/ppm): δ 8.18 (s, 2H), 7.89 (s, 2H), 7.40 (d, ^3J = 5.2 Hz, 2H), 7.12 (d, ^3J = 5.6 Hz, 2H), 3.23-3.13 (m, 4H), 1.62-1.38 (m, 16H), 1.27-1.21 (m, 12H), 0.90-0.84 (m, 12H).

4,7-bis[3,3'-bis(2-ethylhexylsulphanyl)-2,2'-bithien-5-yl]-2,1,3-benzothiadiazole (**3e**) → Cyclohexane : CH$_2$Cl$_2$ (90:10). Yield 80%. Dark Red oil; ^{1}H NMR (400 MHz, CDCl3, TMS/ppm): δ 8.20 (s, 2H), 7.87 (s, 2H), 7.40 (d, ^3J = 5.2 Hz, 2H), 7.12 (d, ^3J = 5.2 Hz, 2H), 2.90 (d, 4H), 2.84 (d, 4H), 1.57-1.32 (m, 20H), 1.26-1.20 (m, 16H), 0.88-0.81 (m, 24H).

General procedure for the synthesis of compounds **1c-3c** *and* **1-3.** A mixture of the bromothienyl-derivative **1b-3b, 1f-3f** (1 mmol), bis(pinacolato)diboron (0.6 mmol), PdCl$_2$dppf (0.05 mmol), NaHCO$_3$ (2 mmol) in THF/water 2:1 (3 mL) was irradiated with microwaves at 80°C for 20 min. The reaction mixture was brought to room temperature and the solvent was evaporated under reduced pressure. All compounds were purified by flash chromatography with increasing amounts of CH$_2$Cl$_2$ in cyclohexane as eluent.

3,3'-bis(hexylsulphanyl)-2,2'-bithiophene (**1c**) → Cyclohexane : CH$_2$Cl$_2$ (80:20). Yield 75%. Yellow oil; EI-MS *m/z* 398 (M$^+$);^{1}H NMR (400 MHz, CDCl3, TMS/ppm): δ 7.36 (d, ^3J = 5.2

Hz, 2H), 7.08 (d, ^3J = 5.2 Hz, 2H), 2.77 (t, 4H), 1.57-1.49 (m, 4H), 1.36–1.20 (m, 12H), 0.86 (t, 6H).

3,3'-bis(hexan-2-ylsulphanyl)-2,2'-bithiophene (**2c**) → Cyclohexane : CH$_2$Cl$_2$ (80:20).Yield 60%. Yellow oil; EI-MS *m/z* 398 (M$^+$); ^{1}H NMR (400 MHz, CDCl3, TMS/ppm): δ 7.36 (d, ^3J = 5.2 Hz, 2H), 7.09 (d, ^3J = 5.2 Hz, 2H), 3.10-3.01 (m, 2H), 1.55-1.38 (m, 8H), 1.18 (d, 6H), 0.87-0.84 (m, 6H).

3,3'-bis[(2-ethylhexylsulphanyl)-2,2'-bithiophene (**3c**) → Cyclohexane : CH$_2$Cl$_2$ (85:15). Yield 50%. Yellow oil; EI-MS *m/z* 454 (M$^+$);^{1}H NMR (400 MHz, CDCl3, TMS/ppm): δ 7.35 (d, ^3J = 5.2 Hz, 2H), 7.08 (d, ^3J = 5.2 Hz, 2H), 2.77 (d, 4H), 1.48-1.16 (m, 18H), 0.88-0.79 (m, 12H).

4,4'-(3,3',4'',3'''-tetrakis(hexylsulphanyl)-2,2':5',2'':5'',2'''-quaterthiene-5,5'''-diyl)bis(7-(3,3'-bis(hexylsulphanyl)-2,2'-bithien-5-yl)-2,1,3-benzothiadiazole, **1** (**decamer 1**) → Cyclohexane : CH$_2$Cl$_2$ (80:20). Yield 85%. Dark Violet oil; ^{1}H NMR (400 MHz, CDCl3, TMS/ppm): δ 8.20 (d, ^{3}J = 6.4 Hz, 4H), 7.89 (s, 4H), 7.42 (d, ^{3}J = 5.6 Hz, 2H), 7.24 (s, 2H), 7.13 (d, ^{3}J = 5.2 Hz, 2H), 2.98-2.83 (m, 16H), 1.70-1.55 (m, 16H), 1.45-1.35 (m, 16H), 1.31-1.23 (m, 32H), 0.89-0.82 (m, 24H); ^{13}C NMR (400 MHz, CDCl3): δ 152.5, 138.84, 138.78, 136.4, 133.9, 133.7, 133.1, 133.0, 132.9, 132.3, 132.2, 132.0, 131.4, 131.2, 130.8, 127.5, 126.2, 125.5, 125.4, 125.3, 36.4, 36.1, 31.41, 31.38, 29.7, 29.6, 29.5, 28.5, 28.4, 26.9, 22.58, 22.55, 14.1, 14.0. UV/Vis: UV/Vis: λ$_{max}$ 514 nm (ε 52100 cm^{-1}M^{-1}), λ$_{em.}$ 715 nm in (CH$_2$Cl$_2$).

4,4'-(3,3', 4'',3''' -tetrakis(hexan-2-ylsulphanyl)-2,2':5',2'':5'',2'''-quaterthiene-5,5'''-diyl) bis(7-(3,3'-bis(hexan-2-ylsulphanyl)-2,2'-bithien-5-yl)-2,1,3-benzothiadiazole, **2** (**decamer 2**) → Cyclohexane : CH$_2$Cl$_2$ (80:20). Yield 82%. Dark Violet oil; ^{1}H NMR (400 MHz, CDCl3, TMS/ppm): δ 8.20 (d, ^{3}J = 5.6 Hz, 4H), 7.90 (s, 4H), 7.40 (d, ^{3}J = 5.2 Hz, 2H), 7.25 (s, 2H), 7.13 (d, ^{3}J = 5.2 Hz, 2H), 3.30-3.14 (m, 8H), 1.69-1.38 (m, 32H), 1.32-1.22 (m, 24H), 0.94-0.84 (m, 24H) ^{13}C NMR (400 MHz, CDCl3): δ 152.5, 138.5, 138.4, 136.0, 135.9, 134.4, 134.2, 132.9, 132.7, 132.3, 131.9, 131.8, 131.2, 129.0, 125.8, 125.53, 125.48, 125.41, 125.35, 45.2, 44.9, 39.05, 39.01, 21.3, 20.3, 20.2, 14.0, 13.95, 13.93. UV/Vis: λ$_{max}$ 518 nm (ε 53400), λ$_{em.}$ 700 nm in CH$_2$Cl$_2$.

4,4'-(3,3',4'',3'''-tetrakis((2-ethylhexylsulphanyl)-2,2':5',2'':5'',2'''-quaterthiene-5,5'''-diyl)bis(7-(3,3'-bis(2-ethylhexylsulphanyl)-2,2'-bithien-5-yl)-2,1,3-benzothiadiazole, **3** (**decamer 3**) → Cyclohexane : CH$_2$Cl$_2$ (80:20). Yield 80%. Dark Violet oil; ^{1}H NMR (400 MHz, CDCl3, TMS/ppm): δ 8.22 (d, ^{3}J = 6.4 Hz, 4H), 7.88 (s, 4H), 7.40 (d, ^{3}J = 5.2 Hz, 2H), 7.24 (s, 2H), 7.13 (d, ^{3}J = 5.2 Hz, 2H), 2.97-2.84 (m, 16H), 1.64-1.33 (m, 40H), 1.29-1.19 (m, 32H), 0.91-0.82 (m, 48H); ^{13}C NMR (400 MHz, CDCl3): δ 152.5, 138.7, 138.6, 136.3, 133.8, 133.7, 133.6, 133.4, 133.3, 132.7, 132.3, 132.0, 131.5, 131.3, 130.9, 127.5, 126.0, 125.5, 125.43, 125.38, 125.35, 41.0, 40.8, 40.7, 39.5, 39.44, 39.38, 39.36, 32.32, 32.31, 32.24, 32.23, 28.9, 28.82, 28.80, 28.77, 25.54, 25.46, 25.43, 23.04, 23.01, 22.98, 14.2, 14.11, 14.08, 10.82, 10.77, 10.73. UV/Vis: λ$_{max}$ 522 nm (ε 58000), λ$_{em.}$ (CH$_2$Cl$_2$) 715 nm in CH$_2$Cl$_2$.

General procedure for the synthesis of polymers **4-6.** A mixture of the bromothienyl-derivative **4a-6a** (1 mmol), 2,1,3-Benzothiadiazole-4,7-bis(boronic acid pinacol ester) (1 mmol), PdCl$_2$dppf (0.1 mmol), NaHCO$_3$ (5 mmol) in THF/water 2:1 (3 mL) was irradiated with microwaves at 80°C. The reaction mixture was brought to room temperature and the solvent was evaporated under reduced pressure.

Poly(4-[3,3'-bis(hexylsulphanyl)-2,2'-bithiophen-5-yl]-2,1,3-benzothiadiazole), **4** (**Polymer**

4) → Mw 15066, Mn 9300, PDI 1.62. UV/Vis: λ_{max} 538 nm, $\lambda_{em.}$ 727 nm in CH_2Cl_2.

Poly (4-[3,3'-bis(hexan-2-ylsulphanyl)-2,2'-bithiophen-5-yl]-2,1,3-benzothiadiazole), **5**
(Polymer 5) → Mw 12800 Mn 8000 PDI 1.60. UV/Vis: λ_{max} 546 nm, $\lambda_{em.}$ 707 nm in CH_2Cl_2.

Poly(4-[3,3'-bis(2-ethylhexylsulphanyl)-2,2'-bithiophen-5-yl]-2,1,3-benzothiadiazole), **6**
(Polymer 6) → Mw 18320 Mn 12400 PDI 1.48. UV/Vis: λ_{max} 612 nm, $\lambda_{em.}$ 748 nm in
CH_2Cl_2.

Figure S1-S27 (¹HNMR and ¹³CNMR) are not reported

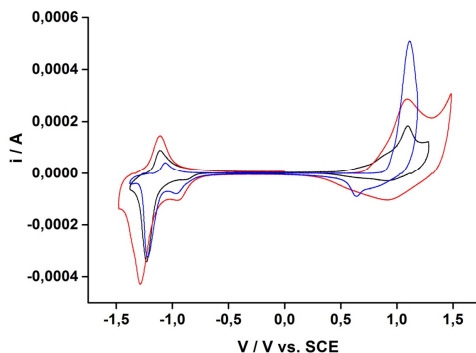## 4.3. Cyclic voltammetries of the thin films of compounds 2, 4 and 5

Figure S28. Cyclic voltammetries of the thin films of compounds **2** (blue trace), **4** (red trace) and **5** (black trace) deposited from 70:30 toluene:acetonitrile.
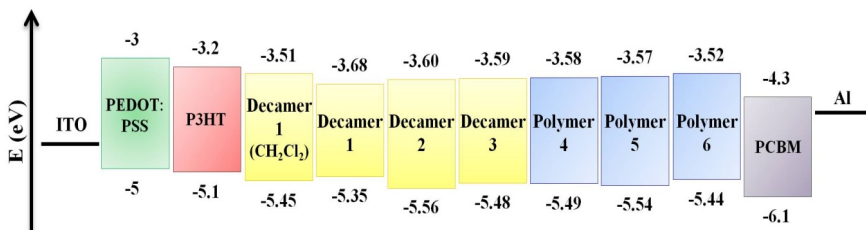

Figure S29. A) Sketch illustrating the relative energy levels of HOMO and LUMO orbitals (from CV data) of compounds **1-6** compared to the corresponding levels of PEDOT:PSS, P3HT and PCBM.

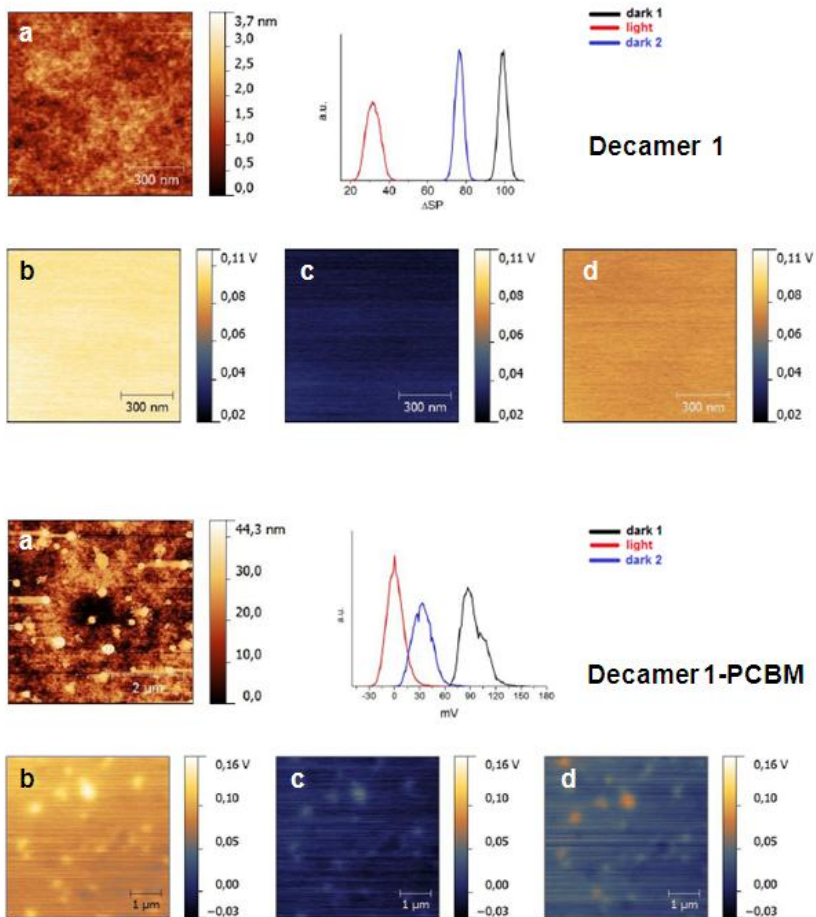## 4.4. Kelvin Probe Force Microscopy (KPFM)

Figure S30. A) (a) Surface topography images of a cast film from toluene:acetonitrile of decamer **1** (R=Hex); (b,c,d) the corresponding KPFM images (dark1, light, dark2) and (e) surface potential distributions. B) The same for decamer **1** in blend with PCBM.
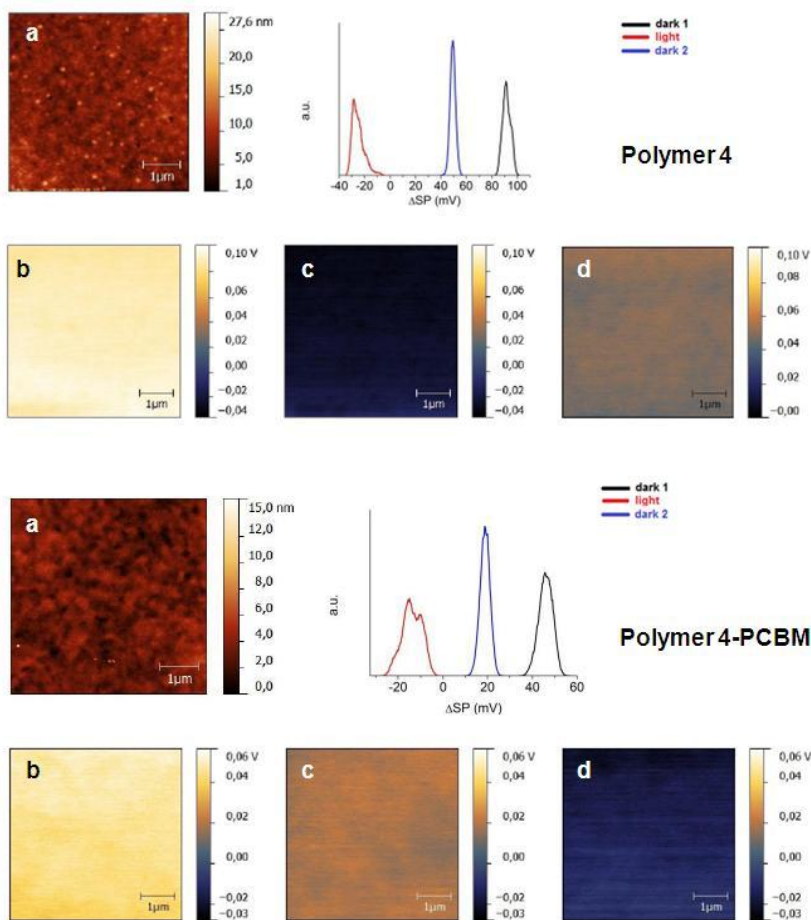
Figure S31. A) (a) Surface topography images of a cast film from toluene:acetonitrile of polymer **4** (R=Hex); (b,c,d) the corresponding KPFM images (dark1, light, dark2) and (e) surface potential distributions. B) The same for polymer **4** in blend with PCBM.

Table S1. *ΔSP$_{light-dark}$* values and conversion efficiency of decamers and polymers

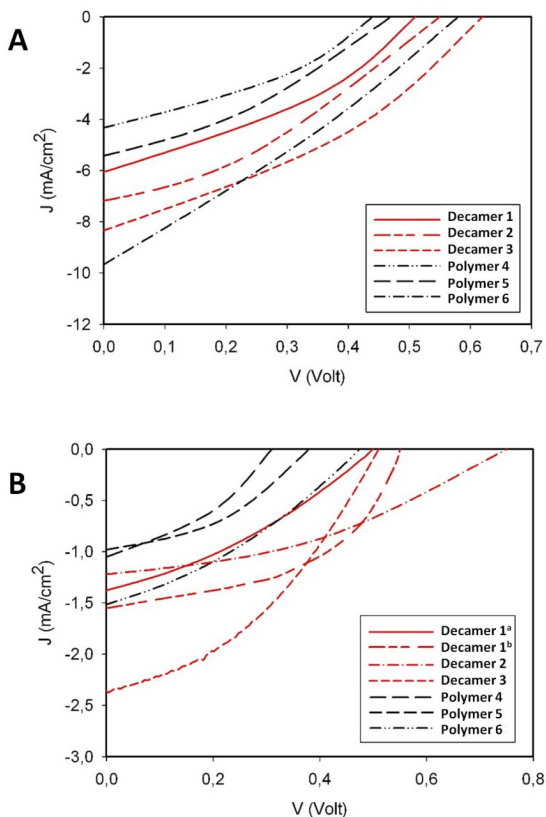| Sample	ΔSP$_{light-dark}$ (mV)	η%
decamer 3-Pcbm	193.25	1.80
decamer 3	94.35	0.54
decamer 1-Pcbm	86.42	1.07
decamer 1	67.75	0.38
polymer 3-Pcbm	90.34	1.56
polymer 3	112.46	0.30
polymer 1-Pcbm	57.63	0.67
polymer 1	102.79	0.12

4.5. J/V plots of BHJ and SMOC devices

Figure S32. A) Bulk heterojunction and B) single component solar cells of compounds **1-6** (a= film deposited from CH_2Cl_2 , b=film deposited from toluene:acetonitrile)

REFERENCES

[1] Mori H, Suetsugu M, Nishinaga S, Chang N, Nonobe H, Okuda Y, Nishihara Y. *J. Polym. Sci. Pol. Chem.*, **2015**, 53, 709-718.

[2] Li H, Liu F, Wang X, Gu C, Wang P, Fu H. *Macromolecules* **2013**, 46, 9211-9219.

[3] Beaujuge PM, Fréchet JMJ. *J. Am. Chem. Soc.,* **2011**, 133, 20009-20029.

[4] Bundgaard E, Krebs FC. *Sol. Energ. Mat. Sol. C.,* **2007**, 91, 954-985.

[5] Cheng Y.-J, Yang S.-H, Hsu C.-S. *Chem. Rev.* **2009**, 109, 5868-5923.

[6] He X, Cao B, Hauger TC, Kang M, Gusarov S, Luber EJ, Buriak JM. *ACS Appl. Mater. Interfaces,* **2015**, 7, 8188-8199.

[7] Zhou P, Zhang ZG, Li Y, Chen X, Qin J. *Chem.Mater.,* **2014**, 26, 3495-3501.

[8] Feng K, Xu X, Li Z, Li Y, Li K, Yu T, Peng Q. *Chem. Commun.,* **2015**, 51, 6290-6292.

[9] Umeyama T, Imahori H. *J. Mater. Chem. A,* **2014**, 2, 11545-11560.

[10] Cao W, Xue J. *Energy Environ. Sci.* **2014**, 7, 2123-2144.

[11] Chen Y, Wan X, Long G. *Acc. Chem. Res.* **2013**, 46, 2645-2655.

[12] Lin Y, Lia Y, Zhan X. *Chem. Soc. Rev.* **2012**, 41, 4245-4272.

[13] Hu S, Bao X, Liu Z, Wang T, Du Z, Wen S, Wang N, Han L, Yang R. *Org. Electron.,* **2014**, 15, 3601-3608.

[14] Di Maria F, Olivelli P, Gazzano M, Zanelli A, Biasiucci M, Gigli G, Gentili D, D'Angelo, P, Cavallini M, Barbarella G. *J. Am. Chem. Soc.,* **2011**, 133, 8654-8661.

[15] DiMaria F, Barbarella G. *J. Sulfur Chem.* **2013**, 34, 627-637.

[16] Melitz W, Shena J, Kummela AC, Lee S. *Surface Science Reports,* **2011**, 66, 1-27.

[17] Glatzel T, Hoppe H, Sariciftci NS, Lux-Steiner MC, Komiyama M. *Jpn. J. Appl. Phys.,* **2005**, 44, 5370-5373.

[18] Huang Y, Kramer EJ, Heeger AJ, Bazan GC. *Chem. Rev.,* **2014**, 114, 7006-7043.

[19] Roncali J. *Adv. Energy Mater.*, **2011**, 1, 147-160.

[20] Koyuncu S, Wang HW, Liu F, Toga KB, Gub W, Russell TPA. *J. Mater. Chem. A,* **2014**, 2, 2993-2998.

[21] Cao J, Du X, Chen S, Xiao Z, Ding LA. *Phys. Chem. Chem. Phys.,* **2014**, 16, 3512-3514.

[22] Miyanishi S, Zhang Y, Tajima K, Hashimoto K. *Chem. Commun.,* **2010**, 46, 6723-6725.

[23] Yamamoto S, Yasuda H, Ohkita H, Benten H, Ito S, Miyanishi S, Tajima K, Hashimoto K. *J. Phys. Chem. C,* **2014**, 118, 10584-10589.

[24] Izawa S, Hashimoto K, Tajima K. *Phys. Chem. Chem. Phys.,* **2012**, 14, 16138-16142.

[25] Arumugam S, Cortizo-Lacalle D, Rossbauer S, Hunter S, Kanibolotsky A, Inigo AR, Lane PA, Anthopoulos TD, Skabara PJ. *ACS Appl. Mater. Interfaces,* **2015**, 7, 27999–28005

[26] Huang Y, Kramer EJ, Heeger AJ, Bazan GC. *Chem. Rev.,* **2014**, 114, 7006-7043.

[27] Adamo C, Barone V. *J. Chem. Phys.,* **1999**, 110, 6158-6170.

[28] Weigend F, Furche F, Ahlrichs R. *J. Chem. Phys.,* **2003**, 119, 12753-12762.

[29] Kresse G, Furthmuller J. *Phys. Rev. B,* **1996**, 54, 11169-11186.

[30] Constantin LA, Fabiano E, Laricchia S, Della Sala F. *Phys. Rev. Lett.,* **2011**, 106, 186406-1/186406-4.

[31] Gentili D, Di Maria F, Liscio F, Ferlauto L, Leonardi F, Maini L, Gazzano M, Milita S, Barbarella G, Cavallini M. *J. Mater. Chem.*, **2012**, 22, 20852-20856.

[32] Di Maria F, Gazzano M, Zanelli A, Gigli G, Loiudice A, Rizzo A, Biasiucci M, Salatelli E, D' Angelo P, Barbarella G. *Macromolecules,* **2012**, 45, 8284-8291.

[33] Azumi R, Mena-Osteritz E, Boese R, Benet-Buchholz J, Bäuerle P. *J. Mater. Chem.,* **2006**, 16, 728-735.

[34] Cardona CM, Li W, Kaifer AE, Stockdale D, Bazan GC. *Adv. Mater.,* **2011**, 23, 2367-2371.

[35] Berlin A, Zotti G, Zecchin S, Schiavon G, Vercelli B, Zanelli A. *Chem. Mater.,* **2004**, 16, 3667-3676.

[36] TURBOMOLE, V6.3; TURBOMOLE GmbH: Karlsruhe, Germany, **2011**. http://www.turbomole.com (accessed 2011).

[37] Fabiano E, Constantin LA, Cortona P, Della Sala F. *J. Chem. Theory Comput.,* **2015**, 11, 122-131.

[38] Grimme S, Antony J, Ehrlich S, Krieg HA. *J. Chem. Phys.,* **2010**, 132, 154104-1/154104-18.

[39] Liscio A, De Luca G, Nolde F, Palermo V, Mūllen K, Samori' P. *J. Am. Chem. Soc.,* **2008**, 130, 780-781.

[40] Chiesa M, Burgi L, Kim JS, Shikler R, Friend RH, Sirringhaus H. *Nano Lett.,* **2005**, 5,559-563.

[41] Loiudice A, Rizzo A, Grancini G, Biasiucci M, Belviso MR, Corricelli M, Curri ML, Striccoli M, Agostiano A, Cozzoli PD, et al. *Energy Environ. Sci.,* **2013**, 6, 1565-1572.

[42] Liscio A, Palermo V, Samori P. *Acc. Chem. Res.,* **2010**, 43, 541-550.

[43] Maturova K, Kemerink M, Wienk MM, Charrier DSH, Janssen RAJ. *Adv. Funct. Mater*., **2009**, 19, 1379-1386.

[44] Bu L, Guo X, Yu B, Qu Y, Xie Z, Yan D, Geng Y, Wang F. *J. Am. Chem. Soc.,* **2009**, 131, 13242-13243.

[45] Cravino A, Leriche P, Alévêque O, Roquet S, Roncali J. *Adv.Mater.,* **2006**, 18, 3033-3037.

[46] Durantini J, Morales GM, Santo M, Funes M, Durantini EN, Fungo F, Dittrich T, Otero L, Gervaldo M. *J.Phys.Chem.C,* **2015**, 119, 4044-4051.

[47] Durantini J, Suarez MB, Santo M, Durantini E, Otero L, Gervaldo M. *Org. Electron,* **2012**, 13, 604-614.

[48] Yang L, Zhou H, You W. *J. Phys. Chem. C,* **2010**, 114, 16793-16800.

[49] Li Y, Chen Y, Liu X, Wang Z, Yang X, Tu Y, Zhu X. *Macromolecules,* **2011**, 44, 6370-6381.

CHAPTER IV: THIOPHENE FLUOROPHORES FOR BIOLOGICAL APPLICATIONS

In the last decade optical probes and fluorescence techniques have received great attention as tools for the detection of the components of complex biological systems and the monitoring of biological processes in real time. To this purpose several families of fluorescent probes with light-emitting frequencies spanning from the visible range to the near- infrared have been developed. Owing to the versatile chemistry of thiophene, its easy functionalization and the fluorescence properties and chemical and optical stability of its oligomers, we have started a research aimed to synthesize thiophene-based fluorophores for biological applications.

Here we report two studies showing that thiophene fluorophores are not only bright markers of biomolecules but are also capable to specifically interact with intracellular fribrillar or globular proteins.

Part I: Live Cell Cytoplasm Staining and Selective Labeling of Intracellular Proteins by Non-Toxic Cell-Permeant Thiophene Fluorophores

I. INTRODUCTION

Synergistic advances in fluorescent probes[1] and imaging techniques[2] have made visualization of live cells one of the most powerful techniques, at the interface of chemistry and biology, to obtain information on cell components in their native context in real time. Among the various components present in live cells much interest is devoted to proteins and related biological mechanisms at the basis of cell physiology and dysfunction.[3] Presently, chemical tagging methods to visualize specific proteins inside live cells are increasingly being employed in alternative to fluorescent proteins labelling.[4] Genetically encoded fluo-rescent proteins can be covalently fused to the protein of interest which is then targeted with high precision. However, given their significant size, the fusion may alter the function of the targeted protein. Various methods for protein tagging inside live cells using non-genetically encoded probes have been described so far, differing for labelling difficulties and versatility, specificity and toxicity. Nevertheless, despite the development of various smart procedures, it is widely accepted that new and simpler methods are still needed for the routine use of fluorescent probes in the cellular environment. Organic fluorophores have the advantage of being small size tags, easy to tune via organic synthesis, and some of them can even be repeatedly imaged owing to high brightness and resistance to photobleaching.[1f] They have been largely employed for in vitro studies of proteins, however the transition to labelling inside live cells is often limited by the absence of membrane permeance, toxicity and lack of specificity for any particular intracellular protein. In recent years Nilsson et al.[5] have demonstrated that high selectivity in proteins labelling may be achieved by thiophene oligomers through non covalent interactions. Their *in vitro*, *ex vivo* and *in vivo* experiments have demonstrated that molecules made of five to seven thiophene rings and with terminal carboxy groups display great affinity for fibrillar proteins and may act as specific probes for the pathological hallmarks of protein misfolding diseases. Owing to the flexibility of the aromatic backbone, these oligomers undergo subtle conformational changes upon interaction with fibrillar proteins causing appreciable variations in absorption and emission features. In our long-standing research on molecular engineering of functional thiophene oligomers[6] - fluorescent and electroactive com-pounds, capable of an astonishing variety of non bonding interactions in the most diverse environments[7] - we have described thiophene fluorophores for the *in vitro* labelling of proteins and oligonucleotides[6a,b] and have initiated a search for cell-permeant and biocompatible thiophene fluorophores to study their behavior inside live cells.[6c] We have found that some thiophene fluorophores are capable of specific non bonding interactions with *fibrillar* type-I collagen inside live human and murine fibroblasts.[6c,d] In this paper we describe a thiophene fluorophore having the ability to discriminate among the innumerable *globular* proteins present inside living NIH 3T3 mouse fibroblast cells. These results open the door to the possibility of using specifically engineered thiophene fluorophores, cell-permeant and biocompatible, for the easy and direct tagging of proteins in live cells and their detection by fluorescent techniques.

II. RESULTS AND DISCUSSION

Chart 1 shows the molecular structure of the cell-permeant thiophene N-succinimidyl esters whose synhesis is described here for the first time, namely compounds 1-2 and 7-8. For comparison, the molecular structure of all the other cell-permeant thiophene fluorophores identified so far, namely compounds 3-6 and 9,[6c] are also reported.

Chart 1. Molecular structure and emission color inside live NIH 3T3 cells of all cell-permeant thiophene fluorophores identified so far (grey structures are described in reference 6c).
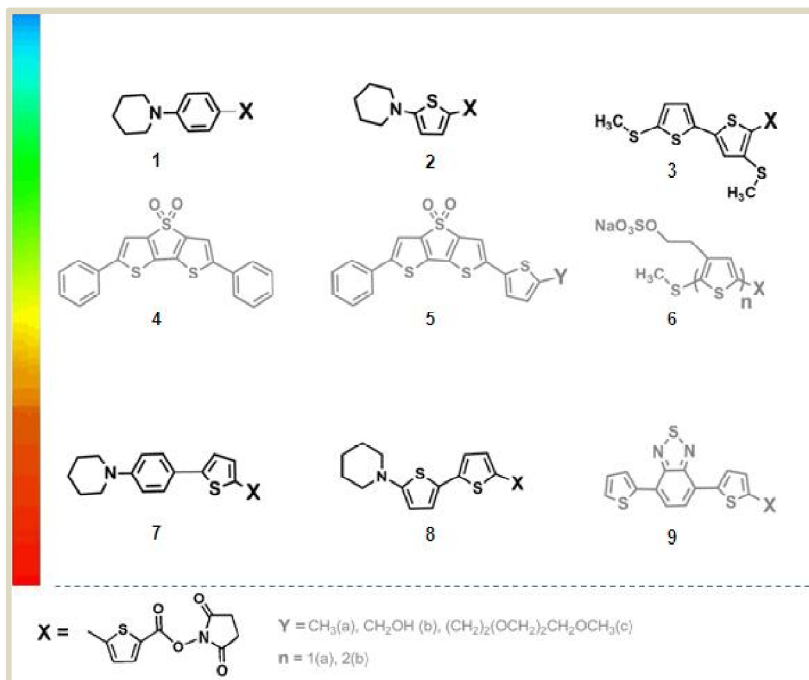
It is easily seen that any rationalization of the structural elements leading to cell permeability is difficult and that the identification of the structures depicted in the chart is due to a trial and error procedure on a large number of thiophene fluorophores. In Chart 1 the fluorophores are organized according to their emission color inside live mouse embryonic fibroblast NIH 3T3 cells. In agreement with previous observations, [6c] the emission color of the fluorophores inside live cells is similar to the fluorescence color in dichloromethane (DCM) solution. Notably, most of these fluorophores emit in the green region of the visible spectrum whereas only three display fluorescence in the red region. Two fluorophores, 3 and 5b, are toxic (this paper for 3 and reference 6c for 5b) and one, compound 8, photobleaches inside the live cells but not in solution in organic solvents. Compounds 1-2 and 7-8 were synthesized by means of the Suzuki cross-coupling reaction[8] in aqueous solvents. Although similar products have already been

synthesized in our laboratory by the Stille reaction,[9,10] the Suzuki coupling is by far a better reaction to prepare ultrapure fluorophores. Enabling techniques such as microwave[11] and ultrasound[12] assistance make the preparation rapid (minutes instead of hours) and the yields high. Moreover, owing to reduced metal-halogen exchange and number of byproducts, reaction workup and separation are much easier.

2.1. Optical properties and environment sensitivity

Table 1 shows maximum absorption and emission wavelengths, molar absorption coefficients, quantum yields and fluorescence lifetimes of compounds 1-3 and 7-8 in toluene, a solvent endowed with a low dielectric constant (2.408[13]). Table 1S reports a few data in ethyl acetate (EA) and dichloromethane (DCM) with dielectric constants 6.02 and 8.9[13], respectively. Figure 7S shows the absorption and emission spectra of 1-3 and 7-8 in toluene, CDM and DMSO. Having large dipolar moments (Table 2S) and in agreement with already reported data[6b,14] both absorption and emission wavelengths increase on increasing the dielectric constant of the solvent. Owing to their absorption wavelength range, compounds 1-3 and 7-8 are a blue-absorbing palette of fluorophores, suitable for excitation by a blue-violet laser line. However, they have very large Stokes shifts, as is generally observed for thiophene oligomers.[6] Thus, in DCM the emission wavelengths attain values in the red region, 619 nm for 7 and 660 nm for 8. Note that red fluorescent labels are particularly useful in biological fluorescence microscopy to prevent problems due to autofluorescence of the cells. Table 1 shows that all fluorophores are bright fluorescent owing to high molar absorption coefficients and fluorescence quantum yields.

Table 1. Maximum absorption (λ_{max}, nm) and emission (λ_{PL}, nm) wavelengths, molar absorption coefficients (ε, cm^{-1}mol^{-1}), quantum yields (ϕ) and fluorescence lifetimes of 1-3 and 7-8.[a]

Item	λ_{max}	λ_{PL}	ε	ϕ	τ (ns)
1	381	465	28400	1.00	2.1
2	430	509	22300	0.92	2.7
3	418	515	33000	0.12	1.3
7	414	530	59800	0.92	2.3
8	443	581	19200	0.80	2.7

[a] In toluene. [b] with respect to perylene in ethanol, ϕ_{ref} = 0.92.

Compound 7 stands out among the others for its high ε value and quantum yield (also in EA, as shown in Table 2S), indicating very bright fluorescence.[15] Table 2S shows that despite the small difference in dielectric constant between EA and DCM, compounds 1-2 and 7-8 display significant emission solvatochromism. This effect should be attributed to their marked hyperconjugated push-pull structural features. The maximum absorption wavelengths always follow the trend $1 < 7 < 2 < 8$, suggesting that the introduction of a phenyl ring on the piperidine side increases the energy of S0-S1 electron transition more than it decreases the same energy gap by increasing electronic conjugation (compare 7 with 2). Conversely, replacement of a phenyl ring with an electron rich thienyl ring on the piperidine side leads to a

lower S0-S1 energy gap (compare 2 with 1 and 8 with 7). In all cases, fluorescence decays were found to be strictly monoexponential and falling in the 2-3 ns range. The lifetime trend in EA followed the number of aromatic rings in the compound, being higher in 7 and 8. Yet an analogous pattern could not be observed in DCM, suggesting that solute-solvent interactions have a strong influence on the non-radiative decay kinetics and, ultimately, on the fluorescence lifetime. In most cases, emission red-shift was associated with a reduced emission lifetime, in keeping with the typical photophysical behavior of solvatochromic compounds for which the excited state energy stabilization favors fast internal conversion down to ground state.[13] Conventional thiophene fluorophores are poorly sensitive to pH changes. Fluorophores 1-2 and 7-8 were engineered for enhanced pH sensitivity, owing to the presence of the nitrogen atom in the piperidine moiety. As expected, these fluorophores display great sensitivity to acidity changes in organic solvents. Protonation of the nitrogen atom caused reversible changes in fluorescence emission. The process is illustrated in detail in Figure 1 for fluorophore 7. The Figure shows the variations of proton chemical shifts and fluorescence wavelengths upon stepwise addition of CF_3COOH in toluene and subsequent neutralization with stoichiometric amounts of $N(CH_2CH_3)_3$. Protonation induces sizeable upfield shifts of theprotons of the phenyl group, adjacent to the protonation site, accompanied by a blue shift in fluorescence and its decrease in intensity. These changes were reversible and after several cycles of acidification/neutralization both the chemical shifts and the fluorescence came back to the starting values. Apparently, 7 is a good acidity sensor and could be usefully checked in pathological cells to detect acidity variations.
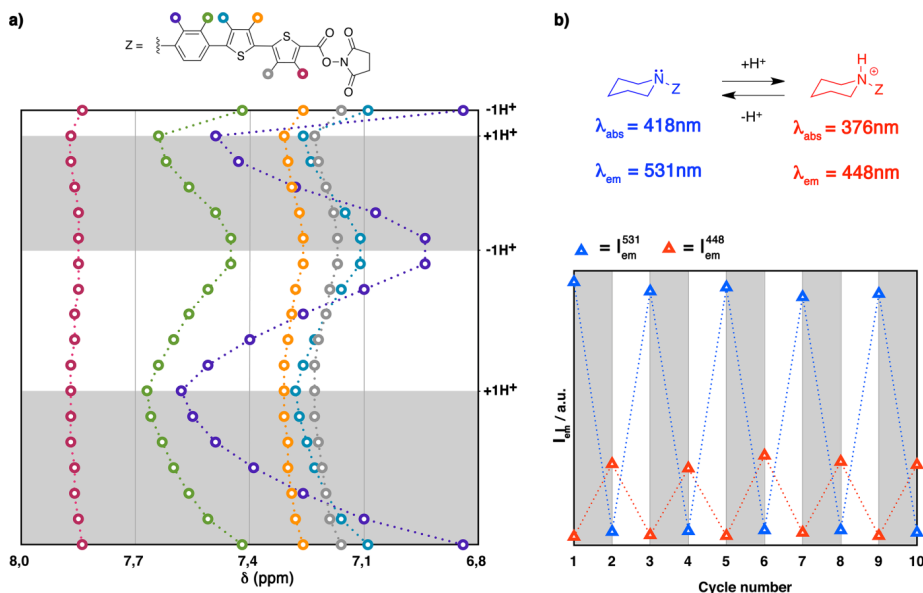

Figure 1. A) Variation of the chemical shifts in toluene of the aromatic protons of fluorophore **7** upon stepwise addition of CF_3COOH and subsequent neutralization with stoichiometric amounts of $N(CH_2CH_3)_3$. **B)** Corresponding variations in wavelength and intensity of fluorescence emission.

2.2. Uptake of the fluorophores by live NIH 3T3 mouse fibroblast cells

Fluorophores 1-3 and 7-8 displayed excellent cell permeability and were rapidly internalized, showing efficient retention inside the cells. Fluorophores 1-2 and 7 showed bright and persisting staining of the cytoplasm with fluorescence transmitted from mother to daughter cells during the replication process. By contrast, the brilliant red emission of fluorophore 8 was quenched after a few seconds examination with both the laser scanning confocal microscope or fluorescence microscope. Initial experimental data and theoretical calculations aimed to elucidate this behaviour are reported in experimental section (Figures 8S,14S). The cytotoxicity of the fluorophores towards NIH 3T3 cells was analyzed by means of the MTT cytotoxicity test, a commonly used method of measuring the viability of living cells via mitochondrial dehydrogenase activity, whose key component is 3-[4,5-dimethylthiazol-2-yl]-2,5-diphenyl tetrazolium bromide. The results are shown in Figure 2.[16]
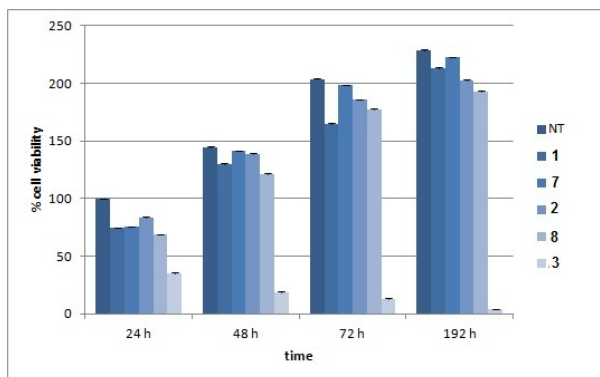

Figure 2. MTT cytotoxicity tests on NIH 3T3 cells treated with fluorophores 1-3 and 7-8 compared to untreated cells (NT). Representative measurements of three distinct sets of data (t-Student test, $P < 0.05$).

No reduced cell viability was found for the cells treated with fluorophores 1-2 and 7-8, while those treated with fluorophore 3 displayed drastically reduced viability. Incidentally, we note that while 3 is cell-permeant but toxic to the cells, its regioisomer with the SCH_3 substituent in the α−position[6a,b] is cell-impermeant. Since for different reasons neither 8 nor 3 could be examined in live cells by LSCM, their emission was checked in fixed NIH 3T3cells. The relative images are shown in Figures 12S and 13S, respectively. Figure 3 shows the LSCM images of live NIH 3T3 cells treated with the green emitting fluorophores 1,2 and monitored after 1h, 24h and 192h from treatment. Additional images are reported in Figures 9S and 10S. Both fluorophores caused the intense fluorescent staining of the cytoplasm of the cells - deep green in the case of 1, green with a green-yellow shade in the case of 2 - while the nucleus remained rigorously unstained. Being activated esters, once crossed the cell membrane, the fluorophores can react with the amine primary groups of proteins present in the cytoplasm, i.e. in the basic region of the cells, to form a covalent amide bond.[6a-c] However, which ones of the NH_2 groups of cytoplasmic proteins has reacted and to what extent cannot be established.

Figure 3 shows the presence of multiple intensely fluorescent spots indicating the accumulation of the fluorophore in the perinuclear region, i.e. the region where proteins synthesis takes place. This behaviour is similar to that observed upon treatment of the same type of cells with fluorophore 4 (Chart 1). In that case the accumulation of green spots in the perinuclear region was followed by formation of green fluorescent microfibers, mainly made of type-1 collagen embedding the fluorophore, that were subsequently extruded in the extracellular matrix.[6c,d] By contrast, in the case of fluorophores **1** and **2**, the accumulation in the perinuclear region is followed by elimination of the fluorophore by cell machinery.
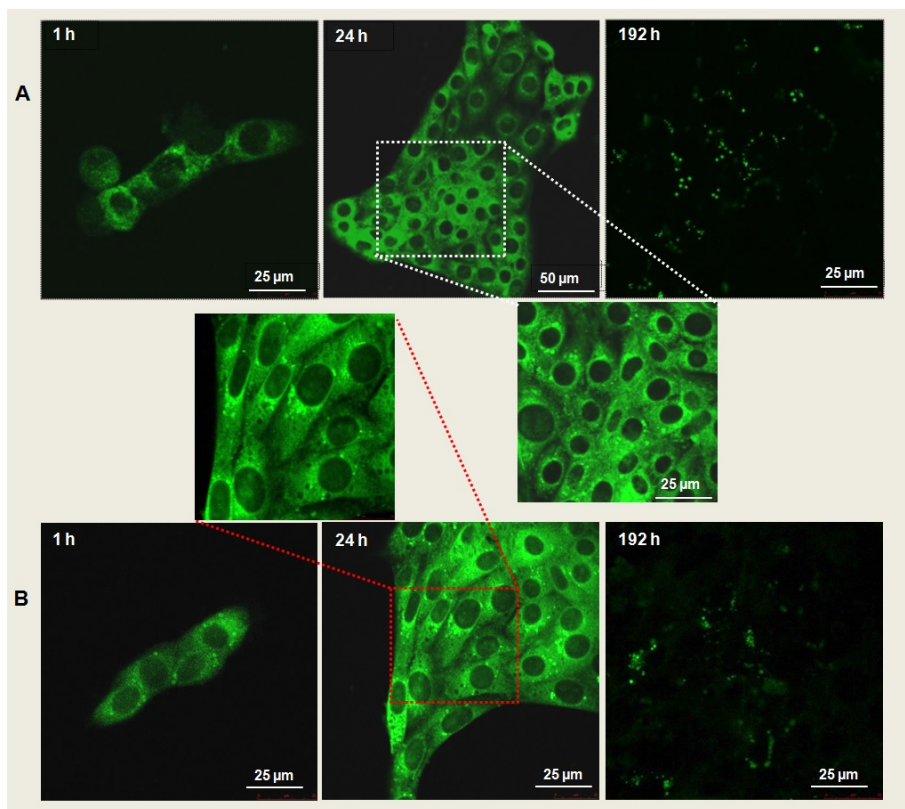

Figure 3. A), B) LSCM images of live NIH 3T3 cells after 1h, 24h and 192h from treatment with fluorophores 1 and **2**, respectively. 63x oil immersion.

Indeed, after 192h from treatment, only feeble traces of green fluorescence are still present. Figure 4 shows the LSCM images of live NIH 3T3 cells 1h, 24h, 48h, 72h and 192h after treatment with fluorophore 7. Additional images are reported in Figure 11S.
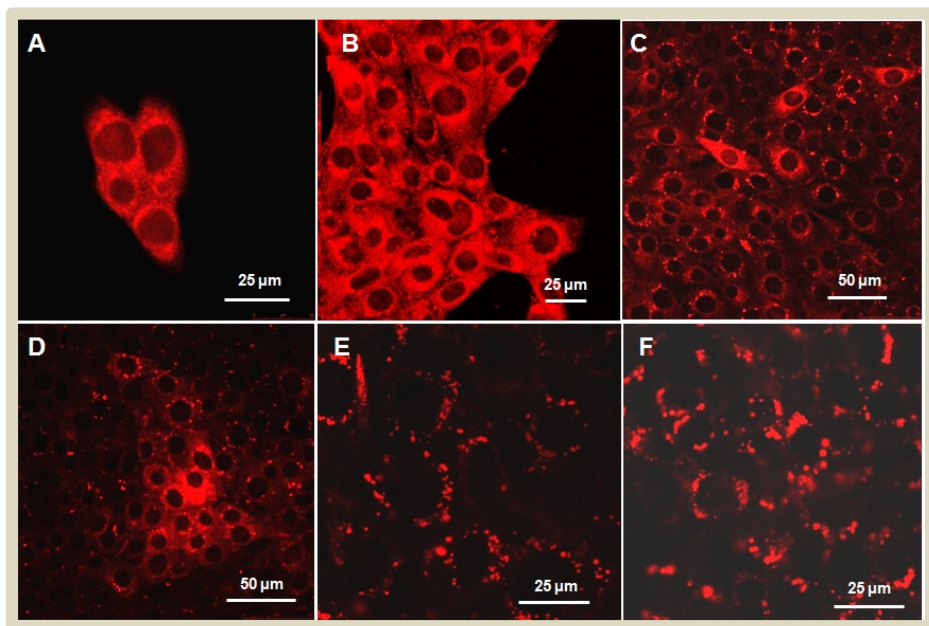
Figure 4. LSCM images of live NIH 3T3 cells after 1 hour (A), 24 hours (B), 48 hours (C), 72 hours (D) and 192 hours (E,F) from treatment with fluorophore 7.

The spontaneous uptake of fluorophore 7 by the cells caused the rapid red fluorescent staining of the cytoplasm while the nucleus remained dark. As in the case of fluorophores 1-2, during cell proliferation the fluorescence was transmitted from mother to daughter cells and accumulation of fluorescent spots in the perinuclear region was observed. However, contrary to what was found with 1 and 2, the appearance of red spots in the perinuclear region was followed by the progressive formation of bright red clusters. The bright red clusters accumulated with time and after 192h from treatment appeared numerous, large and diffuse. The treatment of the cells with fluorophore 7 (as well as with fluorophores 1-3 and 8) was repeated several times and the results were highly reproducible. The red fluorescent clusters formed after 192 hours from treatment with 7 were isolated from NIH 3T3 cell lysate (see ESI) and were found to be soluble in water. This ruled out the possibility that they were aggregates of 7, since this fluorophore is insoluble in H_2O. The water solution of the red clusters was used for a sodium dodecyl sulfate polyacrylamide gel electrophoresis (SDS-PAGE) and for spectroscopic analyses, namely UV, PL and circular dichroism (CD). Despite the very low concentration (we tentatively set the upper limit of concentration to 10^{-6}M), the spectra were rather intense. All results are reported in Figure 5. The SDS-PAGE trace (Figure 5A) was surprisingly simple and revealed the presence of only four low weight proteins, two around 60 kDa and two in the range 10-20 kDa. Given their solubility in water, these proteins must be *globular* (*fibrillar* proteins are insoluble in water). The cells contain innumerable components, including very many globular proteins. Thus, fluorophore 7 is capable to discriminate among

all these components and be (and remaining) associated to four specific globular proteins. The spectra of the water solution of the red clusters were also clean and simple and confirmed this conclusion, as shown in Figure 5B (a-d).
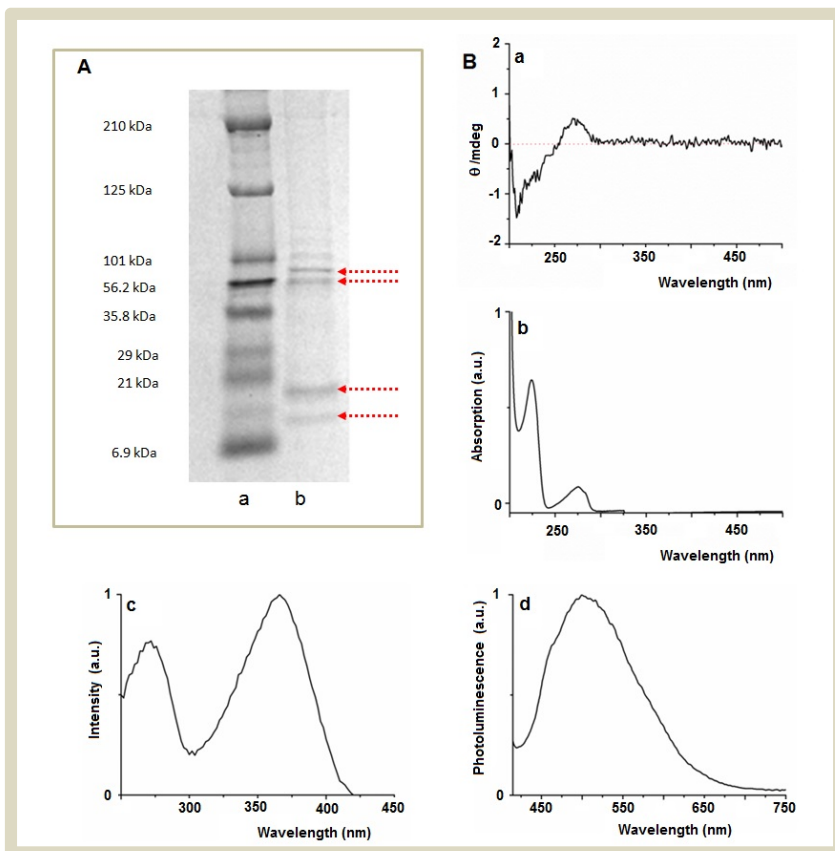

Figure 5. A) SDS-PAGE gel electrophoresis of the red fluorescent clusters formed by live NIH 3T3 live cells 192 hours after treatment with fluorophore 7 (a= broad range marker, b = sample). B) Circular dichroism (a), UV-Vis absorption (b), excitation (c,) and fluorescence (d, λ_{exc}= 375 nm) spectra of the sample dissolved in water.

The UV spectrum (a) displays only the signals tipical of proteins in the range 200-300 nm, corresponding to the CD spectrum (b). Note that fluorophore 7 is an achiral molecule which does not afford any CD signal when dissolved in DMSO-H$_2$O. In the UV spectrum the signals pertaining to the thiophene fluorophore were barely visible. However, these signals were observed in the excitation spectrum (c) showing two broad peaks centered at 275 nm and 375 nm. The fluorescence signal (d, λ_{exc} = 375 nm) is broad, intense and structured (maxima around 460 nm, 500 nm and 575 nm). The difference between absorption and emission is large and in

the order of those generally observed for thiophene fluorophores. We conclude that the 'objects' under examination, i.e. the red clusters, associate the properties typical of proteins (in particular the CD spectrum) with the fluorescence typical of a thiophene fluorophore. The identification of the four globular proteins interacting with 7 inside live NHI 3T3 cells requires more extensive studies, in particular the biochemical analysis of the red clusters, which is currently under way. However, what matters to this stage is that fluorophore 7 is selectively recognized by a few specific globular proteins inside live cells. Most probably, this fluorophore possesses the right size and stereoelectronic requisites to be accommodated by the proteins via non bonding interactions such as H-bondings, electrostatic and hydrophobic interactions. It could be argued that the proteins might be linked to the fluorophore by a covalent bond formed by reaction of the N-succinimidyl group with some NH_2 groups of the proteins. However, this hypothesis seems unlikely due to the fact that the reactivity of the N-succinimidyl group in 7 should be very close to that in its shorter analogue 1, which is instead eliminated by the cells. Clearly, establishing the nature of the protein-fluorophore conjugate is a priority for further studies. Identifying the proteins will help to guide rational efforts to design more selective thiophene fluorophores. But no matter what the nature of the conjugate is, it is remarkable that it does not cause any harm to the cells, as shown by the viability tests reported in Figure 1. The mutual recognition between thiohene fluorophores and specific proteins inside the cells is driven by cell's own metabolism without the need of any additional cofactor. An essential feature for molecular recognition is the flexibility of the systems involved, facilitating binding through a large number of weak interactions. In the present case, the well known ability of proteins to adjust their conformation in order to make specific interactions with a given ligand feets well with the geometric adaptability of the sulfur atom.[6f]

III. CONCLUSION

Besides their uncommon combination of properties - lack of cytotoxicity, brightness, long-lasting fluorescence transmittable from mother to daughter cells and environment sensitivity - the most striking result concerning the thiophene fluorophores described here is that one of them (compound 7, Chart 1) has the right size, steric and electronic properties to be selectively recognized inside live NIH3T3 cells by four low weight *globular* proteins. The importance of this result is stressed by the fact that another thiophene fluorophore (compound 4, Chart 1) has already been shown to be selectively recognized by the *fibrillar* protein type-I collagen inside the same type of live cells.[6c,d] Thus, some biocompatible thiophene fluorophores have the capability to discriminate between protein types, *fibrillar* or *globular*, at the molecular level, inside living cells, depending on their molecular structure, shape and stereoelectronic properties. To the best of our knowledge no other class of organic (least of all inorganic) dyes has displayed so far similar properties. We believe that our results may open the door to the use thiophene fluorophores as a new tool for visualizing specific proteins and their dynamics inside live cells. These small traceable fluorescent dyes display indeed great affinity to proteins, a topic which is just starting to be developed.[5] The derivatives of thiophene have been studied for decades and are still matter of intense research for application in organic devices such as field-effect transistors, light-emitting diodes, light-emitting transistors and photovoltaic cells.[17-

[20] The results presented here indicate that they might have a brilliant future also in the fields of chemical biology and biotechnology.

## IV. EXPERIMENTAL SECTION

4.1.. General

4.1.1. Optical Characterizations. UV-Vis and PL spectra in Table 1 were obtained with a Perkin Elmer Lambda 20 spectrometer and a Perkin Elmer LS50 spectrofluorometer, respectively. For the data reported in Table 2 typically 500-1500 µL samples were used in appropriate quartz cuvettes displaying an absorption/excitation optical path of 1 cm. Absorption data were recorded at 25°C with a JASCO V550 spectrophotometer using 1 nm band-pass, 1 nm step-size and 0.25 s integration time. PL spectra were collected by a Fluoromax-4 spectrofluorimeter using 2 nm excitation band-pass, 1 nm emission band-pass and 0.2-0.5 s integration time. Lifetime measurements were performed by the Time-Correlated Single Photon Counting accessory of Fluoromax-4 using 455 nm pulsed excitation (1 MHz repetition rate) and collecting at fluorophore's emission maximum with 1-5 nm band-pass. CD spectra were recorded with a spectropolarimeter JASCO J-715 under ambient conditions.

4.1.2. Laser Scanning Confocal Microscopy (LSCM). Confocal micrographs were obtained with a Leica confocal scanning system mounted into a Leica TCS SP5 equipped with oil immersion objectives and spatial resolution of approximately 200 nm in *x-y* and 100 nm in *z*.

4.1.3. Uptake of fluorophores by live NIH 3T3 cells. Mouse embryonic fibroblasts (NIH T3 cell line) were seeded at a density of 100.000 cells in tissue culture plate in 1 mL of complete culture medium. The fluorophores were dissolved in the minimum amount of DMSO in order to obtain a stock solution and were then administered to cells by adding the appropriate dilution in DMEM serum free to obtain the final concentration of 0.05 mg/mL ($\sim 10^{-7}$ M) and incubated at 37°C in 5% CO2, 95% relative humidity for 1h. At the end of incubation period unbound dye was removed washing repeatedly the cell cultures with DMEM medium serum free.

4.2. Synthesis and characterization. *General.* Organic solvents were dried by standard procedures. Lithiation and cross coupling reactions were carried out under nitrogen atmosphere. Glass columns of different sizes were used for silica gel chromatographies (particle sizes 0.040-0.063 mm, Merck) or florisil (100-200 mesh, Aldrich). Bis(pinacolato)diboron, namely 2-isopropoxy-4,4,5,5-tetramethyl-1,3,2-dioxaborolane, was purchased from Alfa Aesar GmbH & Co KG; sodium bicarbonate from Sigma-Aldrich Co; 1,1′-bis(diphenylphosphino)ferrocene palladium(II)chloride dichloro methane complex (PdCl$_2$dppf), *n*-butyllithium 2.5 M solution in hexane from Acros Organics. All reagents and solvents were used as received. Microwave irradiation was achieved in a Milestone Microsynth Labstation operating at 2450 MHz equipped with pressure and temperature sensors. Reactions were performed in 10 mL glass vessels sealed with a septum. Microwave irradiation was power controlled (maximum power input: 100 W) and the samples were irradiated with the required power output to achieve the desired temperature. *Melting* points were obtained on *Kofler bank* apparatus and are uncorrected. All ^{1}H NMR and ^{13}C NMR spectra were recorded on a Varian Mercury-400

spectrometer equipped with a 5-mm probe. Chemical shifts are referenced to TMS. Mass spectra were collected on a Finningan Mat GCQ spectrometer.
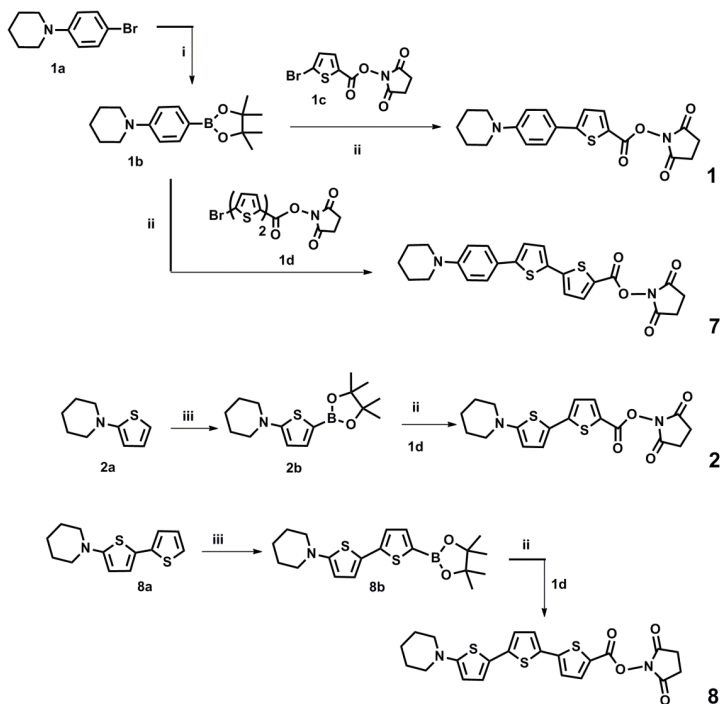
*Reagents and conditions: i) PdCl$_2$(dppf), bis(pinacolato)diboron, NaHCO$_3$, THF/H$_2$O, MW, 10 min, 80°C; ii) PdCl$_2$(dppf), 3 mL DMF/H$_2$O 2:1 v/v, 1 eq **1c** or **1d**, 3 eq **1b**, or **2b** or **8b**, MW 10 min, 80°C; iii) BuLi 2.5 M, 2-isopropoxy-4,4,5,5-tetramethyl-1,3,2-dioxaborolane, THF, -70°C. Compounds **1c** and **1d** have already been described.[6a]*

General procedure for the synthesis of compounds **1-2** *and* **7-8.** A mixture of monobromo derivatives 1c or 1d (0.38 g, 1 mmol), thienylboronic ester (1b, 2b, 8b) (3 mmol), Pd (dppf)$_2$Cl$_2$ (0.05 mmol) and NaHCO$_3$ (2 mmol) in DMF/H$_2$O (2:1, 3 mL) was irradiated with microwaves at 80°C for 10 min. The reaction mixture was brought to room temperature and the solvent was evaporated under reduced pressure. All compounds were isolated by flash chromatography on florisil.

2,5-dioxopyrrolidin-1-yl 5-(4-(piperidin-1-yl)phenyl)-thiophene-2-carboxylate (1)

→ Hexane : AcOEt : CH$_2$Cl$_2$ 70:20:10 Yield 80%. Yellow pale solid; mp>230°C; EI-MS *m/z* 384; absorption maximum, 390 nm (ε 28423 cm^{-1}M^{-1}), emission maximum, 513 nm in CH$_2$Cl$_2$; ^{1}H NMR (CD$_2$Cl$_2$, ppm) δ 7.95 (d, ^3J=4.0Hz, 1H), 7.58 (d, *J*=8.8Hz, 2H), 7.29 (d, ^3J=4.0Hz, 1H), 6.97 (s, 2H), 3.30 (t, 4H), 2.88 (s, 4H), 1.68 (m, 6H); ^{1}H NMR (CD$_3$COCD$_3$, ppm) δ 8.00 (d, ^3J=4.0Hz, 1H), 7.66 (d, *J*=8.8Hz, 2H), 7.48 (d, ^3J=4.0Hz, 1H), 7.04 (d, *J*=8.8Hz, 2H), 3.30 (t, 4H), 2.95 (s, 4H), 1.67 (m, 6H); ^{13}C NMR (CD$_2$Cl$_2$, ppm) δ 169.4, 157.4, 137.9, 137.8, 127.4, 127.3, 122.2, 115.3, 49.3, 25.7, 25.65, 25.6, 25.4, 24.2.

2,5-dioxopyrrolidin-1-yl 5′ –(piperidin-1-yl)-2,2′-bithiophene-5-carboxylate (2)
→ Hexane : AcOEt : CH_2Cl_2 70:20:10. Yield 85%. Yellow solid; mp>230°C; EI-MS *m/z* 390; absorption maximum, 440 nm (ε 28423 $cm^{-1}M^{-1}$), emission maximum, 544 nm in CH_2Cl_2; ^{1}H NMR (CDCl₃, TMS/ppm) δ 7.84 (d, ³*J*=4.4Hz, 1H), 7.09 (d, *J*=4.0Hz, 1H), 6.94 (d, ³*J*=4.0Hz, 1H), 5.98 (d, *J*=4.4Hz, 1H), 3.20 (t, 4H), 2.88 (s, 4H), 1.72 (m, 4H), 1.60 (m, 2H); ¹³C NMR (CDCl₃, ppm) δ 169.3, 161.6, 157.2, 149.9, 137.8, 127.0, 121.0, 120.5, 119.9, 104.5, 51.7, 25.6, 25.0, 23.6.

2,5-dioxopyrrolidin-1-yl 5′-(4-(piperidin-1-yl)phenyl)-2,2′-bithiophene-5-carboxylate (7)
→ Hexane : AcOEt : CH_2Cl_2 60:25:15 Yield 70%. Yellow solid; mp>230°C; EI-MS *m/z* 466; absorption maximum, 421 nm (ε 59869 $cm^{-1}M^{-1}$), emission maximum, 602 nm in CH_2Cl_2; ^{1}H NMR (CD₂Cl₂, ppm) δ 7.94 (d, ³*J*=4.0Hz, 1H), 7.51 (d, *J*=8.8Hz, 2H), 7.35 (d, ³*J*=3.6Hz, 1H), 7.26 (d, ³*J*=3.6Hz, 1H), 7.18 (d, ³*J*=4.0Hz, 1H), 6.93 (d, *J*=8.8Hz, 2H), 3.25 (t, 4H), 2.88 (s, 4H), 1.70 (m, 4H), 1.62 (m, 2H); ¹³C NMR (CD₂Cl₂, ppm) δ 169.5, 157.4, 152.2, 148.5, 147.4, 137.8, 132.7, 127.7, 126.8, 123.9, 123.4, 122.4, 121.0, 115.8, 49.8, 26.4, 25.8, 24.5.

2,5-dioxopyrrolidin-1-yl 5′ –(piperidin-1-yl)-(2,2′;5′,2″)-terthiophene-5-carboxylate (8)
→ Hexane : AcOEt : CH_2Cl_2 60:25:15. Yield 60%. Orange; mp>230°C; EI-MS *m/z* 472; absorption maximum, 454 nm (ε 19256 $cm^{-1}M^{-1}$), emission maximum, 649 nm in CH_2Cl_2; ^{1}H NMR (CD₂Cl₂, ppm) δ 7.89 (d, ³*J*=4.0Hz, 1H), 7.20 (d, ³*J*=4.0Hz, 1H), 7.13 (d, ³*J*=4.0Hz, 1H), 6.94 (d, ³*J*=4.0Hz, 1H), 6.88 (d, ³*J*=4.0Hz, 1H), 5.98 (d, ³*J*=4.0Hz, 1H), 3.20 (t, 4H), 2.89 (s, 4H), 1.72 (m, 4H), 1.59 (m, 2H); ¹³C NMR (CDCl₃, ppm) δ 169.2, 160.2, 157.2, 148.2, 141.0, 137.7, 131.4, 127.1, 124.6, 123.3, 123.0, 121.8, 121.3, 104.6, 52.0, 25.6, 25.1, 23.7.

General procedure for the syntesis of compound 2b, 1b and 8b. To a stirred solution of 2a, 8a and 1a (1 mmol) in anhydrous THF (10 mL) at –70°C, BuLi (2.5M in hexane) (1.2 mmol) was slowly added. The mixture was allowed to react at this temperature for 1 h, then at room temperature for an additional hour. After cooling at –70°C, 2-isopropoxy-4,4,5,5-tetramethyl-1,3,2-dioxaborolane (2.2 mmol) was added and the resulting mixture was allowed to warm to room temperature and stirred for 12 h. The product was extracted with CH_2Cl_2 (2x100 mL). The combined organic phases were dried over anhydrous sodium sulphate and the solvent was removed under reduced pressure.
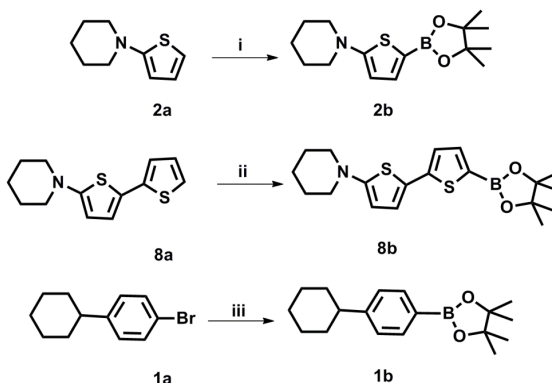
Reagents and conditions: i, ii) BuLi 2.5 M, 2-isopropoxy-4,4,5,5-tetramethyl-1,3,2-dioxaborolane, THF, -70°C; iii) PdCl₂(dppf), bis(pinacolato)diboron, NaHCO₃, THF/H₂O, MW, 10 min, 80°C.

1-(5-4,4,5,5-tretramethyl-1,3,2-dioxaborolan-2-yl)thiophen-2-yl)piperidine (2b)

Yield 99%. Dark-green solid; EI-MS *m/z* 293; ^{1}H NMR (CDCl$_3$, ppm) δ 7.37 (d, ^3J=4.0Hz, 1H), 6.13 (d, ^3J=4.0Hz, 1H), 3.20 (t, 4H), 1.69 (m, 4H), 1.56 (m, 2H) 1.31 (s, 12H).

1-(5-(4,4,5,5-tetramethyl-1,3,2-dioxaborolan-2-yl)-2,2'-bithiophen-5-yl)piperidine (8b)

Dark-green solid. ^{1}H NMR of the crude product showed a mixture of 8b: 7 (starting material) in the ratio 50:50. The crude was utilized as obtained for the last synthetic step. ^{1}H NMR (CDCl$_3$, ppm) δ 7.46 (d, ^3J=3.6Hz, 1H), 7.00 (d, ^3J=3.6Hz, 1H), 6.94 (m, 2H), 3.14 (t, 4H), 1.71 (m, 4H), 1.58 (m, 2H) 1.33 (s, 12H).

1-(4-(4,4,5,5-tetramethyl-1,3,2-dioxaborolan-2-yl)-phenyl)piperidine (1b)

A mixture of compound **1a** (1 mmol), bis(pinacolato)diboron (1.2 mmol), PdCl$_2$(dppf) (0.05 mmol), NaHCO$_3$ (2 mmol) in THF/water 2:1 (3 mL) was irradiated with microwaves at 80°C. The reaction mixture was brought to room temperature and the solvent was evaporated under reduced pressure. the crude product which did not need further purification. Yield 90%. Dark white solid; EI-MS *m/z* 287; ^{1}H NMR (CDCl$_3$, ppm) δ 7.69 (d, *J*=8.8Hz, 2H), 6.87 (d, *J*=8.8Hz, 2H), 3.25 (t, 2H), 1.67 (m, 3H), 1.60 (m, 2H), 1.32 (s, 12H)
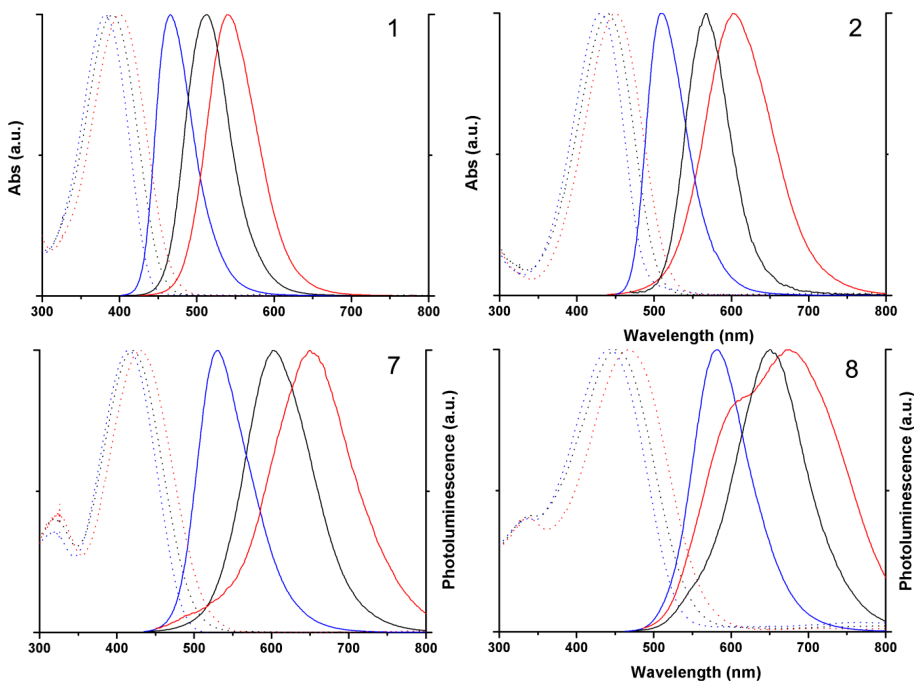
4.3. Optical properties

Figure 7S. Absorption and fluorescence spectra of fluorophores **1**, **2**, **7, 8**

121

Table 1S. Maximum absorption (λ_{max}, nm) and emission (λ_{PL}, nm) wavelengths and fluorescence lifetimes (τ, ns) of 1-2,7-8 in EA and DCM, and fluorescence quantum yield (ϕ) of 7 in DCM.

Item	λ_{max}	λ_{PL}	τ	ϕ [a]	λ_{max}	λ_{PL}	τ	ϕ [a]
	EthylAcetate				*Dichloromethane*			
1	383	449	2.51	0.70	390	513	2.30	0.62
2	429	533	2.83	0.54	442	548	2.51	0.51
7	412	589	3.00	0.45	421	619	2.46	0.45
8	448	635	3.24	0.38	458	660	3.39	0.35

[a] *Calculated with respect to fluorescein. in toluene (blue), DCM (black) and DMSO (red).*

Production of reactive singlet oxygen species by fluorophores 1, 2, 7 and 8

The typical luminescence of the lowest electronically excited singlet state of molecular oxygen, O_2 ($^1\Delta_g$) with a maximum at ca. 1270 nm was detected upon excitation at 442 nm of air equilibrated toluene solutions of the thiophene fluorophores. The figure below displays the results of the NIR luminescence experiment compared with a standard of 5,10,15,20-tetraphenylporphyrin (TPP) in toluene ($\phi_\Delta = 0.70$). The measured yield of $^1\Delta_g$ is 0.08, 0.07, 0.05 and 0.08 for **8**, **7**, **2** and **1**, respectively. The data shown in Figure S11 clearly show that none of the investigated compounds is able to sensitize the production of the reactive singlet oxygen species.
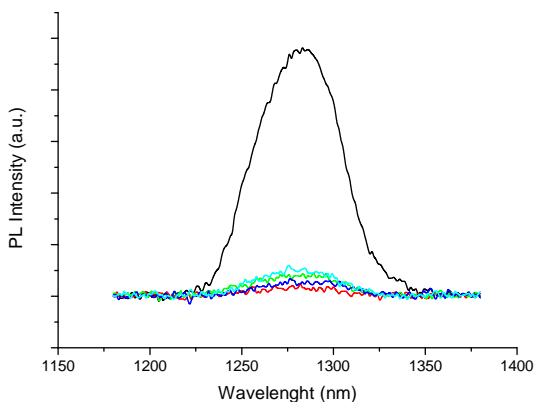

Figure 8S. Sensitised singlet oxygen emission spectra of isoabsorbing TOL solutions of **1** (red), **7** (green), **2** (blue), **8** (magenta) with respect to tetraphenyl porphyrine (black); $\lambda_{exc} = 442$ nm.

4.4. Cell staining. *General.* Tissue culture media and serum were purchased from Sigma, cell line from American Tissue Type Collection (ATTC). The suppliers of the chemicals were: fetal bovine serum (FBS, Sigma, USA), penicillin-streptomycin solution (Sigma, USA), L-glutamine 200 mM (Sigma, USA), DMEM medium (Sigma, USA), sodium pyruvate solution (Sigma, USA), trypsin-EDTA (Sigma, USA), phosphate buffered saline, Dulbecco A (Sigma, USA), 3-[4,5-dimethylthiazol-2-yl]-2,5- diphenyl tetrazolium bromide (MTT, Sigma, USA).

Cell cultures. Mouse embryonic fibroblast cell line (NIH 3T3) was maintained in DMEM supplemented with FBS (10%), penicillin (100 U/mL culture medium), streptomycin (100 µg/mL culture medium), L-glutamine (5%) and sodium pyruvate (5%). Cells were grown in a humidified incubator at 37°C, 5% CO2, and 95% relative humidity.

Live NIH 3T3 cells labeling. Mouse embryonic fibroblasts (NIH 3Laser ScanninT3 cell line) were seeded at a density of 100.000 cells in tissue culture plate in 1 mL of complete culture medium. The fluorophores were dissolved in the minimum amount of DMSO in order to obtain a stock solution and were then administered to cells by adding the appropriate dilution in DMEM serum free to obtain the final concentration of 0.05 mgmL^{-1} and incubated at 37°C in 5% CO2, 95% relative humidity for 1h. At the end of incubation period unbound dye was removed washing the cell cultures with DMEM medium serum free. The samples were examined after 1-24 hours and 7 days by confocal laser scanning microscopy (LSCM). More details in experimental section.

Cytotoxicity tests. Mouse embryonic fibroblasts (NIH 3T3) were analyzed with the cytotoxicity test MTT, a reproducible means of measuring the activity of living cells via mitochondrial dehydrogenase activity whose key component is 3-[4,5-dimethylthiazol-2-yl]-2,5-diphenyl tetrazolium bromide. Mitochondrial dehydrogenases of viable cells cleaved the tetrazolium ring, yielding purple MTT formazan crystals which were insoluble in aqueous solutions. The crystals were dissolved in acidified isopropanol and the resulting purple solution was spectrophotometrically measured. An increase in cell number results in an increase in the amount of MTT formazan formed and an increase in absorbance. Dye suspension at 0.05 mgmL^{-1} concentrations were diluted with appropriate cultural medium. The MTT method of cell determination is most useful when cultures are prepared in multiwall plates. NIH 3T3 cells (10^5 cells/mL) were added to well culture plates at 1000 µL/well and incubated at 37°C in 5% CO2, 95% relative humidity for 24-48 and 72 hours with the 1-3 and 7-8 fluorophores suspension. The control was complete culture medium. After an appropriate incubation period, the cultures were removed from the incubator and the MTT solution added in an amount equal to 10% of the culture volume. Then the cultures were returned to incubator and incubated for 3 hours. After the incubation period, the cultures were removed from the incubator and the resulting MTT formazan crystals were dissolved with acidified isopropanol solution to an equal culture volume. The plates were read within 1 hour after adding acidified isopropanol solution. The absorbance was spectrophotometrically measured at wavelength 570 nm and the background absorbance measured at 690 nm substracted. The percentage viability was expressed as the relative growth rate (RGR) by equation: RGR = (D_{sample}/ $D_{control}$) *100%

where D_{sample} and $D_{control}$ are the absorbances of the sample and the negative control. [Mosmann, T.T. Rapid colorimetric assay for cellular growth and survival: application to proliferation and cytotoxicity assays. *Journal of Immunological Methods* 1983,12-16]

Isolation of red fluorescent aggregates from NIH 3T3 cell lysate. Fluorescent 'spots' present inside the cytoplasmatic region of the mouse embryonic fibroblast (NIH 3T3) cells after treatment with fluorophore 7, were purified by whole cell lysates in 50 mM Tris HCl, pH 7.4; 1% Triton X-100; 5 mM EDTA; 150 mM NaCl; 1 mM Na3VO4; 1 mM NaF; 1 mM phenylmethylsulfonyl fluoride (PMSF), in the presence of protease inhibitor cocktail (10 µM benzamidine-HCl and 10 µg each of aprotinin, leupeptin and pepstatin A per mL) followed by incubation at 4°C. 7-conjugates were left to decant, harvested into fresh reaction tube, washed

three times with fresh lysis buffer by centrifugation, and stored at 4°C. Analyses by fluorescence microscopy were performed to confirm the isolation of fluorescent 'spots' from the cells.

SDS-PAGE. Samples dilution of red fluorescent 7-protein conjugates into SDS-loading buffer (1:1) were separated on SDS-polyacrylamide gels without prior heating. Resolved proteins bands were visualized under Coomassie Brillant Blue.
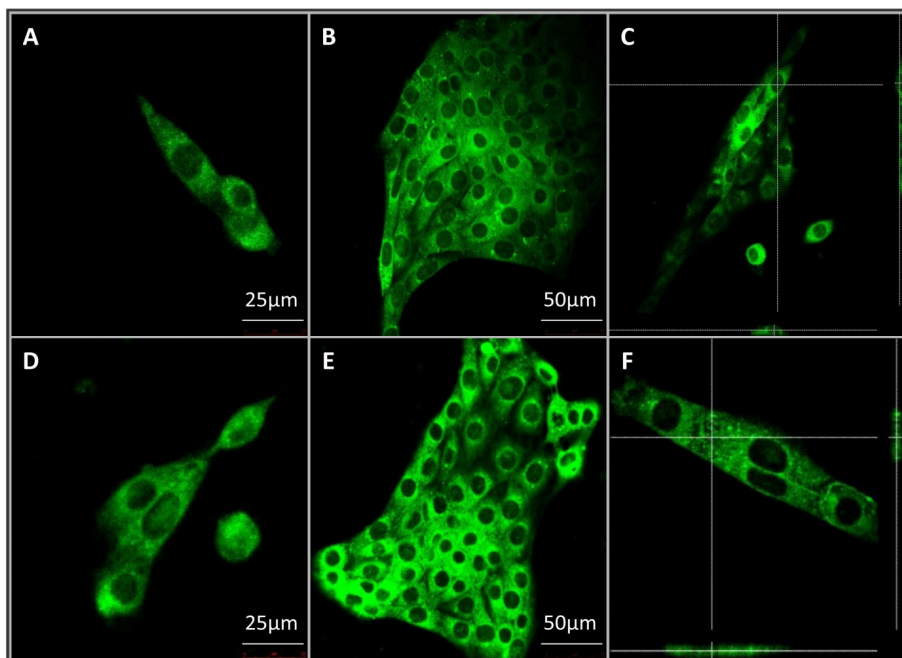

Figure 9S. A), B) LSCM images of live NIH 3T3 cells after 1 hour and 24 hour from treatment with fluorophore 1. D, E) LSCM images of live 3T3 cells after 1 hour and 24 hour from treatment with fluorophore 2. C), F) Cross sections along the z direction (thickness of the slice: 200 nm).
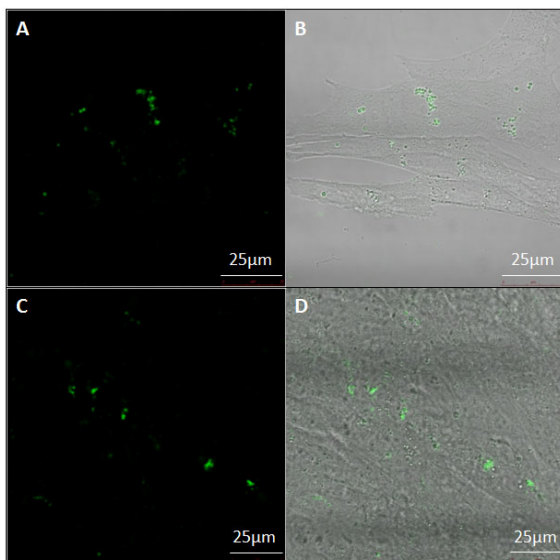
Figure 10S. A), C) LSCM images of live NIH 3T3 cells after 192h from treatment with fluorophores 1 and 2, respectively. B), D) Overlay of light transmission and fluorescence images after 192h from treatment with 1.
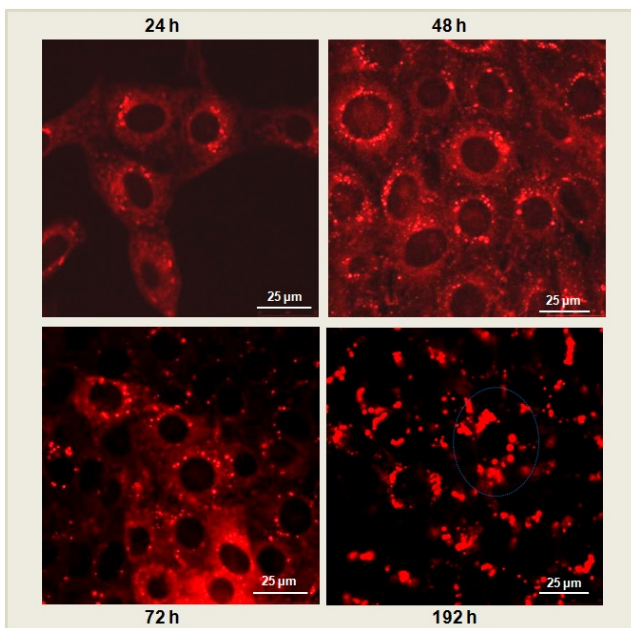

Figure 11S. LSCM images of live NIH 3T3 cells taken 24h, 48h, 72h and 192h after treatment with fluorophore 7.

Fixed NIH 3T3 cells stained with fluorophores 3 and 8. Mouse embryonic fibroblasts (NIH 3T3 cell line) were seeded at a density of 100.000 cells in tissue culture plate in 1 mL of complete culture medium. Fluorophores 3 and 8 were dissolved in the minimum amount of DMSO in order to obtain a stock solution which was then administered to the cells by adding the appropriate dilution in DMEM serum free to obtain the final concentration of 0.05 mgmL^{-1} and incubated at 37°C in 5% CO_2, 95% relative humidity for 1h. At the end of the incubation period unbound dye was removed washing the cell cultures with DMEM medium serum free. After 24 hours each sample was rinsed twice with PBS to remove all unattached cells and was fixed in formaldehyde 3.7%. Nuclei were stained with DAPI (Sigma-Aldrich). The samples were examined using a Leica confocal scanning system mounted on a Leica TCS SP5 (Leica Microsystem GmbH, Mannheim, Germany) and equipped with 63X oil immersion objectives and spatial resolution of approximately 200 nm in x-y and 100 nm in z.
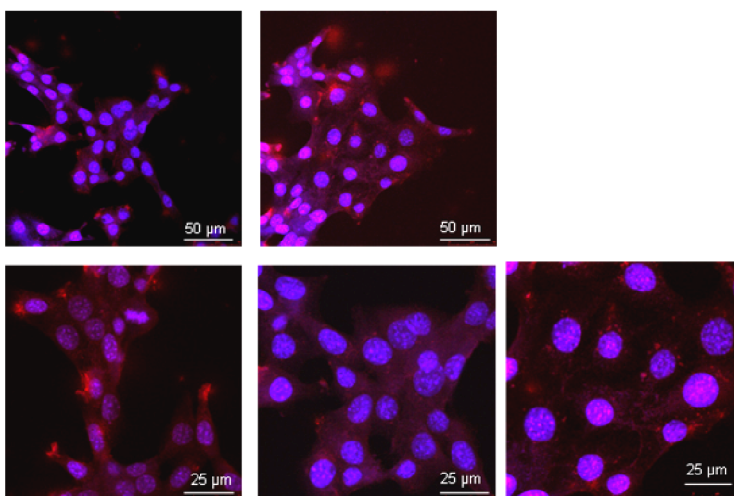

Figure 12S. LSCM images of fixed NIH 3T3 cells incubated with fluorophore **8** (0.05 mg/mL). Green: fluorophore 3. Blue: DAPI.
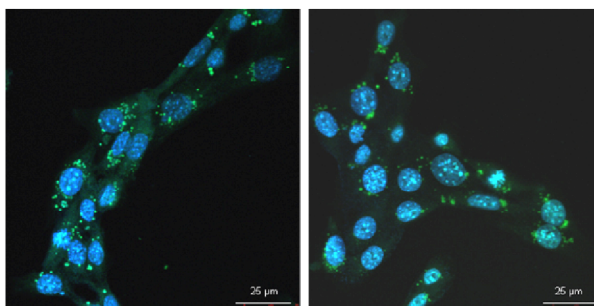

Figure 13S. LSCM images of fixed NIH 3T3 cells incubated with fluorophore **3** (0.05 mg/mL). Red: fluorophore **8**. Blue: DAPI.

4.5.. Theoretical calculations

A) To have an idea of the decomposition mechanisms of compounds 1, 2,7 and 8 we carried out theoretical calculations on the photostability of 2-dimethylamino-thiophene, 2-thienyl-carboxylic acid and 2-thiomethyl-thiophene, for comparison.

It has been suggested that the relative population of Dewar and triplet structures has to be considered responsible for the photochemical isomerization or degradation of thiophene derivatives (M. D'Auria *Journal of photochemistry and photobiology A: Chemistry* 2002, 149, 31-37 and references therein). We have therefore investigated by density functional theory (DFT) calculations the availability of Dewar and triplet structures for 2-dimethylamino-thiophene taken as model for the 2-piperidyl-thiophene moiety of compounds 1, 2,7 and 8. It was found that the Dewar structure is 15 kcal/mol lower than the triplet one, and therefore it is the Dewar structure that has to be taken into account for the observed behaviour. We have then compared this structure with the Dewar structures of 2-thienyl-carboxylic acid and 2-thiomethyl-thiophene, taken as model for the terminal part of stable oligomers, and of thiophene itself (Figure S12).
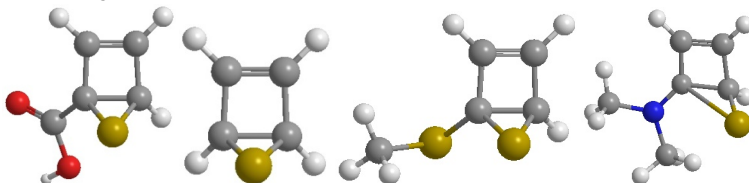

Figure 14S. DFT calculated geometries of the Dewar structures.

We note that the presence of a carboxyl group or a thiomethyl group does not perturb the structure of the Dewar thiophene, characterized by the projection of the sulfur atom out of the plane of the carbon atoms and by the equidistance of the sulfur atom from C2 and C5 (1.85 Å). On the contrary, the presence of an ammino group, owing to its mesomeric effect, strongly perturbs the Dewar structure. In fact, the C-N bond is 0.08 Å shorter than the parent compound (1.31 Å *vs* 1.39 Å) and the S-C2 bond is almost broken (2.78 Å). As a consequence, the molecule results more reactive than the more symmetric carboxylic ones. Furthermore, the energy difference between the Dewar and the classic thiophene structure has been calculated to be 57.1 kcal/mol for thiophene itself and 2-thiomethylthiophene, 61.4 kcal/mol for carboxyl derivative and 44.8 kcal/mol for ammine derivative. This latter results therein to be at the same time the more available by energy and the more reactive by structure, and can further evolve on other structures more easily than the carboxylated and thiomethylated ones.

B) Conjugative effect. To have an insight into the efficiency of conjugative effect of thiometyl and amino groups on our push-pull chromophores, DFT calculations have been performed on the two N-succinidimyl esters a,b as well as on 2,2'-bithiophene itself (T-T) for sake of comparison. We can note that the presence of the push-pull chromophores leads to a significative increase of the planarity of the bithiophene moiety and to a decreasing of the inter-ring distance. Both these geometrical parameters are a good indicator of the efficiency of a conjugative effect. The ammino group, due to its strong mesomeric effect, is by far more

efficient than the thiomethyl group. Moreover, it is also more effective in the decreasing of the energy gap and in the batochromic effect of UV absorption.

Table 2S. Inter-ring torsion ω(°), inter-ring distance d(Å), HOMO-LUMO energy gap ΔE_{H-L}(eV), dipolar moment μ(Debye), absorption wavelength λ_{max}(nm)

Compound[*]	ω(°)	d(Å)	ΔE_{H-L}(eV)	μ(Debye)	λ_{max}(nm)[**]
T-T	158	1.451	4.36	0.27	322
CH_3S-T-T-COONSu **a**	164	1.448	3.72	1.27	372
$(CH_3)_2$N-T-T-COONSu **b**	177	1.438	3.22	5.48	410

[*]Nsu = Nsuccinimidyl group. [**]ZINDO/S calculations on optimized DFT geometries

C) Computational methods. All calculations were carried out at the B3LYP/6-31G(d) level within the framework of the Gaussian 03W suite of programs.[1] Unrestricted calculations were used for the Dewar structures. Geometries were fully optimized by standard gradient techniques and the final structures were checked by frequency analysis. Zero point vibrational energy corrections were applied without scaling. The Dewar structures were optimized also at the uMP2/6-31+G(d,p) level, but no difference with DFT structures was found out. UV transitions were calculated by ZINDO/S-C.I. (6 x 6) calculations on DFT geometries using the HyperChem integrated package. [2]

1) Gaussian 03, Revision B05, M. J. Frisch, G. W. Trucks, H. B. Schlegel, G. E. Scuseria, M. A. Robb, J. R. Cheeseman, J. A. Montgomery, Jr., T. Vreven, K. N. Kudin, J. C. Burant, J. M. Millam, S. S. Iyengar, J. Tomasi, V. Barone, B. Mennucci, M. Cossi, G. Scalmani, N. Rega, G. A. Petersson, H. Nakatsuji, M. Hada, M. Ehara, K. Toyota, R. Fukuda, J. Hasegawa, M. Ishida, T. Nakajima, Y. Honda, O. Kitao, H. Nakai, M. Klene, X. Li, J. E. Knox, H. P. Hratchian, J. B. Cross, C. Adamo, J. Jaramillo, R. Gomperts, R. E. Stratmann, O. Yazyev, A. J. Austin, R. Cammi, C. Pomelli, J. W. Ochterski, P. Y. Ayala, K. Morokuma, G. A. Voth, P. Salvador, J. J. Dannenberg, V. G. Zakrzewski, S. Dapprich, A. D. Daniels, M. C. Strain, O. Farkas, D. K. Malick, A. D. Rabuck, K. Raghavachari, J. B. Foresman, J. V. Ortiz, Q. Cui, A. G. Baboul, S. Clifford, J. Cioslowski, B. B. Stefanov, G. Liu, A. Liashenko, P. Piskorz, I. Komaromi, R. L. Martin, D. J. Fox, T. Keith, M. A. Al-Laham, C. Y. Peng, A. Nanayakkara, M. Challacombe, P. M. W. Gill, B. Johnson, W. Chen, M. W. Wong, C. Gonzalez, and J. A. Pople, Gaussian, Inc., Pittsburgh PA, 2003. 2) *HyperChem* rel 7.5 from Hypercube Inc. Waterloo, Ontario, Canada

REFERENCES

[1] (*a*) Dedecker P, De Schryver C, Hofkens J. *J. Am. Chem. Soc.*, **2013**, 135, 2387-2402. (*b*) Song F, Tang PS, Durst H, Cramb DT, Chan WCW. *Angew. Chem. Int. Ed.*, **2012**, 51, 8773-8777. (*c*) Zhou K, Liu H, Zhang S, Huang X, Wang Y, Huang G, Sumer BD, Gao J. *J. Am. Chem. Soc.*, **2012**, 134, 7803-7811. (*d*) Chan YH, Ye F, Gallina ME, Zhang X, Jin Y, Wu IC, Chiu DT. *J. Am. Chem. Soc.*, **2012**, 134, 7309-7312. (*e*) Choi Y, Kim K, Hong S, Kim H, Kwon YJ, Song R. *Bioconjugate Chem.*, **2011**, 22, 1576-1586. (*f*) Wysocki LM, Lavis LD. *Current Opinion in Chemical Biology*, **2011**, 15, 752-759. (*g*) Vendrell M, Zhai D, Er JC Chang YT. *Chem. Rev.,* **2012**, 112, 4391-4420.

[2] Ishikawa-Ankerhold HC, Ankerhold R, Drummen GPC. *Molecules*, **2012**, 17, 4047-4132.

[3] Aguzzi A, O'Connor T. *Nature Reviews*, **2010**, 9, 237-248.

[4] (*a*) Jing C, Cornish VW. *Acc. Chem. Res.*, **2011**, 44, 784-792. (*b*) Wombacher R, Cornish VW. *J. Biophotonics*, **2011**, 4, 391-402. (*c*) Chen Z, Jing C, Gallagher SS, Sheetz MP, Cornish VW. *J. Am. Chem. Soc*, **2012**, 134, 13692-13699. (*d*) Uttamapinant C, White KA, Baruah H, Thompson S, Fernández-Suárez M, Puthenveeti S, Ting AY. *PNAS*, **2010**, 107, 10914-10919. (*e*) Uchinomiy S, Nonaka H, Wakayama S, Ojidac A, Hamachi I. *Chem.Commun.,* **2013**, 49, 5022-5024. (*f*) Gandor S, Reisewitz S, Venkatachalapathy M, Arrabito G, Reibner M, Schröder H, Ruf K, Niemeyer CM, Bastiaens PIH, Dehmelt L. *Angew. Chem. Int. Ed.,* **2013**, 52, 4790 - 4794.

[5] (*a*) Zako T, Sakono M, Kobayashi T, Sõrgjerd K, Nilsson KPR, Hammarstrōm P, Lindgren M, Maeda M. *ChemBioChem*, **2012**, 13, 358-363. (*b*) Klingstedt T, Åslund A, Simon RA, Johansson LBG, Mason JJ, Nystrōm S, Hammarstrōm P, Nilsson KPR. *Org. Biomol. Chem.*, **2011**, 9, 8356-8370. (*c*) Konradsson P, Åslund A, Nilsson KPR. *Biochemistry*, **2010**, 49, 6838-6845.

[6] (*a*) Barbarella G, Zambianchi M, Ventola A, Fabiano E, Della Sala F, Gigli G, Anni M, Bolognesi A, Polito L, Naldi M, Capobianco M. *Bioconjugate Chem.*, **2006**, 17, 58-67. (*b*) Zambianchi M, Di Maria F, Cazzato A, Gigli G, Piacenza M, Della Sala F, Barbarella G. *J. Am. Chem. Soc.*, **2009**, 131, 10892-10900. (*c*) Palamà IE, Di Maria F, Viola I, Fabiano E, Gigli G, Bettini C, Barbarella G. *J. Am. Chem. Soc.*, **2011**, 133, 17777-17785. (*d*) Viola I, Palamà IE, Coluccia AML, Biasiucci M, Dozza B, Lucarelli E, Di Maria F, Barbarella G, Gigli G. *Integrative Biol.*, **2013**, 5, 1057-1066. (*e*) Zambianchi M, Barbieri A, Ventola A, Favaretto L, Bettini C, Galeotti M, Barbarella G. *Bioconjugate Chem.,* **2007**, 18, 1004-1009. (*f*) Di Maria F, Olivelli P, Gazzano M, Zanelli A, Biasiucci M, Gigli G, Gentili D, D'Angelo P, Cavallini M, Barbarella G. *J. Am. Chem. Soc.*, **2011**, 133, 8654-8661.

[7] Perepichka IE, Perepichka DF. Handbook of Thiophene-Based Materials Eds.; John Wiley & Sons: Chichester, **2009**.

[8] Alonso F, Beletskaya IP, Yus M. *Tetrahedron*, **2008**, 64, 3047-3101.

[9] Espinet P, Echavarren AM. *Angew. Chem. Int. Ed.*, **2004**, 43, 4704-4734.

[10] Sotgiu G, Galeotti M, Samorí C, Bongini A, Mazzanti A. *Chem. Eur. Journal.*, **2011**, 17, 7947-7952.

[11] (*a*) Kappe CO. *Angew. Chem. Int. Ed.*, **2004**, 43, 6250-6284. (*b*) Bassyouni FA, AbuBakr SM, Rehim MA. *Res. Chem. Intermediat.,* **2012**, 38, 283-322.

[12] Li JT, Wang SX, Chen GF, Li TS. *Curr. Org. Synth.*, **2005**, 2,415-436.

[13] Marsh D. *Biophys. J.*, **2009**, 96, 2549-2558.

[14] Signore G, Nifosì R, Albertazzi RL, Storti B, Bizzarri R. *J. Am. Chem. Soc.*, **2010**, 132, 1276-1288.

[15] Lavis LD, Raines RT. *ACS Chem. Biol.*, **2008**, 3, 142-155.

[16] Denizot F, Lang R. *J. Immunol. Methods,* **1986**, 89, 271-277.

[17] Mei J, Diao Y, Appleton AL, Fang L, Bao Z. *J. Am. Chem. Soc.*, **2013**, 135, 6724-6746.

[18] Dang MT, Hirsch L, Wantz G, West JD. *Chem. Rev.*, **2013**, 113, 3734-3765.

[19] Shunta I, Yanagi H, Hotta S. *Org. Electron.*, **2013**, 14, 80-85.

[20] Chen X, Yao K, Chen L, Chen Y. *Chem. Mater.*, **2013**, 25, 897-904.

Part II: Nanostructured protein-fluorophore microfibers physiologically secreted by live cells can direct cell behavior

I. INTRODUCTION

A living cell contains complex substructures that are spatially and functionally self-organizing[1] and present unique characteristics useful for materials production and patterning. Our understanding of these systems and their dynamics is largely dependent on the possibility to visualize their presence inside the cells, in particular by means of fluorescence imaging. To this aim a variety of organic and inorganic tools have been developed spanning from fluorescent proteins[2] to nanoparticles,[3,4] quantum dots[5] and small organic molecules.[6] A great advantage of the latter is the possibility to employ the methodologies of synthetic chemistry to tailor their optical properties and to direct the position of the fluorophore inside live cells by means of appropriate functionalization.[7]

An emerging class of probes for biochemical imaging is that of thiophene oligomers and polymers. K. P. R. Nillson *et al.* have reported that a charged quinquethiophene can mark amyloid fibers[8] *in vitro* and *in vivo* and it is also able to discriminate between various types of cells.[9] Recently, we have reported that some biocompatible thiophene fluorophores have the capability to selectively recognize protein types, fibrillar or globular, inside living cells, depending on their stereoelectronic properties.[10-12] In particular, thiophene fluorophore DTTO, namely 3,5-dimethyl-2,3'-bis(phenyl) dithieno[3,2-b;2',3'-d]thiophene-4,4-dioxide (see Figure 1), is recognized by type-I collagen during the process of its formation inside live human and mouse fibroblasts leading to the secretion of helical fluorescent microfibres.[11] DTTO being a semiconducting molecule, the collagen containing microfibers are also electroactive.[12]

Here, we report Laser Scanning Confocal Microscopy (LSCM) evidence that: 1) the biocompatible DTTO is also specifically recognized by the fibrillar protein vimentin inside live neuroblastoma B104 cells, leading to the physiological secretion of fluorescent vimentin-DTTO microfibers. Note that vimentin[13] is overexpressed in various type of cancers[14] and in the Alzheimer's disease,[15] and that it may play an important role in cancer cells invasion;[16] 2) upon seeding different types of live cells on the physiologically formed protein-DTTO microfibers, very different effects are observed, suggesting that the microfibers could be used to direct cell behaviour in terms of cellular morphology, cytoskeleton rearrangement and viability. The biocompatibility and biodegradability of our hybrid fluorescent multiscale microfibers, physiologically produced by live cells upon spontaneous uptake of DTTO, represent a proof of concept of innovative multiscale biomaterials for active bioagents delivery systems and for tissue engineering applications.

II. RESULTS AND DISCUSSION

2.1. Vimentin microfibers formation and characterization. The molecular structure of DTTO is shown in Figure 1A. The fluorophore is a chemically and optically stable

compound, characterized by green fluorescence emission.[11] Live mouse neuroblastoma cells were incubated with micromolar DTTO in buffered solution (0.05 mg/mL). Following the removal of unbound fluorophore and extensive washing, the cells were continuously cultured and monitored for 7 days. Figure 1 shows the LSCM images of the evolution with time of the neuroblastoma cells after incubation with DTTO. Thanks to the right hydrophilicity/hydrophobicity balance and the amphiphilicity due to the presence of the oxygen atoms, DTTO spontaneously crosses the cell membrane and diffuses into the cells. Figure 1B shows that after 1 h from washing the fluorophore is gathered inside the cells forming globular aggregates around the perinuclear region, as already observed for other thiophene fluorescent dyes.[10-12] After 24 h (Figure 1C) the cytoplasm of the cells appears intensely green fluorescent while the nuclei remain unstained and dark. Moreover, within the cytoplasm of several cells the formation of fluorescent microfibers of micrometer size is apparent. The microfibers progressively accumulate inside the cells (Figure 1E-F), while fluorescent cells are visible in the background indicating that fluorescence is transmitted from mother to daughter cells during the replication process. It is worth noting that many microfibers display details where helical green fluorescent structures are present, see for example the details shown in Figure 1D or Figure 1S.
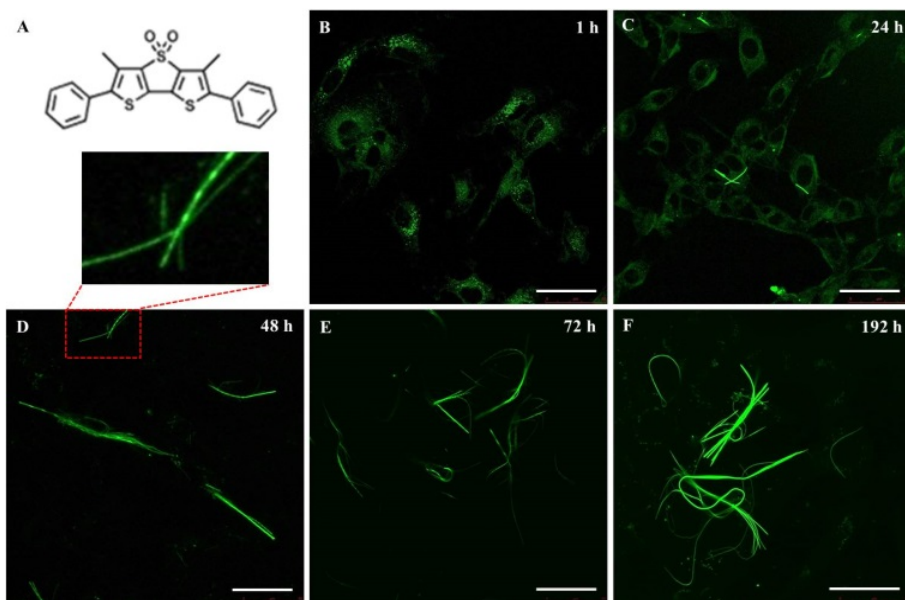

Figure 1. LSCM images of the intracellular formation of fluorescent microfibers in mouse neuroblastoma cells (B104 cell line). (A) Molecular structure of DTTO. (B-F) Time course of the cells incubated with DTTO at concentration of 0.05 mg/mL in DMEM medium. *Scale bars: 50 μm.*

The fluorescent microfibers formed after 7 days from treatment of the cells with DTTO were separated from cell lysate, picked up by LSCM and analyzed by sodium dodecyl sulfate polyacrylamide gel electrophoresis (SDS-PAGE). The results are shown in Figure 2. SDS-PAGE unambiguously indicated the proteic nature of the fluorescent fibrils. Only one single signal was observed in the region around 60 KDa molecular weight.
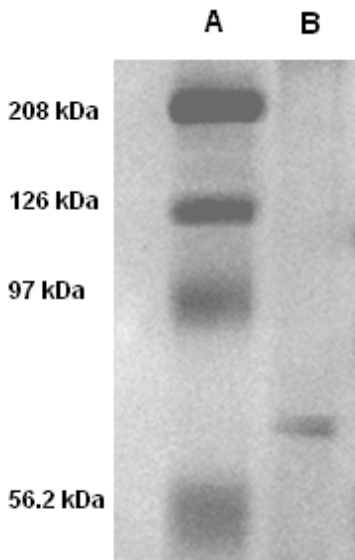

Figure 2. SDS-PAGE of the fluorescent microfibers isolated by live mouse neuroblastoma cells after 192 hours of treatment with DTTO (A= high molecular weight marker, B = sample).

2.2. The fluorescent microfibers isolated by neuroblastoma cells are mainly made of vimentin.

The fluorescent microfibers formed after 7 days from treatment with DTTO and separated from cell lysate were analyzed, after appropriate treatment (see section 2.7), by HPLC-ESI-QToF using the Mascot software[18] for proteins identification.

It was found that the 73.4% (See supplementary attached file denominated 'Fibrille_Rattus') of the fluorescent microfibers was made of vimentin, a protein of the intermediate filaments of the cytoskeleton with a 57 KDa molecular weight.[19] A few percent of nestin, plectin and lamin A were also detected (See again the file 'Fibrille_Rattus'). The presence of the latter proteins is in agreement with the fact that vimentin presents a subcellular distribution and interaction with many proteins as lamin, plectin, etc. In particular, at the nuclear envelope, the 6.6 kDa tail region of vimentin is known to interact with lamin B,[20] while another study shows that vimentin interacts with β3 integrins and plectin, which together regulate the organization and distribution of vimentin in several cell types.[21] In agreement with mass spectrometry data, co-localization experiments of isolated fluorescent microfibers with the monoclonal vimentin antibody showed that there was in fact co-localization between the antibody

and the microfibers. Figure 3 shows the LSCM images of isolated green fluorescent microfibers (a), isolated red fluorescent anti-vimentin antibody (b), merge images (c) and corresponding z-stack sections (d) with z-resolution of 200 nm. Figure 3D shows that there is spatial co-localization with the red fluorescent anti-vimentin antibody inside the green fluorescent microfibers.
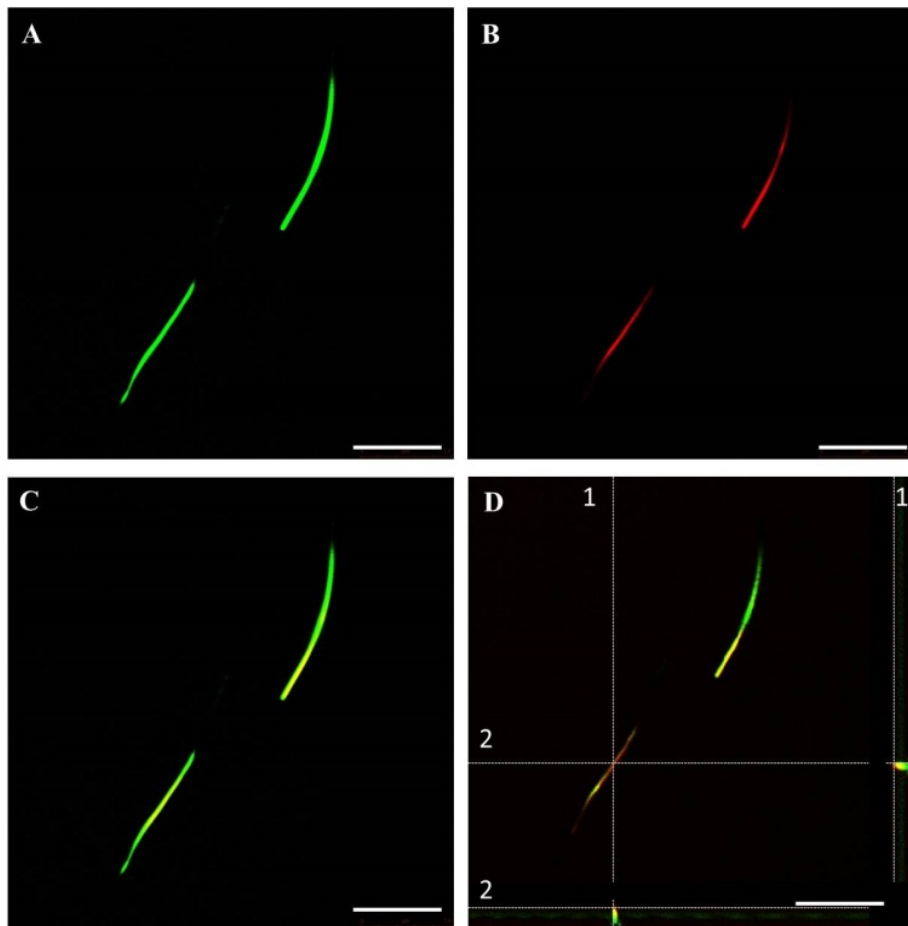

Figure 3. LSCM images of co-localization experiment between isolated fluorescent microfibers secreted by B104 mouse neuroblastoma cells and anti-vimentin antibody. A) Isolated green fluorescent microfibers. B) Isolated red fluorescent anti-vimentin antibody. C) Merge image. D) Corresponding z-stack sections with z-resolution of 200 nm, showing the spatial co-localization of DTTO (green) with anti-vimentin antibody (red) inside the microfibers. *Scale bar: 7.5 µm.*

Figure 4 shows the AFM image of fluorescent microfibers isolated from the cell lysate. The morphology of the largest fiber recalls the structure of the dimer of vimentin

representing the first level of vimentin self-assembly.[22] The figure also displays the coiled coil arrangement of two smaller microfibers. Figure 2S and Figure 3S show another fluorescent microfiber isolated from cell lysate and provide evidence of the lateral growth of the microfibers.
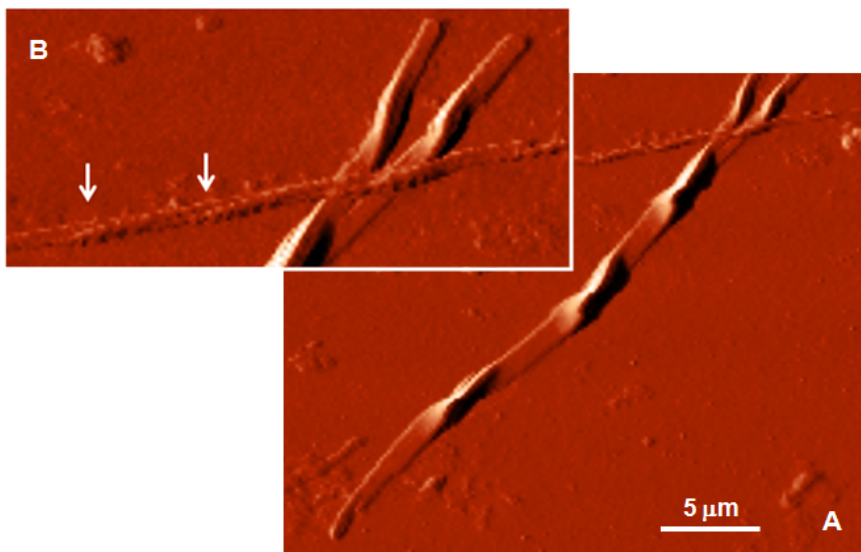

Figure 4. A) AFM image of fluorescent microfibers isolated from the cellular milieu. The morphology of the largest fiber recalls the structure of the dimer of vimentin representing the first level of vimentin self-assembly.[18] B) Magnification of a detail of Figure A. The arrows indicate the coiled coil arrangement of two smaller microfibers.

Vimentin is a polypeptide comprising 466 amino acids with a highly conserved α-helical 'rod' domain that is flanked by non- α-helical N- and C-terminal end domains, the 'head' domain and 'tail' domain, respectively.[13]The self-organization of these molecules leads to the formation of coiled coils, which are the basic structural building blocks for the entire IF family of proteins. Vimentin is also known to form homopolymers and heteropolymers (i.e., it associates with other type III and type IV IFs), a common feature among the members of the IF family ascribed to the presence of a coiled-coil α-helical domain. Highly stable polymers are formed, the stability of which is controlled by the phosphorylation status of the integral proteins.

The fact that fluorescent microfibers mainly made of vimentin are physiologically generated upon treatment of the cells with DTTO is in agreement with our view according to which DTTO is a dye capable to be recognized by selected fibrillar proteins during their formation and growth inside live cells.[11-12] The present results indicate that different types of proteins are recognized by the biocompatible DTTO in different types of live cells. DTTO is a small neutral molecule which can easily be accommodated

within the alpha helical collagen strand of fibroblasts of different origin via hydrogen bonds leading to the stabilization of the helical structure.[11-12] All IF proteins, including vimentin, although varying greatly in their primary structure, are characterized by an alpha-helical central rod domain having the intrinsic capability to form coiled-coil filaments and are terminated by non-helical N- and C-domains of variable size, which play a role in protein self-assembly process. Thus, the α-helical structure present in vimentin and its ability to form non-covalent bonds with DTTO via non-bonding interactions cannot alone justify the fact that it is mainly vimentin that is concerned by DTTO in live neuroblastoma cells. It is more likely that the choice is determined by some co-factors related to the general 'economy' of the cell and its metabolism.Despite the numerous studies reported on vimentin of various origin, including investigations on its *in vitro* self-assembly properties,[23-25] only recently a nearly complete atomic structure of human vimentin rod has been published.[26] The astonishing similarity between the sophisticated shape of the fluorescent microfiber analyzed by AFM in Figure 4 and the shape of human vimentin dimer as determined on the basis of X-ray diffraction at the atomic scale (see figure 4C of reference 26) is unlikely to be the outcome of a mere coincidence. The fact that cell viability remains unaltered upon DTTO uptake (Figure 4S) plaids in favor of the fact that the fluorescent dye is progressively embedded during the protein growth without substantially altering the self-assembly process. This might be the result of the combination of the well-known ability of proteins to adjust their conformation to specifically bind a given ligand via non-bonding interactions with the geometric adaptability of sulfur compounds caused by the polarizability of bound and unbound sulfur electrons. The possibility to separate physiologically formed microfibers by LSCM from cell lysate thanks to their fluorescence offers an unprecedented way to analyze the optical and morphological properties of specific proteins at a given stage of their formation and growth modalities. Apparently, the formation and growth of the fluorescent microfibers inside the cells are a process during for days and, luckily, the lifetime of DTTO fluorescence is also very long.

2.3. Cell interaction with hybrid collagen I and vimentin microfibers. Cellular response to the multiscale hybrid microfibers was analyzed by LSCM. As shown in Figure 5, cells seeded on hybrid collagen I or vimentin microfibers (Figures 5A,E) assumed different morphologies and configurations depending on the stimuli experimented. For C2C12 myoblasts and B104 neuroblastoma cells (Figures 5B,D) a rapid cytoskeleton remodeling, with a remarkable organization of F-actin into intricate branching networks and polarized filopodia protrusions was associated to a more elongated shape whereas the 3T3 fibroblasts (Figure 5C) assumed a spindle-shaped appearance showing a round, contracted cell body when seeded on surfaces coated with hybrid collagen I microfibers. Conversely, 3T3 fibroblasts and B104 neuroblastoma cells (Figures 5G,H) maintained their epithelial morphology of a polygonal shape with many actin cytoplasmic protrusions (filopodia-like processes), while C2C12 myoblasts (Figure 5F) showed a contracted cell body when seeded on surfaces coated with hybrid vimentin microfibers.
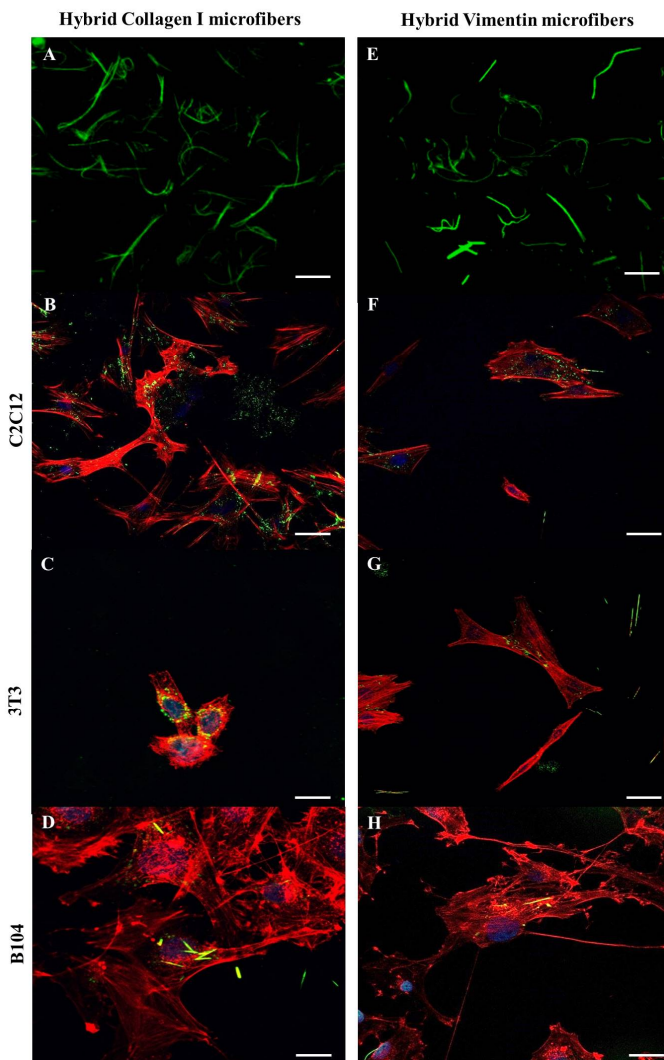
Figure 5. LSCM images of C2C12 myoblasts (B,F) 3T3 fibroblasts (C,G) and B104 neuroblastoma cells (D,H) seeded on hybrid collagen I or vimentin microfibers (A,E, green) for 48 hours and stained for actin (red). Nuclei stained with DAPI (blue). *Scale bar: 10 µm.*

As shown in Figure 6, after 48 h of cell culture, hybrid collagen I and vimentin microfibers appeared as green fluorescent dots, with uniform distribution inside the cytoplasm of C2C12 myoblasts (Figures 6A,D) and 3T3 fibroblasts (Figures 6B,E). It can be guessed that both hybrid microfibers were degraded by the cell,[27,28] conceivably by action of the matrix metalloproteases modifying in this way the microenvironment and resulting in alteration of cellular morphology and cytoskeleton rearrangement

(Figure 5). On the contrary, in B104 neuroblastoma cells hybrid collagen I microfibers were partially degraded, as evident in Figure 6C, while the hybrid vimentin microfibers show their native morphology (Figure 6F). The degradation and possible recycling of hybrid microfibers can be a process used to create protein fragments needed to build new cellular structures.
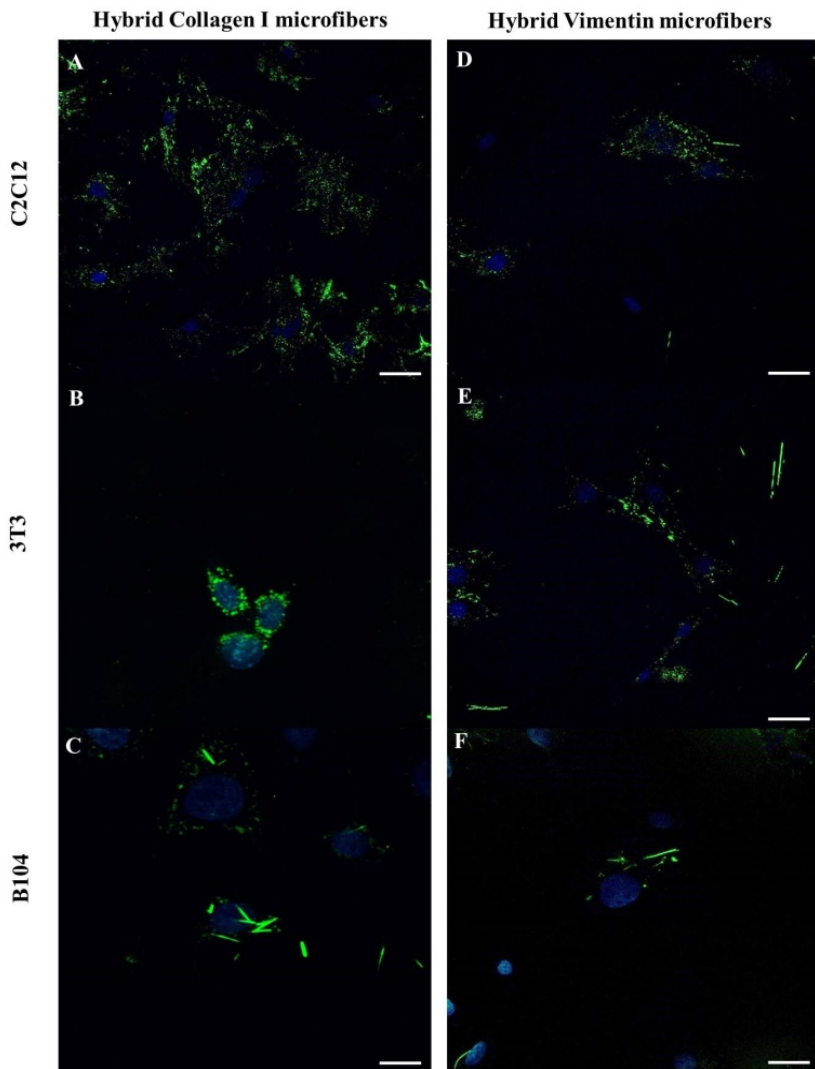

Figure 6. LSCM images of C2C12 myoblasts (A,D) 3T3 fibroblasts (B,E) and B104 neuroblastoma cells (C,F) seeded on hybrid collagen I or vimentin microfibers (green) for 48 hours. Nuclei stained with DAPI (blue). *Scale bar: 10 µm.*

We also evaluated the viability of C2C12 myoblasts, 3T3 fibroblasts and neuroblastoma cells cultured on a glass cover slip coated with fluorescent collagen I or vimentin microfibers by performing a MTT proliferation assay at 24, 48, 72, 192 h. As shown in Figure 7, substrates coated with both hybrid microfibers did not affect cell viability or proliferation, as judged by the increases in total cell numbers over time. The viability of 3T3 fibroblasts was compromised only when cells were seeded on hybrid collagen I microfibers. As evident in Figure 5B all microfibers (1 mg/mL) present on the substrate were degraded and internalized by fibroblasts after 48 h. These result indicates that the massive storage of hybrid collagen I fragments inside fibroblasts leads to apoptosis. This does not exclude that concentrations below 1 mg/mL of hybrid collagen I microfibers might not induce cytotoxic effects on fibroblasts. Further experiments are in progress to elucidate the biochemical mechanisms involved in the degradation of hybrid microfibers and how the mechanical and electrical characteristics of our microfibers direct the cellular behaviour.
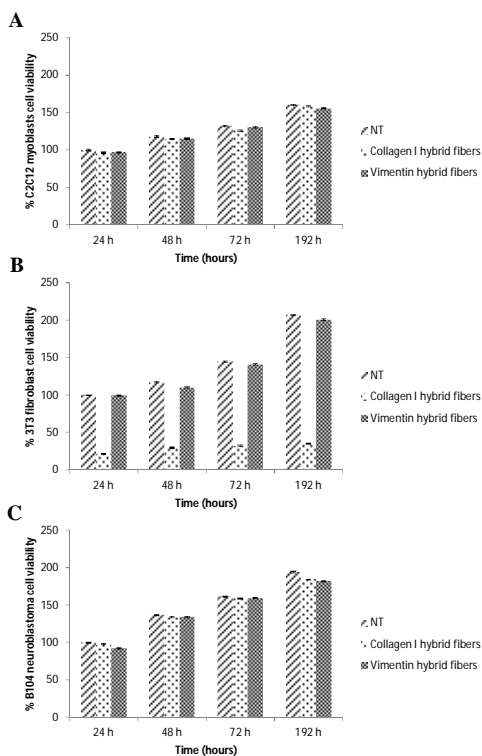

Figure 7. Proliferation assays of C2C12 myoblasts (A), 3T3 fibroblasts (B) and B104 neuroblastoma cells (C) cultured on a uncoated glass cover slip (NT), glass cover slip coated with collagen I or vimentin hybrid microfibers for 24,48,72,192 h. The results are expressed as mean ± standard deviations and are representative of three independent experiments (t-Student test, P< 0.05).

III. CONCLUSION

LSCM studies show that DTTO is a fluorophore recognized by fibrillar intracellular proteins. The results reported here demonstrate that different types of cells employ DTTO for the physiological production of fluorescent fibrillar proteins organized in nanostructured fibres of micrometer size, namely vimentin with neuroblastoma cells (this study) and type-I collagen with fibroblasts of different origin[11]. We show that various types of live cells seeded on these microfibers are able to internalize and degrade them, experiencing in turn different effects on their morphology and viability. The composition and distribution of specific ECM components varies with the type of tissue, and can also be altered by tissue's development stages and/or pathological state. Cells sourced from different tissue typically yield matrices that mimic the relative composition of the natural tissue matrix. In this paper, we demonstrate that the cell source is the primary determinant of the resulting multiscale hybrid microfibers, in particular we used live neuroblastoma cells that produce hybrid vimentin microfibers upon uptake of DTTO. The different composition induce dissimilar cellular behaviour when these multiscale microfibers are used as substrates for cell cultures. The requirements for materials used in biomedical applications are biocompatibility and biodegradability. Our hybrid multiscale microfibers physiologically produced by live cells after uptake of biocompatible DTTO organic dye present both characteristics and represent innovative multiscale biomaterials for active agents delivery systems and for tissue engineering applications. They could also be used to confer bioactivity to synthetic scaffolds through the loading of bioactive molecules as growth factors.

IV. EXPERIMENTAL SECTION

4.1. General

4.1.1. Synthesis and UV, **PL characterization of DTTO.** DTTO was synthesized and characterized according to already described modalities.[11]

4.1.2. Cell culture. Mouse neuroblastoma cell cultures (B104) and mouse embryonic fibroblasts (3T3) were maintained in DMEM supplemented with 10% FBS, 100 U/mL penicillin, 100 mg/mL streptomycin, 5% L-glutamine and 5% sodium pyruvate. Mouse myoblast cells (C2C12) were maintained in growth medium: DMEM medium supplemented with 15% FBS, 50 U/mL penicillin, 0.05 mg/mL streptomycin, 4 mM glutamine and 10 mM HEPES solution. Cells were grown in in a humidified incubator at 37°C, 5% CO_2, and 95% relative humidity. Upon reaching confluence, cells were passaged using 0.25% trypsin-EDTA. Cells at passages 3-10 were used in the following experimental assays.

4.1.3. Live Neuroblastoma cell labelling and LSCM monitoring. Mouse Neuroblastoma cells (B104) were seeded at a density of 100,000 cells in tissue culture plate in 1 mL of complete culture medium. DTTO dye was dissolved in the minimum amount of DMSO in order to obtain a stock solution and then was administered to cells

by adding the appropriate dilution in DMEM serum free to obtain the final concentration of 0.05 mg/mL and incubated at 37°C in 5% CO_2, 95% relative humidity for 1h. At the end of incubation period unbound dye was removed washing the cell cultures with DMEM medium serum free. The samples were examined after 1, 24, 48, 72 hours and 7 days upon treatment with DTTO by laser scanning confocal microscopy (LSCM). Confocal micrographs were taken with Leica confocal scanning system mounted into a Leica TCS SP5 (Leica Microsystem GmbH, Mannheim, Germany), equipped with a 63X oil immersion objective and spatial resolution of approximately 200 nm in x-y and 100 nm in z.

4.1.4. Isolation of fluorescent microfibers from cell lysates. Fluorescent microfibers inside the cells were purified by whole cell lysates in 50 mM Tris HCl, pH 7.4; 1% Triton X-100; 5 mM EDTA; 150 mM NaCl, 1 mM Na_3VO_4; 1 mM NaF; 1 mM phenylmethylsulfonyl fluoride (PMSF), in the presence of protease inhibitor cocktail (10 µM benzamidine-HCl and 10 µg each of aprotinin, leupeptin and pepstatin A per ml) followed by incubation at 4°C. DTTO-conjugates were left to decant, harvested into fresh reaction tubes, washed three times with fresh lysis buffer by centrifugation, and stored at 4°C or -80°C until performing AFM investigations.

4.1.5. SDS-PAGE. Samples dilution of DTTO-microfibers conjugates into SDS-loading buffer (1:1) were separated on SDS-polyacrylamide gels without prior heating. Resolved protein bands were visualized by Coomassie staining (Sigma Chemical Co., St. Louis, MO, USA), according to manufacturer's instructions.

4.1.6. Tryptic digestion and Mass spectrometry analysis. Fiber pellets isolated by mouse neuroblastoma cells (B104) were resuspended with Urea 8 M and treated with 5 µl of ammonium bicarbonate (AMBIC) 100 mM, reduced with Dithiothreitol (DTT 10 mM, 1µl in AMBIC 100 mM) at 56°C for 30min and alkylated with iodoacetamide (55 mM, 1 µl in AMBIC 100 mM) at room temperature in the dark for 1 h. The resulting protein mixture was digested with TPCK-modified sequencing grade trypsin (final ratio of enzyme to substrate 1:50 w/w) at 37°C overnight. Samples were then acidified with 1 µl 5% formic acid (FA) solution and dried in a vacuum evaporator. Trypsinized microfibers were resuspended in 30 µl of 1% FA/acetonitrile 98:2 solution. Chromatographic separation was performed on a high capacity loading chip, with a 150 mm, 300Å, C18 column prior to a desalting step through a 160 nL trap column; injected sample (2 µl, 0.8 µg) was loaded on the trap column with a 4 µl/min 0.1% FA:ACN 98:2 phase; after 3min, the pre-column was switched in-line with the nano flow (400 nl/min, phase A: water:ACN:FA 97:3:0.1, phase B: ACN:water:FA 97:3:0,1), equilibrated in 3% B. The peptides were eluted from the RP column through the following gradient: 3-45% B over a period of 35 minutes, 45-90% in 7 min, 90% B hold for 5 min, and back to 3% B in 3 min - a total of 60 min of runtime, including a 10 min post-run reconditioning step. Mass spectrometry analyses were performed by ESI-Q-TOF Accurate-Mass G6520AA (Agilent Technologies), controlled by MassHunter (v. B.02.00) and interfaced by a CHIP-cube to an Agilent 1200 nano-pump. Centroided MS scan spectra were acquired in positive mode in the range of 300 to 1700 Da with a 6 Hz sampling rate; top 5 ions, preferring +2 and +3 species, were selected for MS/MS analysis, setting an active exclusion of the same precursor after 1 spectra over 0.15

minutes. Tandem mass spectra (N2 CID cell) were recorded in the mass range 50 to 1700 Da with a sampling rate of 3 Hz. Collision energy was calculated according to the following expression: [3.6 (m/z / 100) - 3] V. Automatic QToF calibration was performed before each run. MassHunter (B02.00, from Agilent Technologies) produced mzData.xml raw data that were searched against SwissProt (v. 57.15) database using an in-house Mascot Server (v. 2.3, Matrix Science, UK) with the following settings: 30 ppm parent ion tolerance, 0.15 Da fragment ion tolerance, semitryptic cleavage with one allowed missed cleavage, carbamidomethyl-cysteine as fixed modification and oxidised methionine, lysine and N-terminus carbamylation as variable modifications, narrowing the search to the rodent proteome. A forward-decoy concatenated protein sequence database was used to evaluate the search false discovery rate.

4.1.7. Immuno co-localization of vimentin. The fluorescent microfibers isolated by mouse neuroblastoma cells (B104) were incubated with anti-vimentin monoclonal antibody (1:150, Sigma-Aldrich, USA) in PBS buffer at 37°C for 1 hour. Primary antibody was revealed using TRITC conjugated anti-mouse antibody (1:1000, Millipore, USA) as secondary antibody and mounting with fluoroshield (Sigma-Aldrich, USA). Confocal micrographs were taken with Leica confocal scanning system mounted into a Leica TCS SP5 (Leica Microsystem GmbH, Mannheim, Germany), equipped with a 63X oil immersion objective and spatial resolution of approximately 200 nm in *x-y* and 100 nm in *z*. The 3D confocal scanning was performed by reconstructing the photoluminescence coming from different focalized slices with a sequential image acquisition. The optical sections were collected in transverse *x-z* and *y-z* planes.

4.1.8. Morphological characterization by atomic force microscopy (AFM). The morphological characterization of isolated fluorescent microfibers by neuroblastoma cells was performed by tapping mode AFM using a Solver PRO Scanning Probe Microscope (NT-MDT Europe BV, Eindhoven, The Netherlands) in air at room temperature. We used TESPA (Veeco, Santa Barbara, CA) silicon cantilevers of 20–80 N/m spring constant and resonance frequency of around 300 kHz and scan size 5 µm x 5 µm.

4.1.9. Cellular adhesion. Prior to microfibers deposition cover slip glass were cleaned with a piranha solution consisting of a 3:1 mixture of H_2SO_4 and H_2O_2, rinsed sequentially with deionized water, ethanol, acetone, and finally dried with nitrogen. 1 mg/mL of isolated fluorescent microfibers (Collagen I hybrid microfibers and Vimentin hybrid microfibers) were deposited on cover slip glass and dried overnight. All the substrates were sterilized for 15 min using UV light before seeding cells. Mouse myoblasts (C2C12), Mouse neuroblastoma cells (B104) and mouse embryonic fibroblasts (3T3) were seeded on microfibers at 100,000 cell/mL (approximately 1000 cells/mm^2 of substrate). After 48 hours each specimen was rinsed twice with PBS 1X to remove any unattached cells. Cytoskeleton morphology was investigated by phalloidin-TRITC at a final concentration of 1 mg/mL (Sigma-Aldrich) labeling. Cells were fixed in situ for 5 min in 3.7% formaldehyde, permeabilized with 1%Triton X-100 in PBS 1X, and washed again in PBS 1X. Thereafter, filamentous actin was stained with phalloidin-TRITC for 40 min at room temperature. Subsequently, the cells were washed several times with PBS to remove unbound phalloidin conjugate. The samples were examined

using a Leica confocal scanning system mounted into a Leica TCS SP5 (Leica Microsystem GmbH, Mannheim, Germany) and equipped with a 63xoil immersion objective.

4.1.10 Proliferation assays. Mouse myoblasts (C2C12), Mouse neuroblastoma cells (B104) and mouse embryonic fibroblasts (3T3) seeded on Collagen I hybrid microfibers and Vimentin hybrid microfibers were analyzed with the cytotoxicity test MTT, measuring the activity of living cells via mitochondrial dehydrogenase activity whose key component is 3-[4,5-dimethylthiazol-2-yl]-2,5-diphenyl tetrazolium bromide.[17] The controls were realized by cells culture on glass coverslip surfaces. Mitochondrial dehydrogenases of viable cells cleaves the tetrazolium ring, yielding purple MTT formazan crystals which are insoluble in aqueous solutions. The crystals are then dissolved in acidified isopropanol and the resulting purple solution is spectrophotometrically measured. An increase in cell number results in an increase in the amount of MTT formazan formed and an increase in absorbance. B104 cells (100,000 cells/mL) were added to well culture plates at 1 mL/well and incubated at 37°C in 5% CO_2, 95% relative humidity for 24-48-72 and 192 hours with the DTTO dye suspension. The control was complete culture medium. After an appropriate incubation period, the cultures were removed from the incubator and the MTT solution added in an amount equal to 10% of the culture volume. Then the cultures were returned to incubator and incubated for 3 hours. After the incubation period, the cultures were removed from the incubator and the resulting MTT formazan crystals were dissolved with acidified isopropanol solution to an equal culture volume. The plates were read within 1 hour after adding acidified isopropanol solution. The absorbance was spectrophotometrically measured at wavelength 570 nm and the background absorbance measured at 690 nm substracted. The percentage viability is expressed as the relative growth rate (RGR) by equation:

$$RGR = (D_{sample}/ D_{control}) * 100\%$$

where D_{sample} and $D_{control}$ are the absorbances of the sample and the negative control. Representative measurements of three distinct sets of data have been reported (Student t-test, $P < 0.05$).
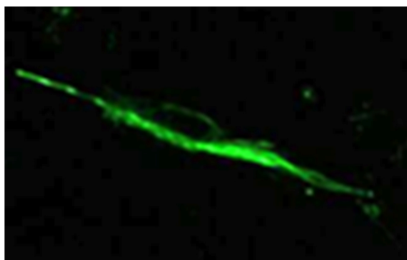
4.2. LSCM image

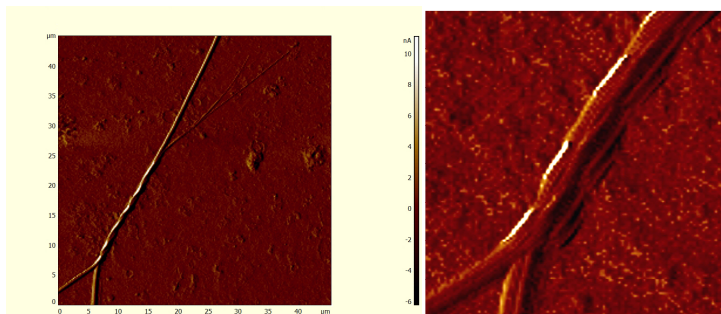**Figure 1S**. A detail of Figure 1D

4.3. AFM images

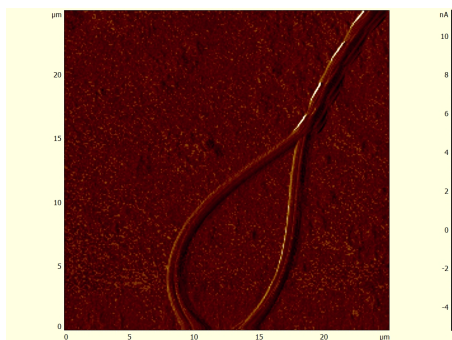**Figure 2S**. AFM image of a fluorescent microfiber isolated from cell lysate.

Figure 3S. Another AFM view of the microfiber of Figure 2S.

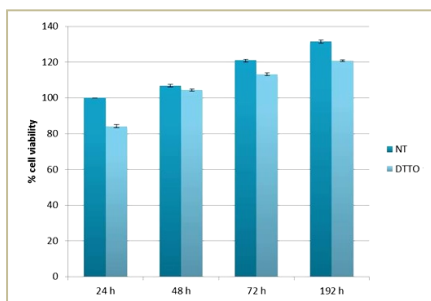## IV. MTT Cytotoxicity tests

Figure 4S. MTT cytotoxicity tests on mouse neuroblastoma cells treated with DTTO dye compared to untreated cells (NT). Representative measurements of three distinct sets of data (t-Student test, $P < 0.05$).

REFERENCES

[1] Harold FM. *Microbiol. Mol. Biol. Rev.,* **2005**, 69, 544-564.

[2] Dedecker P, De Schryver FC, Hofkens J. *J. Am. Chem. Soc.,* **2013**, 135, 2387-2402.

[3] Xie X, Gao N, Deng R, Sun Q, Xu QH, Liu X. *J. Am. Chem. Soc.,* **2013**, 135, 12608-12611.

[4] Li Z, Sun Q, Zhu Y, Tan B, Xu ZP, Dou S. *J. Mater. Chem. B*, **2014**, 2, 2793-2818.

[5] Song F, Tang PS, Durst H, Cramb DT, Chan WCW. *Angew. Chem. Int . Ed.*, **2012**, 51, 8773-8777.

[6] Wysocki LM, Lavis LD. *Current Opinion in Chemical Biology*, **2011**, 15, 752-759

[7] Gandor S, Reisewitz S, Venkatachalapathy M, Arrabito G, Reibner M, Schröder H, Ruf K, Niemeyer CM, Bastiaens PIH, L. Dehmelt. *Angew. Chem. Int. Ed.*, **2013**, 52, 4790-4794.

[8] Aslund A, Sigurdson CJ, Klingstedt T, Grathwohl S, Bolmont T, Dickstein DL, Glimsdal E, Prokop S, Lindgren M, Konradsson P, Holtzman DM, Hof PR, Heppner FL, Gandy S, Jucker M, Aguzzi A, Hammarström P, Nilsson KPR. *ACS Chem. Biol.,* **2009**, 4, 673-684.

[9] Cióslar-Pobuda A, Bäck M, Magnusson K, Jain MV, Rafat M, Ghavami S, Nilsson KPR, Łos MJ. *Cytometry Part A,* **2014**, 85, 628-635. .

[10] Di Maria F, Palamà IE, Baroncini M, Barbieri A, Bongini A, Bizzarri R, Gigli G, Barbarella G, *Org. Biomol. Chem.,* **2014**, 12, 1603-1610.

[11] Palamà IE, Di Maria F, Viola I, Fabiano E, Gigli G, Bettini C, Barbarella G. *J. Am. Chem. Soc.*, **2011**, 133, 17777-17785.

[12] Viola I, Palamà IE, Coluccia AML, Biasiucci M, Dozza B, Lucarelli E, Di Maria F, Barbarella G, Gigli G. *Integrative Biol.*, **2013**, 5, 1057-1066.

[13] Goldie KN, Wedig T, Mitra AK, Aebi U, Herrmann H, Hoenger A. *J. Struct. Biol.*, **2007**, 158, 378-385.

[14] Satelli A, Li S. *Cell. Mol. Life Sci.*, **2011**, 68, 3033-3046.

[15] Levin EC, Acharya NK, Sedeyn JC, Venkataraman V, D'Andrea MR, Wang HY, Nagele RG. *Brain Res.*, **2009**, 1298, 194-207.

[16] Yoneyama MS, Hatakeyama S, Habuchi T, Inoue T, Nakamura T, Funyu T, Wiche G, Ohyama C, Tsuboi S. *Eur. J. Cell. Biol.*, **2014**, 93, 157-169.

[17] Denizot F, Lang R. *J. Immunol. Methods*, **1986**, 89, 271-277.

[18] http://www.matrixscience.com/search_intro.html.

[19] Dahl D, Rueger DC, Bignami A, Weber K, Osborn M. *Eur. J. Cell. Biol.,* **1981**, 24, 191-196.

[20] Georgatos D, Blobel G. *J. Cell. Biol*., **1987**, 105, 117-125.

[21] Bhattacharya R, Gonzalez AM, Debiase PJ, Trejo HE, Goldman RD, Flitney FW, Jones JC. *J. Cell. Sci.*, **2009**, 122, 1390-1400.

[22] Herrmann H, Aebi U. *Annu. Rev. Biochem*., **2004**, 73, 749-89.

[23] Schaffeld M, Herrmann H, Schultess J, Markl J. *Eur. J. Cell. Biol*., **2001**, 80, 692-702.

[24] Pinto N, Yang FC, Negishi A, Rheinstadter M, Gillis TE, Fudge DS. *Biomacromol.,* **2014**, 15, 574-581.

[25] Herrmann H, Häner M, Brettel M, Müller SA, Goldie KN, Fedtke B, Lustig A, Franke WW, Aebi U. *J. Mol. Biol*., **1996**, 264, 933-953.

[26] Chernyatina AA, Nicolet S, Aebi U, Herrmann H, Strelkov SV. *PNAS*, **2012**, 109, 13620-13625.

[27] Monica L, Andersson B, Warburton MJ. *Biochimica et Biophysica Acta (BBA) - Molecular Cell Research*, **1995**, 1268, 27-34.

[28] Virtanen I, Närvänen O, Lehto V. *International Journal of Cancer*, **1988**, 42, 256-260.

- We have synthesized unprecedented classes of functional thiophene based materials by employing enabling technologies such as microwave and ultrasound irradiation in order to obtain oligo and polythiophenes in very pure form and high yields. Preparing oligo- and polythiophenes in very pure form by means of rapid and environmentally friendly procedures is crucial for application of these compounds in materials chemistry as semiconductor and fluorescent compounds for electronic and optoelectronic devices as well as for application in cell imaging and monitoring of intracellular processes. Indeed, the presence of by-products originated by demetalation or dehalogenation of the starting materials or by homo-coupling or boron-halogen exchange side reactions or by the presence of catalyst residues is highly detrimental for their performance in the different fields, altering charge conduction and fluorescence efficiency.

- We have demonstrated that a wide tuning of the optical, charge transport and redox properties of thiophene based oligo- and polythiophenes can be obtained *via* chemoselective oxidation of the thiophene sulfur. In particular, through the synthesis of appropriate polythiophene-S-oxides and the corresponding –S,S-dioxides we have demonstrated that the former have ambipolar charge transport properties while the latter are *n*-type semiconductors.
  We have also found that the chemoselective oxidation of the thiophene sulfur of small fluorescent oligomers allowed to modulate their interaction with intracellular proteins inside live cells *via* H-bonding interactions.

- The synthesis of "sulfur overrich" oligo and polythiophenes, namely compounds having an extra sulfur per ring in the β-position, allowed us to identify a series of decamers and polymers showing photovoltaic properties in Single Material Solar Cells (SMOCs). We ascribed this behaviour to the ability of the compounds - mostly due to S···S non bonding interactions - to self-organize in thin film in such a way as to define separate patterns for holes and electrons transport.

- We have found that in a newly synthesized "sulfur overrich" octamer, the presence of intra- and intermolecular S···S non bonding interactions promotes the spontaneous self-assembly into helical, crystalline, micrometer sized, fibers red fluorescent and electroactive. In appropriate conditions, a different form of crystalline microfibers – straight and yellow emitting - was obtained. Both forms displayed circular dichroism despite the lack of asymmetric carbons; this additional property is only observed when the molecules organize themselves into ordered fibers.

We demonstrated that through accurate design and synthesis the properties of this new class of thiophene based compounds can be tuned opening the way to new materials with peculiar characteristics that allow them to spontaneously organize into ordered structures by cells assistance or by exploiting intra and intermolecular sulfur-sulfur non bonding interactions.